

Aus dem Max von Pettenkofer-Institut für Hygiene und Medizinische Mikrobiologie
Institut der Ludwig-Maximilians-Universität München
Vorstand: Prof. Dr. med. Sebastian Suerbaum

Novel insights into the interaction of *Helicobacter pylori* with host
cells: Impact of Outer Membrane Proteins, Phospholipid
Scramblase I and Annexin binding

Dissertation
zum Erwerb des Doktorgrades der Naturwissenschaften
an der Medizinischen Fakultät der
Ludwig-Maximilians-Universität München

vorgelegt von
Barbara Schmidinger
aus Salzburg

Jahr
2021

Mit Genehmigung der Medizinischen Fakultät
der Universität München

Betreuer: Prof. Dr. Rainer Haas

Zweitgutachter: Prof. Dr. Harald Steiner

Dekan: Prof. Dr. med. Thomas Gudermann

Tag der mündlichen Prüfung: 09.05.2022

Eidesstattliche Erklärung

Ich, Barbara Schmidinger, geb. am 04.04.1991 in Salzburg, erkläre hiermit an Eides statt, dass ich die vorliegende Dissertation mit dem Titel

Novel insights into the interaction of *Helicobacter pylori* with host cells: Impact of Outer Membrane Proteins, Phospholipid Scramblase I and Annexin binding

selbständig verfasst, mich außer der angegebenen keiner weiteren Hilfsmittel bedient und alle Erkenntnisse, die aus dem Schrifttum ganz oder annähernd übernommen sind, als solche kenntlich gemacht und nach ihrer Herkunft unter Bezeichnung der Fundstelle einzeln nachgewiesen habe.

Ich erkläre des Weiteren, dass die hier vorgelegte Dissertation nicht in gleicher oder in ähnlicher Form bei einer anderen Stelle zur Erlangung eines akademischen Grades eingereicht wurde.

München, 18.05.2022

Ort, Datum

Barbara Schmidinger

Unterschrift

Teile dieser Arbeit wurden oder werden unter folgenden Titeln veröffentlicht:

Schmidinger B*, Petri K*, Lettl C, Li H, Namineni S, Ishikawa-Ankerhold H, Jiménez-Soto L, Haas R. “*Helicobacter pylori* binds human Annexins via Lipopolysaccharide to interfere with Toll-like Receptor 4 signaling”, PLoS Pathogens (Manuscript in revision)

*Co-first authors

Bonsor DA, Zhao Q, Schmidinger B, Weiss E, Wang J, Deredge D, Beadenkopf R, Dow B, Fischer W, Beckett D, Wintrobe PL, Haas R, Sundberg EJ. “The *Helicobacter pylori* adhesin protein HopQ exploits the dimer interface of human CEACAMs to facilitate translocation of the oncoprotein CagA”, EMBO Journal, 2018 Jul 2;37(13):e98664.

Table of content

Abstract.....	1
Zusammenfassung.....	3
Chapter 1: Introduction.....	5
1.1 <i>Helicobacter pylori</i>	5
1.1.1 Pathogenicity factors	7
1.1.2 Lipopolysaccharide.....	13
1.2 <i>H. pylori</i> outer membrane proteins	14
1.2.1 HopQ-CEACAM interaction	17
1.3 Annexins.....	18
1.3.1 Intracellular functions.....	19
1.3.2 Extracellular functions	20
1.3.3 Interaction with pathogens.....	21
1.4 Objectives	23
Chapter 2: Material and Methods	24
2.1. Materials	24
2.1.1 Cell lines.....	24
2.1.2 Bacterial Strains	25
2.1.3 Plasmids.....	31
2.1.4 Primers.....	33
2.1.5 Guide RNAs	35
2.1.6 Antibodies	36
2.1.7 Commercially available kits	37
2.1.8 Enzymes	37
2.1.9 Chemicals and buffers.....	37
2.1.10 Consumables	40
2.2 Methods.....	41
2.2.1 Working with eukaryotic cells.....	41
2.2.2 Working with bacteria	43
2.2.3 Molecular biological techniques: RNA.....	50
2.2.4 Molecular biological techniques: DNA.....	51

2.2.5 Protein biochemistry methods	54
2.2.6 Immunofluorescence staining	57
2.2.7 Data analysis and statistics	60
Chapter 3: Results.....	61
3.1 Role of HopQ and CEACAM1 in regulating CagA translocation	61
3.1.1 Influence of the CEACAM1 cytoplasmic tail on CagA translocation	61
3.1.2 Interaction of HopQ with gerbil CEACAM1	63
3.1.3 Effects of targeted mutations in HopQ on CagA translocation	66
3.1.4 Influence of a <i>babC</i> deletion on CagA translocation	68
3.1.5 CagY as a possible interaction partner of HopQ	69
3.2 OMP knockout mutants.....	75
3.2.1 Construction of multiple <i>H. pylori</i> OMP knockout strains.....	75
3.2.2 Deletion of adhesin genes <i>alpA</i> and <i>alpB</i> in different <i>H. pylori</i> strains.....	81
3.3 Impact of the human phospholipid scramblase 1 on CagA translocation.....	91
3.4 Analyzing <i>H. pylori</i> binding to members of the annexin family.....	101
3.4.1 AnxA5 binding of different <i>H. pylori</i> strains	101
3.4.2 Identification of the AnxA5 binding site to <i>H. pylori</i>	102
3.4.3 Influence of lipid A structure on AnxA5 binding.....	108
3.4.4 Influence of mouse stomach passage on AnxA5 binding of <i>H. pylori</i>	111
3.4.5 Influence of AnxA5 binding on the interaction of <i>H. pylori</i> with host cells	111
3.4.6 Analyzing the <i>H. pylori</i> -annexin interaction in human gastric tissue	115
Chapter 4: Discussion	118
4.1 HopQ-CEACAM interaction and CagA translocation	118
4.1.1 The ITIM of CEACAM1 has no impact on CagA translocation	118
4.1.2 Interaction of HopQ with gerbil CEACAM1	118
4.1.3 Targeted HopQ mutations and their impact on CagA translocation.....	119
4.1.4 <i>BabC</i> restricts CagA translocation efficiency in <i>H. pylori</i> P12	120
4.1.5 HopQ-CagY interaction	120
4.2 Adhesins and their impact on CagA translocation	121
4.2.1 Deletion of <i>hopN</i> , <i>hopM</i> and <i>hopA</i> did not influence CagA translocation	121
4.2.2 Deletion of <i>alpAB</i> promotes CagA translocation of <i>H. pylori</i> P12	122
4.2.3 Strain specific differences in adhesion and CagA translocation	122

4.2.4 Stain-specific differences in gene transcription between P12 and G27 <i>alpAB</i> mutants	123
4.3 A novel mechanism for CagA injection.....	125
4.4 The annexin- <i>H. pylori</i> interaction and implications for TLR-4 activation.....	130
4.4.1 AnxA5 binds to the lipid A part of <i>H. pylori</i> LPS	130
4.4.2 AnxA5 can mask recognition by TLR-4.....	131
4.4.3 AnxA5 co-localizes with <i>H. pylori</i> in the human stomach	132
4.5 Outlook	134
Appendix	136
List of figures	136
List of tables	137
List of abbreviations.....	138
Bibliography.....	141
Danksagung	152

Abstract

Helicobacter pylori expresses a multitude of pathogenicity factors for successful establishment of a persistent infection in the stomach mucosa, as well as for evasion of the immune system. One of these pathogenicity factor is the *cag* type IV secretion system, which enables the bacteria to translocate the cytotoxin CagA into their host cells, where it derails several signaling pathways and contributes to development of severe pathologies. The interaction of the *H. pylori* outer membrane protein (OMP) HopQ with CEACAMs is an important co-factor for CagA translocation, however, how this interaction contributes to this process is not clear. Signaling events triggered by the ITIM (immunoreceptor tyrosine-based inhibitory motif) of CEACAM1 don't seem to contribute to CagA translocation efficiency. However, by solving the HopQ-CEACAM1 structure, the β 2- α 4 loop of HopQ was identified as a necessary structure for the interaction with CEACAM1. Furthermore, CagY was identified as a possible interaction partner of HopQ to prime the secretion apparatus for CagA translocation into the host cell. By RNA-Seq analysis, *babC* was identified as an upregulated gene in P12 Δ *hopQ*, however, deletion of this gene led to an increase in CagA translocation.

H. pylori has a remarkably large set of outer membrane proteins, which allow the bacteria to attach to their host cells for establishment of a chronic infection. Several adhesins of *H. pylori* and their host cell receptors are known, like BabA or HopQ, but there are still uncharacterized genes in the OMP family. Deletion of HopQ results in a reduction of CagA translocation to ~50 % in AGS cells. Therefore, to identify other adhesin-receptor pairs impacting CagA translocation, multiple *omp* knockout strains were generated and their influence on CagA translocation was tested. However, none of the analyzed adhesins (HopA, HopN, or HopM) contributed to CagA translocation in AGS cells. In addition, the adhesins AlpA and AlpB were further characterized in this work. Deletion of *alpAB* in P12 resulted in an increase in CagA translocation in AGS and KatOIII cells, even though adhesion to these cell lines was slightly reduced. However, deletion of the same genes in *H. pylori* G27 resulted in a reduction of CagA translocation. These results indicate that *H. pylori* employs strain-specific differences in its expression pattern of adhesins.

The mechanism of CagA internalization in the host cell is still unclear. CagA can bind to phosphatidylserine, a membrane lipid usually localized on the inner leaflet of the plasma membrane. However, contact of *H. pylori* with its host cells leads to externalization of phosphatidylserine. Phospholipid scramblases are Ca^{2+} sensitive enzymes, which mediate externalization of phosphatidylserine. Knockout of the scramblase gene *pslcr1* in AGS cells resulted in a ~50 % reduction of CagA translocation, which was restored by genetic complementation. Thus, this enzyme provides a possible missing link between externalization of

PS upon contact of *H. pylori*, the PS-binding capability of CagA and translocation of the cytotoxin into the cell.

Annexins represent a superfamily of genes that can be found in more than 65 species and they bind to phosphatidylserine in a Ca^{2+} dependent manner. In our laboratory, it was recently discovered that annexins are able to specifically interact with *H. pylori*. This interaction was further characterized in this work. Annexin A5 was discovered to bind to LPS of *H. pylori* and, by analysis of different LPS mutant strains, lipid A was identified as the specific binding partner. As lipid A is the ligand for toll-like receptor-4 (TLR-4), the impact of annexin on TLR-4 activation by *H. pylori* was tested. Indeed, annexin A5 was able to reduce *H. pylori* mediated TLR-4 activation significantly. A mouse re-isolated strain also showed increased annexin binding and TLR-4 activation, which was also reduced by annexin addition, indicating that lipid A modification may be adapted *in vivo*.

In conclusion, this work provides new insights into the HopQ-CEACAM interaction, as well as other outer membrane proteins and their impact on CagA translocation. Furthermore, a putative novel mechanism for the internalization of CagA into the host cell was identified. Lastly, lipid A of *H. pylori* LPS was identified as the bacterial annexin binding partner and this interaction was shown to interfere with TLR-4 signaling, which might help *H. pylori* to evade its host immune recognition.

Zusammenfassung

Helicobacter pylori exprimiert eine Vielzahl an Pathogenitätsfaktoren für die erfolgreiche Etablierung einer persistenten Infektion in der Magenschleimhaut sowie für die Immunevasion. Einer dieser Pathogenitätsfaktoren ist das *cag*-Typ-IV-Sekretionssystem, das es den Bakterien ermöglicht, das Zytotoxin CagA in ihre Wirtszellen zu translozieren, wo es verschiedene Signalwege beeinflusst und zur Entwicklung schwerer Pathologien beiträgt. Die Interaktion des äußeren Membranproteins HopQ mit CEACAMs ist ein wichtiger Kofaktor für die CagA-Translokation, aber es ist nicht klar, wie die Interaktion zu diesem Prozess beiträgt. Signaltransduktionswege, die durch das ITIM von CEACAM1 ausgelöst werden, scheinen nicht zur CagA-Translokation beizutragen. Durch die Auflösung der HopQ-CEACAM1 Struktur wurde jedoch die β 2- α 4-Schleife von HopQ als notwendige Struktur für die Interaktion mit CEACAM1 identifiziert. Darüber hinaus wurde CagY als möglicher Interaktionspartner von HopQ identifiziert, was möglicherweise zur Voraktivierung des Sekretionsapparats beiträgt. Durch RNA-Seq-Analyse wurde *babC* als ein differenziell exprimiertes Gen in P12 Δ *hopQ* identifiziert, jedoch führte die Deletion dieses Gens zu einer Zunahme der CagA-Translokation.

H. pylori verfügt über eine bemerkenswert große Anzahl äußerer Membranproteine (OMPs). Einige dieser OMPs fungieren als Adhäsine und ermöglichen es den Bakterien, sich an ihre Wirtszellen zu heften, um eine chronische Infektion zu etablieren. Neben den bisher bekannten Adhäsinen, wie z.B. BabA oder HopQ, gibt es noch mehrere uncharakterisierte, putative Adhäsingene in der OMP-Familie. In AGS Zellen führt die Deletion von HopQ zu einer Verringerung der CagA-Translokation auf ~50 %. Um andere Adhäsine-Rezeptor-Paare zu identifizieren, die sich auf die CagA-Translokation auswirken, wurden daher mehrere *omp* Deletionsstämme erzeugt und ihr Einfluss auf die CagA-Translokation getestet. Jedoch trug keines der untersuchten Adhäsine (HopA, HopN oder HopM) zur CagA-Translokation in AGS Zellen bei. Um weitere Erkenntnisse über äußere Membranproteine zu gewinnen, wurden die Adhäsine AlpA und AlpB in dieser Arbeit weiter charakterisiert. Die Deletion von *alpAB* in P12 führte zu einer Zunahme der CagA-Translokation in AGS und KatIII Zellen, auch wenn die Adhäsion an diese Zelllinien leicht reduziert war. Die Deletion der gleichen Gene in *H. pylori* G27 führte jedoch zu einer Verringerung der CagA-Translokation. Diese Ergebnisse deuten darauf hin, dass *H. pylori* stammspezifische Unterschiede im Expressionsmuster der Adhäsine aufweist.

Ein weiterer Aspekt einer *H. pylori* Infektion ist der Mechanismus der Internalisierung von CagA in der Wirtszelle, welcher noch unklar ist. CagA kann an Phosphatidylserin binden, ein Membranlipid, das sich normalerweise auf der Innenseite der Plasmamembran befindet. Durch den Kontakt von *H. pylori* mit der Wirtszelle wird Phosphatidylserin externalisiert. Phospholipid-Scramblasen sind

Ca²⁺-empfindliche Enzyme, die zur Externalisierung von Phosphatidylserin beitragen. Die Deletion des Scramblase-Gens *pslcr1* in AGS Zellen führte zu einer ~50 %igen Verringerung der CagA-Translokation, die durch genetische Komplementierung wiederhergestellt werden konnte. Dieses Enzym stellt ein mögliches fehlendes Bindeglied zwischen der Externalisierung von Phosphatidylserin bei Kontakt mit *H. pylori*, der Phosphatidylserin-Bindungsfähigkeit von CagA und der Translokation des Zytotoxins in die Zelle dar.

Annexine sind eine Superfamilie von Genen, die in mehr als 65 Arten vorkommen und Ca²⁺-abhängig an Phosphatidylserin binden. Kürzlich wurde aufgedeckt, dass Annexine in der Lage sind, mit *H. pylori* zu interagieren. Diese Wechselwirkung wurde in dieser Arbeit weiter charakterisiert. Annexin A5 interagiert mit LPS von *H. pylori*, und durch Analyse verschiedener LPS-Mutantenstämme wurde Lipid A als spezifische Bindungsstelle identifiziert. Da Lipid A der Ligand für den Toll-like-Rezeptor-4 (TLR-4) ist, wurde der Einfluss von Annexin auf die TLR-4-Aktivierung durch *H. pylori* getestet. Tatsächlich war Annexin in der Lage, die durch *H. pylori* vermittelte TLR-4-Aktivierung deutlich zu verringern. Ein von Mäusen reisolierter *H. pylori* Stamm zeigte ebenfalls eine erhöhte Annexin-Bindung und TLR-4-Aktivierung, die wiederum durch die Zugabe von Annexin reduziert wurde. Das deutet darauf hin, dass die Lipid-A-Modifikation und damit die Annexin-Bindungsaffinität *in vivo* angepasst werden kann.

Zusammenfassend lässt sich sagen, dass diese Arbeit neue Einblicke in die HopQ-CEACAM-Interaktion sowie in andere äußere Membranproteine und deren Einfluss auf die CagA-Translokation liefert. Darüber hinaus wurde ein mutmaßlich neuer Mechanismus für die Internalisierung von CagA in die Wirtszelle identifiziert. Außerdem wurde gezeigt, dass menschliches Annexin an *H. pylori* LPS bindet und die TLR-4-Signalübertragung beeinträchtigt, was *H. pylori* helfen könnte, sich der Erkennung durch das Wirtsimmunsystem zu entziehen.

Chapter 1: Introduction

1.1 *Helicobacter pylori*

In 1984, Marshall and Warren were able to cultivate a bacterium isolated from human stomach biopsies from patients suffering from gastritis and peptic ulcerations (Marshall & Warren, 1984). The bacterium was at first called *Campylobacter pyloridis*, but was finally named *Helicobacter pylori* (*H. pylori*). Previously, it was thought that the human stomach is a sterile environment, even though Walter Kiernitz could already detect bacteria in the stomach of patients with gastric cancer in 1905 (Rickes, 2011). In 1985, Barry Marshall was able to prove that *H. pylori* is the cause of gastritis. By drinking a culture of *H. pylori* bacteria he subsequently developed gastrointestinal symptoms (Marshall *et al.*, 1985). In 2005, Marshall and Warren were awarded with the Nobel Prize in Physiology and Medicine for their discovery.

H. pylori is a Gram-negative, spiral shaped, microaerophilic ϵ -proteobacterium with two to six flagella. 50 % of the world's population is infected with *H. pylori*, even though the incidence is dependent on socio-economic factors, as well as geography (Suerbaum & Michetti, 2002). In Southern and Eastern Europe, South America and Asia the prevalence of an *H. pylori* infection in adults is often higher than 50 %, whereas in Northern Europe and North America, only about one third of adults are infected (Eusebi *et al.*, 2014). The highest risk factor for an infection is low socio-economic conditions during childhood (Eusebi *et al.*, 2014).

The transmission of *H. pylori* is likely via an oral-to-oral or faecal-to-oral route within a family in early childhood. Other routes of transmission, like water, may be found in developing countries (Suerbaum & Michetti, 2002).

One of the hallmarks of *H. pylori* is its inter-strain genomic diversity. Because of this, an infected individual carries at least one genetically unique strain, usually with a high heterogeneity within this strain and this genetic variability probably contributes to its success as a pathogen (Ailloud *et al.*, 2021). Indeed, *H. pylori* has been associated with modern humans for about 100,000 years, proving its success (Linz *et al.*, 2007, Moodley *et al.*, 2012).

Even though most individuals infected with *H. pylori* are asymptomatic, a small percentage will develop severe diseases associated with an infection, like peptic ulcers, gastric atrophy, adenocarcinoma or MALT (mucosa associated lymphoid tissue) lymphoma (Peek & Blaser, 2002). In 1994, the WHO declared *Helicobacter pylori* as a class I carcinogen (IARC, 1994). Treatment of diseases in connection with an *H. pylori* infection is primarily eradication therapy. Quadruple therapy with proton pump inhibitors (PPI), clarithromycin, amoxicillin and bismuth is used as a first line regimen. However, the increased antimicrobial resistance to clarithromycin represents a

challenge for treatment. In areas with high clarithromycin resistance rates, addition of metronidazole to PPI, clarithromycin and amoxicillin has proven to be effective. Nevertheless, the growing resistance of *H. pylori* to commonly used antibiotics represents a challenge and thus, a focus on research for alternative treatment options should be implemented. (de Brito *et al.*, 2019)

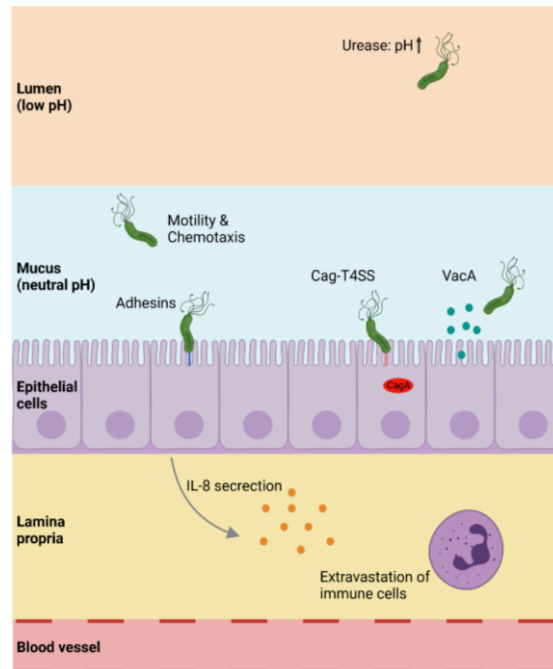


Figure 1.1: Pathogenicity factors of *H. pylori*.

H. pylori expresses a multitude of pathogenicity factors for successful establishment of a persistent infection in the stomach mucosa, as well as for evasion of the immune system. Urease helps to increase the pH value in the gastric lumen; motility, chemotaxis and cell shape enable the bacteria to find their ecological niche, the gastric mucosa. Attachment to their host cells is mediated by multiple adhesins. The Cag-T4SS and VacA are virulence factors that help to establish a chronic infection and manipulate the immune system. (Ansari & Yamaoka, 2019) Figure was created with Biorender.

1.1.1 Pathogenicity factors

H. pylori is able to establish a chronic infection in the human stomach mucosa. Upon reaching the lumen of the stomach, it encounters very harsh conditions, like low pH levels. However, *H. pylori* possesses several factors to counteract these harsh conditions in the stomach, like urease, its bacterial shape, motility and chemotaxis to reach the gastric mucosa still intact (Figure 1.1). There, it attaches to its host cells via adhesins and expresses other pathogenicity factors, like the Cag-Type IV secretion system and vacuolating cytotoxin, to establish an infection and evade the immune system. (Ansari & Yamaoka, 2019)

1.1.1.1 Urease

H. pylori expresses a large amount of the enzyme urease, which catalyzes urea hydrolysis, ultimately resulting in production of ammonia, CO₂ and water. Ammonia neutralizes stomach acidity and creates a neutral microenvironment around *H. pylori* in the gastric lumen. In the periplasmic space, CO₂ is converted to bicarbonate by α -carbonic anhydrase, thereby maintaining the periplasmic pH of 6.1. (Ansari & Yamaoka, 2019)

Urease activity, together with the major building block of flagella, flagellin, alter the properties of the mucus layer by influencing the transcription of mucin genes (Perrais *et al.*, 2014). Additionally, urease expression and its catalytic products are proposed to be important for establishment of infection. Ammonia disrupts tight cell junctions and breaches cellular integrity, resulting in damage of the gastric epithelium (Lytton *et al.*, 2005, Wroblewski *et al.*, 2009). CO₂, on the other hand, protects the bacteria from metabolic products like peroxyxynitrite, a bactericidal metabolite of nitric oxide (Kuwahara *et al.*, 2000). Furthermore, urease seems to trigger pro-angiogenic processes in gastric epithelial cells, playing an additional role in gastric cancer development (Olivera-Severo *et al.*, 2017).

1.1.1.2 Motility and chemotaxis

The *H. pylori* chemotaxis systems allows sensing of a number of environmental and bacterial signals, ensuring movement away from harmful towards more favorable conditions and guiding the bacteria towards the gastric mucosa. The core chemotaxis proteins of *H. pylori* include chemoreceptors (TlpA, TlpB, TlpC, and TlpD), the CheW coupling protein, CheA kinase and the CheY response regulator. (Johnson & Ottemann, 2018)

CheA is the sensor of the two-component system CheA-CheY, regulating flagella movement according to environmental changes (Foyne *et al.*, 2000, Camilo *et al.*, 2017). Auxiliary chemotaxis proteins are three CheV-type coupling proteins, the CheZ phosphatase and the unique chemotaxis protein ChePep. Repellent conditions for *H. pylori* include acidic pH, reactive oxygen

species (ROS) and bile. A bacterial repellent is the quorum-sensing molecule autoinducer-2 (AI-2) that responds to its own electron transport chain and may promote dispersion of *H. pylori in vivo*. Furthermore, *H. pylori* also senses several beneficial chemoattractants, e.g. urea, sensed by TlpB, and arginine, which is an essential amino acid for *H. pylori* and is sensed by TlpA. (Johnson & Ottemann, 2018)

The motility of *H. pylori* is mediated by its flagella and it enables bacteria to escape the harsh conditions of the gastric lumen and reach the gastric mucosa. In addition, the helical cell shape helps the bacteria to penetrate and move within the viscous mucus layer (Ansari & Yamaoka, 2019). *H. pylori* has two to six unipolar sheathed flagella (Geis *et al.*, 1989). Acid exposure actually activates flagellin, resulting in higher speeds of acid-exposed bacteria compared to non-acid exposed ones (Merrell *et al.*, 2003). Besides, *H. pylori* flagellin contributes to evasion of toll-like receptor (TLR) 5 mediated immunity. The bacterium evades TLR-5 recognition *in vitro* by avoiding the shedding of flagellin and even if released, activation of TLR-5 is very weak (Gewirtz *et al.*, 2004).

1.1.1.3 Adhesins

Once the bacteria finally reach the gastric epithelium, they attach to their host cells via adhesins, such as blood group antigen-binding adhesin (BabA), sialic acid-binding adhesin (SabA) and others. Attachment to their host cells is essential for establishing a chronic infection. It also provides several benefits for *H. pylori*: protection of washing out during mucus shedding, nutrient access and delivery of bacterial toxins and other effector molecules. (Ansari & Yamaoka, 2019)

Bacterial adhesins and their host cell receptors will be discussed in depth in chapter 1.2.

1.1.1.4 Cag Type IV Secretion System

The *cag* type IV secretion system (Cag-T4SS) translocates the effector protein cytotoxin-associated antigen A (CagA) across the bacterial and epithelial membranes into the host cell cytoplasm, where it deregulates several cellular signaling pathways and is associated with severe disease development (Backert *et al.*, 2015). It is encoded by the ca. 40 kb *cagPAI* (pathogenicity island), a typical chromosomal insertion element carrying 27-31 genes (Censini *et al.*, 1996). The presence of the *cagPAI* increases the risk to develop severe pathologies upon *H. pylori* infections, therefore these strains belong to highly virulent type-I strains, in contrast to the *cagPAI* negative, less virulent type-II strains (Censini *et al.*, 1996). As this genetic element was acquired only once, more than 60,000 years ago and is still maintained today, it probably provides evolutionary advantages for *H. pylori* (Olbermann *et al.*, 2010).

The Cag-T4SS is a multicomponent protein complex, spanning the inner and outer membranes. It exhibits homology to the prototypical VirB/VirD4 T4SS of *Agrobacterium tumefaciens*, consisting of 12 components (Backert *et al.*, 2015). Compared to this, the Cag-T4SS is unique, as it requires at least 15-16 components to form a functional translocation machinery (Table 1.1) (Backert *et al.*, 2015). It forms pilus-like surface structures, formation of which is induced upon host cell contact (Kwok *et al.*, 2007). Other environmental factors also regulate formation of pili, for example, limitation of iron results in production of more pili and more translocation of CagA (Noto *et al.*, 2013).

Table 1.1: Components of the Cag-T4SS, their localization and function (Backert *et al.*, 2015).

Name	Localization	Function	Essential for CagA translocation
Cag1/Cag ζ	Inner membrane	Unknown	No
Cag2/Cag ϵ	Cytoplasm	Unknown	No
Cag3/Cag δ	Outer membrane	Component of outer membrane complex	Yes
Cag4/Cag γ	Periplasm	PGN hydrolase (VirB1)	Yes
Cag5/Cag β	Inner membrane	Coupling factor (VirD4)	Yes
Cag α /VirB11	Cytoplasm/inner membrane	NTPase	Yes
CagZ	Cytoplasm/inner membrane	Cag5 stabilization	~
CagY	Inner/Outer membrane/Surface	Component of core complex, integrin binding (VirB10)	Yes
CagX	Inner/Outer membrane/Surface	Component of core complex (VirB9)	Yes
CagW	Inner membrane	Inner membrane channel (VirB6)	Yes
CagV	Inner membrane	Component of core complex (VirB8)	Yes
CagU	Inner membrane	Unknown	Yes
CagT	Outer membrane/Surface	Component of core complex, outer membrane lipoprotein (VirB7)	Yes
CagS	Cytoplasm	Unknown	No
CagQ	Inner membrane	Unknown	No
CagP	Inner membrane	Unknown	No
CagM	Outer membrane	Component of outer membrane complex	Yes
CagN	Periplasm/Inner membrane	Accessory factor	~
CagL	Periplasm/Surface	VirB5-like, pilus biogenesis, integrin binding	Yes
CagI	Periplasm/Surface	Pilus biogenesis, integrin binding	Yes
CagH	Inner membrane	Pilus biogenesis	Yes

CagG	Periplasm	Unknown	Yes
CagF	Cytoplasm/Inner membrane	Chaperone of CagA	Yes
CagE	Inner membrane	NTPase (VirB3/VirB4)	Yes
CagD	Inner membrane/Periplasm/Surface	Unknown	~
CagC	Inner/Outer membrane/Surface	Pilus subunit (VirB2)	Yes
CagB	Unknown	Unknown	Unknown
CagA	Cytoplasm/Surface	Effector protein	Yes

Recently, structures of the Cag-T4SS were visualized by single particle electron microscopy or cryo-electron tomography (Frick-Cheng *et al.*, 2016, Chang *et al.*, 2018, Chung *et al.*, 2019). The Cag-T4SS consists of three subassemblies: the outer membrane core complex (OMCC), the periplasmic ring complex (PRC) and the central stalk (Chung *et al.*, 2019). The OMCC forms the cap structure of the T4SS, the crest of which consists of CagY, which likely breaks through the outer membrane (Chung *et al.*, 2019). CagY is a VirB10 homologue, but consists of two additional repeat elements, the 5' repeat region (FRR) and the middle repeat region (MMR) (Aras *et al.*, 2003). Recombination in the MMR regions can happen via deletion or duplication events, altering the T4SS function (Barrozo *et al.*, 2013). Thus, CagY is proposed to act as an immune-sensitive regulator for adaption of host inflammatory responses to sustain persistent *H. pylori* infection (Barrozo *et al.*, 2016). CagY also binds to $\alpha_5\beta_1$ integrin via the MMR, therefore promoting attachment to epithelial cells. Recombination events in the MMR modulate function of the Cag-T4SS by altering attachment to $\alpha_5\beta_1$ integrin (Jiménez-Soto *et al.*, 2009, Skoog *et al.*, 2018).

The Cag-T4SS components CagI, CagA and CagL also interact with $\alpha_5\beta_1$ integrin, CagL specifically interacts via its RGD (arginine-glycine-aspartic acid) motif (Kwok *et al.*, 2007, Jiménez-Soto *et al.*, 2009). Additionally, CagL can bind to $\alpha_v\beta_5$ integrin (Wiedemann *et al.*, 2012). CagL binding to $\alpha_5\beta_1$ integrin activates nonreceptor host cell kinases FAK and c-Src, as well as the epidermal growth factor receptor and epidermal growth factor receptor family member Her3/Erb3 (Kwok *et al.*, 2007, Tegtmeyer *et al.*, 2010). CagL also upregulates gastrin expression via $\alpha_v\beta_5$ integrin (Wiedemann *et al.*, 2012). Furthermore, CagL has a flagellin D1 domain like motif, through which it can activate TLR-5 and thereby modulate the immune response against *H. pylori* (Pachathundikandi *et al.*, 2019).

The Cag-T4SS exhibits two major phenotypes: CagA translocation and IL-8 induction (Backert *et al.*, 2015). For translocation of CagA into epithelial cells, the interaction of HopQ with CEACAMs (carcinoembryonic antigen-related cell adhesion molecules) is necessary (Javaheri *et al.*, 2016,

Königer *et al.*, 2016) (see chapter 1.2.1). However, interaction with integrins is not required to inject CagA (Zhao *et al.*, 2018).

In addition to CagA, the T4SS translocates some other effector molecules, like LPS metabolites, chromosomal DNA and peptidoglycan. LPS metabolites include ADP-*glycero*- β -D-*manno*-heptose (ADP-heptose), which acts as a pathogen-associated molecular pattern and activates the nuclear factor κ B (NF- κ B) pathway in human epithelial cells. For that, α -protein kinase-1 (ALPK1)/TRAF-interacting protein with forkhead-associated domain (TIFA) is activated, resulting in pro-inflammatory signaling events (Pfannkuch *et al.*, 2019). Furthermore, chromosomal DNA activates TLR-9, which recognizes hypo-methylated CpG motifs (Varga *et al.*, 2016). Nod1, an intracellular pattern recognition receptor, recognizes peptidoglycan of *H. pylori* upon translocation into epithelial cells (Viala *et al.*, 2004).

Upon contact of *H. pylori* with its host cells, phosphatidylserine (PS), a phospholipid normally localized in the inner leaflet of the plasma membrane, is externalized. CagA interacts with PS via a K-Xn-R-X-R motif (R619/R621), located in the central region of the protein. Through this interaction, CagA translocation is thought to be initiated. Once delivered into the host cell, CagA is tethered to the plasma membrane in polarized epithelial cells via this PS binding motif. (Murata-Kamiya *et al.*, 2010)

Delivered CagA is phosphorylated by host cell kinases at Glu-Pro-Ile-Tyr-Ala (EPIYA) motif. According to the conserved flanking sequence of the EPIYA motif, four distinct EPIYA segments were identified, EPIYA-A, -B, -C, and -D. Depending on the geographical region, the composition of EPIYA motifs vary: EPIYA-ABC is mainly found in Western strains (worldwide except East Asia) and EPIYA-ABD in East Asian strains. The EPIYA-C motif is present in variable numbers (usually 1-3 copies) in Western CagA variants. (Takahashi-Kanemitsu *et al.*, 2020)

The different EPIYA motifs are selectively phosphorylated by different kinases. Src family kinases (SFK), like c-Src, specifically phosphorylate EPIYA-C and EPIYA-D motifs, whereas c-Abl kinase phosphorylates all four motifs. Usually, only one or two EPIYA segments are phosphorylated, but never three or more. None of the phosphorylated EPIYA motifs alone are sufficient to induce cell scattering and elongation in AGS cells (“hummingbird phenotype”), indicating a hierarchical process. According to this, EPIYA-C/EPIYA-D is phosphorylated first by SFKs, followed by phosphorylation of EPIYA-A or EPIYA-B by c-Abl. (Mueller *et al.*, 2012)

Furthermore, CagA has a conserved 16 amino acid sequence multimerization motif (CM) immediately next to either EPIYA-C or EPIYA-D segments, by which it multimerizes at the plasma membrane (Ren *et al.*, 2006).

Both phosphorylated and non-phosphorylated CagA act as a pro-oncogenic scaffolding protein, thereby activating host cell signaling pathways leading to secretion of pro-inflammatory cytokines, cell proliferation, actin cytoskeleton rearrangement and disruption of intercellular junction and cell polarity (Takahashi-Kanemitsu *et al.*, 2020). For example, SHP2, a non-receptor type phosphatase, binds to phosphorylated EPIYA-C or EPIYA-D, resulting in a conformational change to an activated conformation (Higashi *et al.*, 2002b). Thus, the RAS-RAF-MEK-ERK pathway is activated, a signaling pathway involved in proliferation and differentiation of cells (Takahashi-Kanemitsu *et al.*, 2020). Binding affinity of SHP2 to EPIYA-D is stronger than to EPIYA-C motifs, thus EPIYA-ABD strains are considered to be more virulent than EPIYA-ABC strains (Higashi *et al.*, 2002a). SHP2 also dephosphorylates the focal adhesion kinase (FAK), which regulates the dynamics of focal adhesion and therefore influences cell morphology and motility (Tsutsumi *et al.*, 2006).

Phosphorylated EPIYA-A and EPIYA-B motifs, on the other hand, are used by C-terminal Src kinase (CSK) as a docking site (Tsutsumi *et al.*, 2006). CSK is a protein tyrosine kinase, which phosphorylates the inhibitory phosphorylation sites of SFKs, thus attenuating the CagA-mediated activation of SHP2 and downregulating of EPIYA-C and -D phosphorylation (Tsutsumi *et al.*, 2003).

1.1.1.5 Vacuolating Cytotoxin VacA

Another protein of *H. pylori*, which is associated with severe disease outcome, is the vacuolating cytotoxin VacA. It induces the formation of vacuoles in different cell types and can form anion selective channels in host cells (McClain *et al.*, 2017). Other functions include interference on the mitochondrial membrane, stimulation of apoptosis, disrupted endocytic trafficking, efflux of various ions and depolarization of the plasma membrane potential (McClain *et al.*, 2017). It can also inhibit function and proliferation of various immune cells, most notably T-cells, therefore helping in modulating the immune response and establishing a persistent infection (Gebert *et al.*, 2003).

VacA is produced as a 140 kDa precursor protein and, via proteolytic cleavage, the 88 kDa secreted toxin is produced (Cover & Blaser, 1992, Schmitt & Haas, 1994). For secretion, the N-terminal signal peptide and the C-terminal β -barrel domain are necessary (type V autotransporter secretion pathway) (Cover *et al.*, 1994, Fischer *et al.*, 2001). The 88 kDa toxin can be further cleaved into a 55 kDa (p55) and 33 kDa (p33) subunit, but there is no evidence that this cleavage is required for function (McClain *et al.*, 2017).

VacA binds to lipid rafts on the plasma membrane of its host cells (McClain *et al.*, 2017). Receptors include sphingomyelin (Gupta *et al.*, 2008), receptor-like protein tyrosine phosphatase alpha

(Yahiro *et al.*, 2003) and beta (Yahiro *et al.*, 1999), and low density lipoprotein receptor-related protein-1 on epithelial cells (Yahiro *et al.*, 2012) and $\beta 2$ integrin on T-cells (Sewald *et al.*, 2008). Upon cell contact, VacA is internalized into endosomal compartments (McClain *et al.*, 2017). It can be integrated into membranes to form hexameric anion selective channels, including in plasma membrane and endosomal membranes (Iwamoto *et al.*, 1999, Szabò *et al.*, 1999). It also forms vacuoles in the cytoplasm of host cells, which contain markers of late endosomes and lysosomes, as they are probably derived from the endosome-lysosome pathway (Papini *et al.*, 1994, Molinari *et al.*, 1997). Association of VacA with mitochondria causes decreased mitochondrial membrane potential and activation of apoptotic pathways (BAK BAX, cytochrome c release, mitochondrial fragmentation) (McClain *et al.*, 2017).

Most *H. pylori* strains contain intact *vacA* open reading frames (ORF), but there is a high variance of alleles between strains (McClain *et al.*, 2017). Differences in VacA toxin activity can be attributed to variations in amino acid sequences or the levels of transcription or secretion (Atherton *et al.*, 1995, Forsyth *et al.*, 1998, Letley & Atherton, 2000).

VacA alleles are categorized in several different families, based on heterogeneity in specific regions. There are three main heterogenic regions of *vacA*, the “s” (signal), the “i” intermediate and “m” (middle) region (Atherton *et al.*, 1995, Rhead *et al.*, 2007). For each region, several sub-families are classified, e.g., s1a, s1b, s1c and s2; m1 and m2; i1, i2 and i3 (Chauhan *et al.*, 2019). The “s” region corresponds to differences in the amino terminal signal peptide (McClain *et al.*, 2017). The s2 variant contains a 12 amino acid extension at the N-terminus, altering the hydrophobicity of the secreted protein, and is impaired in their ability of anion channel formation and vaculation (McClain *et al.*, 2001). The “i” region is found in the p33 domain (Rhead *et al.*, 2007) and the “m” region in the p55 domain (Atherton *et al.*, 1995).

The s1, i1 and m1 type *vacA* alleles are associated with a higher risk of developing gastric cancer or premalignant conditions, as these alleles were found more often in *H. pylori* strains of patients with those pathologies (McClain *et al.*, 2017). Strains, carrying the s1 *vacA* allele, usually also contain the *cagPAI*, as well as OMPs associated with severe pathologies (e.g., *babA*, type I *hopQ*, *oipA*) (Atherton *et al.*, 1995, Gerhard *et al.*, 1999, Dossumbekova *et al.*, 2006, Yakoob *et al.*, 2016).

1.1.2 Lipopolysaccharide

LPS (lipopolysaccharide) of Gram-negative bacteria is usually composed of three domains: the hydrophobic lipid A, anchoring LPS to the outer membrane, the variable O-antigen and a core oligosaccharide, connecting O-antigen and lipid A (Li *et al.*, 2016). *H. pylori* LPS has some unique

features that support persistent infection and immune evasion: The O-antigen is decorated with Lewis antigens, promoting host mimicry and immune escape and lipid A has a unique structure, which results in resistance to host antimicrobial peptides (CAMPs) and immune evasion (Monteiro, 2001, Cullen *et al.*, 2011). It was previously postulated that the core oligosaccharide is structured, similar to other Gram-negative bacteria, in an inner and outer core. However, the structure of the core was redefined and therefore, consists only of the inner core (Li *et al.*, 2017).

De novo synthesis of lipid A is a nine-step enzymatic pathway, known as the Raetz pathway, and gives rise to a *bis*-phosphorylated and *hexa*-acetylated KDO₂ (keto-deoxy-octonate)-lipid A structure (Raetz & Whitfield, 2002). In *H. pylori*, this structure is further modified, resulting in *mono*-phosphorylated and *tetra*-acetylated KDO-lipid A (Tran *et al.*, 2005, Stead *et al.*, 2010, Cullen *et al.*, 2011). In contrast to other bacteria, which modify their lipid A upon specific environmental cues, *H. pylori* lipid A modification appears to be constitutive (Stead *et al.*, 2010).

Lipid A modification is a highly ordered and complex process, consisting of five enzymatic steps. First, the 1-phosphate group is removed by LpxE, allowing addition of phosphatidylethanolamine (PE) catalyzed by EptA. In the next step, a KDO hydrolase (HP0579/HP0580) removes the terminal KDO. Then, LpxF removes the 4'-phosphate, which allows subsequent removal of the two 3-O-linked acyl chains by LpxR. (Li *et al.*, 2016)

Disruption of this modification process usually results in an increased sensitivity to polymyxin A (Stead *et al.*, 2010, Cullen *et al.*, 2011) Due to the low-level phosphorylation and unusual acetylation pattern and acyl chain length, activation of TLR-4 by *H. pylori* lipid A is usually very weak (Li *et al.*, 2016). However, TLR-10, together with TLR-2, was also suggested to be involved in LPS recognition (Nagashima *et al.*, 2015).

1.2 *H. pylori* outer membrane proteins

H. pylori has a remarkably large set of outer membrane proteins (OMP), approx. 4 % of the genome codes for ~ 64 genes. These genes can be divided into five paralogous families of OMPs according to their functions: The Hop (*H. pylori* outer membrane proteins) and Hor (*H. pylori* outer membrane related proteins) family, the Hof (*Helicobacter* OMP) family, the Hom (*Helicobacter* outer membrane) family, iron regulated OMPs, and efflux pump OMPs. The largest family is Hop and Hor, consisting of 33 members, including the putative adhesin branch (Figure 1.2, green rectangle). (Alm *et al.*, 2000)

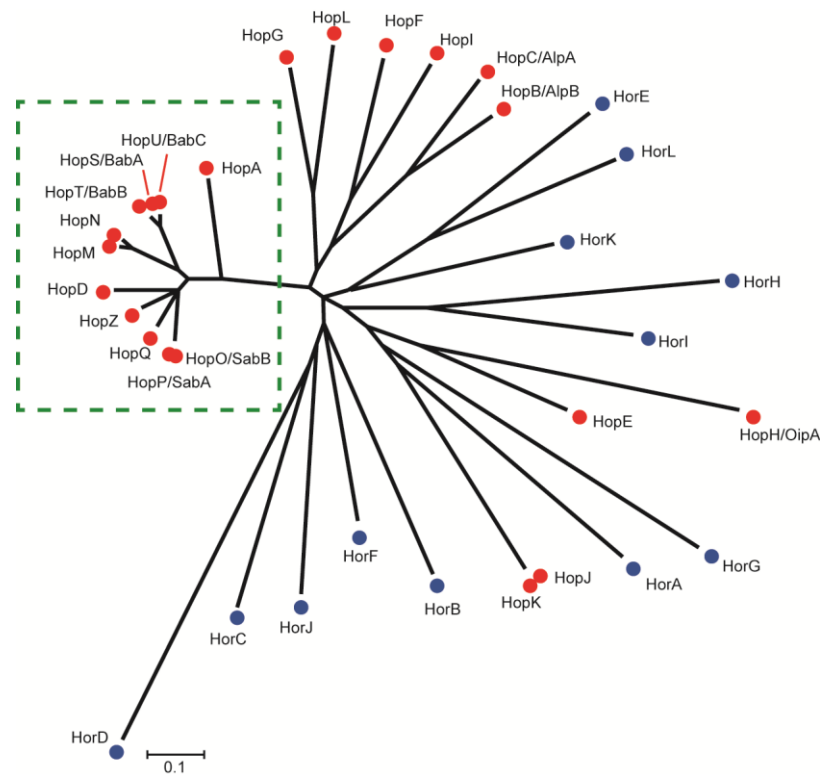


Figure 1.2: Hop and Hor family tree.

One of the 5 families of *H. pylori* OMPs comprises of Hop (red, 21 members) and Hor (blue, 12 members). The putative adhesin branch (green rectangle) consist of 11 Hops, which share a strong sequence identity (Königer *et al.*, 2016).

Adhesins facilitate attachment of the bacteria to their host cells, which is very important for colonization and persistence, evasion from the immune system and efficient delivery of proteins, *e.g.*, CagA (Oleastro & Ménard, 2013). Involved in adhesion are, amongst others, BabA, SabA, adherence-associated lipoprotein A and B (AlpAB), outer inflammatory protein A (OipA) and HopQ. Except for OipA, the host cell receptors were identified for all of these adhesins.

BabA is one of the best characterized adhesins of *H. pylori*. It binds to fucosylated Lewis B (Le^b) blood group antigens (Borén *et al.*, 1993, Ilver *et al.*, 1998). Depending on their BabA binding specificity, strains can be divided into “specialist” and “generalist” (Aspholm-Hurtig *et al.*, 2004). “Specialist strains” can bind only to Le^b antigen corresponding to blood group O. “Generalist strains”, on the other hand, can bind independent of terminal modification on Le^b antigen (Ale^b, BLe^b, and Le^b), corresponding to blood groups A, B and O. These strains are found in populations in Europe and the US, whereas “specialist strains” can only be found in South American Amerindian populations, as most of these individuals have blood group O (Aspholm-Hurtig *et al.*, 2004). Binding of BabA to Le^b is pH-dependent, at a lower pH, binding is reduced, which can be restored by acid neutralization (Bugaytsova *et al.*, 2017). This allows bacteria to escape from

epithelial cells and mucus that was shed into the lumen of the stomach (Bugaytsova *et al.*, 2017). BabA is suggested to enhance CagA translocation into gastric cells and induce severe inflammation in the stomach (Ishijima *et al.*, 2011).

The receptor for SabA is sialyl Lewis X/a glycosphingolipid (sLe^x/sLe^a) (Mahdavi *et al.*, 2002). Interestingly, sLe^x expression is induced during *H. pylori* infection. Highly pathogenic *H. pylori* strains are able to alter expression of the specific glycosyltransferase β 3GlcNAcT5, which is essential for the biosynthesis pathway of Lewis antigens, in a CagA and CagE dependent manner (Marcos *et al.*, 2008). Expression of SabA is regulated by slipped strand mispairing in a 5' CT dinucleotide repeat region, mutations in this region can lead to a pre-mature stop codon in the *sabA* ORF and, thus, expression is switched "off" (Goodwin *et al.*, 2008).

AlpA and AlpB were first identified as adhesins by BlaM-transposon shuttle mutagenesis in the *H. pylori* strain P1, as deletion of these genes resulted in decreased adhesion to the gastric epithelial cell line KatOIII (Odenbreit *et al.*, 1996, Odenbreit *et al.*, 1999). The receptor for AlpAB is suggested to be laminin, a component of the extracellular matrix (Senkovich *et al.*, 2011). In contrast to other OMPs, AlpA and B seem to play an important role in colonization of the human stomach, as these proteins were shown to be expressed in all of the tested clinical isolate strains (Odenbreit *et al.*, 2009). In addition, *alpAB* mutant strains showed low colonization rates in stomachs of mice and Mongolian gerbils (Lu *et al.*, 2007, Senkovich *et al.*, 2011).

OipA was initially identified to induce pro-inflammatory responses, as in an *oipA* mutant IL-8 production in a gastric epithelial cell line was reduced (Yamaoka *et al.*, 2000). However, another study suggested that there is no link between OipA and IL-8 induction, but that OipA acts as an adhesin to host cells (Dossymbekova *et al.*, 2006). Others suggested that IL-8 expression due to the *cagPAI* is increased by the presence of OipA (Odenbreit *et al.*, 2009). Like *sabA* expression, *oipA* is regulated by slipped strand mispairing (Saunders *et al.*, 1998, Yamaoka *et al.*, 2000). Furthermore, OipA activates phosphorylation of FAK, thereby inducing the remodeling of actin stress fibers (Tabassam *et al.*, 2008).

Other adhesins include HopD and HopZ. HopD is also called LabA (N,N'-diacetyllactosediamine (LacdiNAc)-binding adhesin A) due to its receptor LacdiNAc (Rossez *et al.*, 2014). The receptor for HopZ is still unknown (Peck *et al.*, 1999).

1.2.1 HopQ-CEACAM interaction

HopQ is an adhesin of *H. pylori* that was identified as a non-*cagPAI*-encoded co-factor of CagA translocation (Belogolova *et al.*, 2013, Zhao *et al.*, 2018). As receptors for HopQ, CEACAM1, CEACAM3, CEACAM5, and CEACAM6 were identified (Javaheri *et al.*, 2016, Königer *et al.*, 2016).

CEACAMs are a diverse group of surface glycoproteins, belonging to the immunoglobulin (Ig) superfamily. CEACAMs are usually involved in cell-cell recognition and cellular processes, like shaping of tissue architecture, angiogenesis, insulin homeostasis and T-cell proliferation. CEACAM1, 5 and 6 consist of differing numbers of constant (IgC-like) and one N-terminal variable Ig domain (IgV-like). Several isoforms of CEACAM1 are expressed, most of them harboring a transmembrane domain and either a long or short cytoplasmic domain, the long isoform possessing ITIMs. CEACAMs 5 and 6 are linked to the membrane by a glycosylphosphatidylinositol anchor. CEACAM1, 5, and 6 are expressed, amongst others, on epithelial cells and can form homo- and heterodimers via their N-terminal IgV-like domains. CEACAM3, on the other hand, has only one IgV-like domain and a cytoplasmic ITAM (immunoreceptor tyrosine-based activation motif) and can only be found on human granulocytes, where it acts as a receptor for phagocytosis of specific bacterial pathogens. A number of pathogenic bacteria (*e.g.*, *Neisseria gonorrhoeae*, *N. meningitidis*, *Haemophilus influenzae*, and *Moraxella catarrhalis*) also adhere to human CEACAMs. (Gray-Owen & Blumberg, 2006, Kuespert *et al.*, 2006, Tchoupa *et al.*, 2014) HopQ binds CEACAMs via their N-terminal IgV-like domain, exploiting the dimer interface of human CEACAMs for adhesion by a coupled folding and binding mechanism (Bonsor *et al.*, 2018, Moonens *et al.*, 2018). *H. pylori* has two different families of *hopQ* alleles (type I and type II) and type I *hopQ* alleles are more common in *cagPAI/s1 vacA* positive strains from patients with peptic ulcer disease (Cao & Cover, 2002). Apparently, HopQII loses the ability to interact with CEACAM6, but can still bind to CEACAM1, 3 and 5 (Moonens *et al.*, 2018). Furthermore, HopQ does not recognize murine, canine or bovine CEACAMs (Königer *et al.*, 2016). In fact, CagA is not phosphorylated upon translocation in murine polymorphonuclear leukocytes (PMN), but a strong phosphorylation can be detected in CEACAM-humanized murine PMNs (Behrens *et al.*, 2020). Moreover, HopQ interaction with CEACAMs supports Cag-T4SS dependent canonical and non-canonical NF- κ B signaling in host cells (Feige *et al.*, 2018, Maubach *et al.*, 2020).

1.3 Annexins

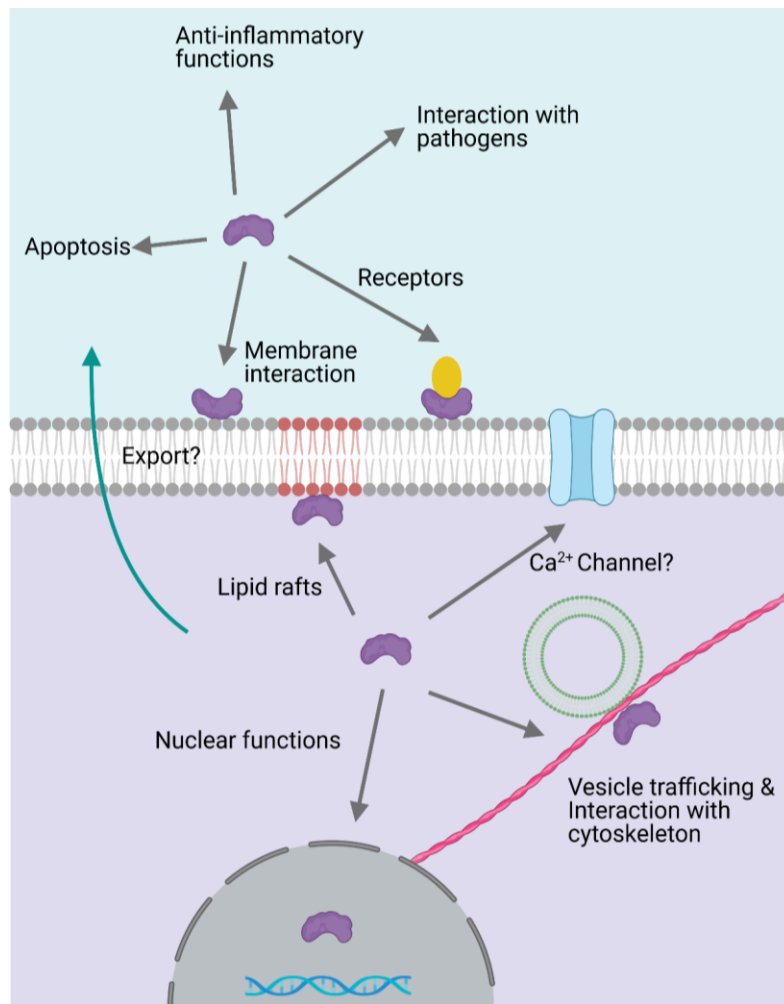


Figure 1.3: Schematic overview of intra- and extracellular functions of annexins.

Intracellular functions include interaction with membranes, interaction with the cytoskeleton, vesicle trafficking and others. Even though the secretion mechanism is not fully understood, several annexins can be found extracellularly. Extracellular functions include interacting with membranes, acting as receptors, regulation of apoptosis, anti-inflammatory functions and interaction with several pathogens. Figure was adapted from Lizarbe *et al.* (2013) and was created with Biorender.

Annexins are a superfamily of genes that can be found in more than 65 species, ranging from fungi to plants and higher vertebrates. They are mostly known for their Ca²⁺ and phospholipid binding abilities. The name annexin is derived from the Greek word *annex*, which means “to hold something together”. It describes the main function of annexins, binding biological structures together, in particular membranes. (Gerke & Moss, 2002)

All annexins are defined by two properties: they must be able to bind to phospholipids in a Ca²⁺ dependent manner and they all consist of a conserved structural element, the annexin repeat (70

amino acids). Four annexin repeats are packed into a highly α -helical, slightly curved disk, which forms the annexin core domain. The convex side of this disk faces the membrane and is therefore responsible for Ca^{2+} and phospholipid binding. The concave side, pointing away from the membrane, is available for interaction with other proteins or the variable N-terminal head domain. Annexins can also interact with other proteins through this N-terminal domain (e.g. annexin (Anx) A1 interaction with S100A11 (Mailliard *et al.*, 1996)). (Gerke & Moss, 2002, Rescher & Gerke, 2004)

In vertebrates, 12 members of the annexin family are known (AnxA1-11 and 13). These subfamilies differ in their N-terminal domains and position of the Ca^{2+} /membrane binding sites within the core domain. Annexins are proposed to have a multitude of functions, both intracellularly and extracellularly (Figure 1.3) (Rescher & Gerke, 2004). Some annexins are ubiquitously expressed throughout the human body (A1, A2, A4, A5, A6, A7, A11), but others can only be found in certain tissues or cell types (e.g., AnxA3 in neutrophils or AnxA9 in tongue tissue) (Moss & Morgan, 2004).

1.3.1 Intracellular functions

Annexins are mainly cytosolic proteins, and the best characterized function is their ability to bind membrane phospholipids in a Ca^{2+} dependent manner. They preferentially bind PS and PE, but some annexins may also interact with phosphoric acid, phosphatidylglycerol, phosphatidylinositol or other membrane lipids, as well as fatty acids, ceramides and lipid-derived metabolites (Bandorowicz-Pikula *et al.*, 2012, Lizarbe *et al.*, 2013)

In fact, fluorescently labelled AnxA5 is commonly known for its use in a laboratory setting as a marker for early apoptotic cells, binding to externalized PS, which subsequently can be detected by flow cytometry or microscopy (Vermes *et al.*, 1995).

Annexins are proposed to play a multitude of functions via their membrane binding abilities (Figure 1.3). For example, they promote membrane stabilization by formation of two-dimensional lattices. AnxA5 can form such lattices on the membrane bilayer and this may function to stabilize plasma membrane structures, changing membrane curvature and cell shape. In addition, some annexins (A1, A2, A4, A6 and A7) can link two membranes together in a Ca^{2+} dependent manner. (Gerke *et al.*, 2005, Lizarbe *et al.*, 2013)

Furthermore, annexins seem to interact with the cytoskeleton and play a role in vesicle trafficking. AnxA2 is found at the site of actin cytoskeleton interaction, where it organizes membrane lipids. Additionally, it was shown that AnxA2 is a component of the filamentous actin-rich comet tails.

These tails are involved in propelling newly formed endocytic vesicles from the plasma membrane to the cell interior. Annexins are also implicated to be involved in exocytosis, more precisely promoting membrane fusion. (Gerke *et al.*, 2005)

Further functions of annexins include promoting membrane repair, establishing membrane domains, involvement in cell signaling and regulating ion channels. They are also proposed to act as Ca²⁺ channels themselves, but the exact mechanism remains to be elucidated. For some annexins, nuclear functions are suggested, as they migrate to the nucleus. Still, their activity and function in the nucleus is not clear yet. (Gerke *et al.*, 2005, Lizarbe *et al.*, 2013)

Annexins can also interact with membranes in a Ca²⁺-independent, cholesterol mediated manner, playing a role in signaling events involving receptors localized in cholesterol and sphingomyelin-enriched membrane microdomains (Bandorowicz-Pikula *et al.*, 2012).

1.3.2 Extracellular functions

Even though it remains unclear, how annexins are secreted, AnxA1, A2, A4 and A5 can be found extracellularly. They all lack the signal peptide for the conventional secretion pathway, but two major pathways are currently proposed for annexin secretion: direct translocation across the plasma membrane or secretion via extracellular vesicles (EV) (Popa *et al.*, 2018). Direct translocation involves either insertion of annexins into the membrane, but there is scarce evidence for this occurring *in vivo*, or it is dependent on binding to phospholipids and lipid flipping activity, e.g. TMEM16F is a membrane phospholipid scramblase implicated in transporting AnxA2 and A5 across the plasma membrane (Stewart *et al.*, 2018). The other proposed annexin secretion pathway involves EVs, where annexins are commonly found. However, another mechanism proposes direct packaging of annexins into exosomes for secretion, but whether EVs actually release their contents still remains unclear. Furthermore, it has been proposed that transport of AnxA1 is mediated via an ABC transporter protein (Popa *et al.*, 2018).

Once in the extracellular space, annexins have a multitude of functions (Figure 1.3). One function is acting as receptors themselves, e.g. for serum proteases, regulators of cell migration and blood coagulation. AnxA2, for example, is a surface receptor for β 2-glycoprotein I (Popa *et al.*, 2018). In addition, AnxA2 is involved in fibrinolysis, as it can act as a co-receptor for plasminogen and tissue plasminogen activator, thus promoting formation of plasmin and degradation of fibrin (Lizarbe *et al.*, 2013).

AnxA5 has an anti-coagulant role by preventing formation of the prothrombinase complex by competing for PS binding on platelets. This function is based on the ability of AnxA5 to form two-

dimensional lattices on membranes, sequestering PS from procoagulant factors that use this phospholipid in the clotting cascade. Antiphospholipid syndrome, linked to recurring pregnancy loss and increased risk for thrombosis, is linked to AnxA5. In the serum of patients suffering from this syndrome, autoantibodies against phospholipid, β 2-glycoprotein-I and AnxA5 can be found. It is suggested, that antibodies against AnxA5 unmask the procoagulant surface of placental syncytiotrophoblasts and thus promote prothrombotic events resulting in fetal loss. (Gerke *et al.*, 2005, van Genderen *et al.*, 2008, Lizarbe *et al.*, 2013)

AnxA1 has anti-inflammatory functions, as it prevents transendothelial migration of leukocytes. Receptors for AnxA1 can be found on neutrophils and monocytes. These receptors belong to the formyl peptide receptor family of chemoattractant receptors (Rescher & Gerke, 2004). Binding of AnxA1 to this receptor induces detachment of adherent leukocytes from activated endothelium (Gavins *et al.*, 2003).

AnxA1 and AnxA2 can promote apoptosis by acting as bridging proteins to macrophages. AnxA5, on the other hand, inhibits phagocytosis most likely by shielding of externalized PS and promoting internalization of the PS-containing membrane domain, harboring additional apoptotic signals. In both cases, the ability of AnxA5 to form two-dimensional crystal structures at the plasma membrane may be involved. (van Genderen *et al.*, 2008)

1.3.3 Interaction with pathogens

Annexins are also known to interact with different pathogens. Many interactions are described between annexins and viruses (e.g. influenza A virus, herpes simplex virus type I), but for the purpose of this work, there will be a focus on annexin-bacteria interactions (Kuehnl *et al.*, 2016). Annexins can act as receptors for pathogens, for example, AnxA2 is a receptor on human endothelial cells for *Pseudomonas aeruginosa* (*P. aeruginosa*), a pathogen critical for patients with cystic fibrosis, sepsis or with an immunocompromised status. Whether binding of *P. aeruginosa* to AnxA2 results in direct signal transmission or AnxA2 only acts as an anchoring protein, remains to be elucidated (Kirschnek *et al.*, 2005).

In addition, AnxA2 is proposed to act as a receptor for *Mycoplasma pneumoniae*, the community-acquired respiratory distress syndrome toxin of this pathogen binds to cell surface-associated AnxA2 (Somarajan *et al.*, 2014). Also, in a *Mycoplasma hyorhinis* infection, the bacterial protein p37 interacts with AnxA2 of their host cell and a synthetic N-terminal AnxA2 polypeptide is able to decrease infection of gastric cancer cells with this bacterium (Duan *et al.*, 2014, Yuan *et al.*, 2016).

On another note, interaction of pathogens with annexins also has the purpose of cytoskeleton rearrangement (Kuehnl *et al.*, 2016). One example for such a rearrangement is the facultative intracellular pathogen *Salmonella enterica* serovar Typhimurium, which recruits AnxA2 through its effector protein SopB, delivered by its type 3 secretion system into the host cell, where dynamic actin-driven ruffling of the membrane takes place, resulting in internalization of the bacterium into a modified phagosome (Jolly *et al.*, 2014).

Other examples for cytoskeleton rearrangement by bacteria are enteropathogenic *Escherichia coli* (EPEC) and enterohemorrhagic *E. coli* (EHEC) that both cause formation of filamentous actin-rich pedestals at their site of attachment and AnxA2 is specifically recruited to those protrusions (Zobiack *et al.*, 2002, Miyahara *et al.*, 2009). The EHEC effector protein EspL2 interacts directly with AnxA2, resulting in increased activity of AnxA2 to aggregate Tir-induced F-actin and thus promoting invasion of the bacteria (Miyahara *et al.*, 2009).

Other functions of AnxA2 include protective roles, *e.g.* in *Klebsiella pneumoniae* in mice, where AnxA2 seems to reduce infection associated inflammation. In addition, in a murine model of a *Cryptococcal* infection, mice lacking AnxA2 showed lower survival rates. (Dallacasagrande & Hajjar, 2020)

AnxA5 is also able to interact directly with bacteria. It was shown previously that AnxA5 binds to Gram-negative bacteria, such as *P. aeruginosa*, *Shewanella putrefaciens* and *H. influenzae* in a Ca²⁺ dependent manner. As the binding site for *P. aeruginosa*, the lipid A part of LPS was identified. This interaction is proposed to play a role in modulating the host response against LPS (Rand *et al.*, 2012). Recently, an interaction between AnxA5, as well as AnxA1 and A2, and *H. pylori* has been shown (Petri, 2020).

1.4 Objectives

The first aim of this thesis is the investigation of the impact of the HopQ-CEACAM interaction on CagA translocation. As pointed out before, HopQ is the only known non-*cagPAI* encoded co-factor of CagA translocation, but the mechanism of CagA delivery into the host cell is still unknown. To address this issue, several hypotheses should be tested in this thesis: CEACAM1, in contrast to CEACAM5 and 6, has a transmembrane domain and a cytoplasmic tail with ITIM domains. Therefore, it will be tested if the signaling cascades activated by ITIM could have an impact on CagA translocation. Next, as Mongolian gerbils develop more severe pathologies upon *H. pylori* infection, the interaction of HopQ with gerbil CEACAM1 will be analyzed. Third, since the structure of the HopQ-CEACAM1 complex was solved, the influence of targeted mutations in HopQ on CagA translocation will be investigated. Lastly, the interaction of HopQ with the Cag-T4SS will be examined.

As deletion of HopQ results in a 50 % reduction of CagA translocation in AGS cells, another unknown putative receptor-adhesin pair(s) responsible for the residual 50 % should be elucidated. For this, several further adhesins of the putative adhesin branch of OMPs should be deleted and their influence on CagA translocation as well as adhesion will be tested. To address strain-specific differences, this will be performed in different *H. pylori* strains.

Another objective of this thesis is the investigation of the mechanism of CagA internalization into the host cell. It has already been reported that PS is externalized upon contact with *H. pylori* and CagA binds to these phospholipids. As PS is usually only found on the inner leaflet of the membrane, externalization requires an enzyme, e.g., a scramblase. Therefore, the influence of human phospholipid scramblase 1 (PLSCR1) on CagA translocation will be tested.

Annexins are proteins binding to PS in a Ca²⁺ dependent manner. Due to the known interaction of CagA with PS, annexins were investigated further in the context of an *H. pylori* infection. In these studies, *H. pylori* was found to interact with AnxA5. In this work, this interaction will be characterized further.

Chapter 2: Material and Methods

2.1. Materials

2.1.1 Cell lines

Table 2.1: Cell lines used in this work

Cell line	Description	Reference
AGS	Human adenocarcinoma cell line ATCC CRL-1739	(Barranco <i>et al.</i> , 1983)
AGS [LgBiT]	Human adenocarcinoma cell line, stably transfected with HaloTag-LgBiT	(Lettl <i>et al.</i> , 2021)
Kat0III	Human gastric carcinoma cell line ATCC HTB-103	(Sekiguchi <i>et al.</i> , 1978)
ITGB1 KO Kat0III	Kat0III cell line carrying a deletion in the integrin β 1 gene	(Zhao <i>et al.</i> , 2018)
ITGAvB1B4 KO Kat0III	Kat0III cell line carrying deletions in integrin α v, β 1 and β 4 genes	(Zhao <i>et al.</i> , 2018)
HEK293	Human embryonic kidney cell line ATCC CRL-1573	(Graham <i>et al.</i> , 1977)
HEK293 CEACAM1	Human embryonic kidney cell line, stably transfected with CEACAM1	(Königer <i>et al.</i> , 2016)
293FT	Clonal derivates of 293T cell line	(Javanbakht <i>et al.</i> , 2003)
3BF3 E6	AGS cell with a deletion of <i>p/scr1</i>	This work
1-A8; 1-D2; 2-B3	<i>AGSΔp/scr1::egfp-p/scr1</i>	This work
HEK-Blue hTLR4	HEK293 cells expressing human TLR4, MD-2 and CD14 and an inducible SEAP reporter gene	Invivogen (hkb-htlr4)

2.1.2 Bacterial Strains

2.1.1.1. *E. coli*

Table 2.2: *E. coli* strains used in this work

Strain	Properties	Reference
Top10	F ⁻ <i>mcrA</i> , $\Delta(mrr-hsdRMS-mcrBC)$, $\Phi80lacZ\Delta M15$, $\Delta lacX74$, <i>recA1</i> , <i>ara</i> Δ 139, $\Delta(ara-leu)$ 7697, <i>galU</i> , <i>galK</i> , <i>rpsL</i> (Str ^R), <i>endA1</i> , <i>nupG</i> (Invitrogen, Karlsruhe)	(Grant <i>et al.</i> , 1990)
OneShot	F ⁻ <i>mcrB mrr hsdS20</i> (rB ⁻ , mB ⁻) <i>recA13 supE44 ara14 galK2</i>	Invitrogen
Stbl3	<i>lacY1 proA2 rpsL20</i> (Str ^R) <i>xyl5 λ-leu mtl1</i>	

2.1.1.2. *H. pylori*

Table 2.3: List of *H. pylori* strains

Strain	Internal ID	Properties	Reference
P12	WSP12	Wildtype, clinical isolate 888-0 (University of Hamburg, Germany)	(Schmitt & Haas, 1994)
G27	BAS-P290	Wildtype, clinical isolate (Grosseto Hospital, Italy)	(Baltrus <i>et al.</i> , 2009)
26695	BAS-P270	Wild-type, clinical isolate	(Tomb <i>et al.</i> , 1997)
P217	BAS-P269	Wildtype	(Jiménez- Soto <i>et al.</i> , 2009)
P145	BAS-P271	Wildtype	(Jiménez- Soto <i>et al.</i> , 2009)
X47	BAS-P273	Wildtype	(Kleanthous <i>et al.</i> , 2001)
Tx30a	BAS-P274	Wildtype, clinical isolate (USA, Texas)	(Atherton <i>et al.</i> , 1995)
P12ΔcagH	WSP696	P12 transformed with pWS423; Strep ^R , Erm ^R	W. Fischer
P12ΔhopQ	VKH80	P12 transformed with pVK13; Strep ^R	(Königer <i>et al.</i> , 2016)
P12ΔhopQ::<i>hopQ</i>	WSP1233	P12(pVK13) transformed with pWS658; Strep ^R , Cm ^R	W. Fischer

P12ΔhopQ::hopQ^{L150A}	WSP1240	P12(pVK13) transformed with pDAB341; Strep ^R , Cm ^R	W. Fischer
P12ΔhopQ::hopQ^{T390A}	WSP1241	P12(pVK13) transformed with pDAB344; Strep ^R , Cm ^R	W. Fischer
P12ΔhopQ::hopQ^{Δ155-156Δ161-162}	WSP1242	P12(pVK13) transformed with pDAB360; Strep ^R , Cm ^R	W. Fischer
P12ΔhopQ::hopQ^{β2-α4:BabA}	WSP1243	P12(pVK13) transformed with pDAB361; Strep ^R , Cm ^R	W. Fischer
P12[TEM-CagA]	RNP3	P12 expressing TEM1-CagA, marker-free, Strep ^R	(Schindele <i>et al.</i> , 2016)
P12[TEM-CagA]ΔcagT	WSP1172	P12[TEM-CagA] transformed with pJP95, Cm ^R	(Bonsor <i>et al.</i> , 2018)
P12[TEM-CagA]ΔhopQ	WSP1229	P12[TEM-CagA] transformed with pFS10, Erm ^R	(Bonsor <i>et al.</i> , 2018)
P12[TEM-CagA]ΔhopQ::hopQ	WSP1232	P12[TEM-CagA](pFS10) transformed with pWS658, Erm ^R , Cm ^R	(Bonsor <i>et al.</i> , 2018)
P12[TEM-CagA]ΔhopQ::hopQ^{L150A}	WSP1236	P12[TEM-CagA](pFS10) transformed with pDAP341, Erm ^R , Cm ^R	(Bonsor <i>et al.</i> , 2018)
P12[TEM-CagA]ΔhopQ::hopQ^{T390A}	WSP1237	P12[TEM-CagA](pFS10) transformed with pDAP344, Erm ^R , Cm ^R	(Bonsor <i>et al.</i> , 2018)
P12[TEM-CagA]ΔhopQ::hopQ^{Δ155-156Δ161-162}	WSP1238	P12[TEM-CagA](pFS10) transformed with pDAP360, Erm ^R , Cm ^R	(Bonsor <i>et al.</i> , 2018)
P12[TEM-CagA]ΔhopQ::hopQ^{β2-α4:BabA}	WSP1239	P12[TEM-CagA](pFS10) transformed with pDAP361, Erm ^R , Cm ^R	(Bonsor <i>et al.</i> , 2018)
P12[TEM-CagA]ΔhopQ	BAS-P138	P12[TEM-CagA] transformed with pVK13, Strep ^R	This work
P12[TEM-CagA]ΔbabC	BAS-P404	P12[TEM-CagA](pLH7) transformed with pLH8, Strep ^R	This work
P12[TEM-CagA]ΔhopQΔbabC	BAS-P333	P12[TEM-CagA](pVK13) transformed with pLH7, Erm ^R	This work
P12[TEM-CagA]ΔbabCΔbabB	BAS-P411	P12[TEM-CagA](pLH7, pLH8) transformed with pLH5, Erm ^R	This work

P12 HopQ^{myc}	BAS-P077	P12(pVK13) transformed with pBAS48, expression of HopQ ^{myc} (after aa 38) under <i>alpA</i> promoter, Strep ^R , Cm ^R	This work
P12 HopQ^{myc} ΔcagY::rpsLerm	BAS-P186	P12(pVK13, pBAS48) transformed with pKG11, Strep ^R , Cm ^R , Erm ^R	This work
P12 CagY^{ΔMMR::myc}	LJH199	P12 deletion of CagY MMR transformed with pKG5-5-3	K. Gramlich, AG Haas
P12 CagY^{S1MC1}		P12(pBlu_cagY-RCAT) transformed with pCR_cagY-MC1, Strep ^R	A. Debowski, AG Haas
P12 CagY^{S1MC2}		P12(pBlu_cagY-RCAT) transformed with pCR_cagY-MC2, Strep ^R	A. Debowski, AG Haas
P12ΔbabA	VKH77	P12(pLH3) transformed with pLH4, Strep ^R	(Königer <i>et al.</i> , 2016)
P12ΔoipA	VKH83	P12 transformed with pVK15, Strep ^R	V. Königer, AG Haas
P12ΔhopA::rpsLerm	BAS-P057	P12 transformed with pBAS2, Erm ^R	This work
P12ΔhopN	BAS-P081	P12(pBAS6) transformed with pBAS5, Strep ^R	This work
P12ΔhopM::rpsLerm	BAS-P089	P12 transformed with pBAS4, Erm ^R	This work
P12ΔhopNΔhopM	BAS-P114	P12(pBAS5, pBAS4) transformed with pBAS3, Strep ^R	This work
P12ΔhopNΔhopMΔhopQ	BAS-P124	P12(pBAS5, pBAS4, pBAS3) transformed with pVK13, Strep ^R	This work
P12ΔhopNΔhopMΔhopQ ΔoipA	BAS-P148	P12(pBAS5, pBAS4, pBAS3, pVK13) transformed with pVK15, Strep ^R	This work
P12ΔhopNΔhopMΔhopQ ΔoipAΔbabA	BAS-P148	P12(pBAS5, pBAS4, pBAS3, pVK13, pVK15, pLH3) transformed with pLH4, Strep ^R	This work
P12[TEM-CagA]ΔoipA	BAS-P156	P12[TEM-CagA] transformed with pVK15, Strep ^R	This work
P12[TEM-CagA] ΔhopA	BAS-P067	P12[TEM-CagA](pBAS2) transformed with pBAS1, Strep ^R	This work
P12[TEM-CagA]ΔhopN	BAS-P085	P12[TEM-CagA] (pBAS6) transformed with pBAS5, Strep ^R	This work
P12[TEM-CagA] ΔhopM::rpsLerm	BAS-P093	P12[TEM-CagA] transformed with pBAS4, Erm ^R	This work

P12[TEM-CagA] <i>ΔhopNΔhopM</i>	BAS-P118	P12[TEM-CagA] (pBAS5, pBAS4) transformed with pBAS3, Strep ^R	This work
P12[TEM-CagA] <i>ΔhopNΔhopMΔhopQ</i>	BAS-P127	P12[TEM-CagA] (pBAS5, pBAS4, pBAS3) transformed with pVK13, Strep ^R	This work
P12[TEM-CagA] <i>ΔhopNΔhopMΔhopQ ΔoipA</i>	BAS-P152	P12[TEM-CagA] (pBAS5, pBAS4, pBAS3, pVK13) transformed with pVK15, Strep ^R	This work
P12[TEM-CagA] <i>ΔhopNΔhopMΔhopQ ΔoipAΔbabA</i>	BAS-P167	P12[TEM-CagA] (pBAS5, pBAS4, pBAS3, pVK13, pVK15, pLH3) transformed with pLH4, Strep ^R	This work
P12 GFP	BAS-P104	P12 transformed with pCH7c, Cm ^R	This work
P12<i>ΔhopQ</i> GFP	BAS-P109	P12(pVK13) transformed with pCH7c, Cm ^R , Strep ^R	This work
P12<i>ΔhopA</i> GFP	BAS-P311	P12(pBAS2, pBAS1) transformed with pCH7c, Cm ^R , Strep ^R	This work
P12<i>ΔhopN</i> GFP	BAS-P112	P12(pBAS6, pBAS5) transformed with pCH7c, Cm ^R , Strep ^R	This work
P12<i>ΔhopM</i> GFP	BAS-P122	P12(pBAS4) transformed with pCH7c, Cm ^R , Erm ^R	This work
P12<i>ΔhopNΔhopM</i> GFP	BAS-P144	P12(pBAS6, pBAS5, pBAS4, pBAS3) transformed with pCH7c, Cm ^R , Strep ^R	This work
P12<i>ΔhopNΔhopMΔhopQ</i> GFP	BAS-P144	P12(pBAS6, pBAS5, pBAS4, pBAS3, pVK13) transformed with pCH7c, Cm ^R , Strep ^R	This work
G27[TEM-CagA]	WSP1471	G27 expressing TEM1-CagA, marker-free, Strep ^R	W. Fischer
G27[TEM-CagA]<i>ΔcagT</i>	WSP1499	G27[TEM-CagA] transformed with pJP95, Strep ^R , Cm ^R	W. Fischer
G27[TEM-CagA]<i>ΔhopA</i>	BAS-P396	G27[TEM-CagA] transformed with pBAS2, Erm ^R	This work
G27[TEM-CagA]<i>ΔhopM</i>	BAS-P398	G27[TEM-CagA] transformed with pBAS4, Erm ^R	This work
G27[TEM-CagA]<i>ΔhopN</i>	BAS-P400	G27[TEM-CagA] transformed with pBAS6, Erm ^R	This work

P12ΔalpAB	BAS-P235	P12(pBAS8) transformed with pBAS7, Strep ^R	This work
P12ΔalpAB::alpAB	BAS-P297	P12(pBAS8) transformed with gDNA of BASP-250, Erm ^R , Cm ^R	This work
P12[TEM-CagA]ΔalpAB	BAS-P232	P12[TEM-CagA](pBAS8) transformed with pBAS7, Strep ^R	This work
P12[TEM-CagA]ΔalpAB::alpAB	BAS-P250	P12[TEM-CagA](pBAS8, pBAS7) transformed with pBAS75, Strep ^R , Cm ^R	This work
P12[TEM-CagA]ΔalpABΔhopQ	BAS-P238	P12[TEM-CagA](pBAS8, pBAS7) transformed with pVK13, Strep ^R	This work
G27[TEM-CagA]ΔalpAB	BAS-P268	G27[TEM-CagA] transformed with pBAS8, Erm ^R	This work
G27[TEM-CagA]ΔhopQ	BAS-P286	G27[TEM-CagA] transformed with pVK13, Strep ^R	This work
G27[TEM-CagA]ΔalpAB::alpAB	BAS-P289	G27[TEM-CagA](pBAS8) transformed with PCR product of BAS16/125, Strep ^R	This work
G27[TEM-CagA] GFP	BAS-P318	G27[TEM-CagA] transformed with pCH7c, expressing GFP, Strep ^R , Cm ^R	This work
G27[TEM-CagA]ΔalpAB GFP	BAS-P320	G27[TEM-CagA](pBAS8) transformed with pCH7c, expressing GFP, Erm ^R , Cm ^R	This work
G27[TEM-CagA]ΔhopQ GFP	BAS-P322	G27[TEM-CagA](pVK13) transformed with pCH7c, expressing GFP, Strep ^R , Cm ^R	This work
G27[TEM-CagA]ΔalpAB::alpAB GFP	BAS-P324	G27[TEM-CagA](pBAS8, gDNA BAS-P250) transformed with pCH7c, expressing GFP, Strep ^R , Cm ^R	This work
G27ΔwaaL	BAS-P292	G27 with deletion of <i>waaL</i> gene	(Li <i>et al.</i> , 2017)
G27Δhp1284	RHP297	G27 with deletion of <i>hp1284</i> gene	(Li <i>et al.</i> , 2017)
G27Δhp0805	RHP298	G27 with deletion of <i>hp0805</i> gene	(Li <i>et al.</i> , 2019)
G27ΔrfaE	BAS-P313	G27 transformed with pCL1, Cm ^R	This work

P12[TEM-CagA]ΔrfaE	CLH35	P12[TEM-CagA] transformed with pCL1, Strep ^R , Cm ^R	C. Lettl, AG Haas
26695ΔrfaE	BAS-P316	26695 transformed with pCL1, Cm ^R	This work
26695Δhp1284	RHP291	26695 with deletion of <i>hp1284</i> gene	(Li <i>et al.</i> , 2017)
P12ΔlpxF	BAS-P361	P12 transformed with pBAS102, Cm ^R	This work
P12ΔeptA	BAS-P363	P12 transformed with pBAS103, Cm ^R	This work
P12ΔlpxE	BAS-P376	P12 transformed with pBAS101, Erm ^R	This work
P12ΔlpxE/F	BAS-P377	P12(pBAS103) transformed with pBAS101, Cm ^R , Erm ^R	This work
26695ΔlpxF	BAS-P365	26695 transformed with pBAS102, Cm ^R	This work
26695ΔeptA	BAS-P367	26695 transformed with pBAS103, Cm ^R	This work
26695ΔlpxE	BAS-P379	26695 transformed with pBAS101, Erm ^R	This work
26695ΔlpxE/F	BAS-P381	26695 (pBAS103) transformed with pBAS101, Cm ^R , Erm ^R	This work
G27ΔlpxF	BAS-P369	G27 transformed with pBAS102, Cm ^R	This work
G27ΔeptA	BAS-P371	G27 transformed with pBAS103, Cm ^R	This work
G27ΔlpxE	BAS-P383	G27 transformed with pBAS101, Erm ^R	This work
G27ΔlpxE/F	BAS-P385	G27 (pBAS103) transformed with pBAS101, Cm ^R , Erm ^R	This work
PMSS1-RFP	PP-35	PMSS1 strain expressing RFP, able to infect mice, Kan ^R	(Arnold <i>et al.</i> , 2018)
PMSS1-RFP isolated	SN-56	PMSS1-RFP re-isolated from CEACAM _{all} mice after 3 weeks of infection, Kan ^R	S. Namineni, AG Haas
P12[HiBiT-CagA]	CLH41	P12 expressing HiBiT-CagA, Strep ^R	(Lettl <i>et al.</i> , 2021)
P12[HiBiT-CagA]ΔcagT	CLH42	P12[HiBiT-CagA] transformed with pJP95, Strep ^R , Cm ^R	(Lettl <i>et al.</i> , 2021)
P12[HiBiT-CagA]ΔrfaE	BAS-P373	P12[HiBiT-CagA] transformed with pCL1, Strep ^R , Cm ^R	This work
P12ΔcagPAI	BAS-P413	P12 transformed with pJP46, Kan ^R	This work

P12ΔlpxE/FΔcagPAI	BAS-P415	P12(pBAS103, pBAS101) transformed with pJP46, Cm ^R , Erm ^R , Kan ^R	This work
G27ΔcagPAI	BAS-P417	G27 transformed with pJP46, Kan ^R	This work
G27ΔlpxE/FΔcagPAI	BAS-P419	G27 (pBAS103, pBAS101) transformed with pJP46, Cm ^R , Erm ^R , Kan ^R	This work

2.1.3 Plasmids

Table 2.4: Plasmids used in this work

Name	Backbone	Properties	Reference
pBAS1	pBluescriptSK	up- and downstream flanking regions of P12 hopA without rpsLerm cassette	This work
pBAS2	pBluescriptSK	up- and downstream flanking regions of P12 hopA with rpsLerm cassette	This work
pBAS3	pBluescriptSK	up- and downstream flanking regions of P12 hopM without rpsLerm cassette	This work
pBAS4	pBluescriptSK	up- and downstream flanking regions of P12 hopM with rpsLerm cassette	This work
pBAS5	pBluescriptSK	up- and downstream flanking regions of P12 hopN without rpsLerm cassette	This work
pBAS6	pBluescriptSK	up- and downstream flanking regions of P12 hopN with rpsLerm cassette	This work
pBAS7	pBluescriptSK	up- and downstream flanking regions of P12 alpAB without rpsLerm cassette	This work
pBAS8	pBluescriptSK	up- and downstream flanking regions of P12 alpAB with rpsLerm cassette	This work
pBAS48	pHel12	HopQ ^{Myc} complementation plasmid	This work
pBAS53	PX462	sgRNA for PLSCR1 Exon 1.1 Guide A	This work
pBAS54	PX462	sgRNA for PLSCR1 Exon 1.1 Guide B	This work
pBAS55	PX462	sgRNA for PLSCR1 Exon 1.2 Guide A	This work
pBAS56	PX462	sgRNA for PLSCR1 Exon 1.2 Guide B	This work

pBAS57	PX462	sgRNA for PLSCR1 Exon 4.1 Guide A	This work
pBAS58	PX462	sgRNA for PLSCR1 Exon 4.1 Guide B	This work
pBAS59	PX462	sgRNA for PLSCR1 Exon 4.2 Guide A	This work
pBAS60	PX462	sgRNA for PLSCR1 Exon 4.2 Guide B	This work
pBAS75	pHel12	Complementation of P12 <i>alpAB</i>	This work
pBAS91	pEGFP-C1	Complementation of EGFP-PLSCR1	This work
pBAS101	pSMART-hcKan	up- and downstream region of HPP12_0019 with rpsLerm cassette	This work
pBAS102	pSMART-hcKan	up- and downstream region of HPP12_1571 with cat cassette	This work
pBAS103	pSMART-hcKan	up- and downstream region of HPP12_0020 with cat cassette	This work
pVK13	pUC19	up- and downstream flanking regions of <i>hopQ</i> with dif-rpsLcat-dif cassette	(Königer <i>et al.</i> , 2016)
pWS658	pHel12	Complementation of <i>hopQ</i> under control of <i>alpA</i> promoter	(Bonsor <i>et al.</i> , 2018)
pDAP341	pHel12	Complementation of HopQ ^{L150A} under control of <i>alpA</i> promoter	(Bonsor <i>et al.</i> , 2018)
pDAP344	pHel12	Complementation of HopQ ^{T370A} under control of <i>alpA</i> promoter	(Bonsor <i>et al.</i> , 2018)
pDAP360	pHel12	Complementation of HopQ ^{Δ135-136Δ141-142} under control of <i>alpA</i> promoter	(Bonsor <i>et al.</i> , 2018)
pDAP361	pHel12	Complementation of HopQ ^{β2-α4:BabA} under control of <i>alpA</i> promoter	(Bonsor <i>et al.</i> , 2018)
pLH7	pBluescript	up- and downstream flanking region of <i>babC</i> with rpsLerm cassette	(Königer <i>et al.</i> , 2016)
pLH8	pBluescript	up- and downstream flanking region of <i>babC</i>	(Königer <i>et al.</i> , 2016)
pKG11	pBluescript KS	up- and downstream flanking region of <i>cagY</i> with rpsLerm cassette	K. Gramlich, AG Haas
pLH3	pBluescript	up- and downstream flanking region of <i>babA</i> with rpsLerm cassette	(Königer <i>et al.</i> , 2016)
pLH4	pBluescript	up- and downstream flanking region of <i>babA</i>	(Königer <i>et al.</i> , 2016)
pLH5	pBluescript	up- and downstream flanking region of <i>babB</i> with rpsLerm cassette	(Königer <i>et al.</i> , 2016)
pVK15	pBluescript	up- and downstream flanking region of <i>oipA</i>	V. Königer, AG Haas
pCH7c	pBluescript	GFP expression plasmid in <i>H. pylori</i>	C. Höfler, AG Haas
pCL1	pSMART-hcKan	up- and downstream region of <i>rfaE</i> with cat cassette	C. Lettl, AG Haas

pJP46	pBluescript	Deletion of <i>cagPAI</i> , <i>aphA3</i> cassette	(Odenbreit <i>et al.</i> , 2001)
pVSV-G		Envelope protein for production of lentiviral particles	B. Busch, AG Haas
pCMVΔ8.9		Packaging plasmid for lentiviral transfection	B. Busch, AG Haas
pLL3.7 GFP	pLL3.7	Expression of GFP for lentiviral transfection	C. Hauck, University Konstanz
pLL3.7 CC1-4L wt GFP	pLL3.7	Expression of full length CEACAM1 for lentiviral transfection	C. Hauck, University Konstanz
pLL3.7CC1ΔCT	pLL3.7	Expression of CEACAM1ΔCT for lentiviral transfection	C. Hauck, University Konstanz

2.1.4 Primers

Table 2.5: List of primers

Name	Sequence	Comment
BAS3	agggataccCAACGAGTGTAGCTTTTTAATTC	fwd, upstream <i>hopN</i> (P12), <i>KpnI</i>
BAS4	agggatcccTTTTTGATTTTCATGTTTTCTCC	rev, upstream <i>hopN</i> (P12), <i>BamHI</i>
BAS5	taggatcccGTGTTTGCTTACTAGGTGGCGC	fwd, downstream <i>hopN</i> (P12) <i>BamHI</i>
BAS15	tagagctcCTCTTTCTACACCGCATGGC	rev, downstream <i>hopN</i> (P12) <i>SacI</i>
BAS7	ttggtaccTTTATGCACCTTCTCATTAGCC	fwd, upstream <i>hopM</i> (P12), <i>KpnI</i>
BAS8	tgggatcccGTGTTTGCTTACTAAAACCCCTC	rev, upstream <i>hopM</i> (P12), <i>BamHI</i>
BAS9	caggatcccGATTTTCATGTTTTCTCCTTTTG	fwd, downstream <i>hopM</i> (P12) <i>BamHI</i>
BAS10	cgtctagaTAAGCTTTCTATCGTGCCTACTAG	rev, downstream <i>hopM</i> (P12) <i>XbaI</i>
BAS11	tcggtaccTTATTTACCTCTTTCTTTAATCAC	fwd, upstream <i>hopA</i> (P12), <i>KpnI</i>
BAS12	ctggatcccGGCCTATTGATATTGAATCGG	rev, upstream <i>hopA</i> (P12), <i>BamHI</i>
BAS13	ccggatcccTTTCATAAAATGTTCCTTAAAG	fwd, downstream <i>hopA</i> (P12) <i>BamHI</i>
BAS14	gccgtctagaCCCCTATTTTGGCTTACAAAG	rev, downstream <i>hopA</i> (P12) <i>XbaI</i>
BAS16	agggataccAAGGGCTAAGGAAAATTTATGGCTTTC	fwd, upstream <i>alpAB</i> (P12), <i>KpnI</i>
BAS17	agggatcccTTTCTTTATCATGATTTTCCTTATCAATG GGATGC	rev, upstream <i>alpAB</i> (P12), <i>BamHI</i>
BAS18	taggatcccGCCTTCTAAAAAGCTCAAGGCC	fwd, downstream <i>alpAB</i> (P12) <i>BamHI</i>
BAS125	cgtctagaTTTTAATCAAGTGGTAGCGTTAAGATTAC	rev, downstream <i>alpAB</i> (P12) <i>XbaI</i>
BAS60	agactagtgaacaaaaattaatttcagaagaagattt aAAGGTGCAAAAACCTTCAGACACTTATG	fwd, HopQ ^{myc} complementation, c-myc-tag, <i>SpeI</i>
BAS61	gaactagtGTCGGCGTTTTTCACTTTTTGAAC	rev, HopQ ^{myc} complementation, <i>SpeI</i>
BAS62	ATCTCAATCAAGGAGCATCCC	sequencing pBAS48 (HopQ ^{myc})
BAS105	GACAAACGTCTCTGGAGTCTCTC	fwd, amplification and sequencing of <i>plscr1</i> knockout locus, exon 4

BAS106	AGTTCCCGCGCCCAAGTC	rev, amplification and sequencing of <i>plscr1</i> knockout locus, exon 4
BAS107	ACATAGAGGTGATTATGATTTTCGTC	fwd, amplification and sequencing of <i>plscr1</i> knockout locus, exon 4
BAS108	GGGCAGAAATTCTTGCTGAAC	rev, amplification and sequencing of <i>plscr1</i> knockout locus, exon 4
BAS140	atgtcgacATGATAAAGAAAAATGGAACGCTG	fwd, complementation of <i>alpAB</i> , <i>Sall</i>
BAS141	atagatctTTAGAAGGCGTAGCCATAGACC	rev, complementation of <i>alpAB</i> , <i>BglII</i>
BAS170	GGGAAGAAAAGGAATATCGG	sequencing of pBAS75
BAS171	TAAAGGGTTCAATCAAAGCC	sequencing of pBAS75
BAS191	ATGTCGACATGAATGCTTCTCACCCGG	cloning of <i>plscr1</i> (RC207485) in pEGFP_N1; <i>SacI</i>
BAS192	ATGGATCCTTAAACCTTATCGTCGTCATCCTTG	cloning of <i>plscr1</i> (RC207485) in pEGFP_N1; <i>BamHI</i>
BAS201	TAGGATCCAACTTAATTAATAAAAACTTAATTAAGC TTTAATTC	knockout of <i>lpxE</i> (HP0021) in P12, <i>BamHI</i>
BAS202	TAGTCGACTAATTTTTTCATGAGTGTTATTTTACTCT TTTTTG	knockout of <i>lpxE</i> (HP0021) in P12, <i>Sall</i>
BAS203	TAGGATCCTATCAATGGTAAAGGGATAAAGTGC	knockout of <i>lpxF</i> (HP1580) in P12, <i>BamHI</i>
BAS204	TAGTCGACTCATTGAAACGCTCGCTTTTC	knockout of <i>lpxF</i> (HP1580) in P12, <i>Sall</i>
BAS205	TAGGATCCCACAAAAAGAGTAAATAACACTCATG	knockout of <i>eptA</i> (HP0022) in P12, <i>BamHI</i>
BAS206	TAGTCGACGAATAATGATGCCAAACACGC	knockout of <i>eptA</i> (HP0022) in P12, <i>Sall</i>
BAS207	TAGAGCCTGGTGAAGCCATAG	fwd, confirmation of <i>lpxE/eptA</i> deletion (P12)
BAS208	GCAATTCTTTGGGAAAAACAAACG	rev, confirmation of <i>lpxE/eptA</i> deletion (P12)
BAS209	GACCTGTTGGGTGAAAGAGC	fwd, confirmation of <i>lpxF</i> deletion (P12)
BAS210	CAATATTCAATCCAAAACGCATGG	rev, confirmation of <i>lpxF</i> deletion (P12)
BAS211	GCAATTCTTTGGGAAAAGAAATG	rev, confirmation of <i>lpxE/eptA</i> deletion (G27)
CL23	ACAATCAAAGCCATATCGCT	confirmation of <i>rfaE</i> deletion
CL24	CCGCTGTTTCTGATACGACCA	confirmation of <i>rfaE</i> deletion
UB110	AACGATGAAGCTTCTAGCTTGCTA	gDNA contamination for RNA purification
UB111	GTGCTTATTCSTNAGATACCGTCAT	gDNA contamination for RNA purification
LH3	gatcctcgagGTAGTTGGTTTTAAGCGGTTG	confirmation of <i>babA</i> deletion

LH6	gatcccgcggTATCGTTACAAGCGCATTTG	conformation of <i>babA</i> deletion
LH7	gatcctcgagATGCCGGCATTAGTAAAAAG	conformation of <i>babB</i> deletion
LH10	gatccgcggccgcGAGAGAGTAAAAGGGTTTTTC	conformation of <i>babB</i> deletion
VK23	GATCCTCGAGTTAACGGGCTTAAGAATTGG	conformation of <i>babC</i> deletion
VK26	GATCCCGCGGTTGAAACTAAGGAGAATGC	conformation of <i>babC</i> deletion
VK70	GATCGGTACCCATGTATTGGGTTTTTTTTGC	conformation of <i>oipA</i> deletion
VK73	GATCCCGCGGAAGCGTTTGAGGTTAAATCG	conformation of <i>oipA</i> deletion
CE82	TGGTGATAAAGGTCGTTAAACCCGC	conformation of <i>hopQ</i> deletion
CE83	CGGCGATGGAATAAATACTAAGGC	conformation of <i>hopQ</i> deletion
m13for	TGTAAAACGACGGCCAGT	Sequencing of pBluescript
m13rev	CAGGAAACAGCTATGACC	Sequencing of pBluescript
EGFP_ FP	TTTAGTGAACCGTCAGATC	Sequencing of pEGFP-C1
EGFP_ RP	TTTAAAGCAAGTAAACCT	Sequencing of pEGFP-C1
EGFP_ C2_FP	GATCACATGGTCCTGCTG	Sequencing of pEGFP-C1
HP519	GCTTGCTTGTATTGGCCTTG	conformation of <i>cagPAI</i> deletion
HP549	GCATGCACATTCCCTAAAGTG	conformation of <i>cagPAI</i> deletion

2.1.5 Guide RNAs

Table 2.6: List of gRNAs for CRISPR/Cas9

Name	Sequence	Comment
BAS87	CACCGAGAGAGCCGGGGCCAGGCGA	PLSCR1 Exon 1, top oligo
BAS88	AAACTCGCCTGGCCCCGGCTCTCTC	PLSCR1 Exon 1, bottom oligo
BAS89	CACCGACCTTGTCTCGCTCGGGAG	PLSCR1 Exon 1, top oligo
BAS90	AAACCTCCCAGAGCGAGACAAGGTCC	PLSCR1 Exon 1, bottom oligo
BAS91	CACCGAGGTCCAGAGAGCCGGGGCC	PLSCR1 Exon 1, top oligo
BAS92	AAACGGCCCCGGCTCTCTGGACCTC	PLSCR1 Exon 1, bottom oligo
BAS93	CACCGTCGCTCGGGAGCGGAAACAG	PLSCR1 Exon 1, top oligo
BAS94	AAACCTGTTTCCGCTCCCGAGCGAC	PLSCR1 Exon 1, bottom oligo
BAS95	CACCGAGATGGCCACAGCAATTTTC	PLSCR1 Exon 4, top oligo
BAS96	AAACGAAATTGCTGTGGGCCATCTC	PLSCR1 Exon 4, bottom oligo
BAS97	CACCGCTTGAGGATTATTGATAATA	PLSCR1 Exon 4, top oligo
BAS98	AAACTATTATCAATAATCCTCAAGC	PLSCR1 Exon 4, bottom oligo
BAS99	CACCGCTCAAGGTAAAAGGTCTAGA	PLSCR1 Exon 4, top oligo

BAS100	AAACTCTAGACCTTTTACCTTGAGC	PLSCR1 Exon 4, bottom oligo
BAS101	CACCGGGGTCAAGAAGTCATAACTC	PLSCR1 Exon 4, top oligo
BAS102	AAACGAGTTATGACTTCTTGACCCC	PLSCR1 Exon 4, bottom oligo

2.1.6 Antibodies

Table 2.7: List of primary antibodies

Name	Target	Supplier	Dilution	Application
AK299	CagA	This lab	1:5000	WB
AK298	HopQI	This lab	1:5000	WB
AK263	RecA	This lab	1:10000	WB
AK214	AlpA	This lab	1:1000	WB
AK262	AlpB	This lab	1:2500	WB
AK273	CagY C-terminus	This lab	1:5000	WB
AK280	CagY N-terminus	This lab	1:5000	WB
AK175	<i>H. pylori</i>	This lab	1:1000	IF
PY99	P-Tyr	Santa Cruz	1:2500	WB
4D1	Tubulin	abcam	1:50000	WB
JL-8	GFP	Takara	1:1000	WB
EPR14249	PLSCR1	abcam	1:100 (flow cytometry), 1:5000 (WB)	WB, Flow cytometry
PA5-21649	PLSCR1	Thermo Fisher	1:1000-1:2000	WB
ab196830	Annexin A1	abcam	1:50	IF
EPR13052(B)	Annexin A2	abcam	1:50	IF
1F4-1A5	Annexin A5	abcam	1:50 (IF), 1:1000 (Dot Blot)	IF, Dot blot
PA1-73178	Lipid A	Thermo Fisher	1:5000	Dot blot
F3	Lewis Y	abcam	1:2000	Dot blot
9B11	Myc-tag	Cell signaling	1:100	IP

Table 2.8: List of secondary antibodies

Name	Supplier	Dilution	Application
Goat α -mouse IgG-Alexa 488	Invitrogen	1:500-1:1000	IF
Goat α -rabbit IgG-Alexa 555	Invitrogen	1:500-1:1000	IF
Goat α -rabbit IgG-Alexa 488	Invitrogen	1:500-1:1000	IF
Goat α -rabbit IgG-Alexa 647	Invitrogen	1:1000	Flow cytometry
α -mouse IgG-POX		1:10000	WB, Dot blot

α -rabbit IgG-Pox	1:10000	WB
α -mouse IgM-Pox	1:4000	Dot blot
α -goat IgG Pox	1:5000	Dot blot
Protein A-AP	1:5000	WB
α -mouse IgG-AP	1:5000	WB

2.1.7 Commercially available kits

Table 2.9: List of commercially available kits

Name	Description	Supplier
QIAamp Tissue Kit	Isolation of gDNA	Qiagen
illustra GFX PCR DNA and Gel Band Purification Kit	Purification of DNA from PCR reactions or agarose gels	GE Healthcare
RNeasy Plus Mini Kit	Isolation of RNA	Qiagen
RNase-free DNase Set	Isolation of RNA	Qiagen
TURBO DNA-free™ Kit	Isolation of RNA	Thermo Fisher
Experion RNA StdSens Analysis Kit	Determinatin of RNA quality	BioRad
LiveBLazer™ FRET-B/G Loading Kit with CCF4-AM	TEM assay	Thermo Fisher
Nano-Glo® Live Cell Assay System	HiBiT assay	Promega
QUANTI-Blue™	Detection of TLR-4 signaling	Invivogen
Immobilon Chemiluminescent HRP Substrate	Detection of POX-coupled secondary antibodies	Millipore

2.1.8 Enzymes

Restriction enzymes were purchased form New England Biolabs (NEB). T4 DNA Ligase was also obtained from NEB.

2.1.9 Chemicals and buffers

Chemicals were usually purchased from Roth, Merck, or Sigma-Aldrich. Cell culture grade DPBS (Dulbecco's DPBS without calcium and magnesium, Gibco) was used. Composition of buffers is described in Table 2.10.

Table 2.10: Composition of buffers

Buffer	Composition	Application
2x HBS	50 mM HEPES	Lentiviral transfection (2.2.1.3.2)
	280 mM NaCl	
	1.5 mM Na ₂ HPO ₄	
	pH 7.0	
2x SDS sample buffer	100 mM Tris/HCl	Western blot (2.2.5.2)
	4 % (w/v) SDS	
	0.2 % (w/v) Bromophenol blue	
	20 % (v/v) Glycerol	
	10 % (v/v) β-Mercaptoethanol	
pH 6.8		
Annexin A5 binding buffer	10 mM HEPES	Annexin A5 binding assay (2.2.2.2.6)
	150 mM NaCl	
	5 mM KCl	
	5 mM MgCl ₂	
	1.8 mM CaCl ₂	
	pH 7.4	
Anode I	300 mM Tris	Western blot (2.2.5.2)
	10 % (v/v) Methanol	
	pH 10.4	
Anode II	25 mM Tris	Western blot (2.2.5.2)
	10 % (v/v) Methanol	
	pH 10.4	
Cathode buffer	25 mM Tris	Western blot (2.2.5.2)
	40 mM 6-Aminocaproic acid	
	10 % (v/v) Methanol	
	pH 9.6	
GEBS	20 % (v/v) Glycerol	Agarose gel electrophoresis (2.2.4.3)
	50 mM EDTA	
	0.05 % (w/v) Bromophenol blue	
	0.5 % (w/v) N-lauroylsarcosine	
	pH 8.0	
N3 buffer	3 M Potassium acetate	Plasmid preparation (2.2.4.1.1)

P1 buffer	50 mM Tris	Plasmid preparation (2.2.4.1.1)
	10 mM EDTA	
	pH 8.0	
P2 buffer	200 mM NaOH	Plasmid preparation (2.2.4.1.1)
	1 % (w/v) SDS	
PBS	2.7 mM KCl	Staining of paraffin sections (2.2.6.1)
	137 mM NaCl	
	1.47 mM KH ₂ PO ₄	
	8 mM Na ₂ HPO ₄ *2 H ₂ O	
	pH 7.4	
PBS-T	2.7 mM KCl	Staining of paraffin sections (2.2.6.1)
	137 mM NaCl	
	1.47 mM KH ₂ PO ₄	
	8 mM Na ₂ HPO ₄ *2 H ₂ O	
	0.05 % Tween-20	
	pH 7.4	
RIPA	50 mM Tris/HCl	Immunoprecipitation (2.2.2.3.2)
	100 mM NaCl	
	1 mM EDTA	
	1 % (v/v) Nonidet P-40	
	0.25 % (w/v) Sodium deoxycholate	
	pH 7.4	
SDS Electrophoresis Buffer	25 mM Tris	SDS-PAGE (2.2.5.1)
	250 mM Glycine	
	20 % (w/v) SDS	
	pH 8.3	
Sodium Citrate Buffer	10 mM Sodium citrate	Antigen-demasking (2.2.6.1)
	0.05 % Tween-20	
	pH 6.0	
Stripping Buffer	25 mM Glycine	Stripping of membranes (2.2.5.4)
	10 % SDS	
	pH 2.0	

TAE	40 mM Tris	Agarose gel electrophoresis (2.2.4.3)
	20 mM Acetic acid	
	1 mM EDTA	
	pH 8.0	
TBS	150 mM NaCl	Western blot (2.2.5.2)
	200 mM Tris/HCl	
	pH 7.5	
TBS-T	150 mM NaCl	Western blot (2.2.5.2)
	200 mM Tris/HCl	
	0.05 % (v/v) Tween-20	
	pH 7.5	
Tfbl	30 mM Potassium acetate	Chemically competent <i>E. coli</i> (2.2.2.1.2)
	100 mM RbCl	
	10 mM CaCl ₂	
	50 mM MnCl ₂	
	15 % (v/v) Glycerol	
	pH 5.2 (with acetic acid)	
TfbII	10 mM MOPS	Chemically competent <i>E. coli</i> (2.2.2.1.2)
	75 mM CaCl ₂	
	10 mM RbCl	
	15 % (v/v) Glycerol	
	pH 6.5 (with acetic acid)	

2.1.10 Consumables

Plastics and other consumables were purchased from Corning, VWR, Greiner, Omnilab, or Thermo Fisher. Cell culture treated plates and bottles were obtained from Corning or BD Falcon, except for black, clear bottom 96-well plates (4titude).

2.2 Methods

2.2.1 Working with eukaryotic cells

2.2.1.1 Maintenance of eukaryotic cell lines

Eukaryotic cell lines were grown at 37 °C, 5 % CO₂ (Binder) and sub-cultured every two to three days according to their confluence. AGS and 3BF3 E6 were grown in RPMI/10 % fetal calf serum (FCS) and 1-A8, 1-D2, or 2-B3 cells were also grown in RPMI/10 % FCS supplemented with 0.5 mg/ml G418. AGS [LgBiT] cells were grown in RPMI/10 % FCS/0.5 mg/ml hygromycin B. The medium for Katolll and corresponding integrin knockout cells consisted of RPMI/20 % FCS. For HEK293 cells, DMEM supplemented with 15 % FCS and 1 % glutamine was used, 0.5 mg/ml G418 was added when cells were transfected with CEACAM1 (HEK293 CEACAM1). HEK-Blue hTRL-4 cells were grown in DMEM supplemented with 10 % FCS, 1% glutamine and HEK-Blue selection antibiotics (250x, Invivogen).

2.2.1.2 Cryo-conservation of eukaryotic cell lines

For cryo-conservation, approx. 10^4 - 10^5 cells were detached from the culture dish using trypsin/EDTA (Gibco) by incubation at 37 °C for up to 5 min. Cells were supplemented with medium to inactivate trypsin and centrifuged at 900 rpm (Heraeus Megafuge 3.0R) for 5 min. After discarding the supernatant, cells were re-suspended in 1 ml of cryo-conservation medium (FCS/10 % DMSO mixed 1:1 with cell culture medium), transferred to a cryogenic vial and frozen at -80 °C in Cryo 1 °C freezing containers (Nalgene). After at least 24 h, the vials were transferred to liquid nitrogen for long-term storage.

2.2.1.3 Transfection of eukaryotic cells

2.2.1.3.1 Transfection using liposome reagents

Eukaryotic cells were transfected using Lipofectamin2000 (Invitrogen). For this purpose, 4 µg of plasmid DNA and 10 µl of Lipofectamin2000 were diluted in 250 µl OptiMEM (Gibco) each. After 5 min incubation at room temperature (RT), the DNA and the Lipofectamin2000 solution were mixed together by inversion and incubated for another 20 min at room temperature (RT). Meanwhile, the cell culture medium was changed to OptiMEM. The DNA-Lipofectamin2000 mixture was added slowly to the cells and incubated for 1 h at 37 °C, 5 % CO₂. Afterwards, the medium was changed back to the usual cell culture medium. To generate stable cell lines, antibiotics were added for selection 24 h after transfection.

2.2.1.3.2 Lentiviral transfection

To generate viral particles, 293FT cells were transfected with the plasmid of interest and the packaging plasmids using the CaPO₄ method. For this, 293FT cells were seeded in a T75 bottles one day prior to transfection. Cell culture medium was replenished 3 to 4 h prior to transfection and 5 min before transfection was performed, 25 µM chloroquine was added to the cells.

Meanwhile, solution A and solution B were prepared. Solution A contained 2ml of 2x HBS buffer. Solution B consisted of 20 µg of plasmid of interest, 15 µg of pCMVΔ8.9, 10 µg of pVSV-G and 250 µl of 2 M CaCl₂ and was filled up to 2 ml with sterile ddH₂O. Then, solution A was added dropwise to solution B while mixing thoroughly. DNA-HBS mixture was incubated for 1 min at RT and added dropwise to the cells. After an incubation of 4 h at 37 °C and 5 % CO₂, the medium was replenished. Cells were incubated for 48 h at 37 °C and 5 % CO₂, during which the viral particles were produced. The supernatant of transfected 283FT cells was filtered through a 0.45 µm filter and 1 ml aliquots were made and stored at -80 °C or used immediately. 24 h prior to transfection with viral particles, HEK293 cells were seeded in 12-well plates. The supernatant containing the viral particles was added to the cells in different dilutions (1:2-1:10) and incubated for 24 h at 37 °C and 5 % CO₂. The cells were infected again with viral particles and incubated again for 24 h. Then, the viral supernatant was discarded and cell culture medium was added to transfected cells. After 24 h, the cells were split to a 6-well plate. The next day, cells were analyzed for GFP expression using the BD FACS Cantoll flow cytometer.

2.2.1.4 CRISPR/Cas9 system

To knockout a gene of interest in a eukaryotic cell line using the CRISPR/Cas9 system, first guide RNAs (gRNAs) were designed using the tool of the Zhang Lab (<https://zlab.bio/guide-design-resources>, discontinued in 2019).

After cloning the gRNAs in vector PX462 (pSpCas9n-2A-puro), cells were transfected with the respective plasmids. 24 h after the transfection, 2 µg/ml puromycin was added to select for transfected cells. After another 72 h, the antibiotic was removed again.

To obtain single cell clones, cells were diluted and seeded in a 96-well plate to a final concentration of approx. 0.5 cells per well. Wells containing more than one cell clone were excluded and only single cell clones were cultured further.

2.2.1.5 Intracellular staining for flow cytometry

For intracellular staining, 5*10⁵ cells per staining reaction were fixed in 100 µl of 4 % paraformaldehyde for 15 min at RT. After fixation, cells were re-suspended in DPBS/5 % FCS and incubated for 5 min at RT. Cells were centrifuged at 900 rpm for 5 min and the supernatant was

discarded. For permeabilization, cells were re-suspended in 100 μ l of DPBS/0.1 % saponin and incubated for 15 min at RT. After washing once in DPBS/5 % FCS/0.1 % saponin, cells were blocked with DPBS/5 % FCS/0.1 % saponin over night at 4 °C. For staining, the cells were incubated with the respective primary antibody for 1 h at 4 °C. After washing three times, the cells were incubated with the secondary antibody (1:1000 dilution) for 1 h at 4 °C in the dark. The cells were washed three times and re-suspended in DPBS for flow cytometry using the BD FACS Cantoll. All steps washing and incubation steps were performed using DPBS/5 % FCS/0.1 % saponin.

2.2.1.6 Cell sorting

After transfection of 3BF3 E6 cell line with the *egfp-plscr1* construct (pBAS91), cells were sorted into single-cell clones for high green fluorescence intensity using the BD FACSAria III at the CyTUM MIH facility.

2.2.2 Working with bacteria

2.2.2.1 Working with *Escherichia coli* (*E. coli*)

2.2.2.1.1 Cultivation of *E. coli*

E. coli were cultured on LB agar plates (32 g/l, Invitrogen) or in liquid Luria broth (LB medium, Invitrogen) and grown at 37 °C under aerobic conditions. LB agar plates were supplemented with ampicillin (100 μ g/ml), chloramphenicol (30 μ g/ml), kanamycin (50 μ g/ml), or erythromycin (250 μ g/ml) to select for transformed bacteria. For long term storage, bacteria were re-suspended in 1 ml LB medium/20 % glycerol in cryogenic vials and stored at -80 °C.

2.2.2.1.2 Generating chemically competent *E. coli*

An overnight culture of the *E.coli* strain was used to inoculate 200 ml of LB at an OD₅₅₀ (optical density at 550 nm, Chapter 2.2.2.2.2) of 0.2 and grown at 37 °C, 180 rpm. The culture was incubated until an OD₅₅₀ of 0.5 to 0.6 was reached. Meanwhile, the buffers TfbI and TfbII were freshly prepared and cooled. When the optimal OD₅₅₀ was reached, the culture was cooled on ice for 5 min and centrifuged at 4000 rpm (Heraeus Megafuge 16R) for 15 min at 4 °C. After discarding the supernatant, the cell pellet was re-suspended in 80 ml of ice cold TfbI buffer and incubated on ice for 5 min. The bacteria were centrifuged again at 4000 rpm for 15 min at 4 °C and the supernatant was discarded. After re-suspension of the cells in 8 ml TfbII buffer, aliquots of 50 μ l were flash frozen in liquid nitrogen. The competent bacteria were kept at -80 °C for long-term storage.

2.2.2.1.3 Transformation of chemically competent *E. coli*

After thawing an aliquot of competent *E. coli* on ice, plasmid DNA or ligation reaction (see chapter 2.2.4) were added to the bacteria and incubated on ice for 5-30 min. *E. coli* were incubated at 42 °C for 90 sec and immediately supplemented with 1 ml LB medium. After recovery at 37 °C, 180 rpm for 1 h, the bacteria were plated on selective LB agar plates and incubated at 37 °C overnight. The next day, colonies were picked and streaked on new LB agar plates for plasmid preparation (Chapter 2.2.4.1.1).

2.2.2.2 Working with *H. pylori*

2.2.2.2.1 Cultivation of *H. pylori*

For cryo-conservation, bacteria were re-suspended in 1 ml Brucella broth (BB)/10 % FCS/20 % glycerol in cryogenic vials and stored at -80 °C.

H. pylori strains were streaked from their cryo-culture on GC agar plates (36 g/l, Oxoid) supplemented with 8 % horse serum and 1 % vitamin mix (Table 2.11) and incubated for 72 h at 37 °C under microaerobic conditions (85 % N₂, 10 % CO₂, 5% O₂) (Microincubator MI22N, Scholzen). Before experiments were performed with *H. pylori*, the bacteria were at least passaged once to new serum plates and grown at 37 °C under microaerobic conditions for 24 h. For further use, the strains were passaged daily to new serum plates and incubated for 24 h at 37 °C under microaerobic conditions.

Table 2.11: Composition of vitamin mix for serum plates.

Vitamin mix	100 g/l α-D-glucose
	10 g/l L-glutamine
	26 g/l L-cysteine
	1.1 g/l L-cysteine
	0.15 g/l L-arginine
	0.1 g/l Cocarboxylase
	20 mg/l Iron(III)nitrate
	3 mg/l thiamine
	13 mg/l P-aminobenzoic acid
	0.25 g/l nicotinamide adenine dinucleotide
	10 mg/l Vitamin B12
	1 g/l Adenine

2.2.2.2.2 Measuring the optical density of bacterial cultures

To determine the optical density, the amount of light scattered by the bacterial culture was measured at a wave length of 550 nm (OD₅₅₀) using a photometer (DR1900, Hach). Either the OD₅₅₀ of a liquid culture was directly measured or bacteria were re-suspended from agar plates in medium or buffer using a sterile cotton swab. An OD₅₅₀ of 0.1 corresponds to 3*10⁷ cfu (colony forming units)/ml in *H. pylori*.

2.2.2.2.3 Transformation of *H. pylori*

1 ml of BB/10 % FCS was inoculated with an OD₅₅₀ of 0.2 and incubated for 2 h at 37 °C, 10 % CO₂ and 100 rpm (HeraCell 150, Thermo Scientific). 5 µl of plasmid DNA were added to the culture and incubated for 4 h at 37 °C, 10 % CO₂ and 100 rpm. After centrifugation of the bacterial cultures at 4000 rpm (Eppendorf centrifuge 5424 R), the pellet was re-suspended in 100 µl BB/10 % FCS and plated on a selective serum plate. For selection of transformed bacteria, serum plates were additionally supplemented with chloramphenicol (6 µg/ml), kanamycin (8 µg/ml), erythromycin (10 µg/ml), or streptomycin (250 µg/ml). Transformed bacteria were incubated at 37 °C under microaerobic conditions (Microincubator MI22N, Scholzen) for at least 72 h or until colonies could be detected.

To generate *H. pylori omp* knockout mutants, about 1000 bp up- and downstream of the gene of interest were clone in a pBluescript II SK vector with a *rpsL^{Serm}^R* resistance cassette (*Bam*HI/*Bam*HI). To generate marker-free *H. pylori* mutants, the up- and downstream regions were ligated in a pBluescript II SK vector without a resistance cassette. Primers for amplification of up- and downstream regions can be found in Table 2.5.

H. pylori mutants in *lpxE*, *lpxF* and *eptA* genes were constructed by transformation of the wildtype strains with plasmids pBAS101, pBAS102, and pBAS103, respectively. For construction of these plasmids, a pSMART-hcKan vector containing bp 20052-22245, bp 1664943-1667251, or bp 20022-23512 of the P12 chromosome (=HP2kb07_L02 (*lpxE*)/HP2kb08_K01 (*lpxF*)/HP5kb04_C19 (*eptA*)) was amplified by inverse PCR using primer BAS201/BAS202 for *lpxE* deletion, BAS203/BAS204 for *lpxF* deletion, and BAS205/BAS206 for *eptA* deletion. The product of BAS201/BAS202 was ligated with an *rpsL^{Serm}^R* (*Sall*/*Bam*HI) cassette for *lpxE* deletion, the products of BAS203/BAS204 and BAS205/206 were ligated with a chloramphenicol resistance cassette (*Sall*/*Bam*HI) for *lpxF* and *eptA* deletion, respectively. For confirmation of successful deletion, PCRs with primers BAS207/BAS208 for *lpxE* and *eptA* and BAS209/BAS210 for *lpxF* were performed. Successful *lpxE* or *eptA* deletion mutants in G27 were confirmed using primers BAS207/BAS211. Primer sequences can be found in Table 2.5.

The *myc-hopQ* complementation plasmid pBAS48 was constructed by inverse PCR of the *hopQ* complementation plasmid pWS658 (Bonsor *et al.*, 2018) with primers BAS60, which has a large overhang encoding the myc-tag, and BAS61 (Table 2.5). Both primers have a *SpeI* restriction site and after restriction enzyme digestion, the plasmid can be re-ligated. The correct integration of the myc-tag was confirmed by sequencing using primer BAS62 (Table 2.5).

The *alpAB* complementation plasmid pBAS75 was derived from pWS658 (Bonsor *et al.*, 2018), which was digested with *Sall/BglII* to cut out the *hopQ* open reading frame (ORF). The *alpAB* gene was amplified using primers BAS140/BAS141 (Table 2.5) and ligated into the digested vector. The sequence of the *alpAB* ORF was confirmed using primers BAS170/BAS171 (Table 2.5).

2.2.2.2.4 Preparation of bacterial lysates for Western blot analysis

Bacteria were diluted to a final OD₅₅₀ of 10 in 100 µl of DPBS and centrifuged at 5000 rpm for 5 min. After discarding the supernatant, the pellet was re-suspended in 100 µl 1x SDS sample buffer (50 µl DPBS + 50 µl 2x SDS sample buffer). Samples were lysed by heating to 95 °C for 10 min (Eppendorf Thermomixer Compact).

2.2.2.2.5 Bacterial pull-down assay

3*10⁷ bacteria (OD₅₅₀ of 0.2 in 500 µl DPBS) were centrifuged at 4000 rpm (Eppendorf centrifuge 5424 R) for 5 min and re-suspended in 500 µl CEACAM-N-GFP cell culture supernatant. After incubation at 4 °C for 1-1.5 h with head-over-head rotation (Kabe Labortechnik), the cells were washed twice with DPBS, re-suspended in 500 µl DPBS and diluted 1:5 in DPBS for flow cytometry analysis (BD FACS Canto II). For Western blot analysis, the bacteria were centrifuged at 4000 rpm for 5 min, re-suspended in 1x SDS sample buffer and heated to 95 °C for 10 min (Eppendorf Themomixer Compact).

2.2.2.2.6 AnxA5 binding assay

3*10⁷ bacteria (OD₅₅₀=0.1) were added to 1 ml RPMI with 2.5 µl of Annexin A5-AlexaFluor647 (Invitrogen). After an incubation of 1 h at 37 °C and 10 % CO₂ (HeraCell 150, Thermo Scientific), the bacteria were washed three times with Annexin A5 binding buffer at 4 °C. For flow cytometry analysis, cells were re-suspended in 500 µl of Annexin A5 binding buffer.

2.2.2.3 *In vitro* infection with *H. pylori*

2.2.2.3.1 *Infection for tyrosine phosphorylation assay*

Cell lines were seeded in a 6-well plate one to two days prior to the infection experiment. For the infection, the medium was changed to 2 ml of DPBS/10 % FCS. Cells were infected with a multiplicity of infection (MOI) of 60 (OD₅₅₀ of 0.1 in 2 ml) for 4 h at 37 °C and 5 % CO₂ (Revco Ultima incubator). After 4h, the cells were put on ice and washed twice with DPBS. 1 ml of DPBS supplemented with 1 mM PMSF, 1 mM sodium vanadate, 1 µM leupeptin, 1 µM pepstatin (DPBS*) was added to each well and cells were scraped off using a rubber policeman and transferred to a fresh tube. After centrifugation at 4000 rpm, 4 °C for 5 min (Eppendorf centrifuge 5424 R), the supernatant was discarded and 60 µl of 1x SDS sample buffer (30 µl DPBS* + 30 µl 2x SDS sample buffer) were added. After boiling at 95 °C for 10 min, samples were used for Western blot analysis (see Chapter 2.2.5). Suspension cells were transferred to a 1.5 ml Eppendorf tube immediately after 4 h of infection and centrifuged at 4000 rpm for 5 min at 4 °C and then washed twice with DPBS. Afterwards, samples were treated the same as adherent cell samples.

2.2.2.3.2 *Immunoprecipitation assays*

Two to three days prior to the experiment, cells were seeded in a 175 cm² bottle and grown to 80-90 % confluence. Cells were infected with an MOI of 150 in DPBS/10 % FCS. After an incubation of 4 h at 37 °C, 5 % CO₂ (Revco Ultima incubator), the cells were transferred to ice, washed twice with DPBS and were scraped off in DPBS* (Chapter 2.2.2.3.1) using a rubber policeman. Cells were centrifuged at 4000 rpm (Heraeus Megafuge 16R) for 20 to 30 min at 4 °C and re-suspended in 650 µl of RIPA* (RIPA + protease inhibitors). Cells were treated with ultrasound (Branson Sonifier 450) to ensure thorough lysis of the bacteria. After centrifugation at 15,000 rpm (Eppendorf centrifuge 5424 R) for 10 min at 4 °C, 500 µl of the supernatant was transferred to a fresh 1.5 ml Eppendorf tube, 5 µl of the antibody was added and incubated at 4 °C with head-over-head rotation (Kabe Labortechnik) over night. 50 µl of the supernatant without the antibody was stored at -20 °C as an input sample. The next day, 50 µl of protein A agarose beads (Roche) were added and incubated for 2 h at 4 °C with head-over-head rotation (Kabe Labortechnik). The beads were washed three times with RIPA* and finally re-suspended in 50 µl of 2x SDS sample buffer. After denaturation of proteins at 95 °C for 10 min, the samples were used for Western blot analysis (chapter 2.2.5).

2.2.2.3.3 TEM-1 β -Lactamase assay (Schindele et al., 2016)

For adherent cells lines, cells were seeded one to two days prior to the experiment in dark, clear bottom 96-well plates (4titude). For this assay, bacterial strains expressing a TEM-1 β -lactamase fused to CagA were used. The bacteria were pre-incubated at an OD₅₅₀ of 0.075 in 500 μ l DPBS/10 % FCS for 2 h at 37 °C, 10 % CO₂ and 100 rpm (HeraCell 150, Thermo Scientific). The cells were infected with an MOI of 100 and incubated for 2.5 h at 37 °C and 5 % CO₂ (Revco Ultima incubator). After discarding the supernatant, the CCF4-AM substrate (see Table 2.12) was added to the cells and they were incubated for 2 h at RT. The blue:green fluorescence ratio was measured using the Clariostar plate reader (BMG lab tech).

Prior to infection of suspension or semi-adherent cells, bacteria were pre-incubated at an OD₅₅₀ of 0.1 in 250 μ l DPBS/FCS for 2 h at 37 °C, 10 % CO₂ and 100 rpm (HeraCell 150, Thermo Scientific). For suspension or semi-adherent cells, the appropriate number of cells was counted (CasyTon, Innovatis) and transferred to a 96-well plate (3×10^5 cells/well), which were centrifuged at 900 rpm (Heraeus Megafuge 3.0) for 5 min and then infected with an MOI of 100 for 2.5 h at 37 °C and 5 % CO₂ (Revco Ultima incubator). After centrifugation at 900 rpm for 5 min, the supernatant was discarded, and the cells were stained with the CCF4-AM dye for 2 h at 28 °C and 750 rpm. The cells were washed three times with DPBS and then re-suspended in 200 μ l DPBS for flow cytometry. For data analysis, the value for not infected cells was subtracted from the other samples and results were depicted as blue:green ratio.

Briefly, the CCF4-AM fluorescent dye is transported into the cells, where it is de-esterified and emits a green fluorescence (measured at 530 nm) when excited at 405 nm. If the TEM-1-CagA fusion protein is translocated into the cells, the TEM-1 β -lactamase is able to cleave the fluorescent dye, which then emits a blue fluorescence (460 nm). Using the blue:green fluorescence ratio, the amount of CagA translocated into the cells can be calculated.

Table 2.12: Composition of CCF4-AM solution for one reaction

	Volume [μl]
Solution A	0.05
Solution B	0.5
Solution C	7.78
0.5 M Probenecid (in 1 M NaOH)	0.25
DPBS	41.4

2.2.2.3.4 HiBiT assay (Lettl et al., 2021)

AGS [LgBiT] cells were seeded in a dark 96-well plate one to two days prior to infection without selection antibiotic. For this assay, bacteria expressing HiBiT-CagA were used. Bacteria were pre-incubated at an OD₅₅₀ of 0.019 in 500 µl of F12/5 % FCS/5 mM CaCl₂ for 2 h at 37 °C, 10 % CO₂ and 100 rpm (HeraCell 150, Thermo Scientific). 1 h prior to infection, 2, 5, or 10 µg/ml recombinant AnxA5 (origene) was added to the respective culture. The cells were infected with an MOI of 25 and incubated for 2.5 h at 37 °C and 5 % CO₂ (Revco Ultima incubator). After discarding the supernatant, the 50 µl of luciferase substrate (Promega) was added (Table 2.13) and the luminescence signal was measured immediately using the Clariostar plate reader (BMG lab tech). Briefly, this assay is based on a split luciferase assay. AGS cells were stably transfected with the LgBiT part of the NanoLuc luciferase (Promega) and CagA was fused to HiBiT. Upon translocation of HiBiT-CagA into AGS [LgBiT] cells, HiBiT and LgBiT form a functional luciferase and, after adding the substrate, luminescence is measured. Luminescence is directly proportional to the amount of translocated CagA.

Table 2.13: Composition of HiBiT reaction solution

	Volume [µl]
Substrate	0.5
Buffer	9.5
Medium	40

2.2.2.3.5 TLR-4 assay

HEK-Blue hTLR-4 cells were seeded in a clear flat bottom 96-well plate one to two days prior to infection without selection antibiotics. Bacterial strains were incubated at an OD₅₅₀ of 0.075 in 500 µl of F12/10% FCS/5 mM CaCl₂ for 2 h at 37 °C and 10 % CO₂ (HeraCell 150, Thermo Scientific) while shaking. 1 h prior to infection, 1, 2, or 5 µg/ml AnxA5 (origene) were added to the bacteria. Cells were infected with an MOI of 100 for 20-24 h at 37 °C and 5 % CO₂.

For quantification, 180 µl of QuantiBlue (Invivogen) solution per well were transferred to a clear flat bottom 96-well plate. 20 µl of infected cell supernatant was added and after 30-120 min, the OD at 655 nm was measured using the Clariostar plate reader (BMG lab tech). As a positive control, cells were also incubated with 1 µg/ml of *E. coli* LPS (K-235, Sigma). For analysis, the value of mock infected cells was subtracted from all other values. Samples were measured in duplicates.

2.2.2.3.6 Adhesion assay

To determine the adherence of different bacterial strains, bacteria were either transformed with a GFP expression plasmid (pCH7c) or stained with DAPI. Bacteria were pre-incubated at an OD₅₅₀ of 0.1 in 1.5 ml DPBS/10 % FCS for 1 h at 37 °C, 10 % CO₂ and 100 rpm (HeraCell 150, Thermo Scientific). For staining with DAPI, bacteria were incubated with 5 µg/ml DAPI for 10 min at RT and washed once before infection. Adherent cells were seeded in a 12-well plate one to two days before infection. Semi-adherent and suspension cells were transferred to a 96-well plate. Cells were infected with an MOI of 60 and incubated for 1 h at 37 °C and 5 % CO₂ (Revco Ultima incubator). Cells were washed three times with DPBS either by centrifugation and discarding the supernatant (suspension and semi-adherent cells) or directly (adherent cells). Suspension or semi-adherent cells were at last re-suspended in 200 µl DPBS. Adherent cells were detached from the 12-well plate using 500 µl of DPBS/2 mM EDTA. Both were analyzed using the BD FACS Cantoll.

To determine adherence of the bacterial strains, the GFP or DAPI fluorescence of the bacterial pre-culture without cells was also measured with the BD FACS Cantoll. This value was used to normalize the GFP or DAPI fluorescence of the bacteria, as this was not constant among the different strains. Results were depicted as median fluorescence intensity (FI) normalized to DAPI staining or GFP expression.

2.2.3 Molecular biological techniques: RNA

2.2.3.1 Isolation of RNA

For the isolation of RNA, *H. pylori* strains were incubated at an OD₅₅₀ of 0.1 in DPBS/10% FCS for 2 h in 10 % CO₂ while shaking. The cultures were centrifuged at 4000 rpm (Heraeus Megafuge 16R) for 20 to 30 min at 4 °C, the supernatant was discarded and the pellets were immediately flash frozen in liquid nitrogen. The pellets were stored at -80 °C until further use.

For lysis of bacterial cells, pellets were re-suspended in 700 µl RLT (Qiagen)/1 % β-mercaptoethanol and disrupted using Lysing Matrix B 2 ml tubes with 0.1 mm silica beads (MP biomedical) and the Precellys 24 lysis & homogenization (Bertin Technologies) for 40 sec at 5500 rpm.

RNA was isolated using the RNeasy Plus Mini Kit (Qiagen) according to the manufacturer's instructions. An on-column DNase digestion (RNase free DNase Set from Qiagen) was performed for 15 min at RT. After elution from the column, a second DNase digestion was performed using the TURBO DNA-free™ DNase Kit (Invitrogen). Briefly, 0.1 volumes of the 10x buffer and 2 µl of DNase were added and incubated for 30 min at 37 °C. 0.2 volumes of the DNase inactivation

reagent were added and incubated for 5 min at RT. After centrifugation at 10,000 xg for 2 min at 4 °C, the supernatant was transferred to a fresh RNase-free tube and a 5 µl aliquot was taken for further analysis of the RNA quality.

2.2.3.2 Analysis of RNA quality

2.2.3.2.1 Determination of RNA concentration

RNA concentration and quality was analyzed using a NanoDrop (peqlab). For this, 1 µl of the RNA was loaded on the NanoDrop and the adsorption at 230 nm, 260 nm and 280 nm was measured. RNA quality was considered good, if the A260/A280 ratio was between 1.8 and 2.

2.2.3.2.2 Determination of genomic DNA contamination

To analyze if RNA was contaminated with genomic DNA, a polymerase chain reaction (PCR) with primers UB110/UB111 (Table 2.5) was performed, targeting the 16S rRNA gene (see chapter 2.2.4.2). If no bands were detected in the RNA samples, there was no genomic DNA contamination and RNA could be further used.

2.2.3.2.3 Determination of RNA integrity

RNA concentration and integrity was analyzed using the Experion Automated Electrophoresis System (Bio Rad) according to the manufacturer's instructions. RNA integrity was high, if the RQI value was between 9 and 10.

2.2.3.3 RNA-Seq analysis

RNA-Seq was performed and analyzed by Genewiz (Leipzig, Germany).

2.2.4 Molecular biological techniques: DNA

2.2.4.1 Isolation of DNA

2.2.4.1.1 Plasmid DNA

Plasmid DNA from *E. coli* was isolated using an adapted protocol from the QIAprep Spin Miniprep Kit (Qiagen). Briefly, bacteria were re-suspended in DPBS, centrifuged at 4000 rpm for 5 min (Eppendorf centrifuge 5424 R) and the resulting pellet was re-suspended in 250 µl buffer P1. 250 µl of the lysis buffer P2 were added, followed by 350 µl of the neutralizing buffer N3. After centrifugation at full speed for 10 min at RT, the supernatant was transferred to a new tube and 500 µl of 2-propanol were added. To precipitate the DNA, the mixture was incubated at -20 °C for 20-30 min and centrifuged at full speed for 10 min at RT. After washing the pellet once with 70 %

ethanol by centrifugation at full speed for 5 min, the pellet was dried in a DNA Speed Vac (DNA110, Savant). The pellet was dissolved in 50 μ l ddH₂O and stored at -20 °C until further use.

2.2.4.1.2 Genomic DNA

For isolation of genomic DNA (gDNA) from either *H. pylori* or tissue culture cells, bacteria or eukaryotic cells were re-suspended in DPBS and centrifuged at 4000 rpm (Eppendorf centrifuge 5424 R) for 5 min at RT. The genomic DNA was isolated using the QIAamp Tissue Kit (Qiagen) according to the manufacturer's instructions.

2.2.4.2 Polymerase chain reaction (PCR)

In Table 2.12, the standard mix for a 50 μ l reaction is shown. Usually, the ExTaq polymerase (Takara) and the peqSTAR thermocycler (peqlab) was used. In Table 2.15, the standard protocol for PCR is shown.

Table 2.14: Standard PCR reaction mix

Reagent	Volume [μ l]
10x buffer	5
2.5 mM dNTPs	4
25 mM MgCl ₂	6
10 μ M forward primer	1
10 μ M reverse primer	1
ddH ₂ O	32
ExTag Polymerase	0.1
plasmid or genomic DNA	1

Table 2.15: Standard PCR protocol

	Temperature	Time	Cycles
Initial denaturation	95 °C	10 min	1
Denaturation	95 °C	30 sec	30
Annealing	52 °C	45 sec	
Extension	68 °C	1 min/1000 kb	
Final extension	68 °C	10 min	1
Storage	4 °C	∞	-

2.2.4.3 Agarose gel electrophoresis

To analyze the PCR reaction, it was mixed with GEBS buffer and loaded on a 1 % agarose gel. Additionally, a DNA molecular weight marker (Thermo Fisher) was loaded on the gel. A constant voltage of 100 V was applied and DNA fragments were separated according to their size. Afterwards, the gel was incubated in an ethidium bromide bath (1 mg/l) for approx. 15 min and analyzed under UV light (Molecular Imager Gel Doc XR System, Bio Rad).

If fragments were needed for further applications, a preparative gel with wider slots was prepared. After separation of the DNA, the gel was stained using 0.1 % methylene blue for approx. 20 min at RT while shaking. The gel was de-stained using tap water and the band of interest was cut out of the gel. DNA was isolated from the gel using the illustra GFX PCR DNA and Gel Band Purification Kit (GE Healthcare) according to the manufacturer's instructions. DNA was eluted in 30 μ l of ddH₂O and stored at -20 °C until further use.

2.2.4.4 Cloning

2.2.4.4.1 Restriction enzyme reaction

For a control digestion, 10 μ l reactions were prepared (Table 2.16). After an incubation of approx. 1 h at 37 °C, reaction was loaded on an agarose gel for further analysis (see chapter 2.2.4.3).

Table 2.16: Control digestion reaction

	Volume [μl]
DNA	3
10 x Buffer	1
Enzyme 1	0.5
Enzyme 2	0.5
ddH₂O	5

For preparative restriction reactions, 40 μ l reactions were prepared (Table 2.17). After an incubation for up to 3 h at 37 °C, the reaction was either loaded on a preparative agarose gel (chapter 2.2.4.3) and the band of interest was cut out and purified as described before. When no agarose gel electrophoresis was necessary, the DNA was immediately purified using the illustra GFX PCR DNA and Gel Band Purification Kit (GE Healthcare) according to the manufacturer's instructions.

Table 2.17: Preparative restriction reaction

	Volume [μl]
DNA	27
10 x Buffer	4
Enzyme 1	1
Enzyme 2	1
ddH₂O	7

2.2.4.4.2 Ligation reaction

For ligation, the T4 DNA ligase from NEB was used. 7 μ l insert DNA were mixed with 1 μ l of vector DNA, 1 μ l of 10x buffer and 1 μ l of T4 DNA ligase. The reaction was incubated at 4 °C over night or at 16 °C for 4 h. The ligation reaction was transformed in chemically competent *E. coli* (Chapter 2.2.2.1.3).

2.2.4.4.3 Sequencing

Sequencing was performed by Eurofins Genomics (Germany, Ebersberg). Samples were prepared according to the company's instructions and sequences were analyzed using the CLC Main workbench 7 software (Qiagen).

2.2.5 Protein biochemistry methods

2.2.5.1 Sodium dodecyl sulfate polyacrylamide gel electrophoresis (SDS-PAGE)

In this work, a discontinuous gel technique was used, consisting of an upper stacking gel (Table 2.19) and a resolving gel with differing amounts of polyacrylamide (PAA; Table 2.18). For SDS-PAGE, the *Mini-PROTEAN® 3 Cell* chamber (Bio-Rad) was used. 5 to 10 μ l of the samples (prepared as described in Chapters 2.2.2.2.4, 2.2.2.2.5, 2.2.2.3.1, or 2.2.2.3.2) as well as a protein marker (PageRuler Pre-stained Protein Ladder, Fermentas) were loaded on the gel. Applying a constant voltage (100 V–180 V) ensured separation of the proteins according to their molecular weight.

Table 2.18: Composition of resolving gels with different amounts of PAA

	Volume [ml] for 6 % gel	Volume [ml] for 8 % gel	Volume [ml] for 10 % gel	Volume [ml] for 12 % gel
ddH₂O	2.6	2.3	1.9	1.6
30 % PAA	1.0	1.3	1.7	2.0
1.5 M Tris-HCl, pH 8.8	1.3	1.3	1.3	1.3
10 % SDS	0.05	0.05	0.05	0.05
10 % APS (Ammoniumperoxodisulfat)	0.05	0.05	0.05	0.05
TEMED (Tetramethylethyldiamin)	0.004	0.003	0.002	0.002

Table 2.19: Composition of a 4 % stacking gel

	Volume [μl]
ddH₂O	680
30 % PAA	170
1.0 M Tris-HCl, pH 6.8	130
10 % SDS	10
10 % APS	10
TEMED	1

2.2.5.2 Immunoblot (Western blot)

To visualize immobilized proteins on a membrane using specific antibodies, immunoblotting was performed. In this work, a semi-dry blotting system was used to transfer proteins from the SDS-PAGE gel to the PVDF (polyvinylidenfluorid) membrane (GE Healthcare, pore size 0.2 μm). First, two thick Whatman filter papers soaked in anode I buffer, followed by two thin Whatman filter papers saturated in anode II buffer, were placed in a blotting chamber (Biotec-Fischer). Then, the PVDF membrane, previously activated in 100 % methanol and equilibrated in anode II buffer, and the gel were laid on top, followed by two thin and two thick Whatman filter papers soaked in cathode buffer. After ensuring no air bubbles were between the gel and the membrane, the proteins were transferred to the membrane by applying a constant current of 1 mA/cm² for 90 min.

2.2.5.3 Detection of immobilized proteins

To block unspecific binding sites, the membranes were immediately transferred to a 50 ml Falcon tube containing 5 % skimmed milk powder in TBS-T (blocking solution) while rolling on a tube roller mixer. After incubation for 1 h at RT, the primary antibody was added and incubated overnight at RT while rolling. The next day, the blots were washed at least three times for 15 min with TBS-T, before the secondary antibody was diluted in 5 ml TBS-T and added to the membranes. After incubation for 1 h at RT, the membranes were washed again trice with TBS-T. For detection of POX-(horseradish peroxidase) coupled secondary antibodies, the chemiluminescence substrate containing luminol (Immobilon Chemiluminescent HRP Substrate, Millipore) was incubated for 1-5 min on the membrane. After an exposure time of 1-10 min in the dark, the X-ray film (Super RX-N, Fuji) was transferred to the developing device (Fuji Film FPM-100A) and protein bands were analyzed afterwards.

For detection using alkaline phosphatase (AP) coupled secondary antibodies, the developing solution containing the substrate BCIP (5-Brom-4-chlor-3-indoxylphosphate) and the dye NBT (Nitro blue tetrazolium chloride) was prepared (Table 2.20) and the blot was added. Bands were detected by a color change to purple.

Table 2.20: Developing solution to detect AP-coupled secondary antibodies

	Volume
0.1 M Tris-HCl, pH 9.6	9 ml
1 M MgCl₂	70 µl
5 mg/ml BCIP	100 µl
1 mg/ml NBT	1 ml

2.2.5.4 Stripping of membranes

To detect another protein on the same membrane after POX detection, the bound antibodies were removed by incubation in stripping buffer (25 mM glycine/HCl, 1 % SDS, pH 2) for 20 min. After washing three times with TBS-T, the membranes were blocked again with 5 % skimmed milk powder in TBS-T and incubated with a different primary antibody.

2.2.5.5 Dot Blot

Two PVDF membranes were activated in 100 % methanol, transferred to ddH₂O for 2 min and finally incubated in TBS-T/5 mM CaCl₂ buffer for at least 5 min.

After samples were diluted accordingly, one thin Whatman paper soaked in TBS-T/5 mM CaCl₂ was placed on the Dot Blot microfiltration apparatus, followed by the two prepared PVDF

membranes. The apparatus was closed and connected to the vacuum line. After applying vacuum briefly to remove excess buffer, the samples were loaded on the membrane by pipetting in the corresponding wells. Vacuum was applied to the unit until all samples were filtered through. To wash down the sides of the wells, DPBS was added to each well and vacuum was applied. After the buffer was filtered through, vacuum was turned off and the top membrane was removed from the unit, briefly washed in TBS-T/5 mM CaCl₂ and then transferred to TBS-T/5 mM CaCl₂/3 % BSA (bovine serum albumin). Unspecific binding sites were blocked for 1 h at RT while rolling on a tube roller mixer. After blocking, the membrane was washed briefly with TBS-T/5 mM CaCl₂ and 2 µg/ml AnxA5 (Sigma, A9460) or other primary antibodies (α-Lewis Y or α-Lipid A) was added in TBS-T/5 mM CaCl₂ and incubated at 4 °C over night. In case of AnxA5 detection, the membrane was washed three times for up to 30 min at RT and the primary antibody was incubated in TBS-T/5 mM CaCl₂ for up to 4 h at RT. After washing the membrane again trice in TBS-T/5 mM CaCl₂, the secondary antibody was incubated for 1 h at RT. The membrane was washed three times with TBS-T/5 mM CaCl₂ and detection with POX was performed as described before (see Chapter 2.2.5.3).

2.2.6 Immunofluorescence staining

2.2.6.1 Staining of paraffin sections

Sections were cut from paraffin blocks using a microtome (Leica) with a thickness of 5 to 6 µm. After transfer to the microscope slide, the sections were dried and stored at RT.

2.2.6.1.1 De-paraffinization

To re-hydrate paraffin sections before staining, they were treated as described in Table 2.21. Afterwards, sections were transferred to ddH₂O. For antigen de-masking, sections were boiled in sodium citrate buffer for 20 min using a microwave.

Table 2.21: Treatment for de-paraffinization

	Time [min]	
100 % Xylene	15	3 times
100 % Ethanol	10	1 time
96 % (v/v) Ethanol	5	1 time
80 % (v/v) Ethanol	2	1 time
70 % (v/v) Ethanol	1	1 time
50 % (v/v) Ethanol	1	1 time

2.2.6.1.2 Staining

After de-masking of antigens, the slides were transferred to an immunostaining chamber (Shandon Sequenza, Thermo Fisher) and washed with PBS-T 3 times.

Unspecific binding sites were blocked with DPBS/1 % BSA/2.5 % goat serum/0.5 % saponin for 1 h at RT or at 4 °C overnight. The primary antibodies were diluted in DPBS/1% BSA/2.5 % goat serum/0.5 % saponin and incubated for 1 h at RT or at 4 °C overnight. After washing the sections 3 times with PBS-T, the secondary antibodies were added in PBS-T/2.5 % goat serum and incubated for 1 h at RT in the dark. Slides were washed again 3 times with PBS-T and stained with 5 µg/ml DAPI in PBS-T/2.5 % goat serum for 10 min at RT in the dark, followed by washing 3 times with PBS-T. Sections were embedded with Fluorescence Mounting Medium (Dako) and stored at 4 °C.

2.2.6.1.3 Microscopy and Analysis

Sections were visualized using the Leica TCS SP5 confocal microscope for quantification of annexin signal or the confocal laser scanning microscope LSM880 (Zeiss) with Ayscan Module for co-localization studies.

To analyze the stained sections, FIJI software (<https://pubmed.ncbi.nlm.nih.gov/22743772>) was used. For this, two macros were written, one counting the nuclei on each image (Figure 2.1) and one measuring the fluorescence intensity of the stained protein of interest (Figure 2.2). The threshold for measuring the fluorescence intensity was chosen accordingly, so that no signal was measured in the isotype control samples. Fluorescence intensity was normalized to the number of nuclei visible on the respective image.

```

run("Options...", "iterations=1 count=1 black pad");
run("Colors...", "foreground=white background=black selection=yellow");
//select input folder, make an output folder
indir = getDirectory("select a source folder");
fs = File.separator;
upperfolder=File.getParent(indir);
foldername=File.getName(indir);
outdir=upperfolder+fs+foldername+"_Output"+fs;
File.makeDirectory(outdir);

//get the image list filtering based on the file extension
indir=getDirectory("select a source folder");
list1=getFileList(indir);
list2=newArray(list1.length);
a=0;
for(i=0; i < list1.length;i++){
    if(endsWith(list1[i], "ch02.tif")){
        list2[a]=list1[i];
        a++;
    }
}
list2=Array.trim(list2,a);
Array.show("Comparison", list1, list2)
setBatchMode(true);
//start batch loop
for(i=0; i<list2.length; i++){
    //open image, grap the file name, make a duplicate for proof
    open(indir + list2[i]);
    nameonly = File.nameWithoutExtension;
    run("Duplicate...", "title=dup");

    //make a binary, watershed, analyse particle
    selectWindow(list2[i]);
    setAutoThreshold("Huang dark");
    setOption("BlackBackground", true);
    run("Convert to Mask");
    run("Watershed");
    run("Set Measurements...", "area mean min redirect=dup decimal=3");
    run("Analyze Particles...", "size=10-Infinity circularity=0.00-1.00 show=[Bare Outlines] display exclude summarize");

    //make proof image
    rename("outline");
    run("Invert");
    imageCalculator("Add", "dup","outline");

    //save proof image to output folder
    selectWindow("dup");
    outname = nameonly + "_result";
    saveAs("tif", outdir + outname);

    //clear up workspace and memory
    run("Close All");
    run("Collect Garbage");
}

```

Figure 2.1: Makro code for counting the nuclei

```

run("Options...", "iterations=1 count=1 black pad");
run("Colors...", "foreground=white background=black selection=yellow");
//select input folder, make an output folder
indir = getDirectory("select a source folder");
fs = File.separator;
upperfolder=File.getParent(indir);
foldername=File.getName(indir);
outdir=upperfolder+fs+foldername+"_Output"+fs;
File.makeDirectory(outdir);

//get the image list filtering based on the file extension
indir=getDirectory("select a source folder");
list1=getFileList(indir);
list2=newArray(list1.length);
a=0;
for(i=0; i < list1.length;i++){
    if(endsWith(list1[i], "ch01.tif")){
        list2[a]=list1[i];
        a++;
    }
}
list2=Array.trim(list2,a);
Array.show("Comparison", list1, list2)
setBatchMode(true);
//start batch loop
for(i=0; i<list2.length; i++){
    //open image, grab the file name, make a duplicate for proof
    open(indir + list2[i]);
    nameonly = File.nameWithoutExtension;
    run("Duplicate...", "title=dup");

    //measure green intensity and create proof image
    selectWindow(list2[i]);
    run("Median...", "radius=1");
    setAutoThreshold("Default dark");
    setThreshold(30, 255);
    run("Set Measurements...", "area mean min area_fraction limit display redirect=None decimal=3");
    run("Measure");
    run("Convert to Mask");
    imageCalculator("Add", "dup", list2[i]);
    run("Green");
    outname = nameonly + "_result";
    saveAs("jpeg", outdir + outname);

    //clear up workspace and memory
    run("Close All");
    run("Collect Garbage");
}

```

Figure 2.2: Makro code for measuring the fluorescence intensity

2.2.7 Data analysis and statistics

Flow cytometry data was analyzed with FlowJo software (version 10). Positive gates were set according to the negative control (~ 2.5 % of negative sample in positive gate). Values of the negative control were subtracted from other samples. Statistics were analyzed with GraphPad Prism 5 with either Dunnett's or Bonferroni's *post hoc* test.

Chapter 3: Results

3.1 Role of HopQ and CEACAM1 in regulating CagA translocation

3.1.1 Influence of the CEACAM1 cytoplasmic tail on CagA translocation

HopQ is the only known non-*cagPAI* encoded co-factor of CagA translocation (Belogolova *et al.*, 2013), but the mechanism is still unknown. Thus, one aim of this thesis was investigating the impact of the HopQ-CEACAM interaction on CagA translocation. One approach to analyze the influence of CEACAM on regulating CagA translocation was to examine the effect of the ITIM of CEACAM1 on CagA translocation.

To test this, full length CEACAM1 (CEACAM1-4L) and a version with a deletion of the cytoplasmic tail (CEACAM1 Δ CT) were expressed in HEK293 cells by lentiviral transfection. Transfection efficiency was very low, but expression of CEACAM1 Δ CT was slightly increased compared to CEACAM1-4L (Figure 3.1 A). Despite the low expression levels, CagA phosphorylation could be detected by Western blot (Figure 3.1 B). To quantify the amount of translocated CagA, TEM-1 β -lactamase assays were performed. For this, the transfected cells were infected with P12[TEM-CagA], a *hopQ* deletion mutant and a complemented Δ *hopQ*::*hopQ* strain and translocation was measured by flow cytometry. As expected, no CagA translocation was measured in the *hopQ* deletion mutant, as translocation in this cell line is solely dependent on the HopQ-CEACAM interaction. This effect was restored by complementation of *hopQ*. There was no significant difference in CagA injection between CEACAM1-4L or CEACAM1 Δ CT (Figure 3.1 C), demonstrating that ITIM or ITIM-dependent signaling was not necessary for CagA translocation. The slight elevation in CEACAM1 Δ CT was probably a result of the higher transfection efficiency of this construct.

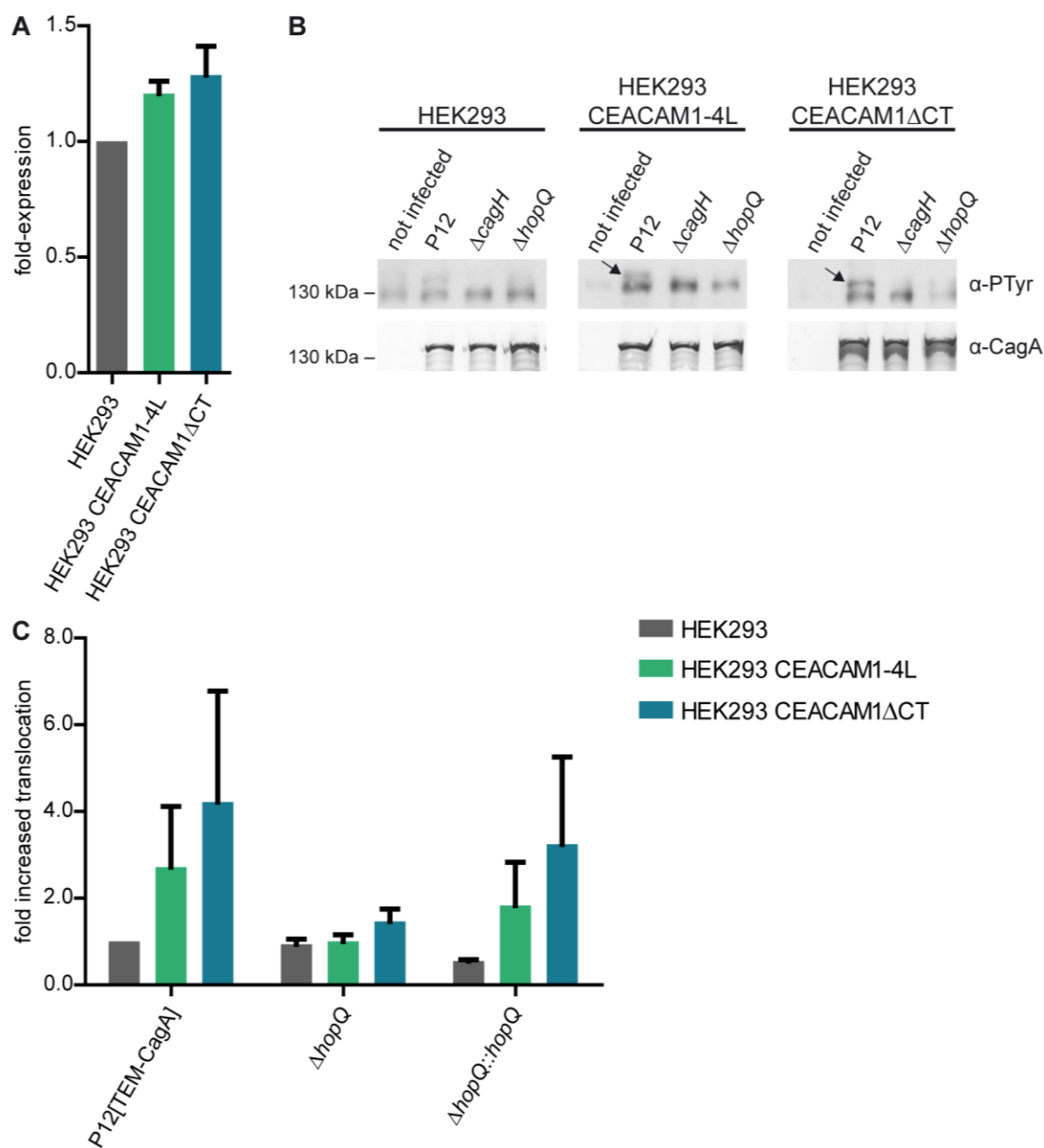


Figure 3.1: Transfection of HEK293 with CEACAM1-4L and CEACAM1ΔCT.

(A) HEK293 cells were transfected with lentiviral particles as described above (Chapter 2.2.1.3.2) for expression of CEACAM1-4L-GFP and CEACAM1ΔCT-GFP. CEACAM1 expression was measured as GFP fluorescence intensity using flow cytometry. Results are shown as mean \pm SEM (standard error of mean). No significances were observed using One-way ANOVA with Bonferroni's Multiple Comparison test. $n=3$

(B) Transfected HEK293 cells were infected *in vitro* with P12, P12ΔcagH (negative control) and P12ΔhopQ. Phosphorylated CagA was detected using an α-PTyr (PY99, Santa Cruz) antibody and CagA was detected using AK299 antibody. The size of CagA is, as expected, 135 kDa.

(C) Cag A translocation was quantified using the TEM-1 β -lactamase assay. The negative control values (P12[TEM-CagA] Δ cagT) were detracted and values were normalized to HEK293 infected with P12[TEM-CagA]. Results are shown as mean \pm SEM. No significances were observed using Two-way ANOVA with Bonferroni's posttest. n=3

3.1.2 Interaction of HopQ with gerbil CEACAM1

Mice are not an optimal model animal for *H. pylori* research due to their mild pathology upon *H. pylori* infection (Ferrero *et al.*, 1998). Thus, Mongolian gerbils (*Meriones unguiculatus*) are frequently used to investigate the pathology of an infection *in vivo*, as these animals develop more severe symptoms (Watanabe *et al.*, 1998). One possible explanation for this could be the lack of interaction between HopQ and murine CEACAM1 (Königer *et al.*, 2016). To gain further insights into the role of CEACAMs and their interaction with *H. pylori* HopQ, the binding of gerbil CEACAM1 to HopQ was analyzed. Recently, the genome of the Mongolian gerbil was published (Zorio *et al.*, 2019) and gerbil CEACAM genes were identified (W. Zimmermann, unpublished; Figure 3.2 A). According to those sequences, gerbil CEACAM1 comprises three IgC-like domains and one IgV-like domain, and therefore show the same structure as human and murine CEACAM1. Human and gerbil CEACAM1 have two ITIM motifs, in contrast to murine CEACAM1, which has one ITIM and one ITSM (immunoreceptor tyrosine-based switch motif).

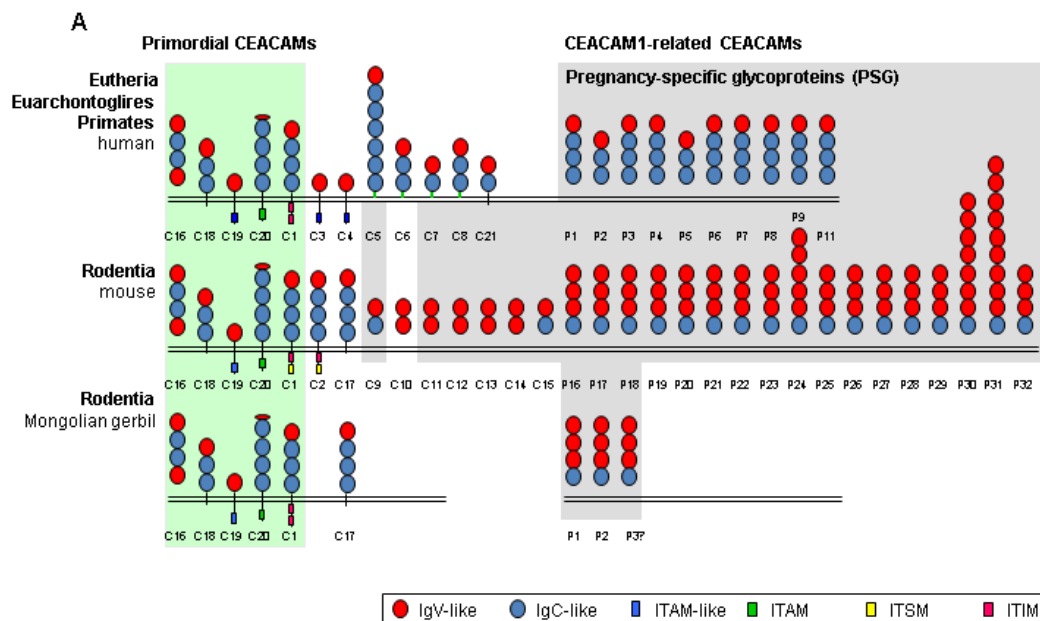


Figure 3.2: Comparison of the structure of human, mouse, and Mongolian gerbil CEACAMs

(A) Schematic overview of the carcinoembryonic antigen family in humans (top), mice (middle) and Mongolian gerbils (bottom). Highlighted in green are CEACAMs, representing the basic set of primordial members. Orthologues to CEACAMs are identified in mice and gerbils. The pregnancy-specific glycoproteins are shaded in gray and can be found in humans, mice and gerbils. (W. Zimmermann, unpublished).

A gerbil CEACAM1-N-GFP construct was generated in the lab of C. Hauck (University Konstanz, unpublished), which was expressed in 293T cells as described previously (Voges *et al.*, 2010). To compare binding of gerbil CEACAM1-N-GFP, human CEACAM1-N-GFP construct, as well as mouse CEACAM1-N-GFP were tested. GFP and human CEACAM1 alone were used as a negative control. Western blotting confirmed that all tested constructs were produced, albeit in differing concentrations (Figure 3.3 A). Pull down assays using gerbil CEACAM1-N-GFP revealed no interaction with *H. pylori* P12 by neither Western Blot (Figure 3.3 B), nor flow cytometry (Figure 3.3 C, D).

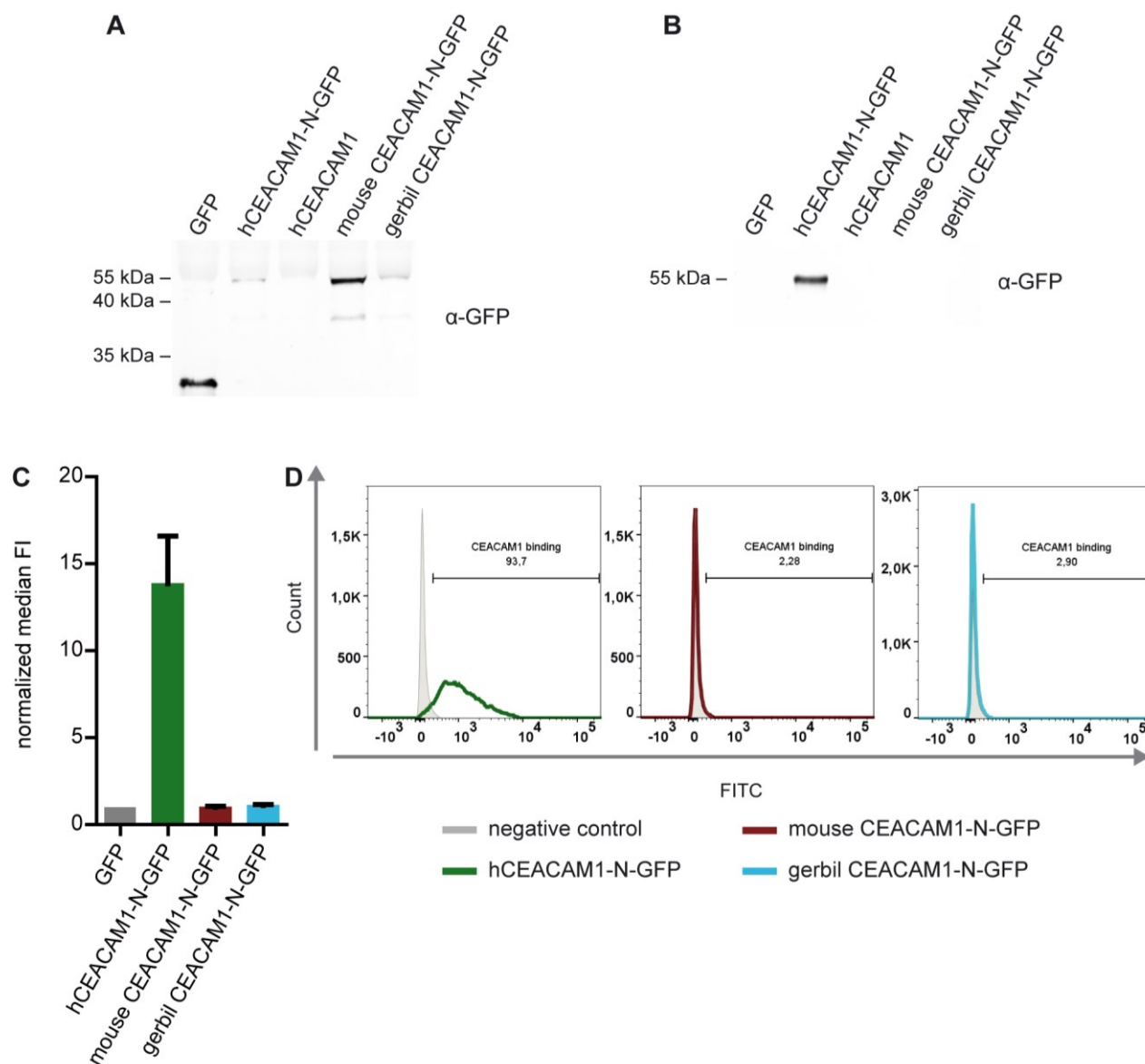


Figure 3.3: Binding of gerbil CEACAM1 to *H. pylori*.

(A) CEACAM1-N-GFP supernatants from human (h), mouse and gerbil, as well as GFP and hCEACAM1 supernatants were analyzed by Western blot to check for GFP expression. GFP was detected using α-GFP (JL-8, Takara) antibody, resulting in bands at 55 kDa (CEACAM1-N-GFP constructs) and 27 kDa (GFP).

(B) A bacterial pull-down assay was performed using GFP alone (negative control), hCEACAM1-N-GFP (positive control), hCEACAM1 without GFP (negative control), mouse CEACAM1-N-GFP, and gerbil CEACAM1-N-GFP. Samples were analyzed by Western blotting using α-GFP (JL-8) antibody. One representative experiment is shown.

(C, D) Bacterial pull-down assays were performed using GFP alone (negative control), hCEACAM1-N-GFP (positive control), mouse CEACAM1-N-GFP, and gerbil CEACAM1-N-GFP and analyzed by flow cytometry. One representative experiment is shown (D). Results are depicted as mean ± SD. n=3 (C)

3.1.3 Effects of targeted mutations in HopQ on CagA translocation

To further investigate the HopQ-CEACAM1 interaction, the structure of this complex was solved in collaboration with the group of E. Sundberg (University of Maryland) (Bonsor *et al.*, 2018). CEACAMs form dimers with themselves and other CEACAMs via interaction of their N-terminal IgV domains (Bonsor *et al.*, 2015). Crystallization of the HopQ-CEACAM1 complex revealed, that HopQ exploits the dimer surface of CEACAM1. Single-site alanine mutations in HopQ were generated and tested for their affinity to CEACAM1 by analytical ultracentrifugation and isothermal titration calorimetry. Only the HopQ^{L150A} variant showed a modest decrease in affinity to CEACAM1. Another variant, the HopQ^{Δ135-136Δ141-142}, which removes the β-hairpin structure in the β2-α4 loop, an important structure for CEACAM1 binding, showed again only a modest decrease in affinity. For the HopQ^{β2-α4:BabA} variant, the β2-α4 loop of HopQ (aa 133-158) was replaced with the corresponding loop of the related but functionally distinct adhesin BabA (aa 136-148). This construct showed no binding to CEACAM1, highlighting the importance of the β2-α4 loop for CEACAM1 binding by HopQ. (Bonsor *et al.*, 2018)

To analyze, whether these mutations in the *hopQ* gene had an impact on their function, a P12Δ*hopQ* deletion strain was complemented with these different HopQ variants and CagA phosphorylation assays as well as TEM-1 β-lactamase assays were performed. AGS cells, a well-established human stomach epithelial cell line frequently used for *H. pylori* infections *in vitro*, were used for these experiments (Barranco *et al.*, 1983, Smoot *et al.*, 1993, Segal *et al.*, 1996). In addition, HEK293 stably transfected with CEACAM1 (HEK293 CEACAM1) were used (Königer *et al.*, 2016).

As these HopQ variations showed only a modest decrease in affinity to CEACAM1 (Bonsor *et al.*, 2018), it not surprising that the HopQ^{L150A}, HopQ^{T370A} and HopQ^{Δ135-136Δ141-142} variations had no impact on CagA translocation or phosphorylation in AGS cells (Figure 3.4 B). Even though the HopQ^{L150A} variant showed a weaker CagA phosphorylation in HEK293 CEACAM1 cells, CagA translocation efficiency was not significantly different between this variant and the wildtype HopQ protein (Figure 3.4 C, D). The HopQ^{T370A} and the HopQ^{Δ135-136Δ141-142} had no influence on either CagA translocation or phosphorylation in HEK293 CEACAM1 cells. The HopQ^{β2-α4:BabA} strain, on the other hand, showed less CagA translocation in AGS cells (approx. 20 %) compared to a *hopQ* deletion mutant (Figure 3.4 B). In addition, the CagA phosphorylation was also significantly reduced (Figure 3.4 A). In HEK293 CEACAM1 cells, this strain showed no CagA translocation or phosphorylation, which is not surprising, as translocation in this cell line is strictly dependent on the HopQ-CEACAM interaction, which was disturbed in this HopQ variant (Figure 3.4 C, D).

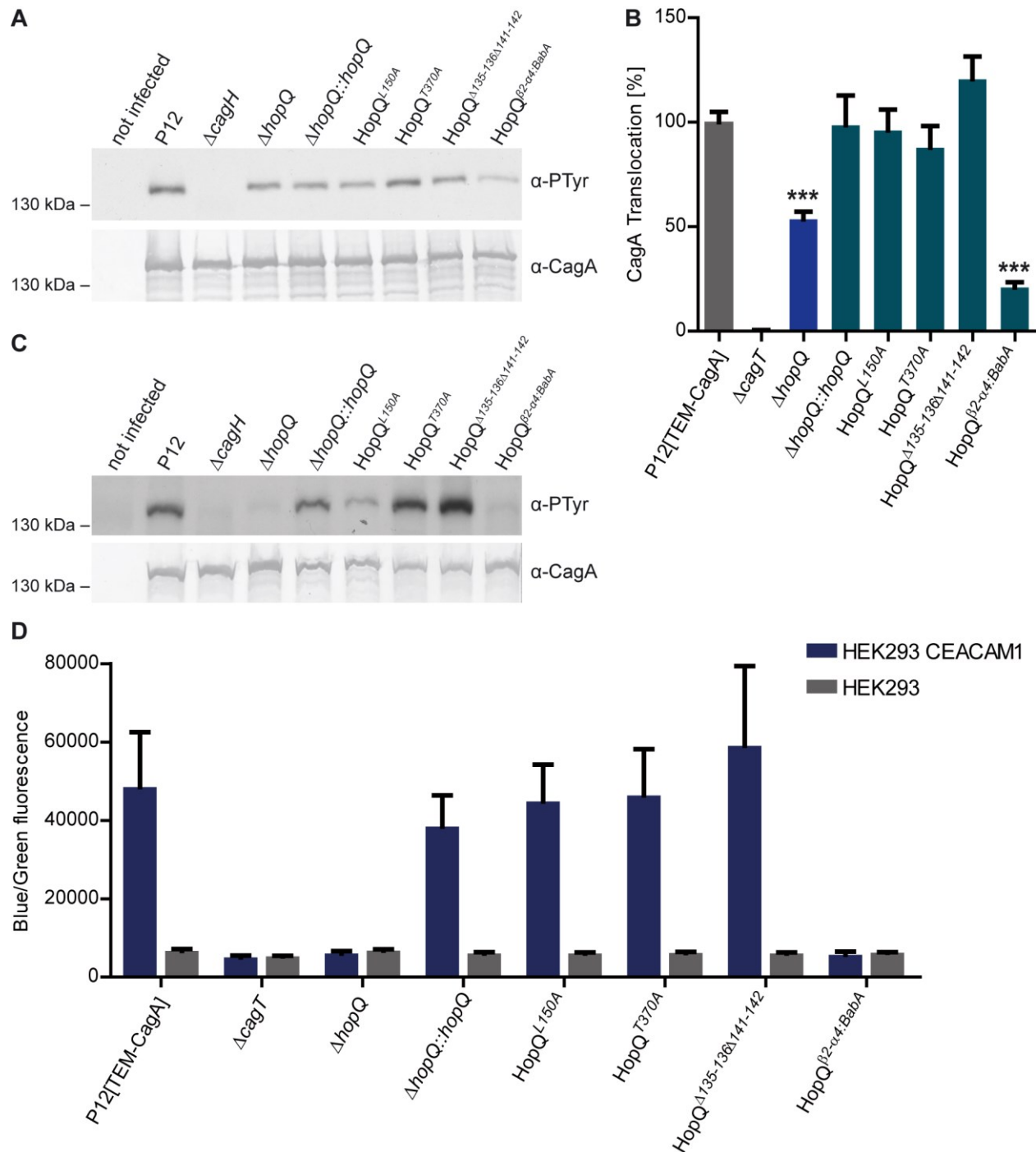


Figure 3.4: Effects of targeted mutations in HopQ on CagA translocation.

(A) An *in vitro* infection of AGS cells with P12 or defined *hopQ* mutant strains was analyzed by Western blot. Phosphorylated CagA was detected with PY99 (Santa Cruz). After stripping, the blot was probed for CagA (AK299). As expected, CagA showed a band at ~ 135 kDa.

(B) CagA translocation in AGS cells of P12[TEM-CagA] and defined *hopQ* mutant strains was quantified using the TEM-1 β -lactamase assay. Values are displayed as mean \pm SEM. A translocation deficient Δ *cagT* mutant was used as a negative control. Statistics were calculated by one-way ANOVA with Dunnett's Multiple Comparison test. n=6. * p < 0.05, ** p < 0.01, *** p < 0.001.

(C) HEK293 CEACAM1 were infected with P12 and defined *hopQ* mutant strains. Phosphorylation of CagA was detected by Western blot (PY99, Santa Cruz). After stripping, CagA was detected with AK299. As expected, CagA showed a band at \sim 135 kDa.

(D) CagA translocation of P12[TEM-CagA] and the defined *hopQ* mutants in HEK293 and HEK293 CEACAM1 cells was analyzed by TEM-1 β -lactamase assay. Results are depicted as mean \pm SEM. n=4.

3.1.4 Influence of a *babC* deletion on CagA translocation

The deletion of *hopQ* results in a 50 % reduction of CagA translocation in AGS cells, in KatolIII cells, however, translocation is almost exclusively dependent on the HopQ-CEACAM interaction, indicating that AGS cells express another receptor exploited by *H. pylori*, which KatolIII cells lack (Königer *et al.*, 2016). KatolIII is another gastric carcinoma cell line, which is frequently used in *H. pylori* research (Sekiguchi *et al.*, 1978). Therefore, the comparison of CagA translocation in AGS and KatolIII cells might contribute to finding the remaining adhesin-receptor pairs impacting CagA injection.

RNA-Seq analysis was performed to identify other up- or downregulated adhesins in an *H. pylori* P12 wildtype strain compared to an isogenic *hopQ* deletion strain (Figure 3.5 A). Indeed, one significant differentially expressed gene (DEG) was *babC-1*, which encodes a putative adhesin in the Bab adhesin family. In strain P12, this gene probably arose from a *babB* duplication in P12 (Königer, 2015). Therefore, the *babC* gene was deleted in P12[TEM-CagA] and CagA translocation was measured in both AGS and KatolIII cells (Figure 3.5 B, C). In addition, a Δ *babC* Δ *babB* double deletion mutant was generated and translocation was measured in AGS cells.

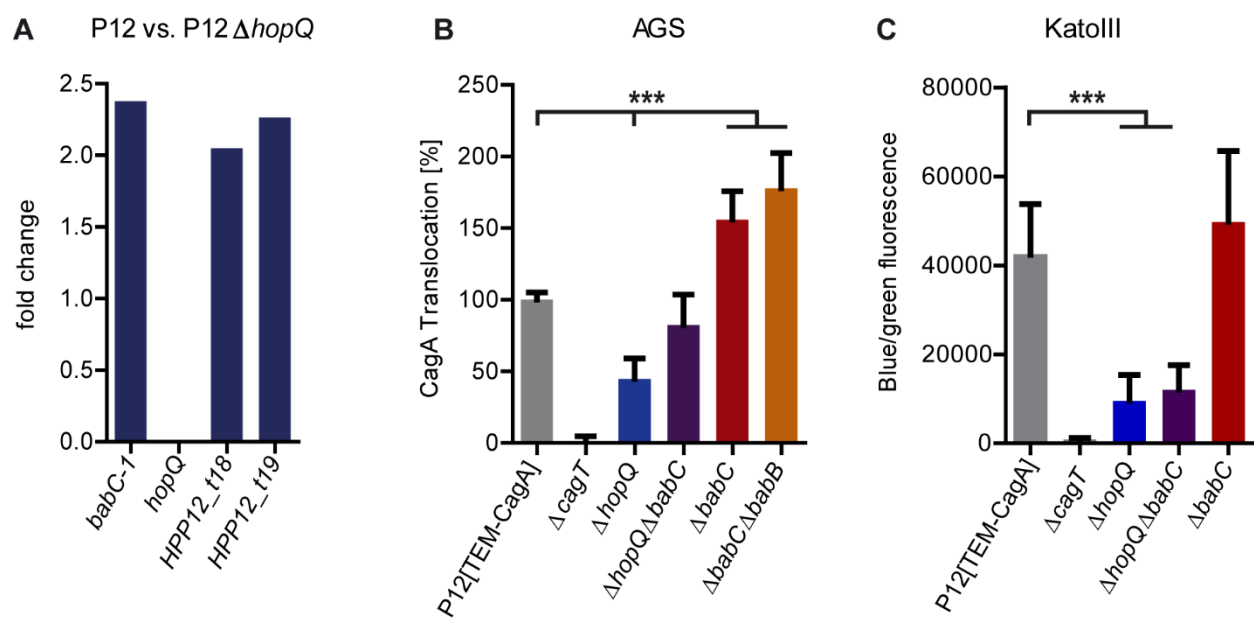


Figure 3.5: Results of RNA-Seq and TEM-assay data for P12 vs. P12 Δ hopQ.

(A) DEGs in P12 vs P12 Δ hopQ.

(B) CagA translocation data of *hopQ*, *hopQ/babC*, *babC* and *babC/babB* deletion mutants were generated using the TEM-1 β -lactamase translocation assay. A Δ cagT mutant was used as a negative control. Results are depicted as mean \pm SD (standard deviation). Statistics were calculated by one-way ANOVA with Dunnett's Multiple Comparison test. $n \geq 4$ (B), $n=6$. * $p < 0.05$, ** $p < 0.01$, *** $p < 0.001$, no asterisk = not significant.

Interestingly, deletion of *babC* resulted in an increase of CagA translocation to about 150 % in AGS cells (Figure 3.5 B, red bar). Double knockout of *babC* and *hopQ* (purple bar) led to almost wildtype translocation rates. Deletion of both *babC* and *babB* again resulted in increased translocation of about 170 %. In contrast, Δ hopQ Δ babC had similar translocation levels as a *hopQ* deletion alone in KatolIII cells. *BabC* deletion had no influence on translocation in KatolIII cells (Figure 3.5 C). Further analysis of the RNA-Seq data is described in chapter 3.2.2.3.

3.1.5 CagY as a possible interaction partner of HopQ

Another possibility for how HopQ impacts CagA translocation, could be an interaction of the adhesin with the Cag-T4SS. This hypothetical interaction of HopQ with one or more components of the Cag-T4SS could be one mechanism to prime the secretion apparatus for CagA translocation into the host cell.

At first, interaction partners of HopQ were tried to be identified using the Bacterial Two Hybrid system (data not shown). As it was difficult to express some *H. pylori* proteins in *E. coli*, other methods were used.

Immunoprecipitation is a useful tool to analyze protein-protein interactions. For this purpose, a HopQ containing a myc-tag was constructed and expressed in a P12 Δ hopQ strain (Figure 3.6 B). The myc-tag was inserted between the first part of the β -barrel (transmembrane domain) and the extracellular domain (Figure 3.6 A). To verify expression of this construct, Western blots were performed (Figure 3.6 C). Similar amounts of HopQ were detected in both P12 wildtype and HopQ^{Myc}. An infection of AGS cells and subsequent Western blotting to detect phosphorylated CagA was performed to ensure functionality of HopQ^{Myc} (Figure 3.6 D).

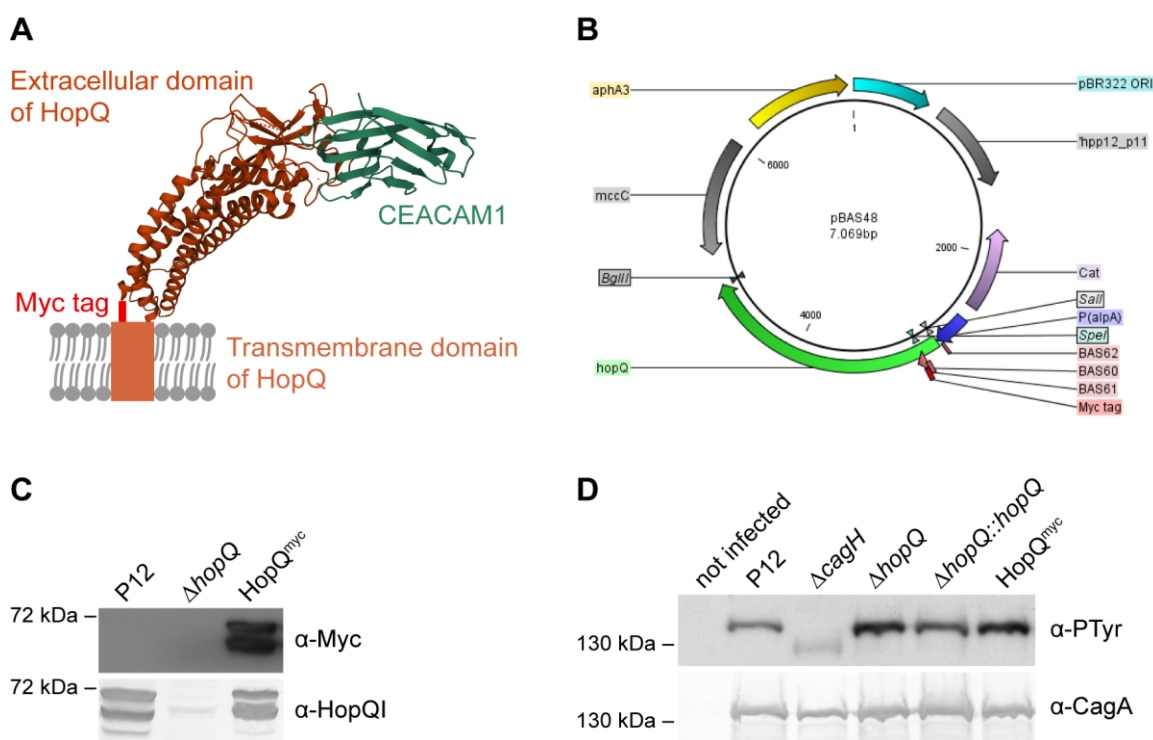


Figure 3.6: Generation of HopQ^{Myc}.

(A) Schematic overview of the HopQ^{Myc} structure with a myc-tag inserted between the transmembrane and the extracellular domain. Adapted from Bonsor, *et al.* (2018) (PDB ID 6AW2).

(B) Plasmid map of pBAS48 encoding HopQ^{Myc}.

(C) Detection of HopQ^{Myc} expression by Western blotting was performed using an α -myc (9B11, Cell Signaling) and an α -HopQI (AK298) antibody.

(D) CagA phosphorylation was analyzed by Western blotting using antibodies α -PTyr (PY99, Santa Cruz) and α -CagA (AK299). AGS cells were infected with P12, P12 Δ cagH (negative control), P12 Δ hopQ, P12 Δ hopQ::hopQ and HopQ^{Myc}.

With the HopQ^{Myc} strain, immunoprecipitation experiments were performed using an α -myc-tag antibody. Different components of the Cag-T4SS, for which antibodies were available, were analyzed to test for an interaction between HopQ and this protein. Only CagY showed a band in the pull-down sample of HopQ^{Myc}, suggesting a possible interaction between HopQ and CagY. In addition, a reverse immunoprecipitation experiment was performed using an α -CagY antibody to precipitate HopQ^{Myc}. To control for unspecific binding, a HopQ^{Myc} Δ cagY strain was generated. Again, only in the HopQ^{Myc} strain sample, HopQ was detected, which confirmed an interaction between CagY and HopQ.

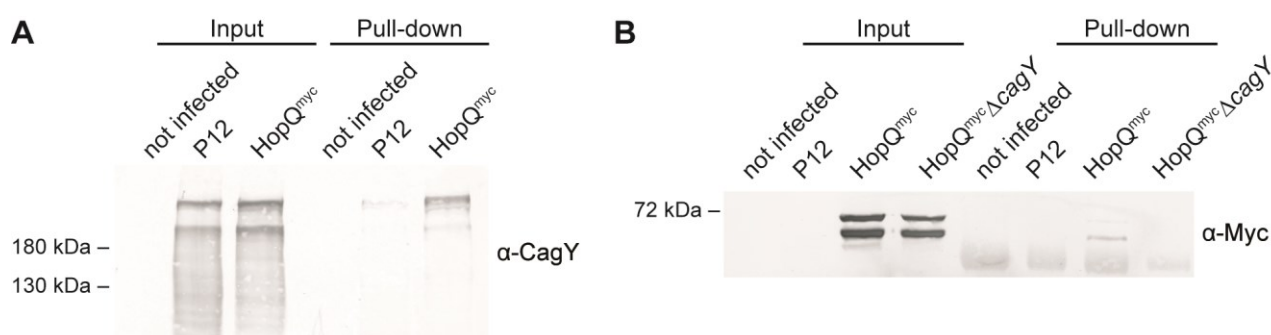


Figure 3.7: Pull-down assays with HopQ^{Myc}.

(A) AGS cells were infected with P12 and the P12 HopQ^{Myc} strain. After lysis, immunoprecipitation was performed using an α -myc antibody (9B11, Cell signaling). Western blot was done using an α -CagY antibody (AK273).

(B) AGS cells were infected with P12, HopQ^{Myc} strain and HopQ^{Myc} Δ cagY. An α -CagY antibody (AK273) was used for pull-down and Western blotting was performed with an α -myc antibody (9B11, Cell signaling), resulting in a band at \sim 70 kDa representing the HopQ^{Myc} protein. One representative image of at least three independent experiment is shown.

For further verification of a HopQ-CagY interaction, immunoprecipitations with different CagY constructs were performed. The CagY Δ MMR::Myc strain is a P12 strain, in which the middle repeat region (MMR) was deleted and replaced by a myc-tag (Figure 3.8 B). Furthermore, in the CagY^{S1MC1} strain, a myc-tag was inserted before the putative second transmembrane region (Figure 3.8 C). The CagY^{S1MC2} strain carries a deletion in the putative integrin-interaction loop (aa 1776-1784), instead containing a myc-tag in this position (Figure 3.8 D). With these modified CagY proteins it was tested, whether the surface localization of CagY was necessary for its interaction with HopQ. Expression of these CagY variants was verified by Western blot (Figure 3.8 E). In contrast to the CagY^{S1MC1} strain, the CagY^{S1MC2} strain was no longer capable of translocating CagA into the host cell (data not shown), suggesting that the putative interaction loop is necessary for successful CagA translocation. Immunoprecipitation experiments were performed with these

modified *H. pylori* P12 strains using an α -myc antibody (Figure 3.8 F). Even though HopQ could be detected in all samples, the precipitated protein amount was slightly elevated in the CagY^{S1MC1} strain, compared to the CagY ^{Δ MMR::Myc} or the CagY^{S1MC2} strain, implicating that a functional CagY protein with a correct insertion into the outer membrane supports interaction with HopQ. However, interaction of HopQ with CagY^{S1MC2} may be possible after lysis of the bacteria before the pull-down assay.

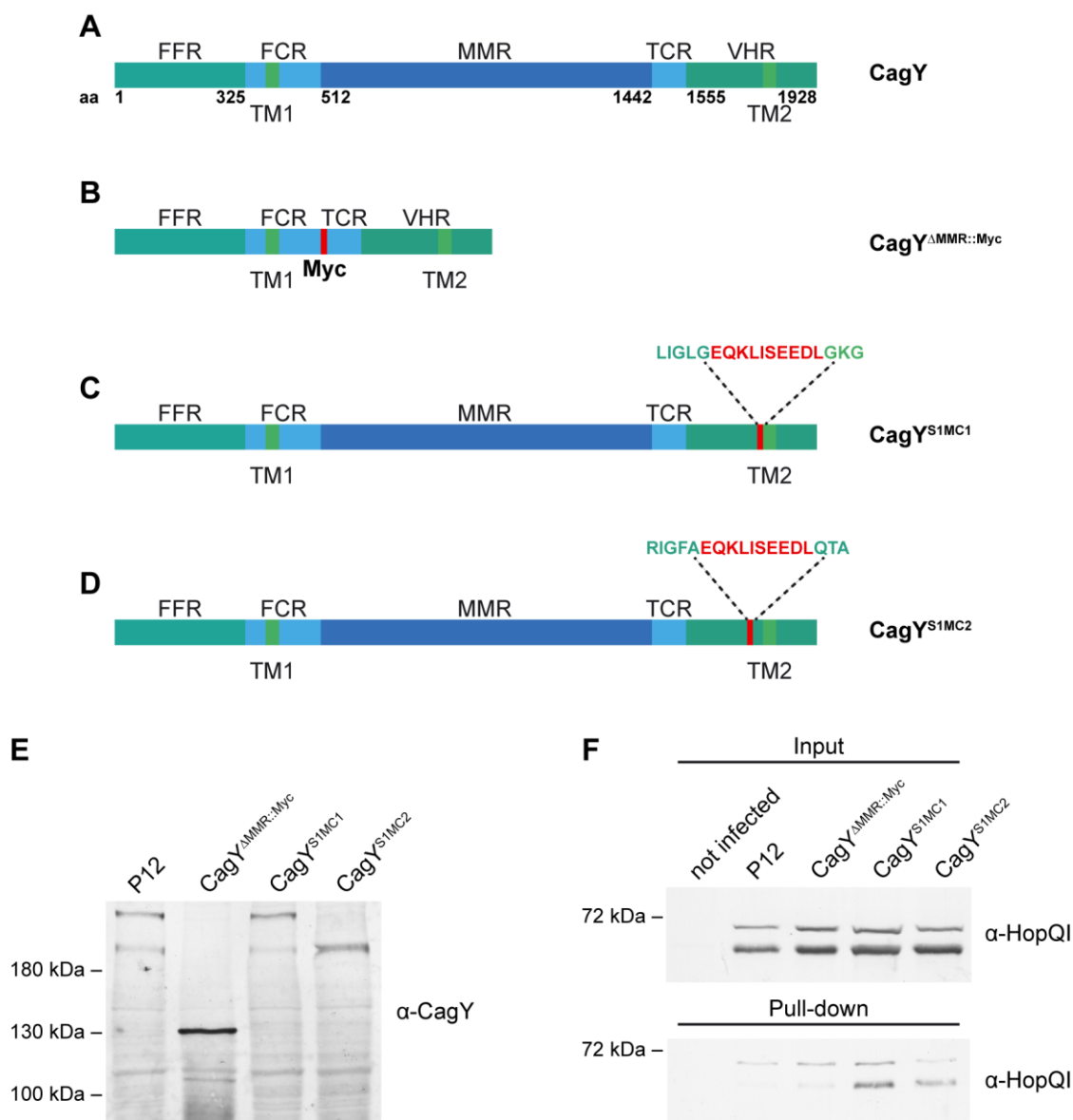


Figure 3.8: Pull-down assays using different CagY constructs.

(A-D) Schematic overview of the domains of CagY wildtype (A), CagY Δ MMR::Myc (B), CagY^{S1MC1} (C), and CagY^{S1MC2} (D). FRR: 5'-repeat region (aa 1-325); FCR: 5'-conserved region (aa 326-511); TM1: transmembrane region 1 (aa 342-362); MMR: middle repeat region (aa 512-1442); TCR: 3'-conserved region (aa 1443-1554); TM2: Transmembrane region 2 (aa 1798-1818); VHR: VirB10 homology region (aa 1555-1928). CagY wildtype domains (Liu *et al.*, 1999). CagY Δ MMR::Myc was constructed by K. Gramlich (B), CagY^{S1MC1} (C) and CagY^{S1MC2} (D) were constructed by A. Debowski.

(E) Western blot using α -CagY (AK280) to show expression of different CagY variants. CagY Δ MMR::Myc had a lower mass (~ 130 kDa) than P12 wildtype. CagY^{S1MC1} showed a similar molecular weight as wildtype, in contrast to CagY^{S1MC2} strain, which lacked the upper of the two CagY bands.

(F) AGS cells were infected with P12, CagY Δ MMR::Myc, CagY^{S1MC1} and CagY^{S1MC2} strains. Immunoprecipitation was performed using an α -myc antibody (9B11, Cell signaling) and Western blot was developed using α -HopQ (AK298) antibody, resulting in a band at ~ 70 kDa. One representative image of at least three independent experiments is shown.

For further analysis of this putative interaction, establishing the NanoBiT protein-protein interaction system (Promega) was attempted. This system is based on a split luciferase complementation reporter system composed of Large BiT (LgBiT) and a small peptide, Small BiT (SmBiT), which has been optimized to have low affinity for LgBiT. Therefore, LgBiT and SmBiT have to be in close contact to form a functional luciferase. Tagging the proteins of interest with LgBiT and SmBiT allows detection of protein-protein interactions. Unfortunately, the expression of the necessary HopQ and CagY fusion proteins were not successful due to technical reasons (data not shown).

3.2 OMP knockout mutants

3.2.1 Construction of multiple *H. pylori* OMP knockout strains

As mentioned previously, disruption of the HopQ-CEACAM interaction results in a reduction of CagA translocation to about 50 % in AGS cells. RNA-Seq analysis of P12 Δ hopQ did not reveal, which other adhesins might be responsible for the remaining 50 % CagA translocation in AGS cells (chapter 3.1.4). To identify the potential additional unknown OMP(s), different adhesin genes were successively deleted in an *H. pylori* P12 strain.

To achieve this, the streptomycin-erythromycin contra-selection method was applied (Figure 3.9). As only few resistance markers are available for *H. pylori*, this method is required for the generation of multiple marker-free knockout mutants. The basis of this method is the streptomycin susceptibility gene (*rpsL^S*) of *Campylobacter jejuni*, which is dominant over the streptomycin resistance (*rpsL^R*) gene. In the first step, a streptomycin resistant *H. pylori* strain was transformed with a plasmid containing an erythromycin (*erm^R*) resistance gene and the *rpsL^S* gene (*rpsL^Serm^R* cassette) flanked by the up- and downstream regions of the gene of interest. By homologous recombination of the up- and downstream flanking regions and selection for erythromycin resistance, the gene of interest is lost and the *rpsL^Serm^R* cassette is integrated into the genome (Figure 3.9, upper row) (Dailidienė *et al.*, 2006).

In the second step, the strain containing the *rpsL^Serm^R* cassette is transformed with a plasmid containing only the flanking regions of the gene of interest. Again, by homologous recombination of the flanking regions, the *rpsL^Serm^R* cassette is lost, resulting in a strain, which is erythromycin sensitive and streptomycin resistant. Using this method repeatedly, multiple adhesin genes can be deleted in the same strain (Figure 3.9, bottom row).

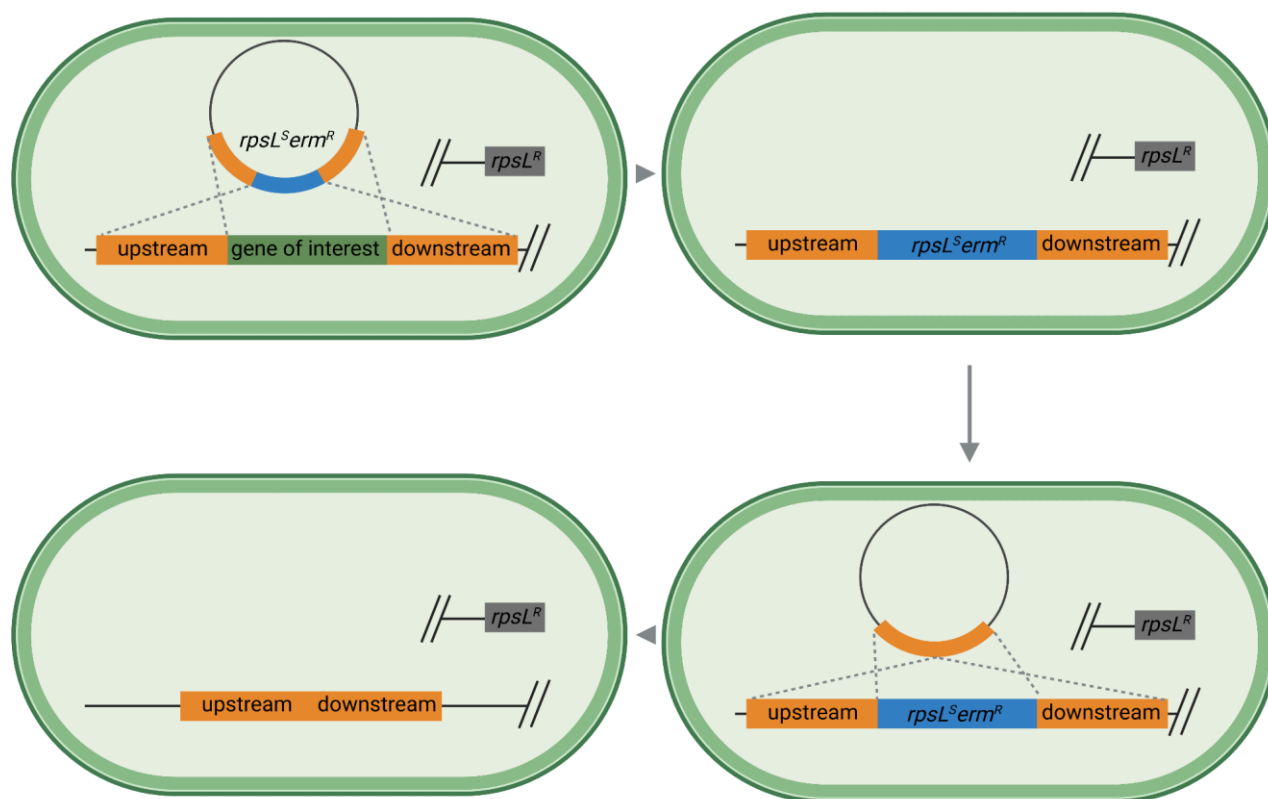


Figure 3.9: Streptomycin-erythromycin contra-selection method to generate marker-free knockout mutants.

Figure was created with Biorender.

Three genes in the putative adhesin branch, *hopM*, *hopN* and *hopA*, were still uncharacterized (Figure 1.2). Therefore, these adhesins were targeted first for knockout. For this, deletion plasmids were cloned and transformed in a streptomycin resistant *H. pylori* P12 strain. Successful knockout clones were screened by amplifying the loci of these genes by PCR (Figure 3.10 B, C, D), as antibodies were not available. Integration of the $rpsL^{Serm^R}$ cassette or marker-free knockout mutants resulted in different sizes of PCR products, as compared to the wildtype P12 strain.

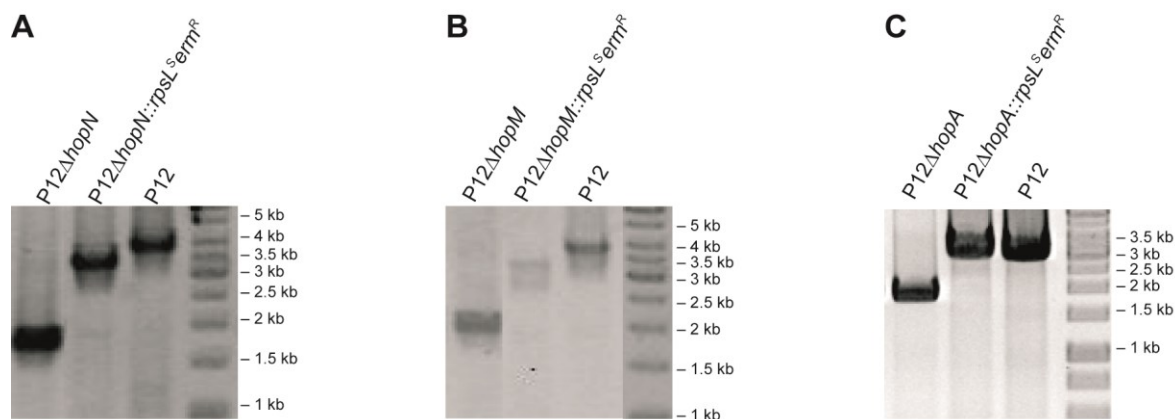


Figure 3.10: Deletion of putative adhesin genes in *H. pylori*.

Verification of *hopN* (A), *hopM* (B), and *hopA* (C) knockout. (A) The PCR product of P12 was 3930 bp, of the P12Δ*hopN*::*rpsL*^{SermR} strain 3434 bp and of the P12Δ*hopN* strain 1886 bp. PCR was performed with primers BAS3/15. (B) PCR was performed with primers BAS 7/10. PCR product length of P12 was 4017 bp, of Δ*hopM*::*rpsL*^{SermR} 3515 bp and of P12Δ*hopM* 1915 bp. (C) The size of the PCR products for strains P12, P12Δ*hopA*::*rpsL*^{SermR} and P12Δ*hopA* were 3346 bp, 3462 bp, and 1922 bp, respectively. PCR was performed using primers BAS 11/14.

After successful generation of Δ*hopN*, Δ*hopM* and Δ*hopA* knockouts, they were screened for their effect on CagA translocation, phosphorylation and adhesion to the host cells. To quantify CagA translocation, the TEM-1 β-lactamase translocation assay was used. For this, the corresponding genes were also deleted in the P12[TEM-CagA] strain. Unexpectedly, none of the knockout mutations had a significant effect on CagA translocation, as tested by two independent assays (CagA phosphorylation assay (Figure 3.11 C) and TEM-1 β-lactamase assay (Figure 3.11 A)). Since the individual gene deletions showed no phenotype, additional outer membrane proteins were deleted in the same strain. First, a Δ*hopN*Δ*hopM* double deletion strain was generated, but its capacity for CagA translocation or phosphorylation was unchanged. The additional deletion of the *hopQ* gene resulted in a 50 % reduction in CagA translocation, which is in accordance with a single Δ*hopQ* knockout. Incremental knockout of other adhesins (OipA and BabA) had no additional effect on CagA translocation, remaining at about 50 % compared to the wildtype strain. These results were also confirmed by a tyrosine phosphorylation assay, showing no decrease in CagA phosphorylation in AGS cells infected with these multiple knockout strains (Figure 3.11 C). Additionally, CagA translocation was measured in KatIII cells. The Δ*hopA* and Δ*hopM* mutation showed no influence on CagA translocation into KatIII cells, whereas Δ*hopN* and the double knockout Δ*hopN*Δ*hopM* showed a slight, but significant reduction in CagA translocation. The triple knockout of Δ*hopN*Δ*hopM*Δ*hopQ*, however, showed a dramatic reduction of CagA injection, in accordance with the effect of a single *hopQ* deletion (Figure 3.11 B).

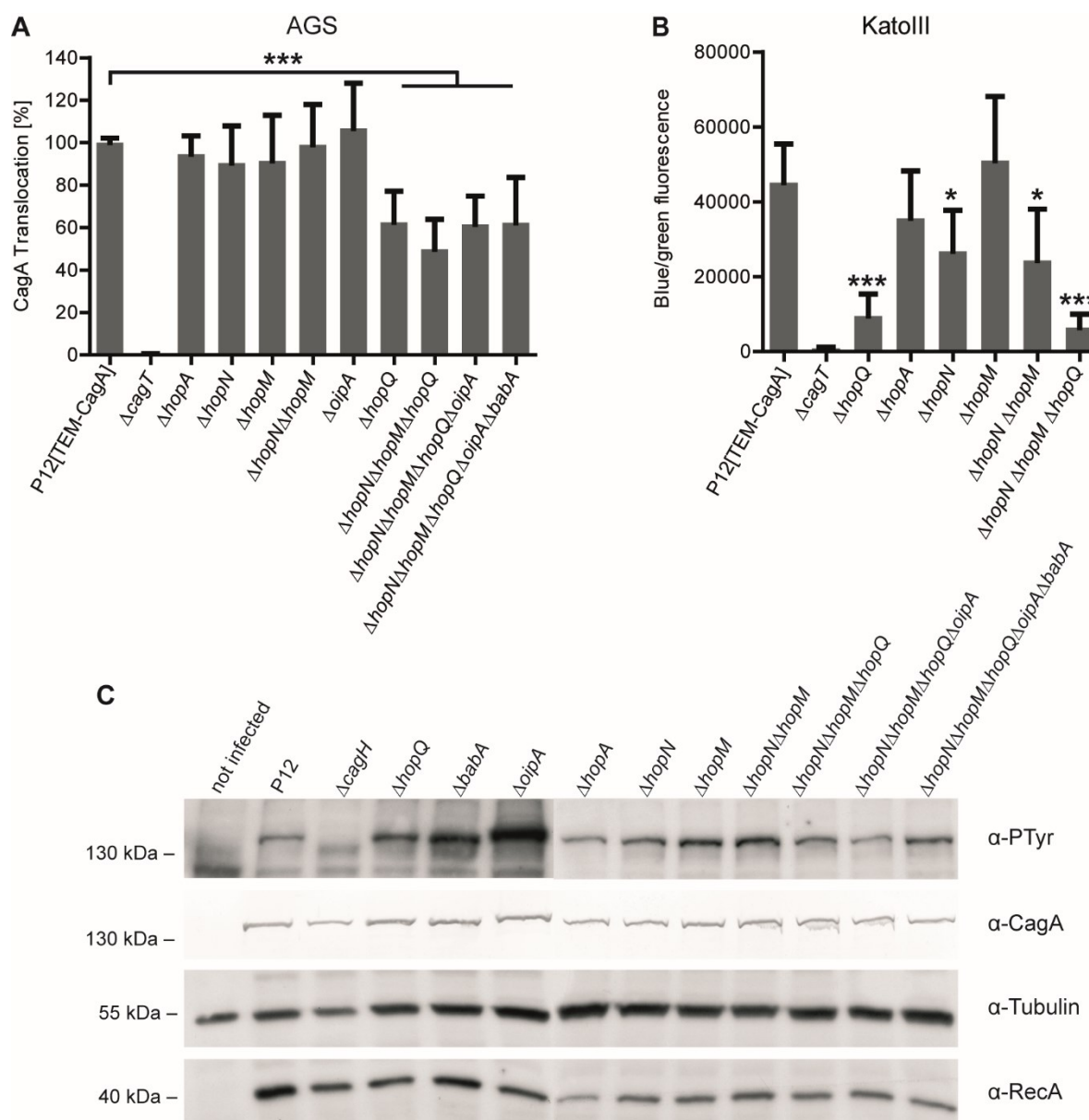


Figure 3.11: Influence of multiple OMP deletions on CagA translocation.

(A, B) CagA translocation into AGS (A) and KatolIII (B) was measured using the TEM-1 β -lactamase translocation assay. Results are shown as mean \pm SD. The translocation deficient $\Delta cagT$ mutant was used as a negative control. Statistical analysis was performed using One-way ANOVA with Dunnett's Multiple Comparison *post hoc* test. $n=7$ (except $\Delta hopA$ $n=3$) (A), $n\geq 4$ (B), * $p<0.05$, ** $p<0.01$, *** $p<0.001$.

(C) An *in vitro* infection of AGS cells was examined by Western blot. An α -PTyr antibody was used to detect phosphorylated CagA. As a loading control for cells and bacteria respectively, detection was performed with an α -CagA antibody (AK299), as well as an α -tubulin and an α -RecA (AK263) antibody. As expected, RecA was detected at ~ 40 kDa, Tubulin at ~ 55 kDa and CagA at ~ 135 kDa. One representative image of three independent experiments is shown.

Deletion of either *babA*, *hopA*, or *oipA* genes had no influence on adhesion (Figure 3.12 A). *HopQ* and *hopN* deletion, however, showed slight reduction in adhesion. Deletion mutants lacking multiple adhesins ($\Delta\text{hopN}\Delta\text{hopM}\Delta\text{hopQ}\Delta\text{oipA}\Delta\text{babA}$) showed an even further reduction in adhesion. Adhesion to KatolIII cells was significantly reduced in the *hopQ* mutant as well as in the triple knock out mutant ($\Delta\text{hopN}\Delta\text{hopM}\Delta\text{hopQ}$), which was not surprising, considering the significant reduction in CagA translocation by these mutants into KatolIII cells (Figure 3.11 B). P12 $\Delta\text{hopN}\Delta\text{hopM}$ showed also a slight reduction in adhesion, which could explain the slight reduction in CagA translocation by this mutant (Figure 3.11 B). However, deletion of *hopA*, *hopN* or *hopM* alone had no impact on adhesion to KatolIII cells (Figure 3.12 B).

Taken together, none of these uncharacterized putative adhesins (*hopN*, *hopM* or *hopA*) seemed to have a significant impact on CagA translocation, phosphorylation or adhesion in AGS cells. However, HopN seemed to contribute to CagA translocation and, in combination with the *hopM* gene, to adhesion in KatolIII cells.

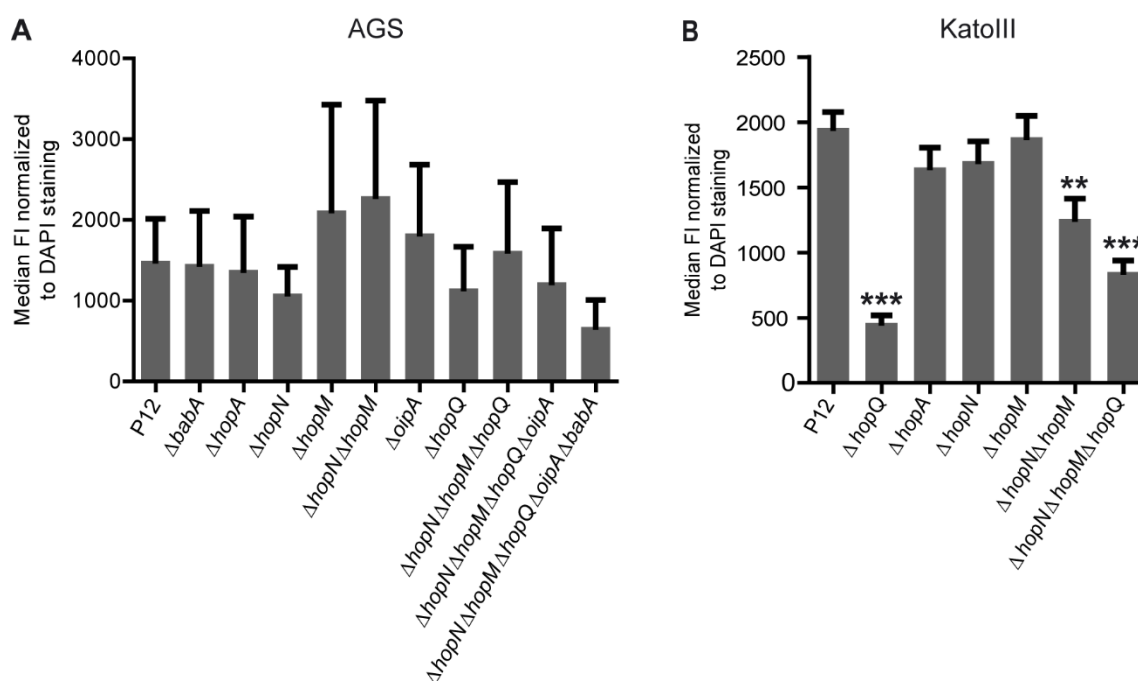


Figure 3.12: Influence of multiple OMP deletions on adhesion.

Adhesion of OMP deletion strains to AGS (A) and KatolIII cells (B) was analyzed by flow cytometry. Results are shown as mean \pm SEM. Statistical analysis was performed using One-way ANOVA with Dunnett's Multiple Comparison *post hoc* test. No statistical significance was observed in adhesion to AGS cells (A). $n \geq 2$ (A), $n \geq 4$ (B), * $p < 0.05$, ** $p < 0.01$, *** $p < 0.001$.

Since there is a high genetic variation between different *H. pylori* strains, *hopA*, *hopM* and *hopN* genes were also deleted in G27[TEM-CagA] and translocation in AGS as well as KatolIII cells was quantified using the TEM-1 β -lactamase assay (Figure 3.13). In contrast to strain P12, the *hopN* knockout in strain G27 had no influence on translocation into AGS or Kato cells. In AGS cells, neither the $\Delta hopA$ nor the $\Delta hopM$ knockout showed a significant difference in CagA injection compared to wildtype (Figure 3.13 A). In contrast, the deletion of *hopA* showed a slight, but significant reduction in KatolIII cells, whereas the deletion of *hopM* again showed no impact (Figure 3.13 B).

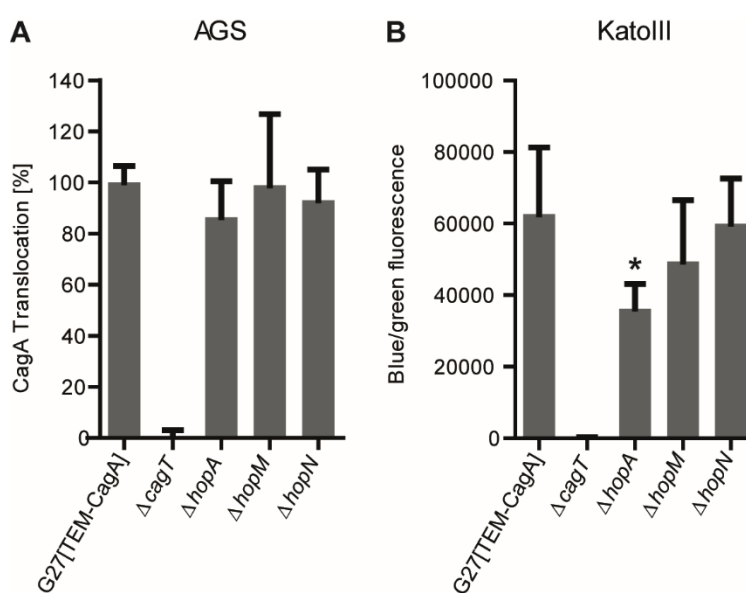


Figure 3.13: Influence on CagA translocation of *hopA*, *hopM* and *hopN* deletion in G27.

CagA translocation was measured using the TEM-1 β -lactamase assay in either AGS (A) or KatolIII (B) cells. The translocation deficient $\Delta cagT$ mutant was used as a negative control. Results are shown as mean \pm SD. Statistical analysis was performed using One-way ANOVA with Dunnett's Multiple Comparison *post hoc* test. n=5 (A, B), * p<0.05, ** p<0.01, *** p < 0.001.

3.2.2 Deletion of adhesin genes *alpA* and *alpB* in different *H. pylori* strains

3.2.2.1 Effect of *alpAB* deletion in *H. pylori* P12

Knockout of the remaining adhesin genes of the putative adhesin branch revealed no additional adhesin influencing CagA translocation to a similar extent as *hopQ*. Thus, OMPs outside of the putative adhesin branch were also taken into consideration (Figure 1.2). Even though the interaction of *alpA* and *alpB* with their receptor laminin is already well established (Senkovich *et al.*, 2011), the effect of these outer membrane proteins on CagA translocation is not well understood.

To elucidate the effect of an *alpAB* deletion on CagA injection, a plasmid containing the flanking regions of *H. pylori* P12 of the *alpAB* gene locus was cloned and deletion mutants were generated (Figure 3.14 A). Deletion and subsequent complementation of the *alpA* and *alpB* genes was additionally verified by Western blot (Figure 3.14 B).

The deletion of *alpAB* in P12 had an unexpected effect on translocation of CagA into AGS cells by the corresponding strains, as shown by the CagA phosphorylation assay (Figure 3.15 C). AGS cell infection experiments using these *H. pylori* strains led to an increase of CagA phosphorylation, which was reversed by genetic complementation ($\Delta alpAB::alpAB$). To quantify this effect, a deletion mutant was also generated in the P12[TEM-CagA] strain and TEM-1 β -lactamase translocation assays were performed (Figure 3.14 E). Compared to wildtype, CagA translocation was increased to about 150 % when an *alpAB* deletion strain was used (dark green bar). This effect was reversed by an additional knockout of *hopQ* ($\Delta alpAB\Delta hopQ$; turquoise bar), which resulted in similar translocation levels as the wildtype strain. Plasmid-mediated complementation of *alpAB* resulted in a decreased translocation efficiency of the strain (light green bar), which may be explained by overproduction of the AlpA and AlpB proteins from the complementation plasmid (Figure 3.14 B).

As the effect of an *alpAB* deletion on translocation in AGS cells was so profound, the experiments were repeated using the Kat0III cell line. The increase in CagA phosphorylation in $\Delta alpAB$ was detectable by Western blotting (Figure 3.14 D), therefore quantification of CagA translocation was performed. CagA injection was elevated similarly in Kat0III as in AGS cells with the *alpAB* deletion (Figure 3.14 F; dark green bar). Complementation of *alpAB* resulted in reduced CagA translocation (light green bar), which again could be explained by overproduction of the two proteins (Figure 3.14 B). The $\Delta alpAB\Delta hopQ$ triple gene deletion resulted in a drastic drop in CagA translocation (turquoise bar), which is mostly due to the $\Delta hopQ$ effect (dark blue bar).

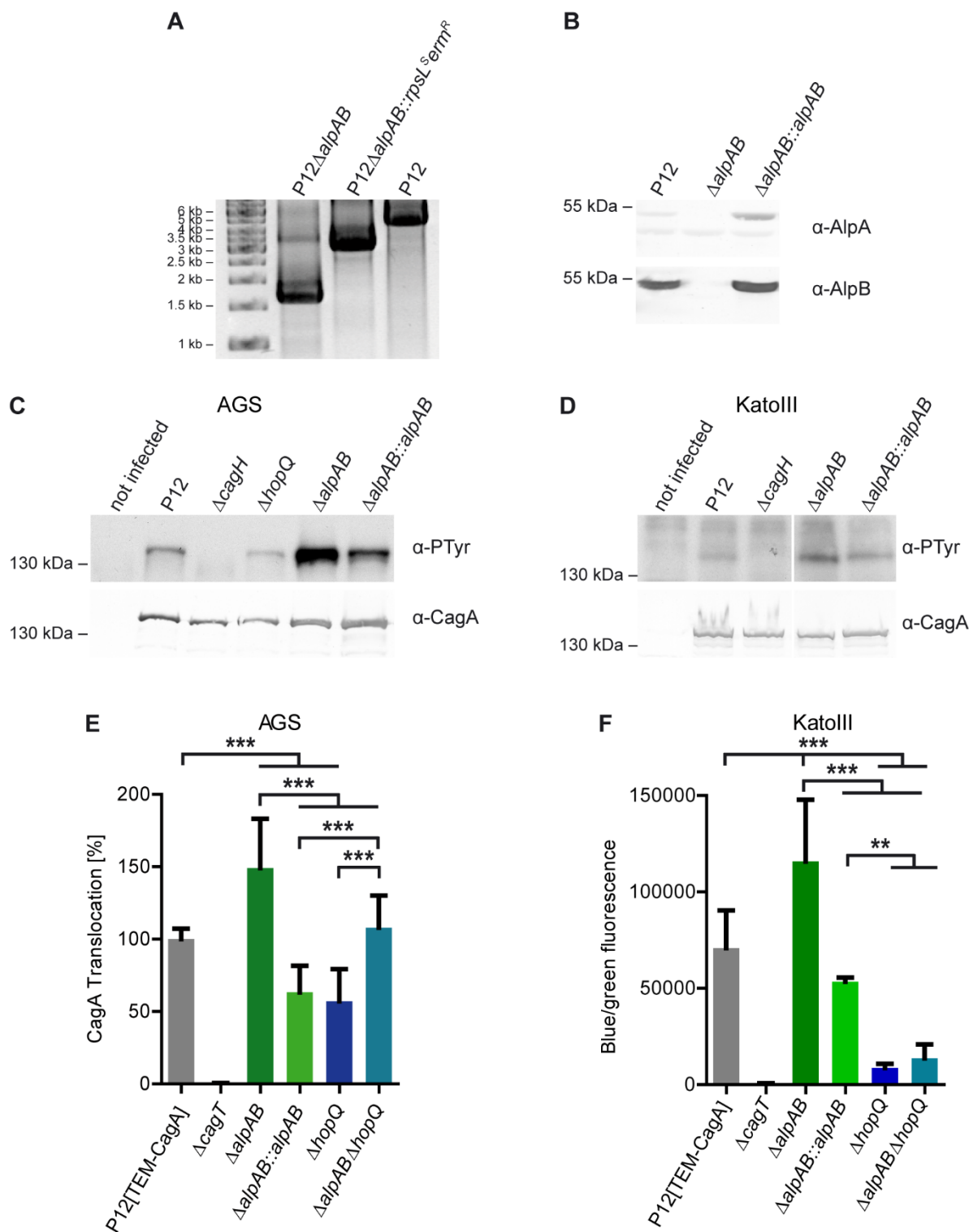


Figure 3.14: Generation of *alpAB* deletion in P12 and the influence on CagA translocation.

(A) PCR of P12 wildtype, P12 Δ *alpAB*::*rpsL*^{SermR}, and P12 Δ *alpAB* using primers BAS16/125 to proof knockout of the *alpA* and *alpB* genes. Length of PCR products were 4789 bp, 3188 bp, and 1648 bp for P12, Δ *alpAB*::*rpsL*^{SermR} and Δ *alpAB* respectively.

(B) Western blot of lysates from P12, $\Delta alpAB$ and $alpAB::alpAB$ using α -AlpA (AK214) and α -AlpB (AK262) antibodies to proof deletion and subsequent complementation of those genes. AlpA and AlpB were detected at approx. 55 kDa.

(C, D) *In vitro* infection of AGS cells (C) or KatolIII cells (D) was analyzed by Western blot for phosphorylated CagA using an α -PTyr antibody (PY99, Santa Cruz). The blot was stripped and re-probed with an α -CagA antibody (AK299). One representative image is shown of at least three independent experiments.

(E, F) CagA translocation of $\Delta alpAB$ strains into AGS cells (E) or KatolIII cells (F) was measured with the TEM-1 β -lactamase assay. The translocation deficient $\Delta cagT$ mutant was used as a negative control. Results are shown as mean \pm SD and statistics were calculated by one-way ANOVA with the *post hoc* Bonferroni's Multiple Comparison test. $n \geq 7$ (E), $n \geq 5$ (F) * $p < 0.05$, ** $p < 0.01$, *** $p < 0.001$.

To further analyze this effect on CagA translocation, adhesion assays using the same deletion mutants were performed. Interestingly, the $\Delta alpAB \Delta hopQ$ triple deletion influenced adhesion to AGS cells (Figure 3.15 A, turquoise bar), resulting in a slight reduction, even though the CagA translocation level of this multiple *omp*-deleted strain was comparable to the wildtype strain. Overall, deletion of *hopQ* or *alpAB* had no influence on adhesion to AGS cells.

In KatolIII cells, *hopQ* deletion reduced adhesion to about half compared to wildtype (Figure 3.15 B; dark blue bar). This result was different from before (Figure 3.12 B), but was probably due to the different methods used to measure adhesion (GFP expressing strains in Figure 3.12 and DAPI staining in Figure 3.15). The triple knockout strain ($\Delta alpAB \Delta hopQ$; turquoise bar) had a significant defect in adhesion compared to the wildtype, even though $\Delta alpAB$ alone showed only a very moderate reduction in adhesion (dark green bar), which was restored by genetic complementation. In conclusion, the effect on adhesion and CagA translocation were not correlated, suggesting that other mechanisms are responsible for the *alpAB* deletion-mediated increase in CagA translocation.

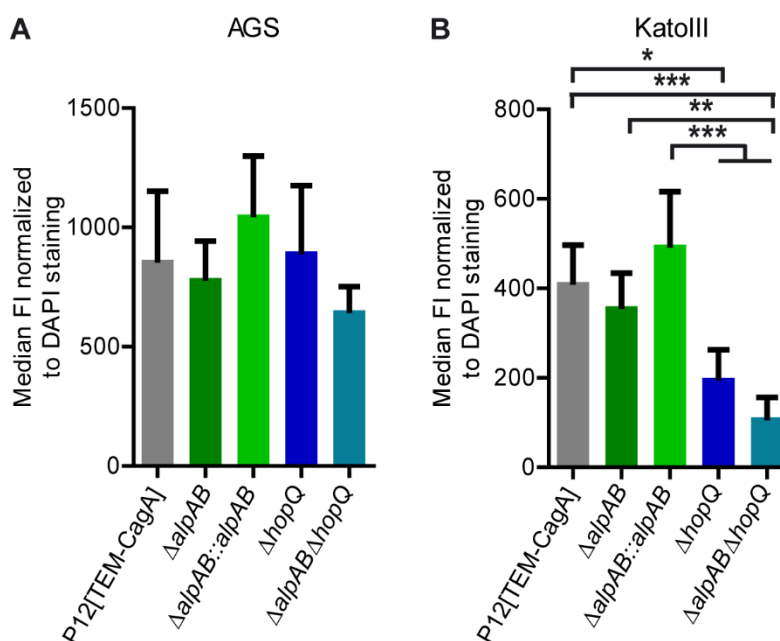


Figure 3.15: The effect of an *alpAB* deletion on adhesion to AGS and KatolIII cells.

(A, B) Adhesion of the different knockout strains to AGS cells (A) and KatolIII cells (B) was measured by flow cytometry. Prior to infection, bacteria were stained with DAPI. Data were analyzed as described above (chapter 2.2.2.3.6). Results are depicted as mean \pm SEM. Statistics was calculated by one-way ANOVA with Bonferroni's Multiple Comparison *post hoc* test. n=3 (A), n=4 (B) * p < 0.05, ** p < 0.01, *** p < 0.001.

The receptor for the AlpA and AlpB adhesins was suggested to be laminin (Senkovich *et al.*, 2011), which is a protein of the extracellular matrix interacting with, amongst others, different integrins (Hall *et al.*, 1990). Thus, CagA translocation was analyzed in KatolIII cell lines, carrying knockouts of different integrin heterodimers. These cells were previously generated using the CRISPR/Cas9 system and either carry a deletion of $\beta 1$ integrin gene only (ITGB1 KO KatolIII, lacking $\alpha 1\beta 1$, $\alpha 2\beta 1$, $\alpha 3\beta 1$, $\alpha 5\beta 1$, $\alpha 6\beta 1$, and $\alpha 9\beta 1$ heterodimers) or a combination of αv , $\beta 1$ and $\beta 4$ integrin genes (ITGA v B1B4 KO KatolIII). The latter KatolIII cell line is therefore devoid of all integrins on the cell surface (Zhao *et al.*, 2018).

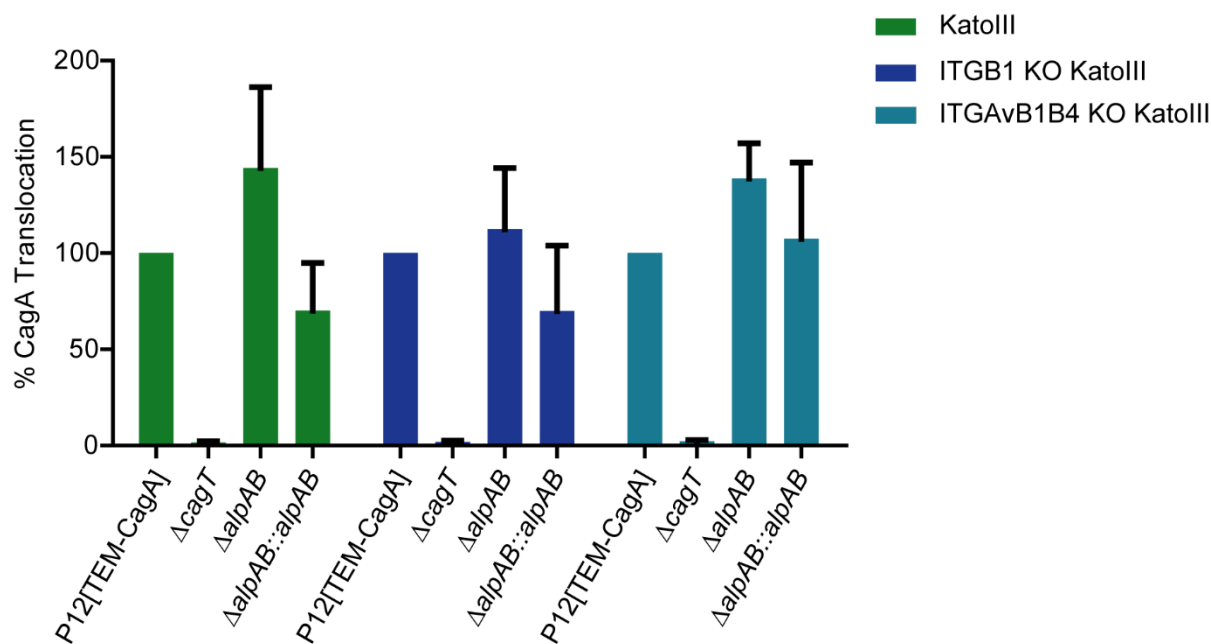


Figure 3.16: Influence of an *alpAB* deletion in P12 on CagA translocation in integrin knockout cell lines.

CagA translocation of P12[TEM-CagA], $\Delta alpAB$, and $\Delta alpAB::alpAB$ in KatolIII wildtype (green), ITGB1 KO KatolIII (blue), or ITGAvB1B4 KO KatolIII (turquoise) cells was measured by flow cytometry using the TEM-1 β -lactamase translocation assay. The translocation deficient $\Delta cagT$ mutant was used as a negative control. Results are depicted as mean \pm SD.

Quantification of CagA translocation in KatolIII, ITGB1 KO KatolIII and ITGAvB1B4 KO KatolIII cells was performed (Figure 3.16). No significant differences were detected in all three cell lines, when infected with an *alpAB* deletion strain, suggesting that the integrin-laminin interaction did not influence CagA translocation.

3.2.2.2 Effect of *alpAB* deletion in G27

Contrary to the findings in this work, a deletion of *alpAB* in *H. pylori* P1 showed an almost complete loss of adhesion to KatolIII cells (Odenbreit *et al.*, 1996). To further analyze these strain specific effects, *alpA* and *alpB* were deleted in a G27[TEM-CagA] strain. Additionally, a $\Delta alpAB::alpAB$ genetic complementation and a $\Delta hopQ$ knockout were generated in the same background. Deletion and complementation of *alpAB* in a G27[TEM-CagA] (Figure 3.17 A) as well as the *hopQ* deletion (Figure 3.17 B) were verified by Western blot.

The impact on CagA translocation was measured by the TEM-1 β -lactamase translocation assay for both AGS and KatolIII cell line. Surprisingly, the $\Delta hopQ$ knockout had no effect on the translocation efficiency of G27 into AGS cells (Figure 3.17 C, blue bar). Additionally, this mutation in G27 resulted in about 30 % CagA translocation efficiency into KatolIII cells (Figure 3.17 D, blue bar), different to a *hopQ* deletion in P12, which reduced CagA translocation efficiency to about 10 % (Figure 3.14 F, blue bar).

In contrast to P12 $\Delta alpAB$ (Figure 3.14 E, dark green bar), the deletion of these outer membrane proteins in a G27 background reduced translocation to about 50 % in AGS cells (Figure 3.17 C, dark green bar). Complementation of the deleted genes led to rescue of this phenotype, as this strain was able to translocate CagA with 100 % efficiency (light green bar). Furthermore, knockout of *alpAB* had a drastic effect on KatolIII cells, reducing CagA translocation significantly (Figure 3.17 D, dark green bar). Complementation of *alpAB* led to a partial restoration of CagA injection (light green bar).

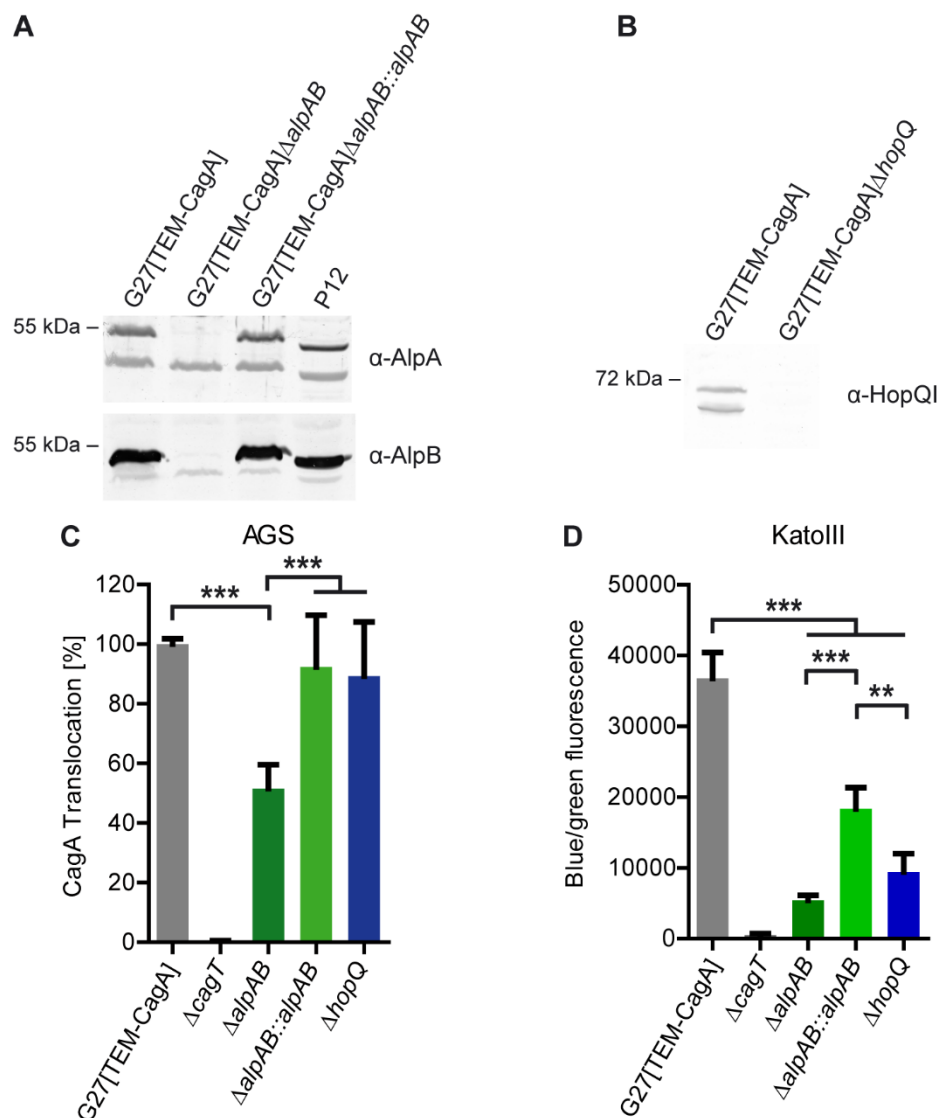


Figure 3.17: Deletion of *alpAB* and *hopQ* in *H. pylori* G27 and the effect on CagA translocation.

(A) Bacterial lysates of G27[TEM-CagA], G27[TEM-CagA]Δ*alpAB*, G27[TEM-CagA]Δ*alpAB*::*alpAB* and P12 were checked for AlpA and AlpB expression using antibodies AK214 (α-AlpA) and AK262 (α-AlpB), resulting in bands at ~ 55 kDa for both proteins.

(B) Proof of HopQ knockout in G27[TEM-CagA] strain. Detection was performed with an α-HopQI antibody (AK298). As expected, HopQ was detected at approx. 70 kDa.

(C, D) CagA translocation of G27[TEM-CagA], Δ*alpAB*, Δ*alpAB*::*alpAB*, and Δ*hopQ* in AGS (C) and KatIII (D) cells was measured using the TEM-1 β-lactamase translocation assay. The translocation deficient Δ*cagT* mutant was used as a negative control. Results are shown as mean ± SD. Statistics were analyzed using one-way ANOVA with a Bonferroni's Multiple Comparison test. n≥6 (C), n=5 (D), * p < 0.05, ** p < 0.01, *** p < 0.001.

For further analysis, the adhesion to AGS and KatolIII cells of these G27 mutant strains was analyzed by flow cytometry (Figure 3.18). The deletion of *alpAB* in G27 had a severe adhesion defect on both AGS and KatolIII cells (Figure 3.18, dark green bar). For AGS cells, adhesion was almost abolished, even though the translocation was still at approx. 50 % (Figure 3.17 C). In KatolIII cells, the adhesion of the same strain was decreased to about a third compared to wildtype (Figure 3.18 B, dark green bar). This phenotype was rescued in both AGS and KatolIII cells by complementation of the *alpAB* genes (Figure 3.18, light green bar). The *hopQ* deletion resulted in no change in adhesion in AGS cells and in a moderate decrease in KatolIII cells (Figure 3.18, blue bar).

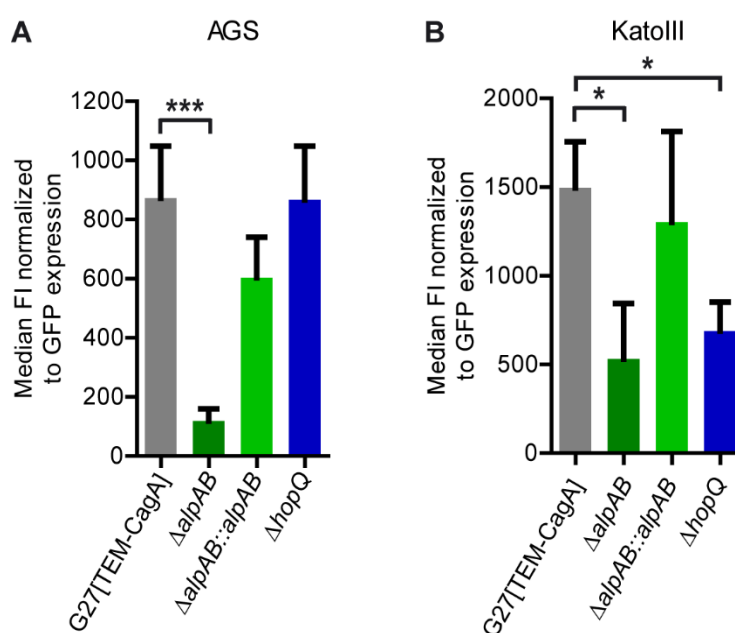


Figure 3.18: Adhesion of G27Δ*alpAB* and Δ*hopQ* to AGS and KatolIII cells.

(A, B) To measure adhesion to AGS (A) and KatolIII cells (B), bacterial strains expressing GFP were used. Data was analyzed as described before (chapter 2.2.2.3.6). Results are depicted as mean \pm SD. Statistics were calculated by one-way ANOVA with Bonferroni's Multiple Comparison as a *post hoc* test. $n \geq 3$ (A), $n = 5$ (B) * $p < 0.05$, ** $p < 0.01$, *** $p < 0.001$.

3.2.2.3 Gene transcription differences between *H. pylori* P12 and G27 by RNA-Seq experiments

To further elucidate the influence of an *alpAB* deletion in P12 on CagA translocation, RNA-Seq experiments were performed. Significant DEGs are depicted in Figure 3.19. For P12 Δ *alpAB*, in addition to *alpA* and *alpB*, only two genes coding for tRNAs were significantly differentially expressed in the deletion mutant compared to the P12 wildtype, providing no indication of the mechanism influencing CagA translocation. Analyzing the RNA-Seq data for all OMPs, no single gene stood out to explain this mechanism (data not shown).

Comparing G27 wildtype to the *alpAB* deletion, more genes were differentially expressed (Figure 3.19 B). In Table 3.1, the function of those genes is described. Most of them play a role in translation, but next to *alpA* and *alpB*, no other *omps* were found to be differentially expressed in the G27 Δ *alpAB* strain.

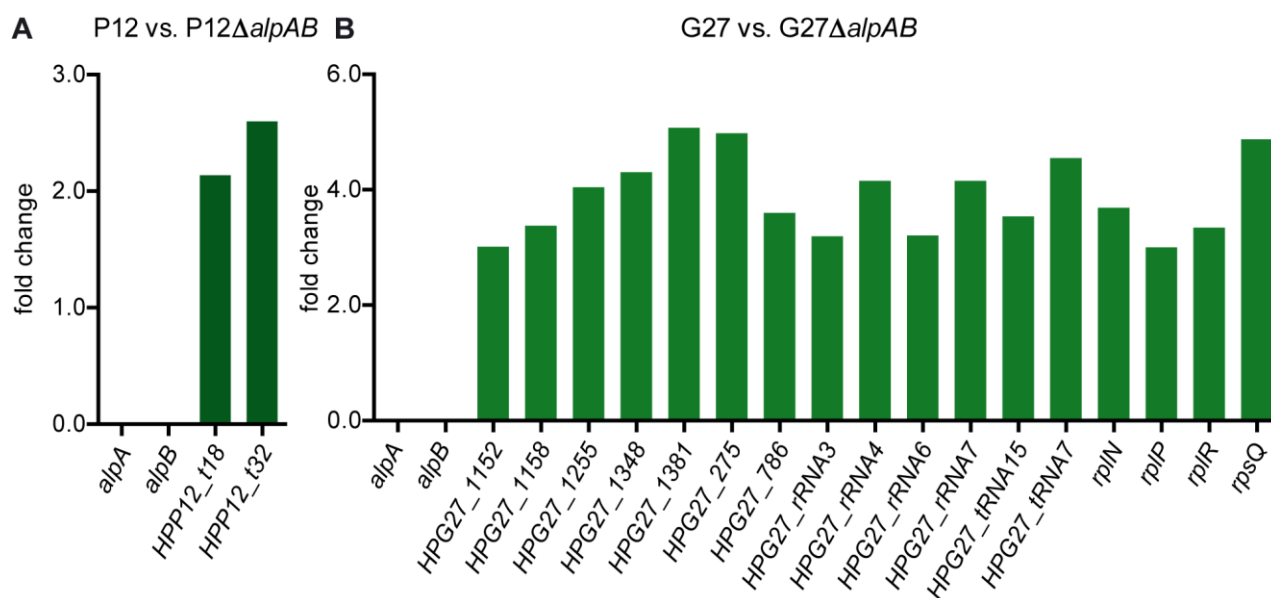


Figure 3.19: DEGs in (A) P12 vs. P12 Δ *alpAB* and (B) G27 vs. G27 Δ *alpAB* according to RNA-Seq results.

In conclusion, new insights into the adhesins AlpA and B were gained in this work. Deletion of *alpAB* in P12 resulted in increased Cag translocation into AGS and KatolIII cells, whereas G27 Δ *alpAB* showed reduced CagA translocation levels. Adhesion of a P12 Δ *alpAB* strain to AGS and KatolIII cells was not significantly changed, but adhesion of G27 Δ *alpAB* to those cells was significantly reduced. These results show that there are strain-specific differences in *H. pylori* regarding their set of expressed adhesins.

Table 3.1: List of differentially expressed genes in G27 vs. G27 Δ *alpAB*

ID	Function
<i>alpA</i>	Adhesin AlpA
<i>alpB</i>	Adhesin AlpB
<i>HPG27_1152</i>	Elongation factor Tu
<i>HPG27_1158</i>	ATP synthase F0, subunit C
<i>HPG27_1255</i>	Ribosomal protein S14
<i>HPG27_1348</i>	Uncharacterized
<i>HPG27_1381</i>	Thioredoxin
<i>HPG27_275</i>	Ribosomal protein L21
<i>HPG27_786</i>	RNA binding protein
<i>HPG27_rRNA3</i>	
<i>HPG27_rRNA4</i>	
<i>HPG27_rRNA6</i>	
<i>HPG27_rRNA7</i>	
<i>HPG27_tRNA15</i>	
<i>HPG27_tRNA7</i>	
<i>rplN</i>	50S ribosomal protein L14
<i>rplP</i>	50S ribosomal protein L16
<i>rplR</i>	50S ribosomal protein L18
<i>rpsQ</i>	30S ribosomal protein S17

3.3 Impact of the human phospholipid scramblase 1 on CagA translocation

In 2010, Murata-Kamiya, *et al.* reported that contact of *H. pylori* with epithelial cells induces externalization of the membrane phospholipid PS. CagA was shown to bind to externalized PS and it was found tethered to the inner leaflet of the plasma membrane in polarized epithelial cells after CagA translocation (Murata-Kamiya *et al.*, 2010). However, it remains unclear, if and how this PS-CagA interaction might be functionally involved in CagA translocation. One possible mechanism could be the exploitation of PLSCR1, a Ca^{2+} responsive, membrane bound protein that flips PS bidirectionally between the membrane leaflets upon activation (Zhao *et al.*, 1998). Other human pathogens, such as herpes simplex virus (HSV) use such a mechanism for entry into their host cells (Cheshenko *et al.*, 2018). During this process, Akt is also translocated to the outer leaflet of the membrane. Akt1 plays a role in *H. pylori* infection, as it is phosphorylated upon contact of the bacteria with the host cell (Sokolova *et al.*, 2014). Therefore, we investigated a potentially new mechanism for delivery of CagA involving PLSCR1 and Akt.

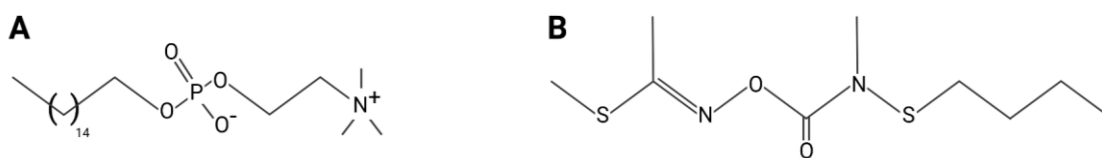


Figure 3.20: Structure of miltefosine (A) and R5421 (B). Figure was created with Biorender.

To verify this, two commercially available inhibitors for Akt1 and PLSCR1 were used. Miltefosine is a drug available for treatment of leishmaniasis and blocks phosphorylation of Akt (Figure 3.20 A) (Ruiter *et al.*, 2003). R5421 (Figure 3.20 B) is a specific scramblase inhibitor (Dekkers *et al.*, 1998) and is used frequently to study the role of scramblase, *e.g.*, in the placenta (Berghold *et al.*, 2015), in virus-host interactions (Cheshenko *et al.*, 2018, Younan *et al.*, 2018) and erythrocytes (Wesseling *et al.*, 2016).

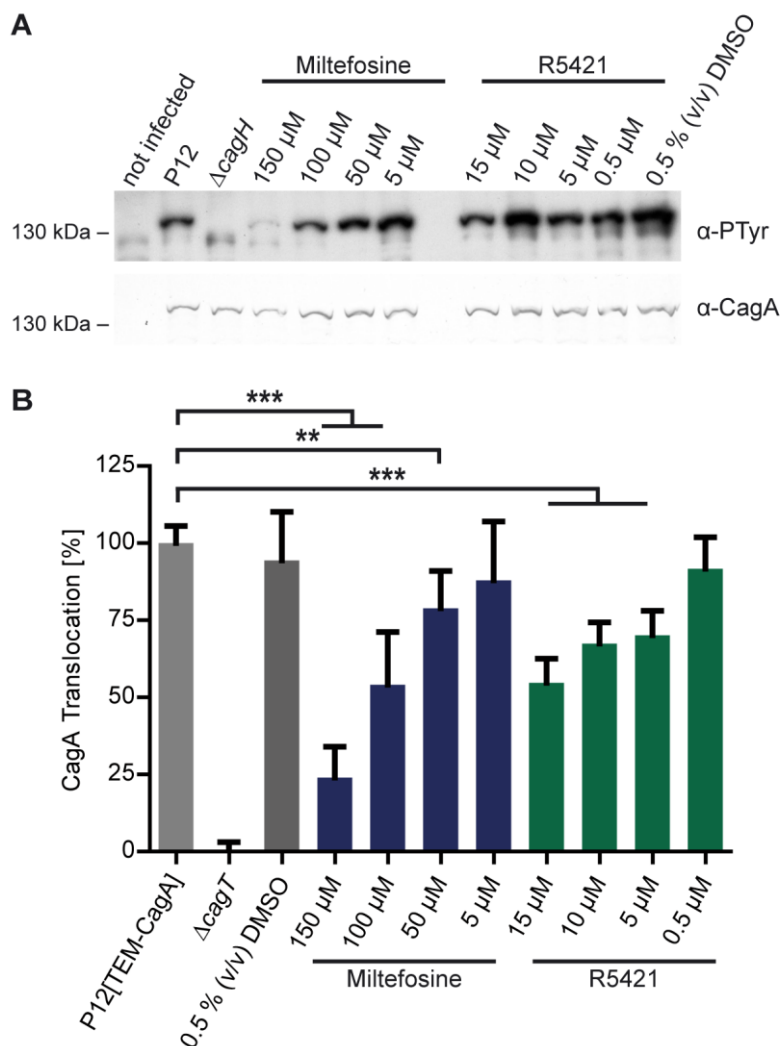


Figure 3.21: Influence of Akt1 and PLSCR1 inhibitors on CagA translocation.

(A) Different concentrations of miltefosine or R5421 were added to *in vitro* infections of AGS cells with P12. Phosphorylated CagA was detected using an α -PTyr (PY99, Santa Cruz) antibody and CagA was detected using AK299 antibody, showing a specific band at \sim 135 kDa.

(B) CagA translocation was measured using the TEM-1 β -lactamase translocation assay. AGS cells were pre-incubated with different concentrations of miltefosine or R5421 15-20 min prior to infection with P12[TEM-CagA]. A Δ cagT mutant served as a negative control. Results are depicted as mean \pm SD. Statistical analysis was performed using One-way ANOVA with Dunnett's Multiple Comparison *post hoc* test. n=4 * p<0.05, ** p<0.01, *** p < 0.001.

As shown in Figure 3.21, addition of miltefosine or R5421 resulted in decreased CagA phosphorylation and translocation into AGS cells by *H. pylori* strain P12 in a concentration dependent manner. 100 μ M miltefosine or 15 μ M of R5421 resulted in an approx. 50 % decrease of CagA translocation (Figure 3.21 B). These results were promising, but it remained unclear,

whether these inhibitors at the tested concentrations might have an additional cytotoxic effect on the eukaryotic cells or the bacteria, which could explain these results.

An alternative approach to avoid the problem of cytotoxicity of the inhibitory substances was the generation of *p/scr1* gene knockout cell line. To do so, the *p/scr1* gene was knocked out in AGS cells using the CRISPR/Cas9 system.

For this, guide RNAs (gRNA) were designed and cloned into the PX462 vector (Figure 3.22). Four sets of gRNAs were designed, two targeting exon 1 and another set targeting exon 4. After transfection and selection with puromycin, single cell clones were generated by serial dilution.

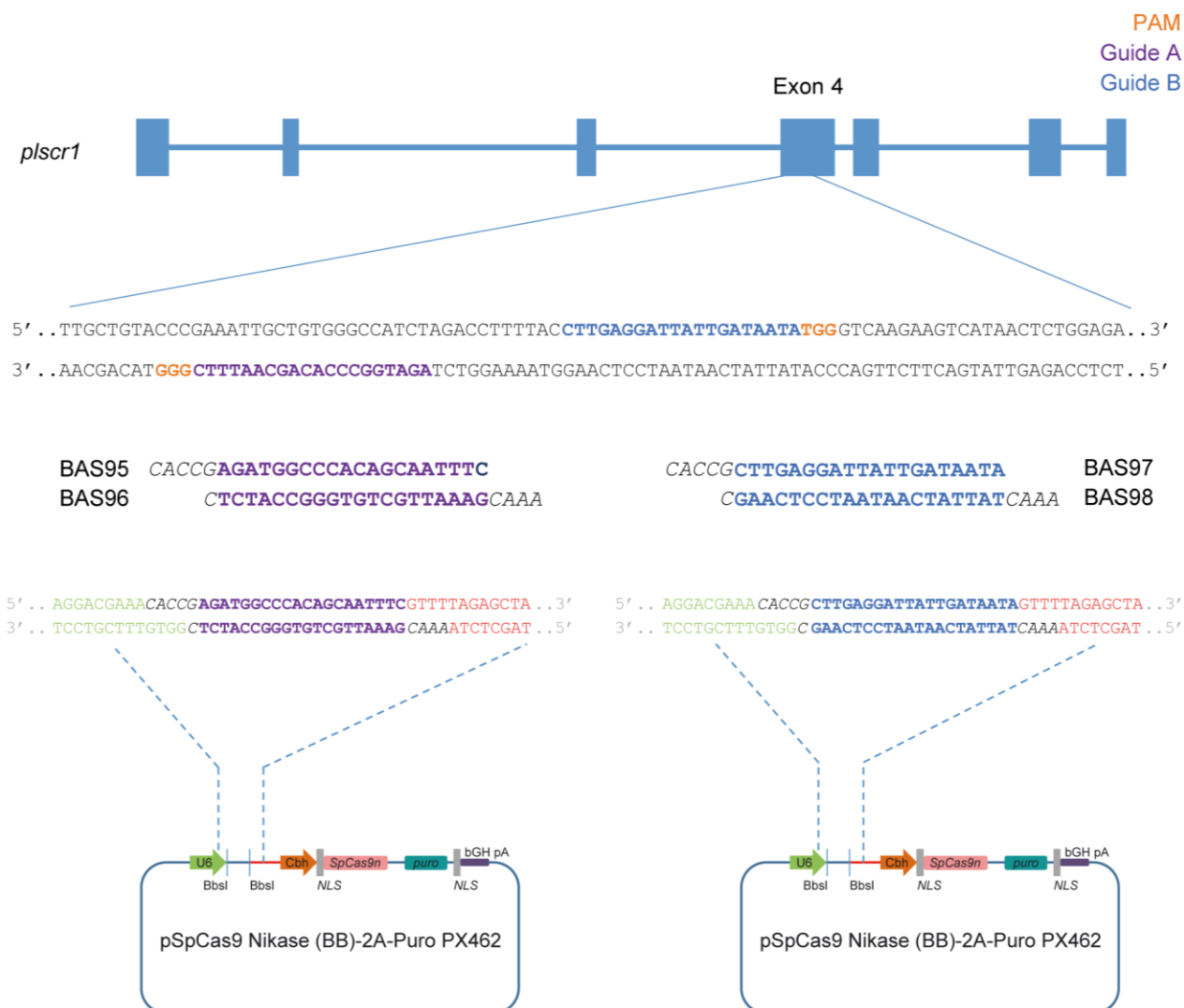


Figure 3.22: Schematic overview for generation of gRNAs for knockout of exon 4 of *plscr1*.

Design of gRNAs for knockout of PLSCR1 in AGS cells using the CRISPR/Cas9 system. The gRNAs were designed using the tool of the Zhang Lab (<https://zlab.bio/guide-design-resources>, discontinued in 2019) and cloned into the pSpCas9 Nikase (BB)-2A-Puro (PX462) vectors. PAM: Protospacer adjacent motif; U6: promoter; BbsI: restriction sites; Cbh: hybrid cytomegalovirus enhancer/chicken β -actin promoter; SpCas9n: *Streptococcus pyogenes* Cas9 D10A nickase mutant; *puro*: puromycin resistance; bGH pA: bovine growth hormone polyadenylation signal; NLS: nuclear localisation sequence nucleoplasmin.

Single cell clones were tested for PLSCR1 expression by Western blot (Figure 3.23). The first two sets (1+2) of gRNAs were not successful in generating knockout cells (*cf.* 1BB4, 2A2A4, 2B2D4), but the other two sets targeting exon 4 (3+4) were able to delete the expression of *plscr1* effectively. Only few single cell clones still showed *plscr1* expression, like 4BF2 or 3AD6.

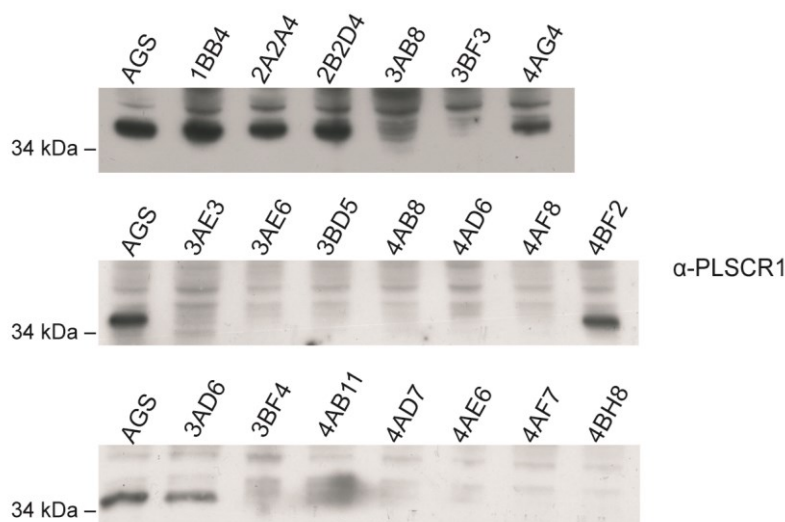


Figure 3.23: Verification of *plscr1* inactivation in AGS cells.

After generation of single cell clones, several clones were tested for *plscr1* expression by Western blotting using α -PLSCR1 antibody (PA5-21649, Invitrogen), giving rise to a specific band of ~ 35 kDa, representing the PLSCR1 protein.

Several of the single cell clones were chosen for quantitative analysis of CagA translocation (Figure 3.24). In three of the six tested single cell clones, CagA translocation was reduced significantly (3BF3, 4AF8, 4BH8), to levels between 50 % (3BF3) and 70 % (4AF8) (Figure 3.24 A, B). Next, a potential contamination of wildtype AGS cells in the tested *plscr1* gene knockout cells was tested. Therefore, the loci targeted by the CRISPR/Cas9 system were amplified from clones 3BD5, 3BF3 and 4AE6 cells by PCR and the products were cloned for sequencing. As it turned out, only in 3BF3 cells no wildtype *plscr1* gene sequence could be detected (data not shown), indicating that the remaining two cell clones still contained small amounts of contaminating wildtype AGS cells. This also explained the higher CagA translocation rate, suggesting that only a small amount of *plscr1* expression might be necessary for CagA translocation. Since the cell line 3BF3 most likely had a complete *plscr1* deletion, it was used for further analysis. 3BF3 cells were serially diluted again, to ensure its derivation from a single cell clone. One clone of this dilution series, named 3BF3 E6, was chosen and was again tested for CagA translocation, verifying the reduction of CagA translocation efficiency of 50 % (Figure 3.24 C).

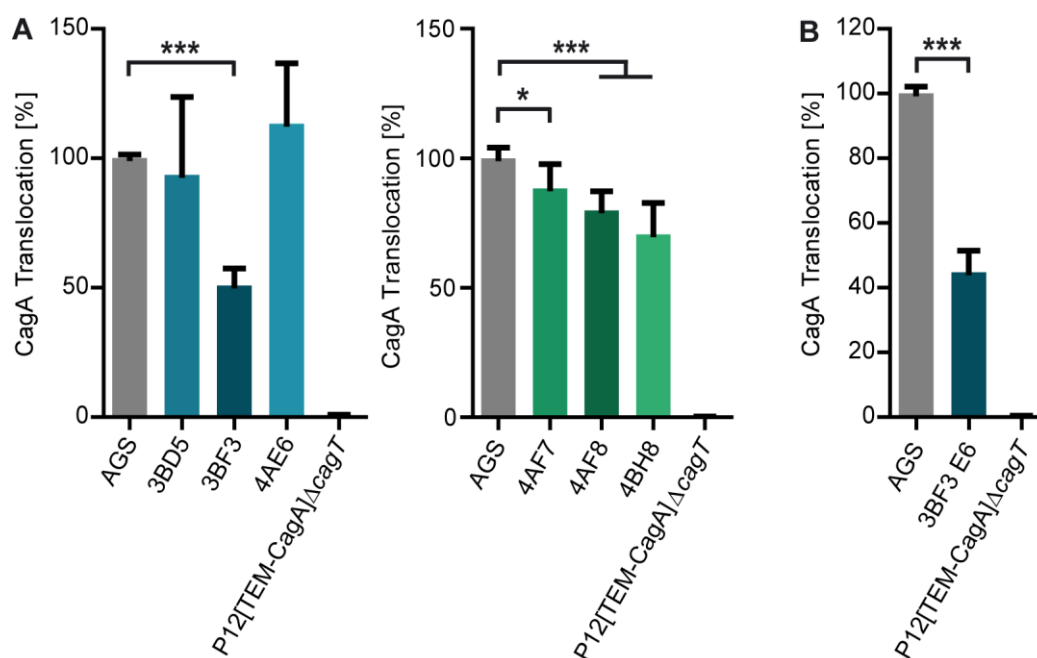


Figure 3.24: Influence of *plscr1* inactivation on CagA translocation.

(A) Six different *plscr1* knockout clones were tested for CagA translocation using the TEM-1 β -lactamase assay and the P12[TEM-CagA] strain, the $\Delta cagT$ mutant was used as a negative control.

(B) 3BF3 E6, a single cell clone derived from 3BF3, was tested for CagA translocation by infection with P12[TEM-CagA] and subsequent TEM-1 β -lactamase assay. Results are depicted as mean \pm SD. Statistical analysis was performed using One-way ANOVA with Dunnett's Multiple Comparison *post hoc* test. $n=4$ (A), $n=5$ (B) * $p < 0.05$, ** $p < 0.01$, *** $p < 0.001$.

To exclude that the reduction in CagA translocation was due to off-target effects, the *plscr1* gene was reintroduced into the 3BF3 E6 cell line by genetic complementation. For this purpose, the *plscr1* ORF was amplified from the plasmid RC207485 (origene) with primers BAS191 (*Sall*) and BAS192 (*Bam*HI) (Table 2.5) and cloned into the EGFP expression vector pEGFP-C1, which was digested with *Sall* and *Bam*HI. This resulted in an N-terminal *egfp*-tagged *plscr1* construct, termed pBAS91 (Figure 3.25 A).

After transfection of pBAS91 into 3BF3 E6 cell line and selection with G418, cells were sorted by high GFP expression into single cell clones. Expression of scramblase was analyzed by Western blot, as well as intracellular staining and subsequent flow cytometry analysis. Western blotting revealed that in the complemented cell clones (1-A8, 1-D2, 2-B3) the EGFP-PLSCR1 fusion protein was produced, indicated by the larger size of this protein (~ 66 kDa) as compared to wildtype (~ 35 kDa) (Figure 3.25 B). Flow cytometry showed that EGFP-PLSCR1 was detected in all three single cell clones, but to varying amounts (Figure 3.25 C). Clone 1-D2 had the lowest expression, as only 50 % of the population shifted to gate Q3 (PLSCR1 positive). In 1-A8 and 2-B3, approx. 60 % and 70 % of the population shifted to the PLSCR1 positive gate. Only a small number of cells were positive for both EGFP and PLSCR1, indicating that EGFP may not be functional in this fusion protein, even though the correct size of EGFP-PLSCR1 was detected by Western blotting. However, it is not clear, why the EGFP protein showed weak fluorescence.

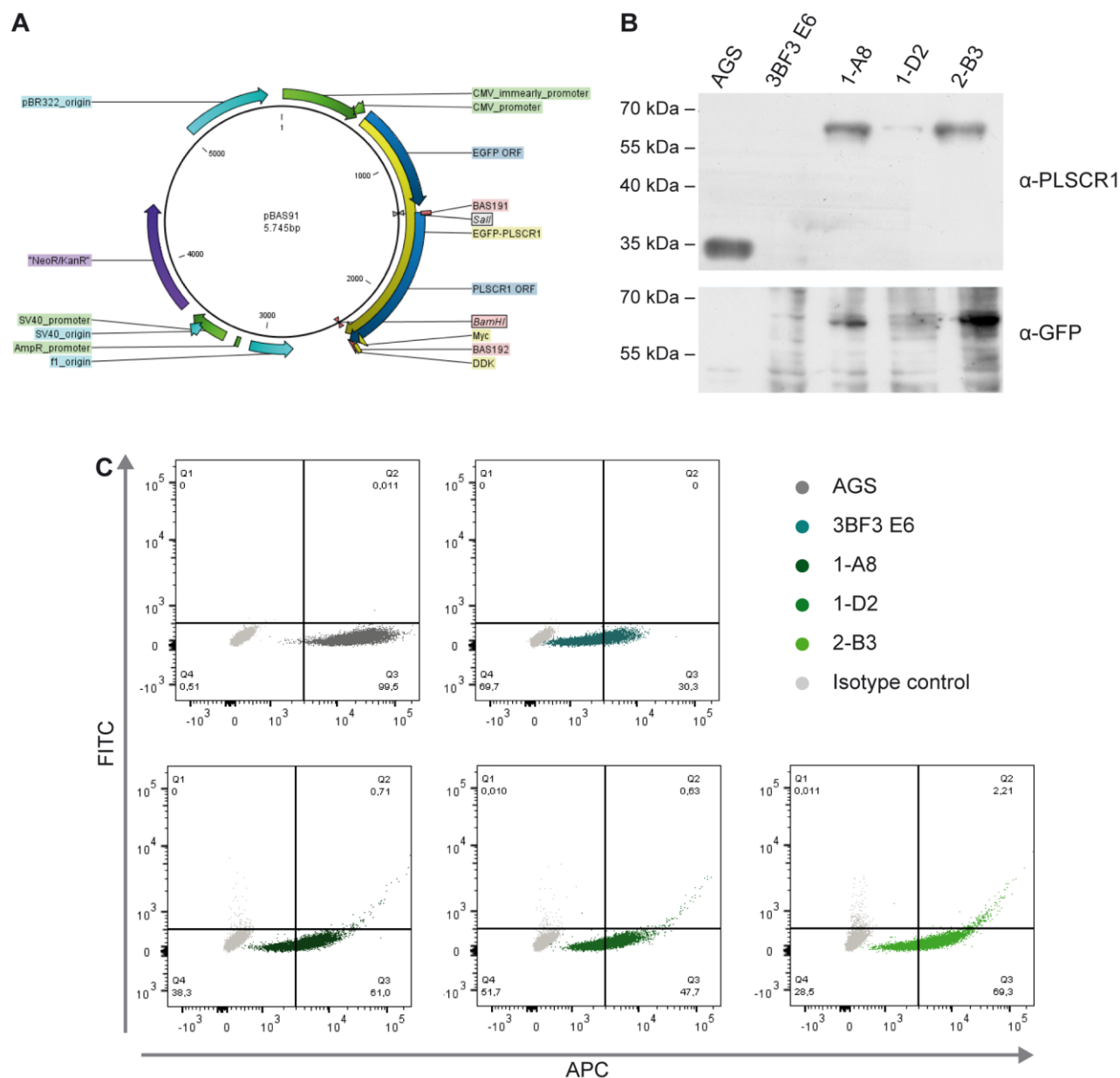


Figure 3.25: Characterization of complemented AGS Δ *plscr1* cells.

(A) Plasmid map of *egfp-plscr1* complementation plasmid (pBAS91).

(B) 3BF3 E6 was complemented with an *egfp-plscr1* plasmid construct (pBAS91). Three complemented single cell clones (1-A8, 1-D2 and 2-B3) were analyzed by Western blot using α -PLSCR1 antibody (EPR14249, abcam) or α -GFP antibody. One of three independent experiments is depicted.

(C) PLSCR1 expression was analyzed by flow cytometry as GFP expression (FITC) and PLSCR1 staining (APC, using α -PLSCR1 from abcam). Double negative cells were located in gate Q4, cells only positive for PLSCR1 in gate Q3 and double positive in Q2. One of three independent experiments is shown.

After successful characterization of the three single cell clones 1-A8, 1-D2 and 2-B3, functional assays were performed. To analyze CagA phosphorylation in these complemented cell lines, tyrosine phosphorylation assays were performed (Figure 3.26 A). Phosphorylated CagA was detected in all tested cell lines, but the amounts differed widely, probably due to different loading (cf. Figure 3.26 A, α -Tubulin blots). To quantify CagA translocation, TEM-1 β -lactamase assays were performed with 1-A8, 1-D2 and 2-B3 cell lines (Figure 3.26 B). Notably, CagA translocation was restored to about 80-90 % in all three clones tested, proving that scramblase is essential for CagA internalization.

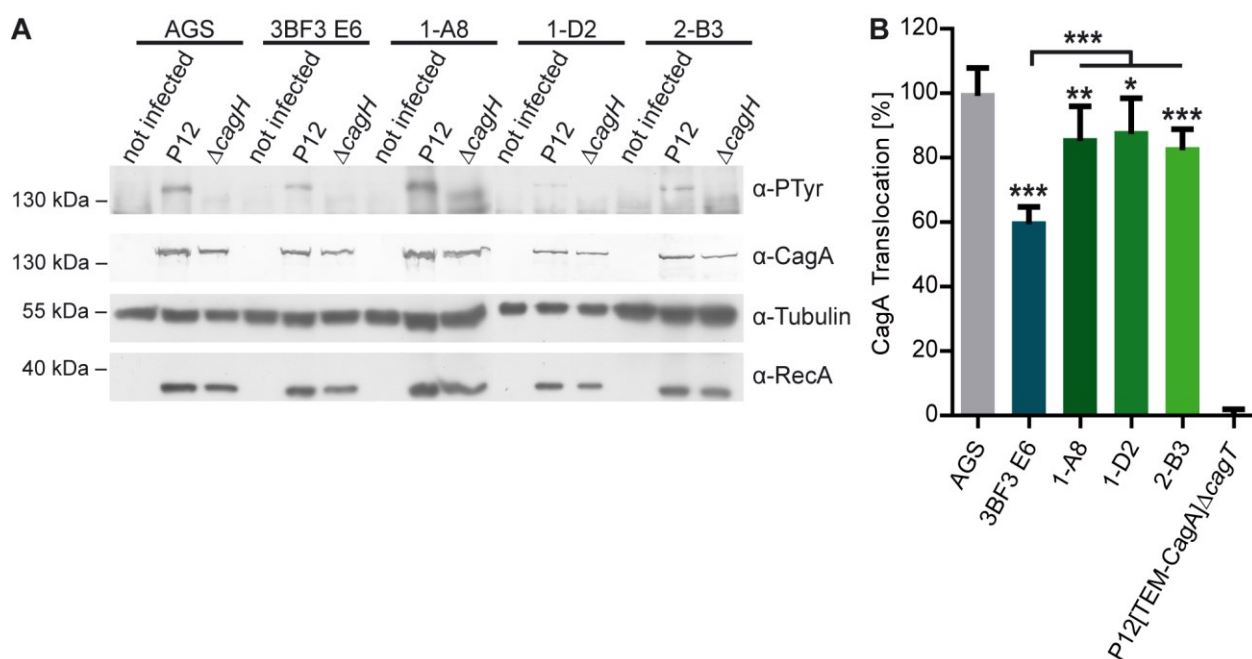


Figure 3.26: CagA translocation in EGFP-PLSCR1 complemented cell lines.

(A) *In vitro* infections of AGS, 3BF3 E6, as well as three complemented single cell clones were analyzed for phosphorylated CagA using an α -PTyr antibody (PY99). Total CagA was detected with AK299. Tubulin and RecA were used as a loading control for eukaryotic cells and bacteria, respectively. Specific bands for CagA, Tubulin and RecA were detected at 135 kDa, 55 kDa and 38 kDa, respectively. One of at least three independent experiments is shown.

(B) Wildtype cells (AGS), as well as *plscr1* deletion cells (3BF3 E6) and EGFP-PLSCR1 complemented cell lines (1-A8, 1-D2, 2-B3) were infected with P12[TEM-CagA] and CagA translocation was quantified using the TEM-1 β -lactamase assay. The translocation deficient Δ cagT mutant was used as a loading control. Results are depicted as mean \pm SD. Statistical analysis was performed using One-way ANOVA with Bonferroni's Multiple Comparison *post hoc* test. n=5. * $p < 0.05$, ** $p < 0.01$, *** $p < 0.001$.

Previously, CagA has been shown to interact with PS via its N-terminus, more specifically through a K-Xn-R-X-R motif (R619, R621) (Murata-Kamiya *et al.*, 2010). In CagA of P12, this corresponds to residues K619 and R621. Using a targeted mutagenesis approach, these residues were exchanged for alanine, rendering the corresponding CagA variant unable to bind PS. The corresponding CagA^{K619A R621A} variant was expressed as an N-terminal HiBiT fusion protein in a P12 strain to analyze CagA translocation using the HiBiT translocation assay (Lettl *et al.*, 2021). At first glance, translocation of this HiBiT-CagA^{K619A R621A} was dramatically reduced (Figure 3.27 A), but expression of the CagA variant was much lower compared to HiBiT-CagA (Figure 3.27 B). Therefore, the amount of translocated CagA was normalized to the total CagA content, revealing that translocation of CagA^{K619A R621A} was reduced to approx. 50-60 % compared to wildtype CagA (Figure 3.27 C). Thus, the mutation of the bacterial protein unable to interact with PS resulted in a similar reduction of CagA translocation as the inactivation of *p/scr1*, which is involved in flipping of PS. The combined data strongly support the hypothesis that CagA binding to PS and the subsequent flipping plays a critical role in the CagA internalization process.

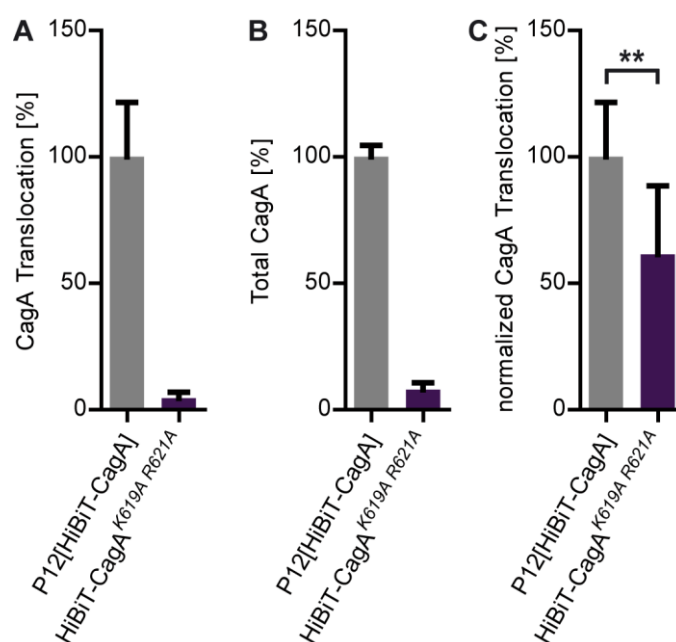


Figure 3.27: CagA translocation of a PS-binding deficient CagA variant.

(A) CagA translocation into AGS-LgBiT cells was measured using the HiBiT translocation assay. (B) Total amount of CagA was measured using a HiBiT assay. (C) CagA translocation was normalized by dividing values of translocated CagA by total CagA. Results are depicted as mean \pm SD. Statistical analysis was performed using Student's t-test. $n=5$, * $p<0.05$, ** $p<0.01$, *** $p < 0.001$. Experiments and data analysis were performed by C. Lettl.

3.4 Analyzing *H. pylori* binding to members of the annexin family

3.4.1 AnxA5 binding of different *H. pylori* strains

Annexins are proteins produced by most eukaryotic cells that bind the membrane phospholipid PS in a Ca^{2+} dependent manner. As outlined in chapter 3.3, PS externalization and binding by CagA plays a critical role in the mechanism of translocation. For this reason, annexins were investigated in the context of an *H. pylori* infection. Another member of the laboratory, K. Petri, discovered that members of the annexin family (annexins A1, A2, and A5) are able to interact with *H. pylori* in a Ca^{2+} dependent manner (Petri, 2020).

For further analysis, the differences in AnxA5 binding between a set of different *H. pylori* strains were investigated. Data were analyzed for percentage of AnxA5-binding bacteria (Figure 3.28 A), and for the median fluorescence intensity (FI), which indicated the median amount of AnxA5 bound per bacterium (Figure 3.28 B). These values were remarkably different between some strains, e.g., P12 and G27 had a similar percentage of AnxA5-positive bacteria, but the median FI was significantly higher in P12. Another interesting finding was strain X47, which bound a similar amount of AnxA5, but the median FI was very low compared to P12, indicating that each bacterium in this population bound less AnxA5. Comparing the percentage of AnxA5-positive bacteria between strains, only strain 26695 and Tx30a showed significant lower percentage of AnxA5 positive bacteria in contrast to P12. Both of these strains had lower median FI values compared to P12.

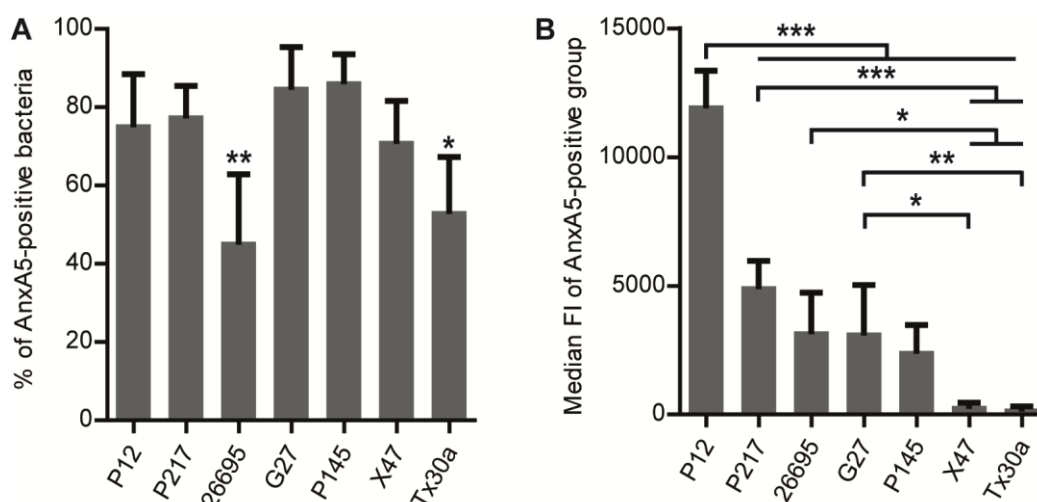


Figure 3.28: AnxA5 binding by different *H. pylori* strains.

Binding of AnxA5-Alexa647 to different *H. pylori* strains was measured by flow cytometry. Data were analyzed for percentage of AnxA5-positive bacteria (A) and median fluorescence intensity (B). Results are depicted as mean \pm SD. Statistical analysis was performed using one-way ANOVA with a Bonferroni's Multiple Comparison test. $n \geq 4$ (A, B). * $p < 0.05$, ** $p < 0.01$, *** $p < 0.001$.

3.4.2 Identification of the AnxA5 binding site to *H. pylori*

The ability of some other Gram-negative bacteria to bind AnxA5 has already been demonstrated, e.g., *P. aeruginosa*, *S. putrefaciens*, and *H. influenzae* (Rand *et al.*, 2012). In these species, AnxA5 binds to the lipid A part of LPS.

As *H. pylori* LPS is unique compared to other bacteria, the binding of AnxA5 to purified LPS from *H. pylori* strain G27, which was provided by H. Li (Sichuan University, China), was investigated. For this purpose, dot blots were performed, in which LPS was incubated with human AnxA5 and detecting with an α -AnxA5 antibody. As shown in Figure 3.29, human AnxA5 was able to bind LPS from strain G27. Lipid A was detected as a loading control for all LPS used and Lewis Y was detected as an *H. pylori* specific loading control.

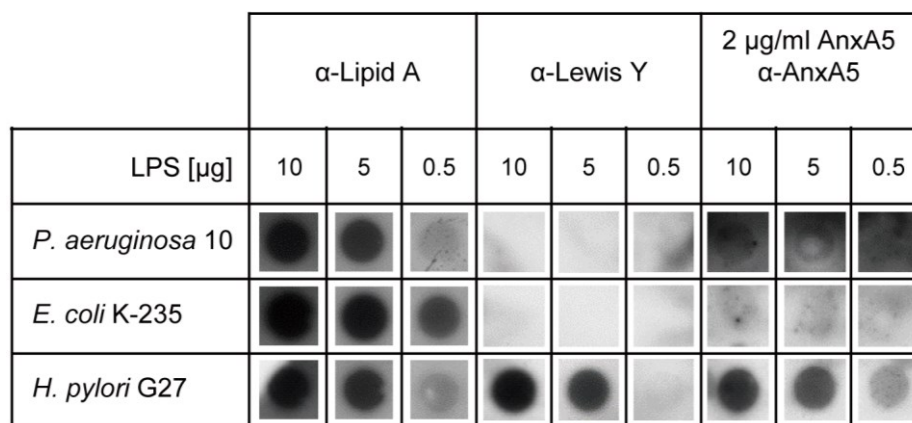


Figure 3.29: LPS dot blots using human AnxA5.

Binding of AnxA5 to LPS from *P. aeruginosa*, *E. coli* and *H. pylori* was analyzed using a dot blot. Different amounts of LPS (10, 5 and 0.5 μg) were dropped onto a PVDF membrane and incubated with an α -Lipid A antibody (PA1-73178, Thermo Fisher), an α -Lewis Y (F3, abcam) or AnxA5 (2 $\mu\text{g/ml}$, A9460, Sigma) and subsequently α -AnxA5 antibody (ab54775, abcam). Lipid A and Lewis Y were used as a loading control. One representative image from at least 3 independent experiments is shown.

To identify the specific binding site of AnxA5, *H. pylori* mutants with shortened LPS versions were utilized. The gene *hp1284* encodes a putative heptosyltransferase, attaching the HepIII residue to the core-oligosaccharide domain (Li *et al.*, 2017). WaaL is responsible for attaching the O-antigen to the core-oligosaccharide. Deletion of *waaL* therefore results in an LPS consisting only of the core-oligosaccharide and lipid A (Li *et al.*, 2017). The bifunctional enzyme RfaE (HP0858) plays a role in the LPS heptose biosynthesis pathway and functions as a kinase and an ADP-transferase. Deletion of *rfaE* leads to an LPS structure consisting only of lipid A and KDO (Stein *et al.*, 2017). LPS structures of these mutants are depicted in Figure 3.30. The gene *hp0805* encodes a putative glycosyltransferase and is postulated to transfer the Gal residue to the HepIII at the core-oligosaccharide, but the structure has not been elucidated completely yet (Pachathundikandi *et al.*, 2019).

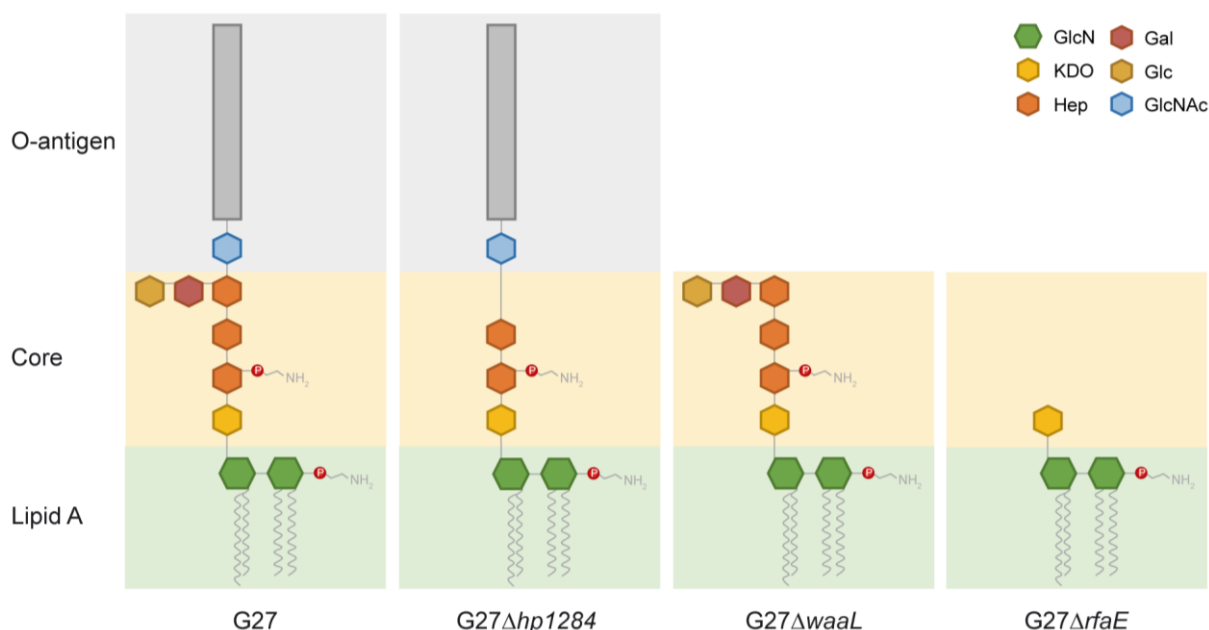


Figure 3.30: Overview of LPS structures of G27 wildtype, $G27\Delta hp1284$, $G27\Delta waaL$ and $G27\Delta rfaE$.

Adapted from (Li *et al.*, 2017, Stein *et al.*, 2017). GlcN: glucosamine; Gal: galactose; KDO: 3-deoxy-D-manno-oct-2-ulosonic acid; Glc: glucose; Hep: heptose; GlcNAc: *N*-acetylglucosamine.

All of the above-mentioned *H. pylori* mutant strains were analyzed for AnxA5 binding (Figure 3.31). As binding differed widely between strains (Figure 3.28), different strain backgrounds (G27, P12, 26695) were used. The $G27\Delta waaL$ strain showed no significant difference in median FI compared to the G27 wildtype (Figure 3.31 A), but the $G27\Delta hp1284$ strain had a significant increase in median FI, which was also the case for 26695 $\Delta hp1284$ (Figure 3.31 A, C).

Interestingly, the average bacterium of $G27\Delta rfaE$ and the 26695 $\Delta rfaE$ strains bound more AnxA5 compared to the wildtype. P12 $\Delta rfaE$ strain also showed a slight but not significant increase (Figure 3.31 B). Since the structure of a $\Delta rfaE$ mutant only consists of KDO and lipid A, the data suggest that AnxA5 binds to either of these structures. Since the binding site for other Gram-negative bacteria was identified as lipid A, our data indicate that AnxA5 also binds to lipid A of *H. pylori*. $G27\Delta hp0805$ showed no difference in median FI compared to the wildtype, but it was difficult to draw any conclusions from this result.

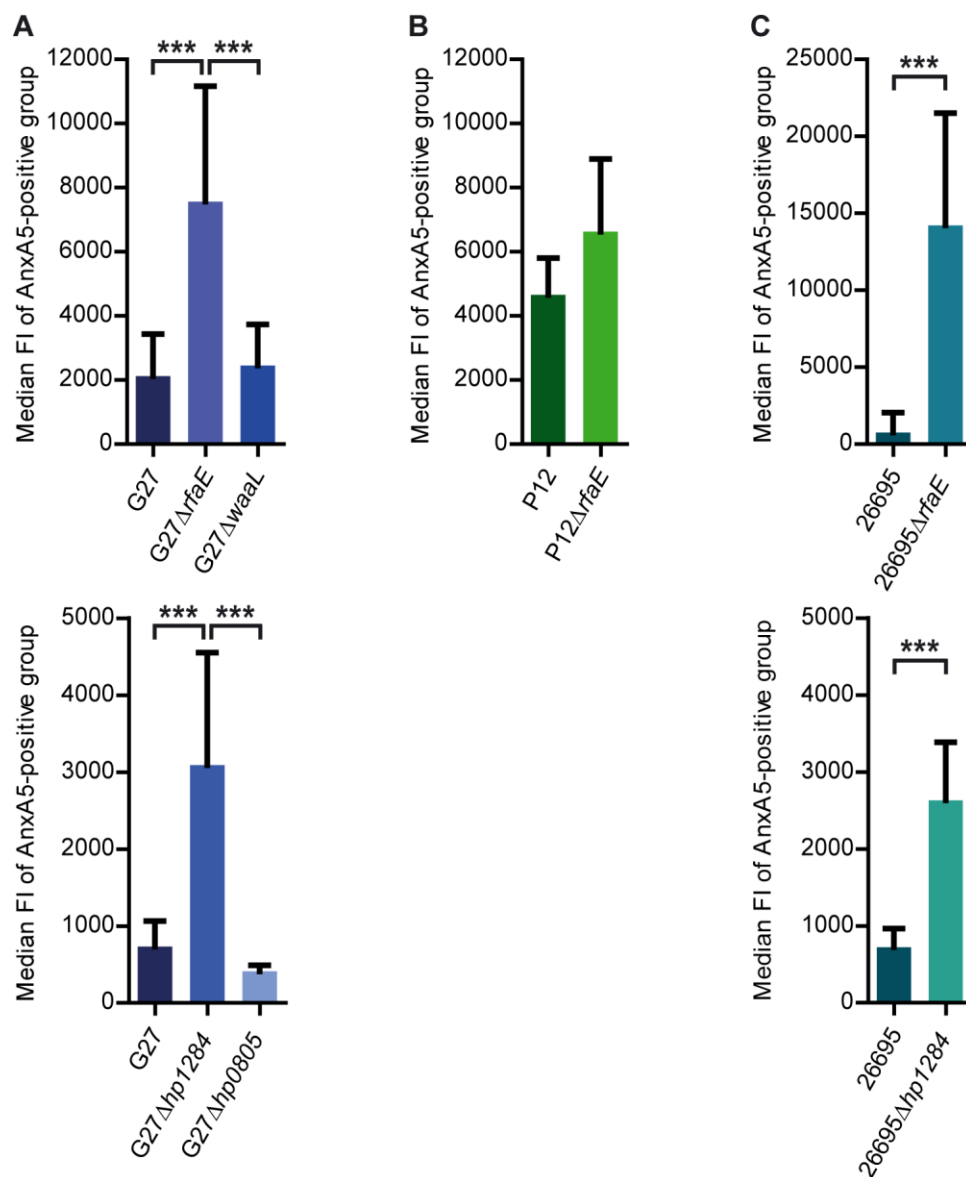


Figure 3.31: LPS mutant strains and AnxA5 binding.

(A) The binding of AnxA5-Alexa647 to G27 and respective mutants, (B) P12 and respective mutants and (C) 26695 and respective mutants was analyzed. Results are depicted as mean \pm SD. Statistics were calculated using one-way ANOVA with Bonferroni's multiple comparison test (A) or Student's unpaired t-test (B, C). $n=8$ (A, top), $n\geq 5$ (A, bottom) $n=5$ (B), $n=7$ (C, top), $n=5$ (C, bottom). * $p < 0.05$, ** $p < 0.01$, *** $p < 0.001$.

The percentage of AnxA5-binding bacteria did not significantly change in the *G27ΔrfaE*, *G27ΔwaaL* or *P12ΔrfaE* compared to their respective wildtype (Figure 3.32 A). In 26695, the *rfaE* mutant showed a higher percentage of AnxA5 binding, indicating that more bacteria of the population were bound by AnxA5 (Figure 3.32 A). In *G27Δhp1284*, percentage of AnxA5-binding bacteria was also increased (approx. 70 % in *G27* compared to approx. 90 % in *G27Δhp1284*), but the *hp1284* mutation in 26695 did not show a difference to the wildtype strain (Figure 3.32 B). Taken together, the binding site of AnxA5 on *H. pylori* was identified to be LPS, more specifically the lipid A part, as AnxA5 binding was significantly increased using a *rfaE* deletion mutant.

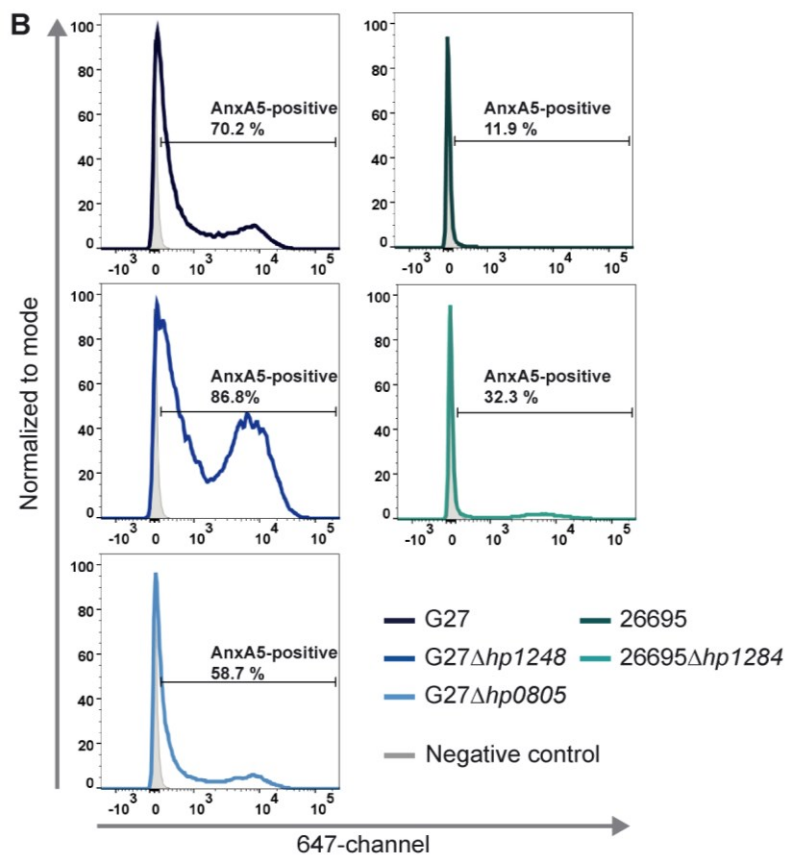
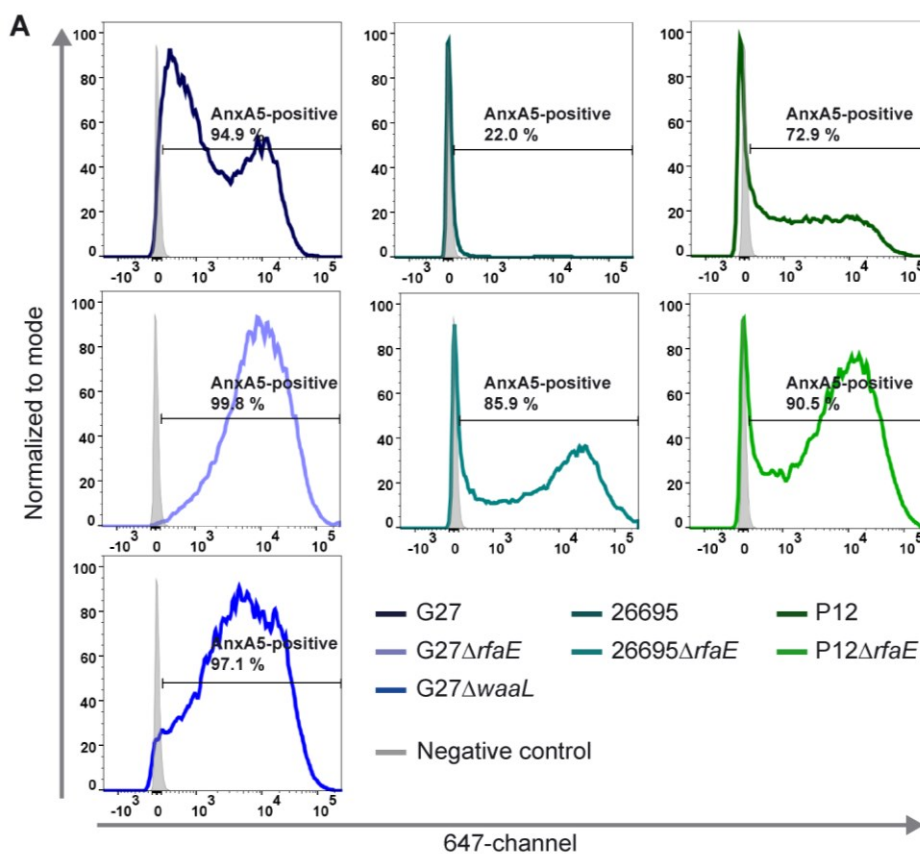


Figure 3.32: Percentage of bacteria bound by AnxA5-Alexa647 in LPS mutant strains.

Percentage of AnxA5 binding was analyzed by flow cytometry. One representative image of at least three independent experiments is shown. (A) G27, G27 Δ *rfaE* and G27 Δ *waaL* (blue), P12 and P12 Δ *rfaE* (green) and 26695 and 26695 Δ *rfaE* (turquoise). (B) G27, G27 Δ *hp1284* and G27 Δ *hp0805* (blue) and 26695 and 26695 Δ *hp1284* (turquoise). Unstained bacteria were used as a negative control.

3.4.3 Influence of lipid A structure on AnxA5 binding

To further assess the influence of lipid A on AnxA5 binding, G27, P12 and 26695 *lpxE*, *lpxF*, double *lpxE/lpxF* and *eptA* knockout mutants were generated. LpxE is the 1-phosphatase of lipid A, dephosphorylation results in transfer of a PE residue to the 1-position, catalyzed by EptA. LpxF dephosphorylates the 4'-position of lipid A (Cullen *et al.*, 2011).

As annexin binding to *H. pylori* requires Ca²⁺ (Petri, 2020), the negatively charged phosphate groups were considered as possible targets for binding sites for AnxA5. Structures of lipid A in wildtype *H. pylori* and the different *lpx* knockout mutants are depicted in Figure 3.33 D.

AnxA5 binding of these knockout mutants in the G27, P12 and 26695 background was analyzed. In P12 (Figure 3.33 B), knockout of the genes had only a slight influence on the median FI. In G27, however, deletion of *lpxE*, *lpxF* and the double knockout resulted in an increase of the median FI, with G27 Δ *lpxE/F* showing the highest increase (about 3-fold) compared to wildtype (Figure 3.33 A). The G27 Δ *lpxE* and G27 Δ *eptA* mutant had similar binding pattern, with a slight increase compared to the wildtype, which was not significant. In 26695, the double knockout mutant (*lpxE/F*) also had the highest impact on AnxA5 binding, resulting in a 1.6-fold increase. The *eptA* deletion had also a significant impact on AnxA5 binding in 26695, but the influence of this gene was unclear, as the structure of this lipid A variant was not known.

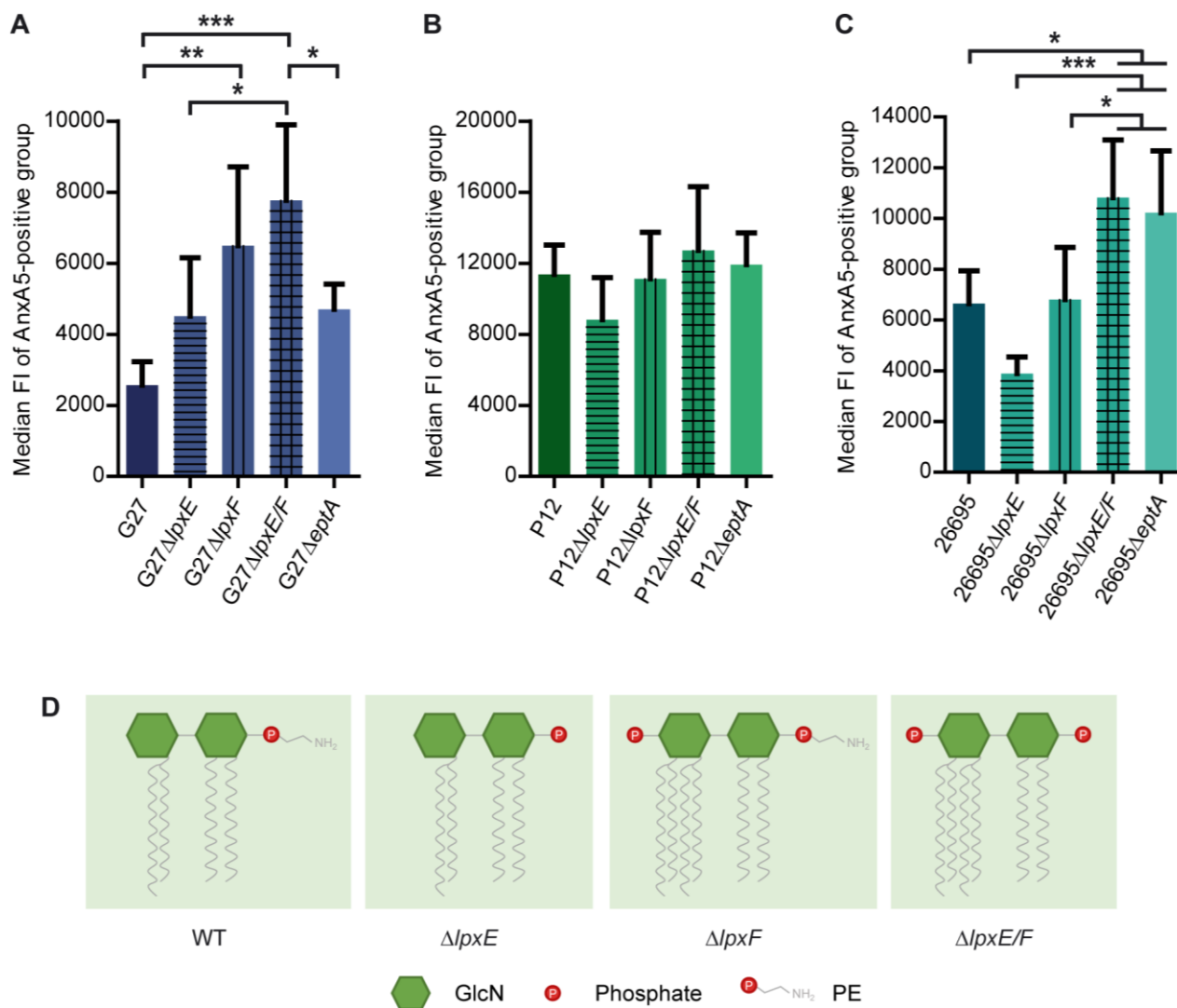


Figure 3.33: AnxA5 binding to lipid A mutants in G27, P12 and 26695.

(A, B, C) Median FI of AnxA5-positive group of G27 (A), P12 (B) and 26695 (C) wildtype, $\Delta lpxE$, $\Delta lpxF$, $\Delta lpxE/F$ and $\Delta eptA$ strains was analyzed as described before. Unstained bacteria were used as a negative control. Results are depicted as mean \pm SD. Statistics were calculated using one-way ANOVA with Bonferroni's multiple comparison test. $n \geq 5$ (A, B, C). * $p < 0.05$, ** $p < 0.01$, *** $p < 0.001$.

(D) Schematic overview of lipid A structures of *H. pylori* wildtype, $\Delta lpxE$, $\Delta lpxF$, and $\Delta lpxE/F$ deletion strains. Adapted from (Cullen *et al.*, 2011). GlcN - *N*-acetylglucosamine, PE – phosphatidylethanolamine.

The average percentage of AnxA5 binding bacteria in the G27 strains, as well as in the P12 strains did not change, remaining at about 80 % for both strain backgrounds (Figure 3.34, blue and green respectively). In 26695 (turquoise), on the other hand, the percentage of AnxA5-positive bacteria increased in 26695 $\Delta lpxE/F$ to about 70 % compared to the wildtype (about 40 %), and in 26695 $\Delta eptA$ strain to about 80 %.

In conclusion, AnxA5 probably bound to the phosphate groups of lipid A, at least in G27 and 26695, as the median FI was significantly increased in a *lpxE/F* deletion mutant in both strains.

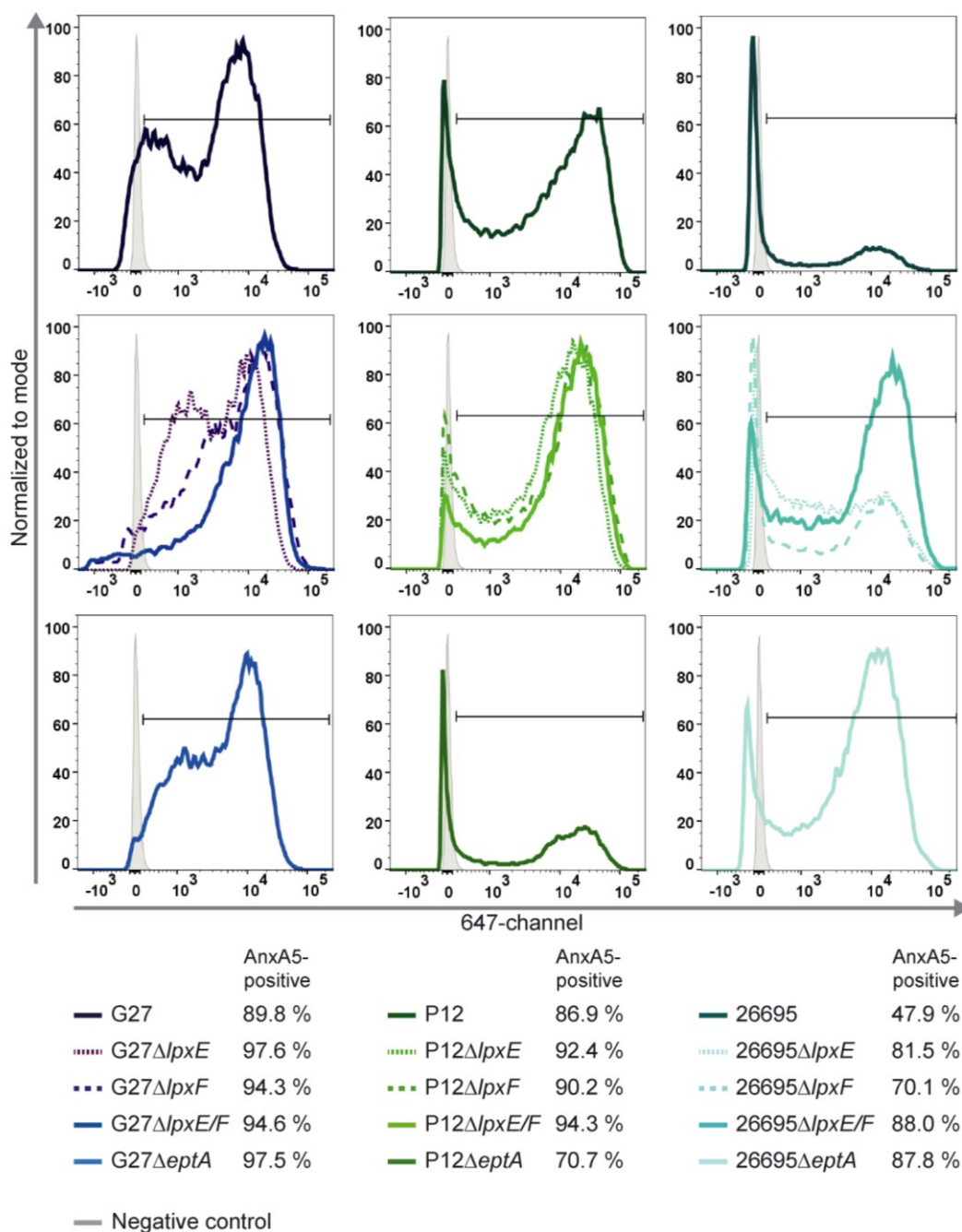


Figure 3.34: Percentage of bacteria bound by AnxA5-Alexa647 in lipid A mutant strains

Percentage of AnxA5-positive bacteria in wildtype, Δ*lpxE*, Δ*lpxF*, Δ*lpxE/F* and Δ*eptA* in the G27 (left column, blue), P12 (middle column, green) and 26695 (right column, turquoise). Unstained bacteria were used as a negative control. One representative image of at least five independent experiments is shown.

3.4.4 Influence of mouse stomach passage on AnxA5 binding of *H. pylori*

For analysis of a possible adaption of AnxA5 binding upon a stomach passage of *H. pylori*, a mouse re-isolated PMSS1 strain was compared to the corresponding lab-passaged strain for its AnxA5 binding capacity (Figure 3.35). Indeed, mouse passage resulted in a higher median FI intensity for PMSS1 compared to the lab-adapted precursor strains. Median FI increased approx. 2.7-fold in the re-isolated strain (Figure 3.35 A), indicating an adaption of AnxA5 binding *in vivo*. The percentage of AnxA5-positive bacteria also increased from 30 % to 70 % in PMSS1 (Figure 3.35 B).

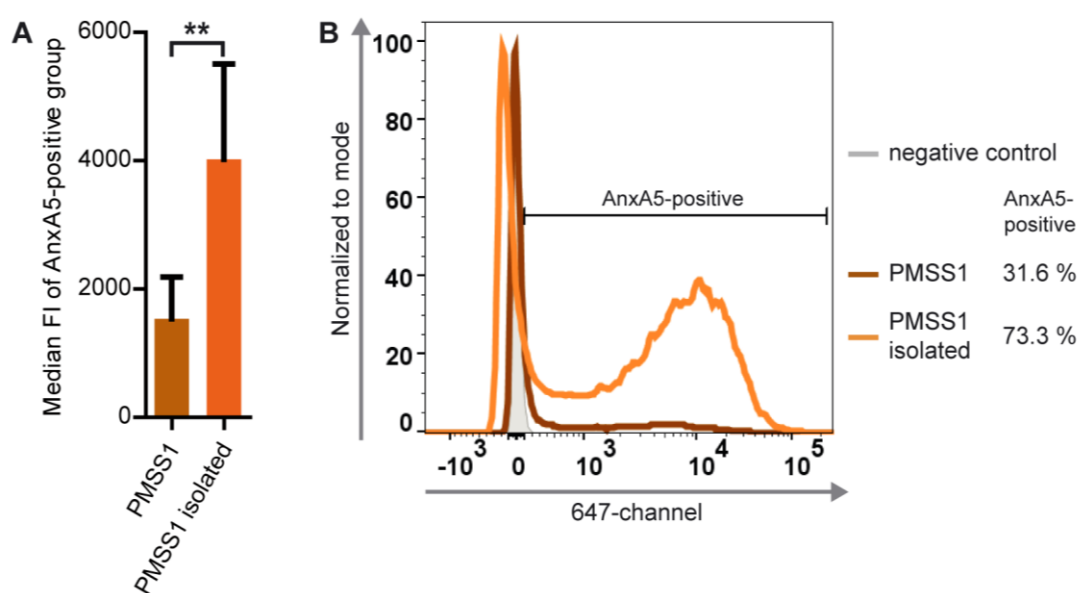


Figure 3.35: AnxA5-binding assay using a mouse-isolated strain.

AnxA5-binding was analyzed in PMSS1 or a mouse-isolated PMSS1 strain by flow cytometry. Data was evaluated for median FI (A) and percentage of AnxA5-positive bacteria (B). Unstained bacteria were used as a negative control. Results are depicted as mean \pm SD (A). Statistics were analyzed using Student's t-test. $n=5$. * $p < 0.05$, ** $p < 0.01$, *** $p < 0.001$. For histograms, one representative image of five independent experiments is shown.

3.4.5 Influence of AnxA5 binding on the interaction of *H. pylori* with host cells

Next, the effect of AnxA5 binding to *H. pylori* on TLR-4 activation as well as CagA translocation was tested. To study the role of AnxA5 binding to *H. pylori* lipid A and the impact on TLR-4 recognition, TLR-4 activation was monitored using the HEK-Blue hTLR-4 reporter cell line (Invivogen). This cell line was generated by stable transfection of HEK293 cells with the TLR-4 machinery and a secreted embryonic alkaline phosphatase reporter gene (SEAP) controlled by

an NF- κ B inducible promoter. Thus, a colorimetric assay allows quantification of TLR-4/MD-2 complex activation of this reporter cell line.

To eliminate the well-known contribution of the *cagPAI* on activation of the NF- κ B signaling, *cagPAI* deletion mutants were generated in a Δ *pxE/F* background. The strains G27 Δ *cagPAI* and P12 Δ *cagPAI* resulted in low levels of TLR-4 activation in the reporter cell line. G27 Δ *pxE/F* Δ *cagPAI* and P12 Δ *pxE/F* Δ *cagPAI* showed higher levels of TLR-4 activation, which was more pronounced in the G27 strain (Figure 3.36 A, B). Addition of 1, 2 or 5 μ g/ml of AnxA5 to the bacteria 1 h prior to infection caused a decreased activation of TLR-4 in G27 Δ *pxE/F* Δ *cagPAI* as well as in P12 Δ *pxE/F* Δ *cagPAI* (Figure 3.36 A, B), indicating that AnxA5 binding to lipid A interferes with *H. pylori*-mediated TLR-4 signaling.

The PMSS1 isolates showed increased activation of TLR-4, as these strains still possess a *cagPAI*, which contributes to NF- κ B activation by translocation of ADP-heptose. Nevertheless, TLR-4 activation was also reduced in the re-isolated PMSS1 strain by addition of 2 or 5 μ g/ml AnxA5. The laboratory-adapted PMSS1 strain showed lower levels of TLR-4 activation and there was no influence of AnxA5 on this strain (Figure 3.36 C).

To rule out that AnxA5 itself reduced TLR-4 activation, the reporter cell line was also treated with 1 μ g/ml LPS of *E. coli* strain K-235 and 1 or 5 μ g/ml AnxA5 (Figure 3.36 D). As AnxA5 was not able to bind to *E. coli* LPS (Figure 3.29) and addition of this protein had no influence on TLR-4 activation, a direct interference by AnxA5 was excluded.

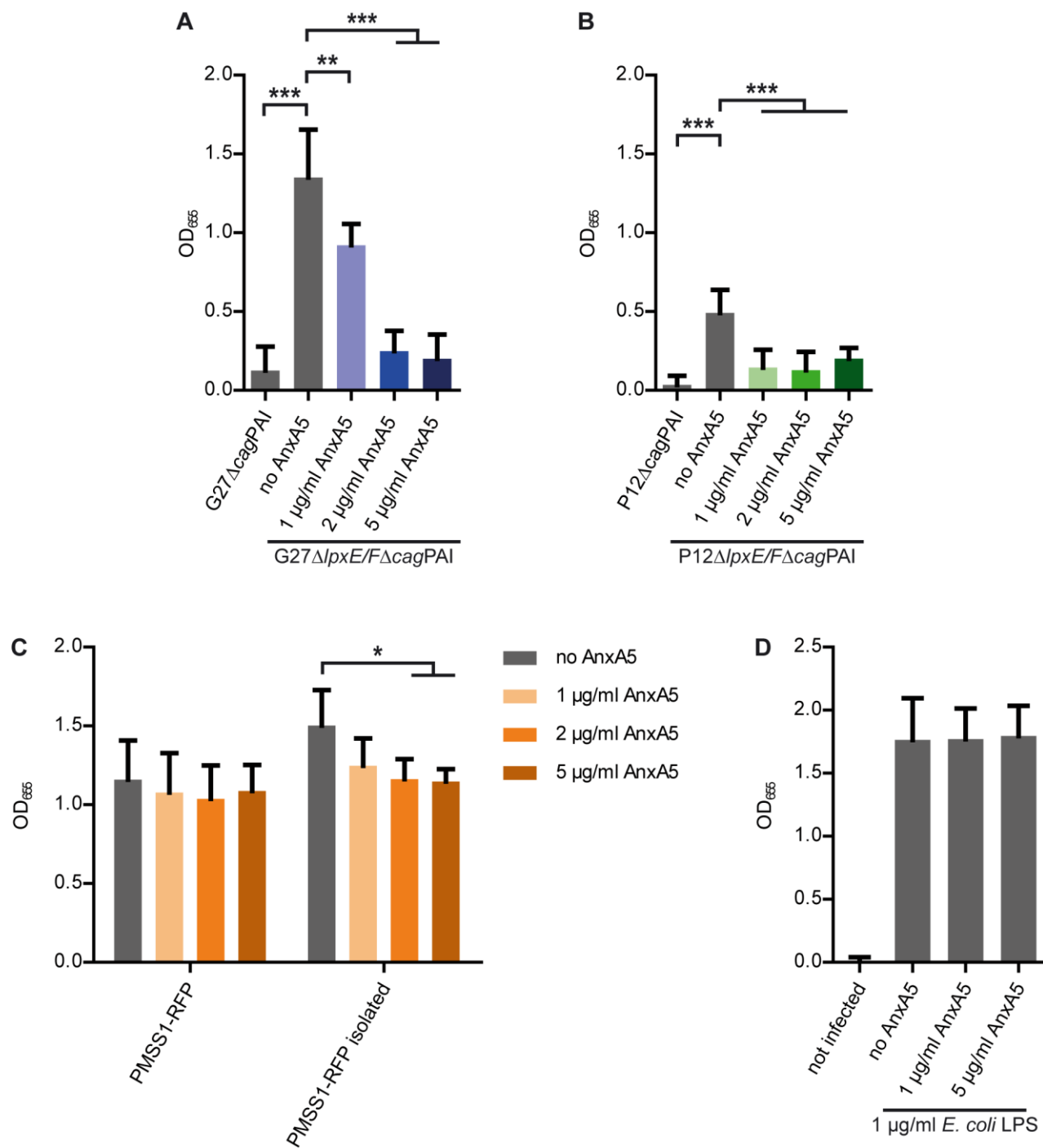


Figure 3.36: Influence of AnxA5 on TLR-4 activation by different *H. pylori* strains.

HEK-Blue hTLR-4 cells were infected with (A) G27 Δ cagPAI or G27 Δ pxE/F Δ cagPAI, with (B) P12 Δ cagPAI or P12 Δ pxE/F Δ cagPAI, and with (C) PMSS1 or re-isolated PMSS1. As a positive control, LPS of *E. coli* K-235 was used (D). Uninfected cells served as a negative control. NF- κ B signaling was determined using QuantiBlue (Invivogen) and OD was measured at 665 nm. Results are depicted as mean \pm SD. Statistics were calculated using one-way ANOVA (A, B, D) with Bonferroni's multiple comparison test or two-way ANOVA (C) with Bonferroni's *post hoc* test. n=5 (A, D), n \geq 5 (B), n=4 (C). * p < 0.05, ** p < 0.01, *** p < 0.001.

For quantification of the influence of AnxA5 binding on CagA translocation, the HiBiT-CagA translocation assay was used (Lettl *et al.*, 2021). Addition of 10 μ g/ml of AnxA5 resulted in a moderate decrease to about 80 % in a P12[HiBiT-CagA] strain (Figure 3.37 A). Since more AnxA5 was able to bind to a P12 Δ rfaE strain (Figure 3.31 C), the experiment was repeated with an *rfaE* knockout strain. Indeed, a reduction to about 70 % was already detected with 2 μ g/ml AnxA5 in this strain. With 5 and 10 μ g/ml AnxA5, CagA translocation was decreased to about 50 % compared to the untreated control (Figure 3.37 B).

To conclude, these results showed that AnxA5 binding to *H. pylori* interfered with TLR-4 activation, as well as with CagA translocation.

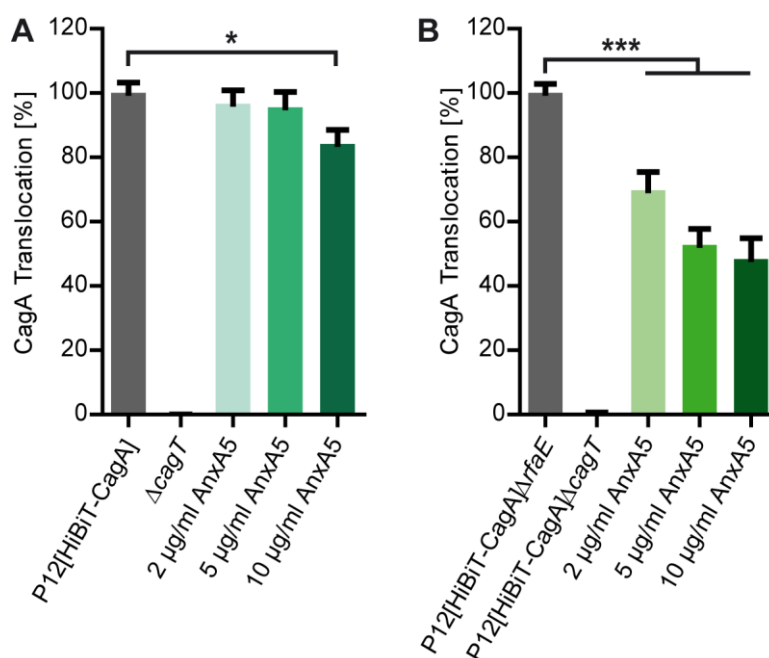


Figure 3.37: Influence of AnxA5 binding on CagA translocation in P12[HiBiT-CagA] and P12[HiBiT-CagA] Δ rfaE. CagA translocation was measured using the HiBiT translocation assay with P12[HiBiT-CagA] (A) and P12[HiBiT-CagA] Δ rfaE (B). P12[HiBiT-CagA] Δ cagT was used as a negative control. 1 h prior to infection, 2, 5 or 10 μ g/ml AnxA5 were added to the bacteria. Results are shown as mean \pm SD. Statistics were calculated using one-way ANOVA with Dunnett's multiple comparison test. n=5 (A, B). * p < 0.05, ** p < 0.01, *** p < 0.001.

3.4.6 Analyzing the *H. pylori*-annexin interaction in human gastric tissue

The results of the re-isolated PMSS1 strain (*cf.* Figure 3.35) indicated that *H. pylori* is able to adapt its AnxA5 binding behavior *in vivo*. Hence, the interaction of *H. pylori* with different members of the annexin family (A1, A2 and A5) was analyzed under *in vivo* stomach infection conditions in humans. For this, sections of stomach biopsies of *H. pylori* positive and negative patients were subjected to immunofluorescence labeling.

To compare the annexin A1, A2 and A5 levels in *H. pylori* positive and negative patients, labeling of annexins by immunofluorescence staining (see Chapter 2.2.6) as well as nuclei was performed in sections of stomach biopsies from corpus and antrum. The quantification results showed a trend towards an increase in annexin A1, A2 and A5 levels in *H. pylori* positive patients, even though the result seemed to be highly variable between individuals (Figure 3.38). AnxA1 staining revealed a trend towards increased levels in *H. pylori* positive patients, which was not significant and varied widely between individual patients (Figure 3.38 A). The same was true for AnxA2 staining, but a significant increase was measured in at least one patient (N1-4-C2) (Figure 3.38 B). For AnxA5, levels were significantly increased in two out of three tested patients (N1-4-C2 and N1-24-C2) (Figure 3.38 C).

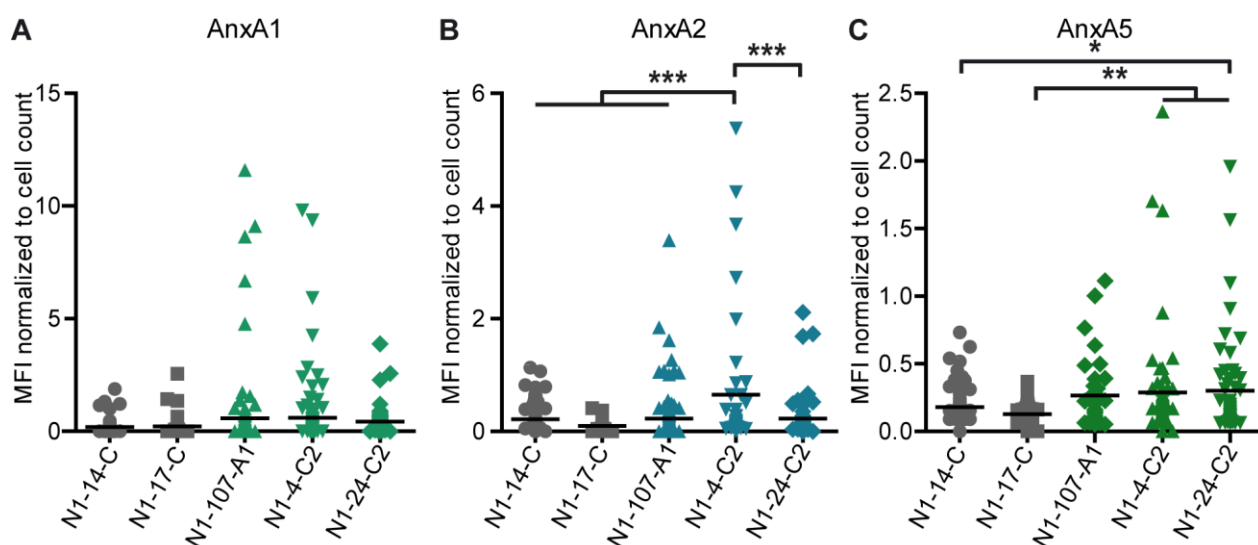


Figure 3.38: Influence of *H. pylori* infection on detected annexin A1, A2 and A5 *in vivo*.

AnxA1 (A), AnxA2 (B) and AnxA5 (C) levels were quantified in *H. pylori* positive (light green/blue/dark green) and negative (grey) samples. Sections were imaged using the Leica TCS SP5 confocal microscope and quantification was performed using Fiji software. Data analysis was performed as described above (chapter 2.2.6.1.3). Statistical analysis was performed using one-way ANOVA with a Bonferroni's Multiple Comparison test. * $p < 0.05$, ** $p < 0.01$, *** $p < 0.001$.

To analyze and visualize a possible co-localization between *H. pylori* and AnxA5, the gastric sections were stained for AnxA5 and *H. pylori*. As controls, sections were either stained with secondary antibodies only (Figure 3.39 F), or for *H. pylori* and secondary antibody of AnxA5 staining only (Figure 3.39 E).

Co-localization was indeed detected in *H. pylori* positive patients (Figure 3.39). The green signal (AnxA5) clearly overlaps with the magenta (*H. pylori*) signal, pointing to an interaction of the bacteria with AnxA5 *in vivo*. Unspecific staining was ruled out using the different controls (Figure 3.39 E, F). In conclusion, the data obtained from the quantification and high resolution microscopic imaging of gastric sections suggest that an *H. pylori* infection might cause an increase of certain annexins in the gastric mucosa and *H. pylori* might be able to interact with AnxA5.

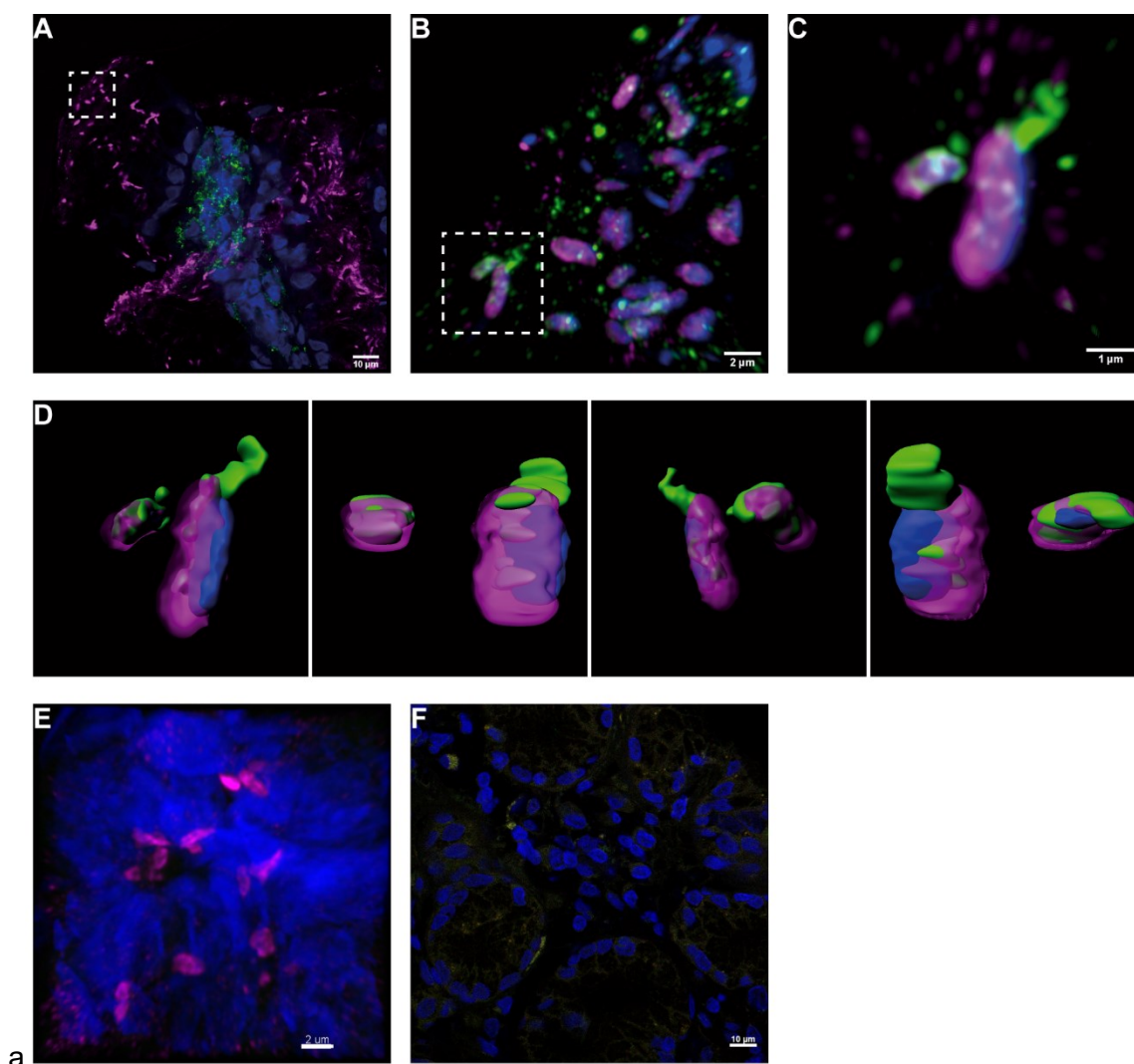


Figure 3.39: Co-localization of *H. pylori* with AnxA5 *in vivo*.

Stomach biopsy sections were stained with AK175 (*H. pylori*, magenta), α -AnxA5 antibody (green) and DAPI (blue). Samples were visualized using the confocal laser scanning microscope LSM880 (Zeiss) with ArysCan Module.

(A) Confocal laser scanning image showing human gastric tissue of an infected patient (N1-24-C2) as an overview after staining *H. pylori* (magenta), AnxA5 (green) and DAPI (blue).

(B, C) Detailed views of *H. pylori* as a confocal image taken with z-stacks and the reconstructed three-dimensional projection.

(D) Image C was modeled using the Imaris software contour surface tool.

(E-F) Control staining for confocal laser scanning microscopy. (E) Gastric tissue of an *H. pylori* infected patient (N2-97-A1) was stained for *H. pylori* (magenta) and DAPI (blue). For AnxA5, only the secondary antibody (green) was applied to control for unspecific binding. Confocal image was taken as a z-stack and the three-dimensional projection was reconstructed. (F) Gastric tissue of an *H. pylori* infected patient (N2-97-A1) was stained with secondary antibodies only.

Chapter 4: Discussion

4.1 HopQ-CEACAM interaction and CagA translocation

One of the major unsolved questions in *H. pylori* research is the mechanism of CagA translocation and how the bacterial adhesin HopQ, a non *cagPAI* encoded co-factor of the Cag-T4SS, is involved. In this work, we attempted to answer this question using different approaches to gain further insight into the mechanism of HopQ-CEACAM interactions and their influence on CagA translocation.

4.1.1 The ITIM of CEACAM1 has no impact on CagA translocation

First, the influence on CagA translocation of the ITIMs of CEACAM1 was tested. Even though expression of CEACAM1 with and without the cytoplasmic tail was difficult, CagA translocation could still be measured (Figure 3.1). As it turned out, signaling events triggered by ITIM did not have an influence on CagA translocation. These results were in line with Moonens, *et al.* (2018). Furthermore, this outcome was expected, as CagA translocation is also mediated by CEACAMs lacking a cytoplasmic tail, like CEACAM5 and 6 (Javaheri *et al.*, 2016, Königer *et al.*, 2016). In fact, it was already suggested that no cellular signaling event, but the high affinity of HopQ for CEACAM is responsible for promoting CagA translocation. This might allow sufficient “dwell time” for CagA to be translocated (Bonsor *et al.*, 2018). However, it is still controversial if HopQ contributes to adhesion to host cells at all. One study found a reduction of adhesion due to deletion of *hopQ* (Javaheri *et al.*, 2016), but others reported no influence on adhesion (Belogolova *et al.*, 2013, Königer *et al.*, 2016). In this work, only a slight reduction in adhesion to AGS cells due to a *hopQ* deletion was detected (Figure 3.11), but a 50 % reduction in CagA translocation was observed. Furthermore, in CEACAM1/5/6 knockout KatolIII cell line, adhesion of a *hopQ* deficient strain was only reduced to approx. 75 %, but CagA translocation was nearly abolished (Zhao *et al.*, 2018). Therefore, it is more likely that the interaction of HopQ with CEACAMs does trigger a signal necessary for CagA to be translocated rather than acting as a pure adhesion event.

4.1.2 Interaction of HopQ with gerbil CEACAM1

The interaction of HopQ with gerbil CEACAM1 was tested using bacterial pull-down assays, but no binding of gerbil CEACAM1-N-GFP to *H. pylori* was detected (Figure 3.3). However, for human CEACAM3 an interaction using a bacterial pull-down assay was only possible when using CEACAM3-Fc constructs (Javaheri *et al.*, 2016). Due to the addition of a secondary antibody, cross-linking occurred, which was necessary to detect the interaction. Isolated soluble CEACAM3-N-GFP constructs without the ability to dimerize showed no interaction with HopQ (Königer *et al.*,

2016). Therefore, it would be interesting to test gerbil CEACAM1 binding using an Fc-construct. Another approach could be the expression of gerbil CEACAM1 in a cell line without CEACAMs (e.g., HEK293) and test the adhesion and CagA translocation capacity of *H. pylori*. Interestingly, binding of rat CEACAM1 to HopQ was shown previously and a *hopQ* deficient strain was not able to colonize rats, demonstrating that HopQ can interact with CEACAMs from rodents (Javaheri *et al.*, 2016). In contrast, others reported that a *hopQ* deficient strain had no disadvantage in colonization in a gerbil infection model (Königer *et al.*, 2016). This implicates that the interaction of HopQ with CEACAM doesn't play a role in this animal model and that other receptors may play a role in triggering the severe pathologies observed in gerbils (Rieder *et al.*, 2005).

4.1.3 Targeted HopQ mutations and their impact on CagA translocation

Like other bacterial adhesins, e.g., the Opa proteins from *N. gonorrhoeae*, HopQ exploits the dimerization interface of CEACAMs for binding (Bonsor *et al.*, 2018). Solving of the HopQ-CEACAM1 complex highlighted the structures in HopQ necessary for CEACAM binding. Therefore, targeted HopQ mutants were generated according to these results. Interestingly, none of targeted mutations had a significant impact on CagA translocation and phosphorylation, except for the HopQ ^{β 2- α 4:BabA} variant, which showed an even more reduced CagA injection into AGS cells than a *hopQ* deletion mutant (Figure 3.4). In HEK293 CEACAM1 cells, this HopQ variant showed no CagA translocation. As CagA translocation in HEK293 CEACAM1 cells is only dependent on the HopQ-CEACAM1 interaction, the affinity of HopQ ^{β 2- α 4:BabA} for CEACAM1 was probably too low for efficient injection of CagA into the host cell. These results were in agreement with the observed affinities of the HopQ variants to CEACAM1 (Bonsor *et al.*, 2018). In this work, no effect of the HopQ^{L150A} mutation on CagA translocation was detected. However, another study found that point mutation of this residue to asparagine (L150N) abolished CagA translocation into MKN28 cells transfected with CEACAM1-4L (Moonens *et al.*, 2018). One reason for this could be the levels of HopQ expression of these mutants. Hop^{L150A} production was similar to wildtype levels (Bonsor *et al.*, 2018), but production of the L150N variant was reduced compared to wildtype HopQ (Moonens *et al.*, 2018). Another reason for this discrepancy might be the difference in the chosen amino acid. The L150N mutation inserted a sterically bulky polar group in the hydrophobic binding interface, which is not the case for L150A. However, according to results observed in this study, the β 2- α 4 loop of HopQ was particularly important for binding to CEACAM1 and for translocation of CagA into the host cells.

4.1.4 *BabC* restricts CagA translocation efficiency in *H. pylori* P12

To elucidate, which adhesin is responsible for the remaining 50 % of translocated CagA of a P12 Δ *hopQ* mutant into AGS cells, RNA-Seq data comparing P12 wildtype to a P12 Δ *hopQ* strain was generated (Figure 3.5). Indeed, one of the upregulated DEGs was *babC-1*, an adhesin closely related to BabA (Figure 1.2). Interestingly, deletion of *babC* in P12 resulted in increased CagA translocation rates. A double deletion of *hopQ* and *babC*, on the other hand, led to translocation levels similar to wildtype. In contrast to AGS cells, CagA translocation in KatOIII cells is mostly mediated through the HopQ-CEACAM interaction (Zhao *et al.*, 2018), thus, it was expected that additional knockout of *babC* in a *hopQ* mutant had no further effect. In addition, *babC* deletion showed no effect on CagA translocation in KatOIII cells. However, to rule out the possibility of polar effects and secondary mutations, *babC* complementation should be attempted. In addition, the adhesion behavior of the mutant should be assessed to determine if this is an adhesion effect.

4.1.5 HopQ-CagY interaction

As activation of signaling cascades by ITIMs of CEACAMs promoting CagA injection could not be proven in this work, the interaction of HopQ with the Cag-T4SS was analyzed further. Immunoprecipitation assays revealed a possible interaction of HopQ with the VirB10 homologue CagY (Figure 3.7). This result was verified using several different CagY constructs. Interaction of HopQ was still detected, albeit at lower levels, using a CagY variant with a deletion of the MMR (CagY Δ MMR::Myc), indicating that HopQ may interact with other domains of this protein (Figure 3.8). A CagY mutant defective in CagA translocation (CagY^{S1MC2}) also resulted in lower interaction levels, suggesting that a functional T4SS, such as the wildtype CagY or the CagY^{S1MC1}, has to be present for an efficient interaction with HopQ.

It was recently shown that CagA translocation is a rapid process, as translocated CagA was already detected 10 min after infection (Lettl *et al.*, 2021). The question therefore arises, if the putative HopQ-CagY complex is already pre-assembled and interaction of HopQ with CEACAMs activates translocation, or if the complex formation is very rapid as well. Compared to wildtype, the translocation kinetics using a *hopQ* deletion mutant are different, as half-maximal luminescence values were reached later (Lettl *et al.*, 2021). This may indicate that priming of the secretion apparatus by HopQ promotes CagA translocation. However, the interaction of HopQ with CagY should be verified using different assays in future.

Taken together, there is a lot of evidence that the HopQ-CEACAM interaction promotes CagA translocation through complex mechanisms and is not just based on adhesion, but elucidating the exact processes is still a challenge. ITIM-based signaling events triggered by HopQ-CEACAM1 interaction play no role in the CagA translocation process. Binding of HopQ to gerbil CEACAMs should be investigated further. In case that no interaction can be verified, other adhesin-receptor pairs may be responsible for the severe pathogenesis seen in Mongolian gerbils after *H. pylori* infection.

Other adhesins, like BabC, on the other hand, show regulatory effects on CagA translocation. However, interaction of HopQ with the T4SS seems to be a promising mechanism, by which the HopQ-CEACAM interaction promotes translocation of CagA and further experiments are necessary to elucidate this interaction.

4.2 Adhesins and their impact on CagA translocation

4.2.1 Deletion of *hopN*, *hopM* and *hopA* did not influence CagA translocation

There is ample evidence that other adhesin-receptor pairs play a role in promoting CagA translocation. For example, deletion of *hopQ* reduces CagA translocation in AGS cells to about 50 %, suggesting that the remaining 50 % is mediated by other adhesins (Königer *et al.*, 2016). Furthermore, CagA translocation and phosphorylation in human macrophages is independent of HopQ-CEACAM interaction, indicating that other receptors play a role there (Behrens *et al.*, 2020). For discovery of other adhesin-receptor pair(s), the uncharacterized putative adhesins, HopA, HopN, and HopM, were deleted and CagA translocation as well as adhesion was measured in AGS cells. None of these adhesins had an impact on CagA translocation and additional knockout of other known adhesins (BabA and OipA) did not influence translocation (Figure 3.11 A). Only *hopQ* deletion showed a significant reduction. A slight reduction in CagA translocation in KatoIII cells was detected with a *hopN* deletion mutant (Figure 3.11 B), however, translocation is mostly mediated by CEACAMs in this cell type (Zhao *et al.*, 2018). To address strain-specific effects, the same genes were deleted in a G27 strain and again, no impact on CagA translocation in AGS cells was detected (Figure 3.13). The deletion of *hopA* in G27 had a slight impact on translocation in KatoIII cells. Adhesion experiments using these strains should be performed to rule out an attachment defect. Taken together, none of these putative adhesins had a significant impact on CagA translocation or adhesion.

4.2.2 Deletion of *alpAB* promotes CagA translocation of *H. pylori* P12

Next, adhesins outside of the putative adhesin branch were targeted. The adhesins AlpA and B were selected, as not much is known about their influence on CagA translocation. Deletion of *alpAB* in P12 actually increased CagA translocation 1.5-fold in AGS as well as KatIII cells (Figure 3.14). Interestingly, triple deletion of *hopQ* and *alpAB* resulted in CagA translocation levels similar to wildtype, suggesting a modulatory role of *alpAB*. The same effect was observed for a *babC* mutation and translocation into AGS cells (Figure 3.5). This represents a novel effect on CagA translocation, which was never observed before. It appeared that *H. pylori* can modulate the amount of translocated CagA through its adhesins. The only similar finding is observed for OipA, which increases *cagPAI* dependent IL-8 production (Odenbreit *et al.*, 2009). More experiments are needed to further analyze this novel CagA translocation modulating effect due to different adhesins.

The role of *alpAB* for pathogenesis in an *H. pylori* infection is still controversial. Previously, no influence on CagA translocation or IL-8 production was observed (Odenbreit *et al.*, 2002, Lu *et al.*, 2007). However, in this work the TEM-1 β -lactamase assay was used to measure CagA translocation (Schindele *et al.*, 2016). This assay allows more accurate quantification than a CagA phosphorylation assay, thereby probably accounting for the differences in this work compared to previous work. Indeed, others found that infection of Mongolian gerbils with an *alpAB* mutant resulted in increased pathogenesis (Senkovich *et al.*, 2011), but a *cagPAI* negative strain (SS1) was used for these experiments, so there is no direct causal link.

Even the host cell receptor of AlpAB is controversial. Senkovich *et al.* (2011) suggest the extracellular matrix protein laminin as a receptor for AlpAB, but others actually observe binding of SabA to laminin (Walz *et al.*, 2005). As integrins interact with laminin, integrin knockout cell lines were used to investigate a possible connection between the AlpAB-laminin interaction and CagA translocation (Figure 3.16), but no effect was detected. However, this is not definitive proof that the AlpAB-laminin interaction plays no role in CagA translocation. Furthermore, AlpAB could have an additional receptor on the cell surface, so further experiments are needed to investigate the host cell receptors of AlpAB on epithelial cells.

4.2.3 Strain specific differences in adhesion and CagA translocation

During this work, interesting strain specific differences in adhesion and CagA translocation were observed. Adhesion of P12 Δ *alpAB* was not changed compared to wildtype, which contrasted with previous findings (Figure 3.15). Deletion of *alpAB* in P1 almost completely abolishes adhesion to KatIII cells (Odenbreit *et al.*, 1996). This indicates that attachment to host cells is mediated by

different adhesins in different *H. pylori* strains. In fact, deletion of *alpAB* in G27 decreased adhesion to AGS and Kat0III cells significantly (Figure 3.18), which also resulted in reduced CagA translocation levels (Figure 3.17). Interestingly, G27 AlpA and AlpB showed slightly different sizes in a Western blot compared to P12 (Figure 3.17), even though genetic complementation of G27 Δ *alpAB* was performed with the *alpAB* genes of P12. This indicates different post-translational modifications of the adhesins in the two strains, which could account for the differences in binding. Another unexpected finding was that deletion of *hopQ* in G27 strain did not have an influence on CagA translocation in AGS cells, which is surprising, as *hopQ* was first identified as a co-factor for T4SS function in G27 (Belogolova *et al.*, 2013). This difference may be due to the different modes of deletion, as in this work, streptomycin-erythromycin contra-selection was performed to achieve a marker-free *alpAB* deletion, whereas Belogolova *et al.* (2013) used transposon mutagenesis. On the other hand, CagA translocation in Kat0III cells was reduced significantly due to the *hopQ* deletion (Figure 3.17), indicating that the HopQ-CEACAM interaction is the major pathway for CagA translocation in Kat0III cells.

Another interesting observation was that CagA translocation and adherence to epithelial cells is not a linear correlation (Figure 3.17 & Figure 3.18). Even though *alpAB* deletion in G27 almost abolished adherence to AGS cells, CagA translocation was only decreased by about 50 %. In Kat0III cells, on the other hand, adherence was reduced to about a third compared to wildtype, but translocation was almost abolished. Thus, one or more other adhesins might mediate attachment of G27 to Kat0III cells in addition to AlpAB. Furthermore, a putative receptor mediating translocation might be more highly expressed on AGS cells than on Kat0III cells. Comparing expression of cell surface receptors of Kat0III and AGS cells might be a good starting point to investigate these discrepancies. In addition, comparison of RNA-Seq data between P12 and G27 might help in elucidating differences in *omp* gene expression patterns (Figure 3.19). Emphasizing the strain specific differences, deletion of *alpAB* resulted in a reduction of IL-8 production only in East Asian strains, but not in Western strains (Lu *et al.*, 2007). Therefore, measurement of IL-8 induction in gastric cells infected with the strains used in this work should be performed.

4.2.4 Strain-specific differences in gene transcription between P12 and G27 *alpAB* mutants

To further investigate these differences in CagA translocation due to AlpAB, RNA-Seq experiments were performed (Figure 3.19). Comparison of P12 and G27 with their respective *alpAB* deletion mutant revealed no significant change in mRNA levels of additional *omp* genes. This does not necessarily correlate with the expression of *omps*, as inhibition of translational initiation by small noncoding RNAs is a frequent event in bacteria (Bouvier *et al.*, 2008). Direct

measurement of expression levels of different OMPs, e.g. by flow cytometry or by tagging with HiBiT (Lettl *et al.*, 2021), may help to elucidate this issue.

In G27 Δ *alpAB*, one significantly upregulated DEG, *hpg27_1381*, encodes thioredoxin-2 (Table 3.1), a part of the Trx system, which is essential for maintenance of thiol/disulfide balance (Kuhns *et al.*, 2015). The *H. pylori* Trx system consists of two thioredoxin genes, *trx1* (*hp0824*) and *trx2* (*hp1458*), and a thioredoxin reductase (*trxR*) (Baker *et al.*, 2001). Trx1 is an electron donor for some antioxidant enzymes (Baker *et al.*, 2001). In addition, Trx1 and Trx2 are important for maintaining macromolecule integrity and survival of *H. pylori* under oxidative stress conditions (Kuhns *et al.*, 2015). The upregulation of *trx2* in an *alpAB* mutant is an interesting observation, as it was shown previously that the thioloxydoreductase HP0231 affects HopQ-dependent CagA translocation. HopQ possesses three consecutive disulfide bridges and is a substrate of HP0231 (Grzeszczuk *et al.*, 2018). Disruption of one disulfide bond (in loop CL1) abolishes CEACAM1 binding and CagA translocation (Hamway *et al.*, 2020). An additional effect of this thioloxydoreductase on other adhesins is possible. Disruption of the redox state in an *alpAB* deletion could explain the severe effects on host cell adhesion in G27. However, there is no evidence for a direct link between the Trx system and OMPs. An investigation of the effects on the redox state of OMPs in the presence of *trx2* deletion should be performed to further clarify this issue. In addition, a *trx2* deletion might also affect CagA translocation.

4.3 A novel mechanism for CagA injection

In this thesis, a novel mechanism of CagA injection involving human PLSCR1 is described for the first time (Figure 4.1) and provides a possible missing link between externalization of PS upon contact of *H. pylori*, the PS-binding capability of CagA and translocation of the cytotoxin into the cell.

PS is a major component of the mammalian plasma membrane and is usually only found in the internal leaflet. Exposure of PS is an important physiological signal, e.g., for apoptosis. There are two basic enzymatic activities that regulate distribution of PS between the two leaflets of the plasma membrane. One is mediated by members of type IV subfamily of P-type ATPases and removes PS from the external leaflet. The second group of enzymes, termed scramblases, catalyze rapid and nonspecific exchange of phospholipids between inner and outer leaflet of the plasma membrane. (Beyers & Williamson, 2016)

Phospholipid scramblases are ATP-independent lipid translocators, which are activated by Ca^{2+} . Scramblases are conserved in all eukaryotic organisms and disrupt the asymmetrical distribution of phospholipids during cellular events like cell activation, apoptosis, or blood coagulation. In humans, PLSCRs constitute a family of four homologous proteins, PLSCR1-4, but PLSCR1 is best characterized. (Sahu *et al.*, 2007)

Several human pathogens induce externalization of PS, like *H. pylori* (Murata-Kamiya *et al.*, 2010), several *Chlamydia* species (Goth & Stephens, 2001), influenza virus (Fujimoto *et al.*, 1998), and *Legionella pneumophila* (Gao & Abu Kwaiq, 1999). Interestingly, PLSCR1 has been identified to play a role during cellular entry of herpes simplex virus (Cheshenko *et al.*, 2018).

Evidence for involvement of PLSCR1 in CagA translocation was found in this work. Specific inhibition of PLSCR1 (inhibitor R5421) showed a dose-dependent reduction of CagA translocation, with a 50 % decrease at the highest inhibitor concentration (15 μM ; Figure 3.21). These results were rather promising, therefore a *p/scr1* knockout cell line was generated using the CRISPR/Cas9 system (Figure 3.24). After generating single cell clones, it turned out that deletion of *p/scr1* in AGS cells resulted in a 50 % reduction of CagA translocation (Figure 3.24 B). Complementation of *p/scr1* restored CagA translocation levels to almost wildtype levels (Figure 3.26 B), thus ruling out off-target effects due to unspecific activity of the Cas9 enzyme.

Furthermore, targeted mutation of the PS-binding motif in CagA led to a reduction of CagA translocation to about 50-60 % in AGS [HiBiT] cells (Figure 3.27 C). This result further emphasized the importance of PS-binding for CagA translocation. Still, further experiments to verify translocation of PLSCR1, PS and CagA into the intracellular space may be needed. Activation of

PLSCR1 seems to be linked to its tyrosine phosphorylation (Cheshenko *et al.*, 2018), so further experiments to detect phosphorylated PLSCR1 upon *H. pylori* infection are needed.

Interestingly, inhibition of Akt by miltefosine also reduced CagA translocation into AGS cells (Figure 3.21). During HSV entry, Akt is also flipped to the external leaflet of the plasma membrane, where it interacts with a viral glycoprotein, promoting conformational changes in Akt, resulting in phosphorylation by unknown kinases (Cheshenko *et al.*, 2018). As Akt is also phosphorylated upon *H. pylori* infection (Sokolova *et al.*, 2014), it may be interesting to investigate Akt in connection to PLSCR1 and determine if Akt, upon *H. pylori* infection, is translocated to the external membrane leaflet as well.

In conclusion, our data support a novel model for *H. pylori* CagA translocation, as follows: In the first step, the intracellular Ca^{2+} concentration is increased locally by contact of *H. pylori* with its host cell and thereby PLSCR1 is activated. There is evidence that the intracellular Ca^{2+} concentration is increased upon contact of *H. pylori* with its host cells in a CagA dependent way (Marlink *et al.*, 2003). Cheshenko *et al.* (2018) showed that 100-200 nM Ca^{2+} is sufficient for activating PLSCR1 and the initial increase in Ca^{2+} concentration upon contact with *H. pylori* is also in that range (Marlink *et al.*, 2003). In addition, the intracellular Ca^{2+} chelator BAPTA reduced CagA translocation into AGS cells significantly (Jiménez-Soto *et al.*, 2009). Therefore, Ca^{2+} dependent activation of PLSCR1 by *H. pylori* may be a possible first step.

After its activation by phosphorylation, the scramblase flips PS together with Akt to the outer leaflet of the plasma membrane. PS externalization during *H. pylori* infection was observed previously and translocation of CagA was reduced by addition of an α -PS antibody (Murata-Kamiya *et al.*, 2010). CagA is proposed to bind to this externalized PS and is translocated into the cell together with PS by scramblase-mediated flipping of PS. PS externalization, triggered by *H. pylori*, is rapid and transient and induces no sign of apoptosis in the infected cells (Murata-Kamiya *et al.*, 2010).

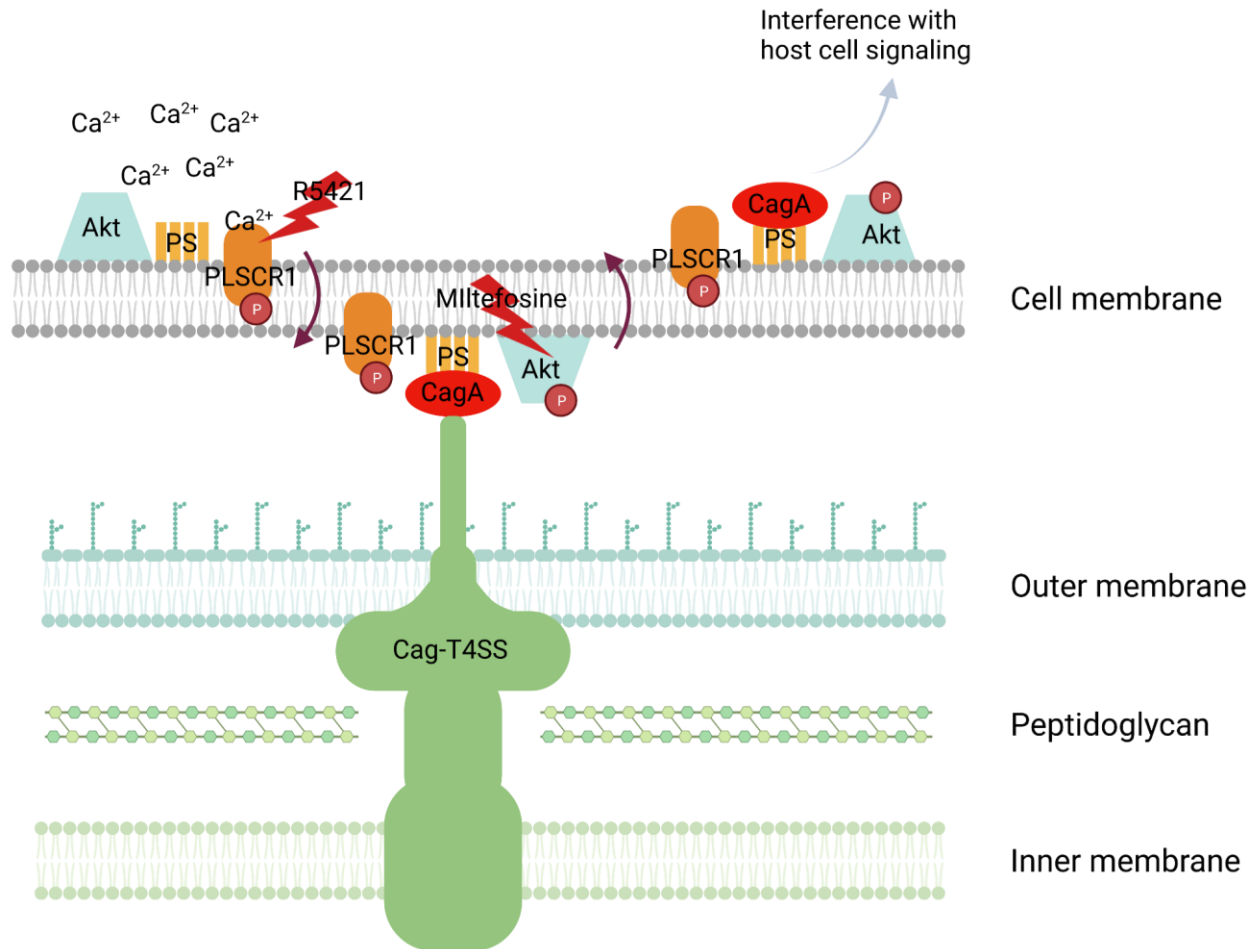


Figure 4.1: Overview of proposed mode of action of PLSCR1 in CagA translocation.

Upon interaction of *H. pylori* with their host cell, intracellular calcium (Ca²⁺) is released and PLSCR1 is activated. PLSCR1 translocates PS and Akt from the inner to the outer leaflet of the membrane. CagA can then bind to PS and PLSCR1, Akt and PS with bound CagA, is translocated back into the cell. R5421 and miltefosine are inhibitors of PLSCR1 and Akt phosphorylation respectively. Figure was created with Biorender.

However, it remains unclear, why CagA translocation is only reduced to about 50 % upon deletion of *plscr1* in AGS cells. There is evidence that PLSCR1 is not sufficient or necessary for PS externalization (Sahu *et al.*, 2007). Disruption of PLSCR1 in mice results in delayed fetal production of mature blood granulocytes and defective granulocytosis, but no defect in externalization of PS in blood cells can be detected (Zhou *et al.*, 2002). PLSCR1, isolated from erythrocytes of Scott syndrome patients, a disease with a defect in blood coagulation due to a disruption in PS externalization, show normal scramblase activity (Stout *et al.*, 1997). However, these studies focused on blood cells, and little is known about the contribution of PLSCR1 in phospholipid scrambling in epithelial cells. PLSCR1 was detected in the stomach epithelial cell

line AGS (Figure 3.23), however, PS externalization in *p/scr1* knockout cell line should be investigated.

Regardless, additional membrane components may be necessary for efficient PS externalization and internalization at the plasma membrane (Sahu *et al.*, 2007). These could also play a role in CagA injection and might account for the remaining 50 % of translocation. Other members of the PLSCR family may have a redundant function in phospholipid scrambling (Kodigepalli *et al.*, 2015). In addition to PLSCRs, two other scramblases have been identified, TMEM16F is proposed to play a role in Scott syndrome, and XKR8, which mediates PS exposure upon apoptotic stimuli (Suzuki *et al.*, 2010, Suzuki *et al.*, 2013). These scramblases could be potential targets for further investigations in the connection of PS externalization and CagA translocation. Additionally, there is some evidence that PLSCR1 is overexpressed in various cancers, *e.g.*, ovarian, colorectal, and metastatic liver cancers (Kodigepalli *et al.*, 2015). As PLSCR1-mediated reduction in CagA translocation was detected in a human adenocarcinoma cell line (Barranco *et al.*, 1983), further research is needed to verify the effect of PLSCR1 in non-transformed cell lines or *in vivo*.

Furthermore, as the role in phospholipid scrambling of PLSCR1 is controversial, other mechanisms could play a role in CagA translocation. PLSCR1 is proposed to be involved in several signaling events (Sahu *et al.*, 2007). For example, PLSCR1 interacts with epidermal growth factor (EGF) receptor (EGFR) (Sun *et al.*, 2001). Activation of EGFR leads to tyrosine phosphorylation of PLSCR1 by c-Src, which is required for interaction of phosphorylated PLSCR1 with Shc (Nanjundan *et al.*, 2003). PLSCR1 usually promotes c-Src activation through its interaction with Shc (Nanjundan *et al.*, 2003). Interestingly, EGFR is also activated by *H. pylori* in a *cagPAI* dependent way via activation of the endogenous ligand heparin-binding EGF-like growth factor (Keates *et al.*, 2001). *Cag*-T4SS components CagE (Keates *et al.*, 2001) and CagL (Wiedemann *et al.*, 2012) are involved in EGFR activation, but it is independent of CagA (Keates *et al.*, 2001). *H. pylori* induced EGFR phosphorylation leads to activation of the PI3K/Akt pathway, thereby protecting gastric epithelial cells from apoptosis (Yan *et al.*, 2009). Hence, *H. pylori* induced activation of EGFR could also activate PLSCR1, subsequently activating c-Src, which phosphorylates CagA (Mueller *et al.*, 2012). Depletion of PLSCR1 could therefore influence the phosphorylation status of CagA. In this study, however, the reduction in CagA translocation in *p/scr1* knockout cells was measured independently of the CagA phosphorylation status using the TEM-1 β -lactamase assay (Figure 3.25). Furthermore, CagA translocation was also reduced in a CagA variant lacking the PS binding motif K619 R621, suggesting a role for this binding motif, but additional interaction(s) or a more direct interaction of CagA and PLSCR1 might be possible

(Figure 3.27). Interestingly, stimulation with EGF results in internalization of plasma-membrane localized PLSCR1 into endocytic vesicles, which is then recycled back to the plasma membrane (Sun *et al.*, 2002), which could represent another possible mechanism for CagA internalization into the host cell.

PLSCR1 was identified as one of the most potently induced interferon (INF)-stimulated genes in response to INF- α , INF- β , or INF- γ (Der *et al.*, 1998). *H. pylori* infection results in recruitment of CD4⁺ T-cells, which control *H. pylori* via secretion of INF- γ (Sayi *et al.*, 2009). Gastric epithelial cells themselves also secrete INF- α and INF- β (Watanabe *et al.*, 2010). Therefore, INF-stimulated expression of PLSCR1 in response to an *H. pylori* infection should be investigated. Furthermore, in a *Staphylococcus aureus* infection, INF- α promotes expression of PLSCR1, protecting lung epithelial cells from α -toxin-induced ATP-depletion (Lizak & Yarovinsky, 2012). This shows that PLSCR1 activity could play a part in a protective mechanism against a bacterial pore-forming toxin (Lizak & Yarovinsky, 2012). Thus, it might be interesting to investigate a possible link between PLSCR1 and the *H. pylori* pore-forming toxin VacA.

Even though further experiments are needed, the results obtained in this study give strong evidence that PLSCR1 is involved in CagA translocation. This provides an opportunity to develop inhibitors of CagA translocation by blocking PLSCR1 mediated injection of the cytotoxin without negatively affecting normal cellular signaling pathways.

4.4 The annexin-*H. pylori* interaction and implications for TLR-4 activation

In this work, the previously reported *H. pylori*-annexin interaction (Petri, 2020) was further characterized. Annexin binding to different *H. pylori* strains was analyzed and strong strain-specific differences were detected (Figure 3.28). Especially the type II strains Tx30a and X47 showed significantly reduced median FI levels compared to the P12 strain. The influence of CagA on annexin binding was analyzed previously and no significant difference was detected, but VacA seems to have some impact on annexin binding (Petri, 2020).

The binding site for annexin was indentified to be LPS (Figure 3.29). Analysis of AnxA5-binding to different G27 LPS mutants revealed that deletion of *waaL* had no influence on the interaction (Figure 3.31 A). As the *waaL* deletion mutant results in the loss of its O-antigen (Li *et al.*, 2017), this structure is probably not the AnxA5 binding site. The *rfaE* and the *hp1284* mutant showed the highest increase in median FI in G27. Both the *rfaE* and the *hp1284* mutant do not possess the side chain at the HepIII residue (Figure 3.30) (Li *et al.*, 2017, Stein *et al.*, 2017), indicating that this structure might be involved in shielding the binding site from AnxA5. By far the highest increase in median FI in both G27 and 26695 showed the *rfaE* mutant (Figure 3.31 A, C). As this structure only consists of lipid A and a KDO residue (Stein *et al.*, 2017), the lipid A part of LPS is the most probable binding site for AnxA5. In P12, *rfaE* deletion also resulted in a not significant increase in AnxA5 binding.

Interestingly, CagA translocation of a P12[HiBiT-CagA] Δ *rfaE* was significantly decreased due to addition of AnxA5 (Figure 3.37 B). Reduction in CagA translocation due to AnxA5 addition was reported previously (Murata-Kamiya *et al.*, 2010). However, they hypothesized that this reduction was due to AnxA5 binding to externalized PS and not to *H. pylori* itself. K. Petri could show that pre-incubation of the bacteria with AnxA5 could further reduce CagA translocation (Petri, 2020), therefore showing that the interaction of AnxA5 with *H. pylori* rather than with PS was more important for inhibition of CagA translocation. This was also quantified in this work (Figure 3.37 A), as pre-incubation with 10 μ g/ml AnxA5 reduced CagA translocation to about 80 %.

4.4.1 AnxA5 binds to the lipid A part of *H. pylori* LPS

As the *rfaE* mutant LPS only consists of lipid and a KDO residue, lipid A mutants were generated in *H. pylori* strains G27, P12 and 26695 (Figure 3.33 D). In both G27 and 26695, the double deletion of *lpxE/lpxF*, which results in a *bis*-phosphorylated, *hexa*-acetylated lipid A species, resulted in an increase in median FI, indicating that the phosphates at the 1- and 4'-positions of lipid A could be the AnxA5-binding site (Figure 3.33 A, C). As the binding of annexin to *H. pylori* is dependent on Ca²⁺ (Petri, 2020), these negatively charged structures are a likely target for the

interaction. The phosphate group at the 4'-position was more important for AnxA5 binding, as deletion of *lpxF* had more impact on the median FI than *lpxE* deletion in G27.

In contrast to G27, the *eptA* deletion in 26695 resulted in a significant increase in AnxA5 binding (Figure 3.33). This may indicate that an *eptA* deletion gives rise to different species of lipid A in *H. pylori* strains G27 and 26695. There is some evidence that lipid A modification works differently in 26695, as the majority of detected lipid A corresponds to a *hexa*-acetylated and *bis*-phosphorylated lipid A species in a *lpxE* deletion strain, whereas in other strains, deletion of this gene results in *tetra*-acetylated lipid A, which is phosphorylated at the 1-position (Tran *et al.*, 2005). This could also explain, why the deletion of *lpxE* in 26695 resulted in a not significant decrease compared to the wildtype.

Interestingly, deletion of these genes in P12 had no impact on AnxA5 binding. An additional binding site for AnxA5 could also be a possible explanation for this discrepancy, as well as other lipid A modifications in P12. The lipid A species synthesized in a *lpxE/F* mutant is *hexa*-acetylated and *bis*-phosphorylated, similar to *E. coli* lipid A (Cullen *et al.*, 2011), but LPS of *E. coli* is not bound by AnxA5 (Figure 3.29). Therefore, additional experiments are necessary to elucidate if annexins are capable to bind to additional structures besides lipid A of *H. pylori*.

4.4.2 AnxA5 can mask recognition by TLR-4

Lipid A of *H. pylori* is usually poorly recognized by TLR-4 due to its modifications (Li *et al.*, 2016). Deletion of *lpxE/F*, however, results in a lipid A species capable of activating TLR-4 signaling (Cullen *et al.*, 2011). Therefore, TLR-4 activation was measured in *lpxE/F* knockout strains with the addition of AnxA5 (Figure 3.36 A, B). To rule out NF- κ B signaling triggered by the Cag-T4SS, all experiments were performed with an additional *cagPAI* deletion.

As expected, G27 and P12 showed almost no activation of TLR-4. In G27, the activation of TLR-4 by Δ *lpxE/F* was much stronger compared to P12 Δ *lpxE/F*. As AnxA5 binding of the *lpxE/F* deletion in P12 was different to G27 and 26695, it was not surprising that this strain also behaved differently in connection to TLR-4 activation. Nevertheless, in both strains, addition of AnxA5 resulted in decreased TLR-4 signaling, indicating that AnxA5 binding masked lipid A from recognition by TLR-4.

Surprisingly, a PMSS1 strain, re-isolated from the mouse stomach after 3 weeks of infection, showed increased AnxA5 binding compared to the lab-adapted precursor strain (Figure 3.35). This strain was also tested for TLR-4 signaling (Figure 3.36 C). The re-isolated strain induced more TLR-4 activation than the precursor strain, but the background was very high due to the Cag-T4SS, so this increase was not significant. Addition of AnxA5 to the re-isolated strain,

however, reduced TLR-4 mediated signaling, whereas no effect of AnxA5 was detected in the PMSS1 lab-adapted strain. This interesting result indicated that an adaption of lipid A occurred *in vivo*.

In contrast to other bacterial species, modifications of lipid A in *H. pylori* are constitutive, giving rise to only one form of lipid A under laboratory conditions (Stead *et al.*, 2010). However, there is some evidence that *H. pylori* does indeed produce variations of lipid A. For example, a minor *bis*-phosphorylated and *hexa*-acetylated lipid A species, resembling that of *E. coli*, can be found in *H. pylori*, which corresponds to the precursor species before modification (Tran *et al.*, 2005).

Furthermore, lipid A might be modified in response to stressors *in vivo*, e.g., calprotectin (CP) (Gaddy *et al.*, 2015). CP is an antimicrobial factor, which, upon release from neutrophils, sequesters nutrients, restricting access to essential metals (manganese and zinc) (Hood & Skaar, 2012). *H. pylori* alters its lipid A molecules in response to CP, resulting in increased biofilm formation and increased bacterial fitness by restricting enzymes of the lipid A modification pathway, including LpxF (Gaddy *et al.*, 2015). In other organisms, lipid A modification occurs upon environmental cues (Stead *et al.*, 2010). Thus, lipid A modifications might also occur in *H. pylori in vivo*, as results presented in this study and by Gaddy *et al.* (2015) could indicate. Identification of the lipid A species in the re-isolated PMSS1 strains might give insights into the modifications occurring *in vivo*.

Interestingly, one of the first immune cells, encountering *H. pylori* in the stomach mucosa, are conventional dendritic cells (cDC2s) (Necchi *et al.*, 2009, Sebrell *et al.*, 2019). TLR-4 activation in these cDC2s drives secretion of inflammatory cytokines and chemokines, which can be blocked by an α -TLR-4 antibody, indicating that these cells are capable of recognizing LPS of *H. pylori* (Neuper *et al.*, 2020). It would be interesting to analyze if AnxA5 binding could attenuate TLR-4 activation in cDC2s.

Lipid A of *H. pylori* mediates resistance to CAMPs because of its unique structure (Monteiro, 2001, Cullen *et al.*, 2011). However, deletion of enzymes in the lipid A modification pathway results in increased sensitivity to CAMPs (Tran *et al.*, 2006, Cullen *et al.*, 2011). It may be possible that the annexin binding to lipid A could mediate increased resistance to CAMPs. Further experiments to test this hypothesis are necessary.

4.4.3 AnxA5 co-localizes with *H. pylori* in the human stomach

Analysis of human stomach sections revealed an increase in AnxA2 and AnxA5 levels probably due to an *H. pylori* infection (Figure 3.38). Overexpression of AnxA2 and AnxA4 in patients

infected with *H. pylori* as well as in human epithelial cell lines was described before (Lin *et al.*, 2008). AnxA2 upregulation can also be found in *H. pylori* infected human epithelial cell lines, AGS and NCI-N87 (Conlin *et al.*, 2004). Thus, the rise in AnxA5 levels in *H. pylori* infected patients has not been described before. However, it is still unclear whether the increase in annexin levels is directly attributable to *H. pylori* infection or to inflammation caused by *H. pylori*. There is some evidence that AnxA5 acts as a tumor suppressor in gastric cancer cells (Wang *et al.*, 2021), however, further investigations in the connection of AnxA5 and gastric cancer are necessary.

Co-localization of *H. pylori* with AnxA5 was detected in human stomach tissue (Figure 3.39). As expected, some bacteria bind a lot of AnxA5, whereas others bind only a small amount or no AnxA5 at all. This is in accordance with the *in vitro* data of this study, as AnxA5 binding varies, depending on the strain, between 50 and 80 % (Figure 3.28 A). The 3D-reconstruction revealed that AnxA5 mostly bound to the surface of the bacteria (Figure 3.39 D), as it was expected due to the interaction with lipid A.

4.5 Outlook

This thesis had four main objectives. First, the influence of the HopQ-CEACAM interaction on CagA translocation was investigated. It was shown that the cytoplasmic ITIM domain of CEACAM1 had no influence on CagA translocation. Thus, signal transduction triggered by HopQ was not necessary for efficient translocation of CagA into the host cell. However, it remains to be elucidated how the exploitation of CEACAMs by HopQ promote CagA translocation. Even though no interaction was detected between HopQ and gerbil CEACAM1, other methods should be applied to verify this result. Solving the HopQ-CEACAM1 structure and subsequent analysis of targeted HopQ modifications helped to get further insight into CEACAM recognition by HopQ. These results may be important for development of novel CagA translocation inhibitors by blocking the HopQ-CEACAM interaction *in vivo*. A promising result was the proposed interaction of HopQ with CagY. Priming of the Cag-T4SS through the interaction of HopQ with CagY might be one possible explanation how the binding of HopQ to CEACAMs promotes CagA translocation. However, further studies are needed to verify this interaction. Taken together, further extensive research is needed to elucidate how exploitation of CEACAMs by the bacterial adhesin HopQ is involved in the efficient translocation of CagA into host cells.

The second aim was the identification of novel adhesin-receptor pairs necessary for efficient CagA translocation. For this, several adhesins of the putative adhesin branch were deleted and their influence on CagA translocation was tested. However, none of the targeted adhesins were significantly involved in adhesion or CagA translocation. Deletion of *alpAB* revealed interesting effects on CagA translocation. It is possible that regulation of CagA translocation is dependent on the *H. pylori* strain, as strain-specific differences were detected in connection with *alpAB* and *hopQ* deletion. Analyzing the outer membrane expression profiles of different *H. pylori* strains might help to elucidate these strain-specific differences and in finding novel adhesin-receptor pairs.

The third aim of this thesis was to analyze the mechanisms of CagA translocation in more detail resulting in the proposal of a novel mechanism for CagA translocation. The putative scramblase PLSCR1 is suggested to be involved in CagA translocation by flipping the phospholipid PS onto the outer membrane leaflet, where CagA can bind. Subsequently, PLSCR1 might flip back both, PS and the bound CagA, into the cells. Deletion of PLSCR1 resulted in decreased CagA translocation (50 %), which was restored by genetic complementation. Other scramblases might also be involved in internalization of CagA. In conclusion, the results in this study provide

preliminary evidence that PLSCR1 is involved in internalization of CagA and help to clarify the missing link between the interaction of CagA with PS and translocation into the host cell.

Finally, the novel interaction of *H. pylori* with members of the annexin family was further characterized. Lipid A, as a component of LPS, was shown to be the binding site for AnxA5, but other binding sites are also possible and are the subject of further research. Surprisingly, the interaction of AnxA5 with *H. pylori* was able to inhibit TLR-4 mediated signaling events. In conclusion, annexins are exploited by *H. pylori* to alter its surface and thereby interfere with the immune recognition of the host.

Appendix

List of figures

Figure 1.1: Pathogenicity factors of <i>H. pylori</i>	6
Figure 1.2: Hop and Hor family tree.....	15
Figure 1.3: Schematic overview of intra- and extracellular functions of annexins.....	18
Figure 2.1: Makro code for counting the nuclei	59
Figure 2.2: Makro code for measuring the fluorescence intensity	60
Figure 3.1: Transfection of HEK293 with CEACAM1-4L and CEACAM Δ CT.	62
Figure 3.2: Comparison of the structure of human, mouse, and Mongolian gerbil CEACAMs....	64
Figure 3.3: Binding of gerbil CEACAM1 to <i>H. pylori</i>	65
Figure 3.4: Effects of targeted mutations in HopQ on CagA translocation.....	67
Figure 3.5: Results of RNA-Seq and TEM-assay data for P12 vs. P12 Δ hopQ.....	69
Figure 3.6: Generation of HopQ ^{Myc}	70
Figure 3.7: Pull-down assays with HopQ ^{Myc}	71
Figure 3.8: Pull-down assays using different CagY constructs.....	73
Figure 3.9: Streptomycin-erythromycin contra-selection method to generate marker-free knockout mutants.	76
Figure 3.10: Deletion of putative adhesin genes in <i>H. pylori</i>	77
Figure 3.11: Influence of multiple OMP deletions on CagA translocation.....	78
Figure 3.12: Influence of multiple OMP deletions on adhesion.	79
Figure 3.13: Influence on CagA translocation of <i>hopA</i> , <i>hopM</i> and <i>hopN</i> deletion in G27.	80
Figure 3.14: Generation of <i>alpAB</i> deletion in P12 and the influence on CagA translocation.	82
Figure 3.15: The effect of an <i>alpAB</i> deletion on adhesion to AGS and Kat0III cells.	84
Figure 3.16: Influence of an <i>alpAB</i> deletion in P12 on CagA translocation in integrin knockout cell lines.....	85
Figure 3.17: Deletion of <i>alpAB</i> and <i>hopQ</i> in <i>H. pylori</i> G27 and the effect on CagA translocation.	87
Figure 3.18: Adhesion of G27 Δ <i>alpAB</i> and Δ <i>hopQ</i> to AGS and Kat0III cells.....	88
Figure 3.19: DEGs in (A) P12 vs. P12 Δ <i>alpAB</i> and (B) G27 vs. G27 Δ <i>alpAB</i> according to RNA-Seq results.	89
Figure 3.20: Structure of miltefosine (A) and R5421 (B). Figure was created with Biorender.	91
Figure 3.21: Influence of Akt1 and PLSCR1 inhibitors on CagA translocation.	92
Figure 3.22: Schematic overview for generation of gRNAs for knockout of exon 4 of <i>plscr1</i>	94

Figure 3.23: Verification of <i>plscr1</i> inactivation in AGS cells.	95
Figure 3.24: Influence of <i>plscr1</i> inactivation on CagA translocation.	96
Figure 3.25: Characterization of complemented AGS Δ <i>plscr1</i> cells.	98
Figure 3.26: CagA translocation in EGFP-PLSCR1 complemented cell lines.	99
Figure 3.27: CagA translocation of a PS-binding deficient CagA variant.	100
Figure 3.28: AnxA5 binding by different <i>H. pylori</i> strains.	102
Figure 3.29: LPS dot blots using human AnxA5.	103
Figure 3.30: Overview of LPS structures of G27 wildtype, G27 Δ <i>hp1284</i> , G27 Δ <i>waaL</i> and G27 Δ <i>rfaE</i>	104
Figure 3.31: LPS mutant strains and AnxA5 binding.	105
Figure 3.32: Percentage of bacteria bound by AnxA5-Alexa647 in LPS mutant strains.	108
Figure 3.33: AnxA5 binding to lipid A mutants in G27, P12 and 26695.	109
Figure 3.34: Percentage of bacteria bound by AnxA5-Alexa647 in lipid A mutant strains.	110
Figure 3.35: AnxA5-binding assay using a mouse-isolated strain.	111
Figure 3.36: Influence of AnxA5 on TLR-4 activation by different <i>H. pylori</i> strains.	113
Figure 3.37: Influence of AnxA5 binding on CagA translocation in P12[HiBiT-CagA] and P12[HiBiT-CagA] Δ <i>rfaE</i>	114
Figure 3.38: Influence of <i>H. pylori</i> infection on detected annexin A1, A2 and A5 <i>in vivo</i>	115
Figure 3.39: Co-localization of <i>H. pylori</i> with AnxA5 <i>in vivo</i>	117
Figure 4.1: Overview of proposed mode of action of PLSCR1 in CagA translocation.	127

List of tables

Table 1.1: Components of the Cag-T4SS, their localization and function (Backert <i>et al.</i> , 2015). ...	9
Table 2.1: Cell lines used in this work.	24
Table 2.2: <i>E. coli</i> strains used in this work.	25
Table 2.3: List of <i>H. pylori</i> strains.	25
Table 2.4: Plasmids used in this work.	31
Table 2.5: List of primers.	33
Table 2.6: List of gRNAs for CRISPR/Cas9.	35
Table 2.7: List of primary antibodies.	36
Table 2.8: List of secondary antibodies.	36
Table 2.9: List of commercially available kits.	37
Table 2.10: Composition of buffers.	38

Table 2.11: Composition of vitamin mix for serum plates.....	44
Table 2.12: Composition of CCF4-AM solution for one reaction	48
Table 2.13: Composition of HiBiT reaction solution	49
Table 2.14: Standard PCR reaction mix	52
Table 2.15: Standard PCR protocol.....	52
Table 2.16: Control digestion reaction	53
Table 2.17: Preparative restriction reaction	54
Table 2.18: Composition of resolving gels with different amounts of PAA.....	55
Table 2.19: Composition of a 4 % stacking gel	55
Table 2.20: Developing solution to detect AP-coupled secondary antibodies	56
Table 2.21: Treatment for de-paraffinization	57
Table 3.1: List of differentially expressed genes in <i>G27</i> vs. <i>G27ΔalpAB</i>	90

List of abbreviations

aa	Amino acids
AlpAB	Adherence-associated lipoprotein A and B
AnxA	Annexin
AP	Alkaline phosphatase
BabA	Blood group antigen binding protein A
BB	Brucella broth
BCIP	5-Brom-4-chlor-3-indoxylphosphate
BSA	Bovine serum albumin
CagA	Cytotoxin-associated gene A
cagPAI	Cag pathogenicity island
Cag-T4SS	Cag Type IV secretion system
CAMP	Cationic antimicrobial peptides
CEACAM	Carcinoembryonic antigen-related cell adhesion molecules
cfu	Colony forming units
CP	Calprotectin
CSK	C-terminal Src kinase
ddH ₂ O	Ultrapure water
DEG	Differentially expressed gene
DMSO	Dimethylsulfoxid
DNA	Deoxyribonucleic acid
DPBS	Dulbecco's phosphate buffered solution
EDTA	Ethylenediaminetetraacetic acid
EGFP	Enhanced GFP

EHEC	Enterohemorrhagic <i>E. coli</i>
EPEC	Enteropathogenic <i>E. coli</i>
EPIYA	Glu-Pro-Ile-Tyr-Ala
EV	Extracellular vesicles
FACS	Fluorescence-activated cell sorting
FAK	Focal adhesion kinase
FCS	Fetal calf serum
FI	Fluorescence intensity
gDNA	genomic DNA
GFP	Green fluorescent protein
gRNA	guide RNA
Hof	<i>Helicobacter</i> OMP
Hom	<i>Helicobacter</i> outer membrane
Hop	<i>Helicobacter pylori</i> outer membrane proteins
Hor	<i>Helicobacter pylori</i> outer membrane protein related
IF	Immunofluorescence
IgC	Constant immunoglobulin domain
IgV	Variable immunoglobulin domain
INF	Interferon
IP	Immunoprecipitation
ITAM	Immunoreceptor tyrosine-based activation motif
ITIM	Immunoreceptor tyrosine-based inhibitory motif
ITSM	Immunoreceptor tyrosine-based switch motif
LabA	LacdiNAc-binding adhesin A
LB	Luria Bertani
Le ^b	Lewis B
LPS	Lipopolysaccharide
MFI	Mean fluorescence intensity
MOI	Multiplicity of infection
NBT	Nitro blue tetrazolium chloride
NF-κB	Nuclear factor κB
OD	Optical density
OipA	Outer inflammatory protein A
OMP	Outer membrane proteins
ORF	Open reading frame
PAA	Polyacrylamide
PBS	Phosphate buffered saline
PCR	Polymerase chain reaction
PE	Phosphatidylethanolamine
PLSCR	Phospholipid scramblase
PMN	Polymorphonuclear leukocytes

PMSF	Phenylmethylsulfonyl fluoride
POX	Peroxidase
PS	Phosphatidylserine
PVDF	Polyvinylidenfluorid
RIPA	Radioimmunoprecipitation assay buffer
RNA	Ribonucleic acid
rpm	revolutions per minute
rpsL	Ribosomal protein S12
RT	Room temperature
SabA	Sialic acid binding adhesin A
SD	Standard deviation
SDS-PAGE	Sodium dodecyl sulfate polyacrylamide gel electrophoresis
SEM	Standard error of mean
SFK	Src family kinases
sLe ^a	A glycosphingolipid
sLe ^x	Sialyl Lewis X
TLR	Toll-like receptor
VacA	Vacuolating cytotoxin A

Bibliography

- Ailloud F, Estibariz I and Suerbaum S (2021). 'Evolved to vary: genome and epigenome variation in the human pathogen *Helicobacter pylori*', FEMS Microbiol Rev, **45**:(1).
- Alm RA, Bina J, Andrews BM, Doig P, Hancock RE and Trust TJ (2000). 'Comparative genomics of *Helicobacter pylori*: analysis of the outer membrane protein families', Infect Immun, **68**:(7) 4155-4168.
- Ansari S and Yamaoka Y (2019). '*Helicobacter pylori* Virulence Factors Exploiting Gastric Colonization and its Pathogenicity', Toxins (Basel), **11**:(11).
- Aras RA, Fischer W, Perez-Perez GI, Crosatti M, Ando T, Haas R and Blaser MJ (2003). 'Plasticity of repetitive DNA sequences within a bacterial (Type IV) secretion system component', J Exp Med, **198**:(9) 1349-1360.
- Arnold IC, Artola-Borán M, Tallón de Lara P, Kyburz A, Taube C, Ottemann K, van den Broek M, Yousefi S, Simon HU and Müller A (2018). 'Eosinophils suppress Th1 responses and restrict bacterially induced gastrointestinal inflammation', J Exp Med, **215**:(8) 2055-2072.
- Aspholm-Hurtig M, Dailide G, Lahmann M, Kalia A, Ilver D, Roche N, Vikström S, Sjöström R, Lindén S, Bäckström A, Lundberg C, Arnqvist A, Mahdavi J, Nilsson UJ, Velapatifo B, Gilman RH, Gerhard M, Alarcon T, López-Brea M, Nakazawa T, Fox JG, Correa P, Dominguez-Bello MG, Perez-Perez GI, Blaser MJ, Normark S, Carlstedt I, Oscarson S, Teneberg S, Berg DE and Borén T (2004). 'Functional adaptation of BabA, the *H. pylori* ABO blood group antigen binding adhesin', Science, **305**:(5683) 519-522.
- Atherton JC, Cao P, Peek RM, Jr., Tummuru MK, Blaser MJ and Cover TL (1995). 'Mosaicism in vacuolating cytotoxin alleles of *Helicobacter pylori*. Association of specific vacA types with cytotoxin production and peptic ulceration', J Biol Chem, **270**:(30) 17771-17777.
- Backert S, Tegtmeyer N and Fischer W (2015). 'Composition, structure and function of the *Helicobacter pylori* cag pathogenicity island encoded type IV secretion system', Future Microbiol, **10**:(6) 955-965.
- Baker LM, Raudonikiene A, Hoffman PS and Poole LB (2001). 'Essential thioredoxin-dependent peroxiredoxin system from *Helicobacter pylori*: genetic and kinetic characterization', J Bacteriol, **183**:(6) 1961-1973.
- Baltrus DA, Amieva MR, Covacci A, Lowe TM, Merrell DS, Ottemann KM, Stein M, Salama NR and Guillemin K (2009). 'The complete genome sequence of *Helicobacter pylori* strain G27', J Bacteriol, **191**:(1) 447-448.
- Bandorowicz-Pikula J, Wos M and Pikula S (2012). 'Do annexins participate in lipid messenger mediated intracellular signaling? A question revisited', Mol Membr Biol, **29**:(7) 229-242.
- Barranco SC, Townsend CM, Jr., Casartelli C, Macik BG, Burger NL, Boerwinkle WR and Gourley WK (1983). 'Establishment and characterization of an *in vitro* model system for human adenocarcinoma of the stomach', Cancer Res, **43**:(4) 1703-1709.
- Barrozo RM, Cooke CL, Hansen LM, Lam AM, Gaddy JA, Johnson EM, Cariaga TA, Suarez G, Peek RM, Jr., Cover TL and Solnick JV (2013). 'Functional plasticity in the type IV secretion system of *Helicobacter pylori*', PLoS Pathog, **9**:(2) e1003189.
- Barrozo RM, Hansen LM, Lam AM, Skoog EC, Martin ME, Cai LP, Lin Y, Latoscha A, Suerbaum S, Canfield DR and Solnick JV (2016). 'CagY Is an Immune-Sensitive Regulator of the *Helicobacter pylori* Type IV Secretion System', Gastroenterology, **151**:(6) 1164-1175.e1163.
- Behrens IK, Busch B, Ishikawa-Ankerhold H, Palamides P, Shively JE, Stanners C, Chan C, Leung N, Gray-Owen S and Haas R (2020). 'The HopQ-CEACAM Interaction Controls CagA Translocation, Phosphorylation, and Phagocytosis of *Helicobacter pylori* in Neutrophils', mBio, **11**:(1).
- Belogolova E, Bauer B, Pompaiah M, Asakura H, Brinkman V, Ertl C, Bartfeld S, Nechitaylo TY, Haas R, Machuy N, Salama N, Churin Y and Meyer TF (2013). '*Helicobacter pylori* outer membrane protein HopQ identified as a novel T4SS-associated virulence factor', Cell Microbiol, **15**:(11) 1896-1912.
- Berghold VM, Gauster M, Hemmings DG, Moser G, Kremshofer J, Siwetz M, Sundl M and Huppertz B (2015). 'Phospholipid scramblase 1 (PLSCR1) in villous trophoblast of the human placenta', Histochem Cell Biol, **143**:(4) 381-396.
- Bevers EM and Williamson PL (2016). 'Getting to the Outer Leaflet: Physiology of Phosphatidylserine Exposure at the Plasma Membrane', Physiol Rev, **96**:(2) 605-645.
- Bonsor DA, Günther S, Beadenkopf R, Beckett D and Sundberg EJ (2015). 'Diverse oligomeric states of CEACAM IgV domains', Proc Natl Acad Sci U S A, **112**:(44) 13561-13566.

- Bonsor DA, Zhao Q, Schmidinger B, Weiss E, Wang J, Deredge D, Beadenkopf R, Dow B, Fischer W, Beckett D, Wintrobe PL, Haas R and Sundberg EJ (2018). 'The *Helicobacter pylori* adhesin protein HopQ exploits the dimer interface of human CEACAMs to facilitate translocation of the oncoprotein CagA', Embo j, **37**:(13).
- Borén T, Falk P, Roth KA, Larson G and Normark S (1993). 'Attachment of *Helicobacter pylori* to human gastric epithelium mediated by blood group antigens', Science, **262**:(5141) 1892-1895.
- Bouvier M, Sharma CM, Mika F, Nierhaus KH and Vogel J (2008). 'Small RNA binding to 5' mRNA coding region inhibits translational initiation', Mol Cell, **32**:(6) 827-837.
- Bugaytsova JA, Björnham O, Chernov YA, Gideonsson P, Henriksson S, Mendez M, Sjöström R, Mahdavi J, Shevtsova A, Ilver D, Moonens K, Quintana-Hayashi MP, Moskalenko R, Aisenbrey C, Bylund G, Schmidt A, Åberg A, Brännström K, Königer V, Vikström S, Rakhimova L, Hofer A, Ögren J, Liu H, Goldman MD, Whitmire JM, Adén J, Younson J, Kelly CG, Gilman RH, Chowdhury A, Mukhopadhyay AK, Nair GB, Papadakos KS, Martinez-Gonzalez B, Sgouras DN, Engstrand L, Unemo M, Danielsson D, Suerbaum S, Oscarson S, Morozova-Roche LA, Olofsson A, Gröbner G, Holgersson J, Esberg A, Strömberg N, Landström M, Eldridge AM, Chromy BA, Hansen LM, Solnick JV, Lindén SK, Haas R, Dubois A, Merrell DS, Schedin S, Remaut H, Arnqvist A, Berg DE and Borén T (2017). '*Helicobacter pylori* Adapts to Chronic Infection and Gastric Disease via pH-Responsive BabA-Mediated Adherence', Cell Host Microbe, **21**:(3) 376-389.
- Camilo V, Sugiyama T and Touati E (2017). 'Pathogenesis of *Helicobacter pylori* infection', Helicobacter, **22** **Suppl 1**.
- Cao P and Cover TL (2002). 'Two different families of *hopQ* alleles in *Helicobacter pylori*', J Clin Microbiol, **40**:(12) 4504-4511.
- Censini S, Lange C, Xiang Z, Crabtree JE, Ghiara P, Borodovsky M, Rappuoli R and Covacci A (1996). '*cag*, a pathogenicity island of *Helicobacter pylori*, encodes type I-specific and disease-associated virulence factors', Proc Natl Acad Sci U S A, **93**:(25) 14648-14653.
- Chang YW, Shaffer CL, Rettberg LA, Ghosal D and Jensen GJ (2018). '*In Vivo* Structures of the *Helicobacter pylori* *cag* Type IV Secretion System', Cell Rep, **23**:(3) 673-681.
- Chauhan N, Tay ACY, Marshall BJ and Jain U (2019). '*Helicobacter pylori* VacA, a distinct toxin exerts diverse functionalities in numerous cells: An overview', Helicobacter, **24**:(1) e12544.
- Cheshenko N, Pierce C and Herold BC (2018). 'Herpes simplex viruses activate phospholipid scramblase to redistribute phosphatidylserines and Akt to the outer leaflet of the plasma membrane and promote viral entry', PLoS Pathog, **14**:(1) e1006766.
- Chung JM, Sheedlo MJ, Campbell AM, Sawhney N, Frick-Cheng AE, Lacy DB, Cover TL and Ohi MD (2019). 'Structure of the *Helicobacter pylori* Cag type IV secretion system', Elife, **8**.
- Conlin VS, Curtis SB, Zhao Y, Moore ED, Smith VC, Meloche RM, Finlay BB and Buchan AM (2004). '*Helicobacter pylori* infection targets adherens junction regulatory proteins and results in increased rates of migration in human gastric epithelial cells', Infect Immun, **72**:(9) 5181-5192.
- Cover TL and Blaser MJ (1992). 'Purification and characterization of the vacuolating toxin from *Helicobacter pylori*', J Biol Chem, **267**:(15) 10570-10575.
- Cover TL, Tummuru MK, Cao P, Thompson SA and Blaser MJ (1994). 'Divergence of genetic sequences for the vacuolating cytotoxin among *Helicobacter pylori* strains', J Biol Chem, **269**:(14) 10566-10573.
- Cullen TW, Giles DK, Wolf LN, Ecobichon C, Boneca IG and Trent MS (2011). '*Helicobacter pylori* versus the host: remodeling of the bacterial outer membrane is required for survival in the gastric mucosa', PLoS Pathog, **7**:(12) e1002454.
- Dailidiene D, Dailide G, Kersulyte D and Berg DE (2006). 'Contraselectable streptomycin susceptibility determinant for genetic manipulation and analysis of *Helicobacter pylori*', Appl Environ Microbiol, **72**:(9) 5908-5914.
- Dallacasagrande V and Hajjar KA (2020). 'Annexin A2 in Inflammation and Host Defense', Cells, **9**:(6).
- de Brito BB, da Silva FAF, Soares AS, Pereira VA, Santos MLC, Sampaio MM, Neves PHM and de Melo FF (2019). 'Pathogenesis and clinical management of *Helicobacter pylori* gastric infection', World J Gastroenterol, **25**:(37) 5578-5589.
- Dekkers DW, Comfurius P, Vuist WM, Billheimer JT, Dicker I, Weiss HJ, Zwaal RF and Bevers EM (1998). 'Impaired Ca²⁺-induced tyrosine phosphorylation and defective lipid scrambling in erythrocytes from a patient with Scott syndrome: a study using an inhibitor for scramblase that mimics the defect in Scott syndrome', Blood, **91**:(6) 2133-2138.

- Der SD, Zhou A, Williams BR and Silverman RH (1998). 'Identification of genes differentially regulated by interferon alpha, beta, or gamma using oligonucleotide arrays', Proc Natl Acad Sci U S A, **95**:(26) 15623-15628.
- Dossumbekova A, Prinz C, Mages J, Lang R, Kusters JG, Van Vliet AH, Reindl W, Backert S, Saur D, Schmid RM and Rad R (2006). '*Helicobacter pylori* HopH (OipA) and bacterial pathogenicity: genetic and functional genomic analysis of hopH gene polymorphisms', J Infect Dis, **194**:(10) 1346-1355.
- Duan H, Chen L, Qu L, Yang H, Song SW, Han Y, Ye M, Chen W, He X and Shou C (2014). '*Mycoplasma hyorhinis* infection promotes NF- κ B-dependent migration of gastric cancer cells', Cancer Res, **74**:(20) 5782-5794.
- Eusebi LH, Zagari RM and Bazzoli F (2014). 'Epidemiology of *Helicobacter pylori* infection', Helicobacter, **19 Suppl 1** 1-5.
- Feige MH, Sokolova O, Pickenhahn A, Maubach G and Naumann M (2018). 'HopQ impacts the integrin α 5 β 1-independent NF- κ B activation by *Helicobacter pylori* in CEACAM expressing cells', Int J Med Microbiol, **308**:(5) 527-533.
- Ferrero RL, Thiberge JM, Huerre M and Labigne A (1998). 'Immune responses of specific-pathogen-free mice to chronic *Helicobacter pylori* (strain SS1) infection', Infect Immun, **66**:(4) 1349-1355.
- Fischer W, Buhrdorf R, Gerland E and Haas R (2001). 'Outer membrane targeting of passenger proteins by the vacuolating cytotoxin autotransporter of *Helicobacter pylori*', Infect Immun, **69**:(11) 6769-6775.
- Forsyth MH, Atherton JC, Blaser MJ and Cover TL (1998). 'Heterogeneity in levels of vacuolating cytotoxin gene (*vacA*) transcription among *Helicobacter pylori* strains', Infect Immun, **66**:(7) 3088-3094.
- Foynes S, Dorrell N, Ward SJ, Stabler RA, McColm AA, Rycroft AN and Wren BW (2000). '*Helicobacter pylori* possesses two CheY response regulators and a histidine kinase sensor, CheA, which are essential for chemotaxis and colonization of the gastric mucosa', Infect Immun, **68**:(4) 2016-2023.
- Frick-Cheng AE, Pyburn TM, Voss BJ, McDonald WH, Ohi MD and Cover TL (2016). 'Molecular and Structural Analysis of the *Helicobacter pylori* *cag* Type IV Secretion System Core Complex', mBio, **7**:(1) e02001-02015.
- Fujimoto I, Takizawa T, Ohba Y and Nakanishi Y (1998). 'Co-expression of Fas and Fas-ligand on the surface of influenza virus-infected cells', Cell Death Differ, **5**:(5) 426-431.
- Gaddy JA, Radin JN, Cullen TW, Chazin WJ, Skaar EP, Trent MS and Algood HM (2015). '*Helicobacter pylori* Resists the Antimicrobial Activity of Calprotectin via Lipid A Modification and Associated Biofilm Formation', mBio, **6**:(6) e01349-01315.
- Gao LY and Abu Kwaik Y (1999). 'Apoptosis in macrophages and alveolar epithelial cells during early stages of infection by *Legionella pneumophila* and its role in cytopathogenicity', Infect Immun, **67**:(2) 862-870.
- Gavins FN, Yona S, Kamal AM, Flower RJ and Perretti M (2003). 'Leukocyte antiadhesive actions of annexin 1: ALXR- and FPR-related anti-inflammatory mechanisms', Blood, **101**:(10) 4140-4147.
- Gebert B, Fischer W, Weiss E, Hoffmann R and Haas R (2003). '*Helicobacter pylori* vacuolating cytotoxin inhibits T lymphocyte activation', Science, **301**:(5636) 1099-1102.
- Geis G, Leying H, Suerbaum S, Mai U and Oepferkuch W (1989). 'Ultrastructure and chemical analysis of *Campylobacter pylori* flagella', J Clin Microbiol, **27**:(3) 436-441.
- Gerhard M, Lehn N, Neumayer N, Borén T, Rad R, Schepp W, Miehlke S, Classen M and Prinz C (1999). 'Clinical relevance of the *Helicobacter pylori* gene for blood-group antigen-binding adhesin', Proc Natl Acad Sci U S A, **96**:(22) 12778-12783.
- Gerke V, Creutz CE and Moss SE (2005). 'Annexins: linking Ca²⁺ signalling to membrane dynamics', Nat Rev Mol Cell Biol, **6**:(6) 449-461.
- Gerke V and Moss SE (2002). 'Annexins: from structure to function', Physiol Rev, **82**:(2) 331-371.
- Gewirtz AT, Yu Y, Krishna US, Israel DA, Lyons SL and Peek RM, Jr. (2004). '*Helicobacter pylori* flagellin evades toll-like receptor 5-mediated innate immunity', J Infect Dis, **189**:(10) 1914-1920.
- Goodwin AC, Weinberger DM, Ford CB, Nelson JC, Snider JD, Hall JD, Paules CI, Peek RM and Forsyth MH (2008). 'Expression of the *Helicobacter pylori* adhesin SabA is controlled via phase variation and the ArsRS signal transduction system', Microbiology (Reading), **154**:(Pt 8) 2231-2240.
- Goth SR and Stephens RS (2001). 'Rapid, transient phosphatidylserine externalization induced in host cells by infection with *Chlamydia* spp', Infect Immun, **69**:(2) 1109-1119.
- Graham FL, Smiley J, Russell WC and Nairn R (1977). 'Characteristics of a human cell line transformed by DNA from human adenovirus type 5', J Gen Virol, **36**:(1) 59-74.

- Grant SG, Jessee J, Bloom FR and Hanahan D (1990). 'Differential plasmid rescue from transgenic mouse DNAs into *Escherichia coli* methylation-restriction mutants', Proceedings of the National Academy of Sciences, **87**:(12) 4645-4649.
- Gray-Owen SD and Blumberg RS (2006). 'CEACAM1: contact-dependent control of immunity', Nat Rev Immunol, **6**:(6) 433-446.
- Grzeszczuk MJ, Bocian-Ostrzycka KM, Banaś AM, Roszczenko-Jasinska P, Malinowska A, Stralova H, Haas R, Meyer TF and Jagusztyn-Krynicka EK (2018). 'Thioloxidoreductase HP0231 of *Helicobacter pylori* impacts HopQ-dependent CagA translocation', Int J Med Microbiol, **308**:(8) 977-985.
- Gupta VR, Patel HK, Kostolansky SS, Ballivian RA, Eichberg J and Blanke SR (2008). 'Sphingomyelin functions as a novel receptor for *Helicobacter pylori* VacA', PLoS Pathog, **4**:(5) e1000073.
- Hall DE, Reichardt LF, Crowley E, Holley B, Moezzi H, Sonnenberg A and Damsky CH (1990). 'The alpha 1/beta 1 and alpha 6/beta 1 integrin heterodimers mediate cell attachment to distinct sites on laminin', J Cell Biol, **110**:(6) 2175-2184.
- Hamway Y, Taxauer K, Moonens K, Neumeyer V, Fischer W, Schmitt V, Singer BB, Remaut H, Gerhard M and Mejías-Luque R (2020). 'Cysteine Residues in *Helicobacter pylori* Adhesin HopQ are Required for CEACAM-HopQ Interaction and Subsequent CagA Translocation', Microorganisms, **8**:(4).
- Higashi H, Tsutsumi R, Fujita A, Yamazaki S, Asaka M, Azuma T and Hatakeyama M (2002a). 'Biological activity of the *Helicobacter pylori* virulence factor CagA is determined by variation in the tyrosine phosphorylation sites', Proc Natl Acad Sci U S A, **99**:(22) 14428-14433.
- Higashi H, Tsutsumi R, Muto S, Sugiyama T, Azuma T, Asaka M and Hatakeyama M (2002b). 'SHP-2 tyrosine phosphatase as an intracellular target of *Helicobacter pylori* CagA protein', Science, **295**:(5555) 683-686.
- Hood MI and Skaar EP (2012). 'Nutritional immunity: transition metals at the pathogen-host interface', Nat Rev Microbiol, **10**:(8) 525-537.
- IARC (1994). 'Schistosomes, liver flukes and *Helicobacter pylori*. IARC Working Group on the Evaluation of Carcinogenic Risks to Humans. Lyon, 7-14 June 1994', IARC Monogr Eval Carcinog Risks Hum, **61** 1-241.
- Ilver D, Arnqvist A, Ogren J, Frick IM, Kersulyte D, Incecik ET, Berg DE, Covacci A, Engstrand L and Borén T (1998). '*Helicobacter pylori* adhesin binding fucosylated histo-blood group antigens revealed by retagging', Science, **279**:(5349) 373-377.
- Ishijima N, Suzuki M, Ashida H, Ichikawa Y, Kanegae Y, Saito I, Borén T, Haas R, Sasakawa C and Mimuro H (2011). 'BabA-mediated adherence is a potentiator of the *Helicobacter pylori* type IV secretion system activity', J Biol Chem, **286**:(28) 25256-25264.
- Iwamoto H, Czajkowsky DM, Cover TL, Szabo G and Shao Z (1999). 'VacA from *Helicobacter pylori*: a hexameric chloride channel', FEBS Lett, **450**:(1-2) 101-104.
- Javaheri A, Kruse T, Moonens K, Mejías-Luque R, Debraekeleer A, Asche CI, Tegtmeyer N, Kalali B, Bach NC, Sieber SA, Hill DJ, Koniger V, Hauck CR, Moskalenko R, Haas R, Busch DH, Klaile E, Slevogt H, Schmidt A, Backert S, Remaut H, Singer BB and Gerhard M (2016). '*Helicobacter pylori* adhesin HopQ engages in a virulence-enhancing interaction with human CEACAMs', Nat Microbiol, **2** 16189.
- Javanbakht H, Halwani R, Cen S, Saadatmand J, Musier-Forsyth K, Gottlinger H and Kleiman L (2003). 'The interaction between HIV-1 Gag and human lysyl-tRNA synthetase during viral assembly', J Biol Chem, **278**:(30) 27644-27651.
- Jiménez-Soto LF, Kutter S, Sewald X, Ertl C, Weiss E, Kapp U, Rohde M, Pirch T, Jung K, Retta SF, Terradot L, Fischer W and Haas R (2009). '*Helicobacter pylori* type IV secretion apparatus exploits beta1 integrin in a novel RGD-independent manner', PLoS Pathog, **5**:(12) e1000684.
- Johnson KS and Ottemann KM (2018). 'Colonization, localization, and inflammation: the roles of *H. pylori* chemotaxis in vivo', Curr Opin Microbiol, **41** 51-57.
- Jolly C, Winfree S, Hansen B and Steele-Mortimer O (2014). 'The Annexin A2/p11 complex is required for efficient invasion of *Salmonella* Typhimurium in epithelial cells', Cell Microbiol, **16**:(1) 64-77.
- Keates S, Sougioultzis S, Keates AC, Zhao D, Peek RM, Jr., Shaw LM and Kelly CP (2001). '*cag+* *Helicobacter pylori* induce transactivation of the epidermal growth factor receptor in AGS gastric epithelial cells', J Biol Chem, **276**:(51) 48127-48134.
- Kirschnek S, Adams C and Gulbins E (2005). 'Annexin II is a novel receptor for *Pseudomonas aeruginosa*', Biochem Biophys Res Commun, **327**:(3) 900-906.

- Kleanthous H, Tibbitts TJ, Gray HL, Myers GA, Lee CK, Ermak TH and Monath TP (2001). 'Sterilizing immunity against experimental *Helicobacter pylori* infection is challenge-strain dependent', Vaccine, **19**:(32) 4883-4895.
- Kodigepalli KM, Bowers K, Sharp A and Nanjundan M (2015). 'Roles and regulation of phospholipid scramblases', FEBS Lett, **589**:(1) 3-14.
- Königer V (2015). 'CEACAMs as novel receptors for *Helicobacter pylori* outer membrane protein HopQ', Ludwig Maximilians Universität, Dr. rer. nat.
- Königer V, Holsten L, Harrison U, Busch B, Loell E, Zhao Q, Bonsor DA, Roth A, Kengmo-Tchoupa A, Smith SI, Mueller S, Sundberg EJ, Zimmermann W, Fischer W, Hauck CR and Haas R (2016). '*Helicobacter pylori* exploits human CEACAMs via HopQ for adherence and translocation of CagA', Nat Microbiol, **2** 16188.
- Kuehnl A, Musiol A, Raabe CA and Rescher U (2016). 'Emerging functions as host cell factors - an encyclopedia of annexin-pathogen interactions', Biol Chem, **397**:(10) 949-959.
- Kuespert K, Pils S and Hauck CR (2006). 'CEACAMs: their role in physiology and pathophysiology', Curr Opin Cell Biol, **18**:(5) 565-571.
- Kuhns LG, Wang G and Maier RJ (2015). 'Comparative Roles of the Two *Helicobacter pylori* Thioredoxins in Preventing Macromolecule Damage', Infect Immun, **83**:(7) 2935-2943.
- Kuwahara H, Miyamoto Y, Akaike T, Kubota T, Sawa T, Okamoto S and Maeda H (2000). '*Helicobacter pylori* urease suppresses bactericidal activity of peroxyxynitrite via carbon dioxide production', Infect Immun, **68**:(8) 4378-4383.
- Kwok T, Zabler D, Urman S, Rohde M, Hartig R, Wessler S, Misselwitz R, Berger J, Sewald N, König W and Backert S (2007). '*Helicobacter* exploits integrin for type IV secretion and kinase activation', Nature, **449**:(7164) 862-866.
- Letley DP and Atherton JC (2000). 'Natural diversity in the N terminus of the mature vacuolating cytotoxin of *Helicobacter pylori* determines cytotoxin activity', J Bacteriol, **182**:(11) 3278-3280.
- Lettl C, Haas R and Fischer W (2021). 'Kinetics of CagA type IV secretion by *Helicobacter pylori* and the requirement for substrate unfolding', Mol Microbiol.
- Li H, Liao T, Debowski AW, Tang H, Nilsson HO, Stubbs KA, Marshall BJ and Benghezal M (2016). 'Lipopolysaccharide Structure and Biosynthesis in *Helicobacter pylori*', Helicobacter, **21**:(6) 445-461.
- Li H, Marceau M, Yang T, Liao T, Tang X, Hu R, Xie Y, Tang H, Tay A, Shi Y, Shen Y, Yang T, Pi X, Lamichhane B, Luo Y, Debowski AW, Nilsson HO, Haslam SM, Mulloy B, Dell A, Stubbs KA, Marshall BJ and Benghezal M (2019). 'East-Asian *Helicobacter pylori* strains synthesize heptan-deficient lipopolysaccharide', PLoS Genet, **15**:(11) e1008497.
- Li H, Yang T, Liao T, Debowski AW, Nilsson HO, Fulurija A, Haslam SM, Mulloy B, Dell A, Stubbs KA, Marshall BJ and Benghezal M (2017). 'The redefinition of *Helicobacter pylori* lipopolysaccharide O-antigen and core-oligosaccharide domains', PLoS Pathog, **13**:(3) e1006280.
- Lin LL, Chen CN, Lin WC, Lee PH, Chang KJ, Lai YP, Wang JT and Juan HF (2008). 'Annexin A4: A novel molecular marker for gastric cancer with *Helicobacter pylori* infection using proteomics approach', Proteomics Clin Appl, **2**:(4) 619-634.
- Linz B, Balloux F, Moodley Y, Manica A, Liu H, Roumagnac P, Falush D, Stamer C, Prugnolle F, van der Merwe SW, Yamaoka Y, Graham DY, Perez-Trallero E, Wadstrom T, Suerbaum S and Achtman M (2007). 'An African origin for the intimate association between humans and *Helicobacter pylori*', Nature, **445**:(7130) 915-918.
- Liu G, McDaniel TK, Falkow S and Karlin S (1999). 'Sequence anomalies in the Cag7 gene of the *Helicobacter pylori* pathogenicity island', Proc Natl Acad Sci U S A, **96**:(12) 7011-7016.
- Lizak M and Yarovinsky TO (2012). 'Phospholipid scramblase 1 mediates type I interferon-induced protection against staphylococcal α -toxin', Cell Host Microbe, **11**:(1) 70-80.
- Lizarbe MA, Barrasa JI, Olmo N, Gavilanes F and Turnay J (2013). 'Annexin-phospholipid interactions. Functional implications', Int J Mol Sci, **14**:(2) 2652-2683.
- Lu H, Wu JY, Beswick EJ, Ohno T, Odenbreit S, Haas R, Reyes VE, Kita M, Graham DY and Yamaoka Y (2007). 'Functional and intracellular signaling differences associated with the *Helicobacter pylori* AlpAB adhesin from Western and East Asian strains', J Biol Chem, **282**:(9) 6242-6254.
- Lytton SD, Fischer W, Nagel W, Haas R and Beck FX (2005). 'Production of ammonium by *Helicobacter pylori* mediates occludin processing and disruption of tight junctions in Caco-2 cells', Microbiology (Reading), **151**:(Pt 10) 3267-3276.

- Mahdavi J, Sondén B, Hurtig M, Olfat FO, Forsberg L, Roche N, Angstrom J, Larsson T, Teneberg S, Karlsson KA, Altraja S, Wadström T, Kersulyte D, Berg DE, Dubois A, Petersson C, Magnusson KE, Norberg T, Lindh F, Lundskog BB, Arnqvist A, Hammarström L and Borén T (2002). '*Helicobacter pylori* SabA adhesin in persistent infection and chronic inflammation', Science, **297**:(5581) 573-578.
- Mailliard WS, Haigler HT and Schlaepfer DD (1996). 'Calcium-dependent binding of S100C to the N-terminal domain of annexin I', J Biol Chem, **271**:(2) 719-725.
- Marcos NT, Magalhães A, Ferreira B, Oliveira MJ, Carvalho AS, Mendes N, Gilmartin T, Head SR, Figueiredo C, David L, Santos-Silva F and Reis CA (2008). '*Helicobacter pylori* induces beta3GnT5 in human gastric cell lines, modulating expression of the SabA ligand sialyl-Lewis x', J Clin Invest, **118**:(6) 2325-2336.
- Marlink KL, Bacon KD, Sheppard BC, Ashktorab H, Smoot DT, Cover TL, Deveney CW and Rutten MJ (2003). 'Effects of *Helicobacter pylori* on intracellular Ca²⁺ signaling in normal human gastric mucous epithelial cells', Am J Physiol Gastrointest Liver Physiol, **285**:(1) G163-176.
- Marshall BJ, Armstrong JA, McGeachie DB and Glancy RJ (1985). 'Attempt to fulfil Koch's postulates for pyloric *Campylobacter*', Med J Aust, **142**:(8) 436-439.
- Marshall BJ and Warren JR (1984). 'Unidentified curved bacilli in the stomach of patients with gastritis and peptic ulceration', Lancet, **1**:(8390) 1311-1315.
- Maubach G, Sokolova O, Täger C and Naumann M (2020). 'CEACAMs interaction with *Helicobacter pylori* HopQ supports the type 4 secretion system-dependent activation of non-canonical NF-κB', Int J Med Microbiol, **310**:(6) 151444.
- McClain MS, Beckett AC and Cover TL (2017). '*Helicobacter pylori* Vacuolating Toxin and Gastric Cancer', Toxins (Basel), **9**:(10).
- McClain MS, Cao P, Iwamoto H, Vinion-Dubiel AD, Szabo G, Shao Z and Cover TL (2001). 'A 12-amino-acid segment, present in type s2 but not type s1 *Helicobacter pylori* VacA proteins, abolishes cytotoxin activity and alters membrane channel formation', J Bacteriol, **183**:(22) 6499-6508.
- Merrell DS, Goodrich ML, Otto G, Tompkins LS and Falkow S (2003). 'pH-regulated gene expression of the gastric pathogen *Helicobacter pylori*', Infect Immun, **71**:(6) 3529-3539.
- Miyahara A, Nakanishi N, Ooka T, Hayashi T, Sugimoto N and Tobe T (2009). 'Enterohemorrhagic *Escherichia coli* effector EspL2 induces actin microfilament aggregation through annexin 2 activation', Cell Microbiol, **11**:(2) 337-350.
- Molinari M, Galli C, Norais N, Telford JL, Rappuoli R, Luzio JP and Montecucco C (1997). 'Vacuoles induced by *Helicobacter pylori* toxin contain both late endosomal and lysosomal markers', J Biol Chem, **272**:(40) 25339-25344.
- Monteiro MA (2001). '*Helicobacter pylori*: a wolf in sheep's clothing: the glyco-type families of *Helicobacter pylori* lipopolysaccharides expressing histo-blood groups: structure, biosynthesis, and role in pathogenesis', Adv Carbohydr Chem Biochem, **57** 99-158.
- Moodley Y, Linz B, Bond RP, Nieuwoudt M, Soodyall H, Schlebusch CM, Bernhöft S, Hale J, Suerbaum S, Mugisha L, van der Merwe SW and Achtman M (2012). 'Age of the association between *Helicobacter pylori* and man', PLoS Pathog, **8**:(5) e1002693.
- Moonens K, Hamway Y, Neddermann M, Reschke M, Tegtmeyer N, Kruse T, Kammerer R, Mejías-Luque R, Singer BB, Backert S, Gerhard M and Remaut H (2018). '*Helicobacter pylori* adhesin HopQ disrupts trans dimerization in human CEACAMs', Embo j, **37**:(13).
- Moss SE and Morgan RO (2004). 'The annexins', Genome Biol, **5**:(4) 219.
- Mueller D, Tegtmeyer N, Brandt S, Yamaoka Y, De Poire E, Sgouras D, Wessler S, Torres J, Smolka A and Backert S (2012). 'c-Src and c-Abl kinases control hierarchic phosphorylation and function of the CagA effector protein in Western and East Asian *Helicobacter pylori* strains', J Clin Invest, **122**:(4) 1553-1566.
- Murata-Kamiya N, Kikuchi K, Hayashi T, Higashi H and Hatakeyama M (2010). '*Helicobacter pylori* exploits host membrane phosphatidylserine for delivery, localization, and pathophysiological action of the CagA oncoprotein', Cell Host Microbe, **7**:(5) 399-411.
- Nagashima H, Iwatani S, Cruz M, Jiménez Abreu JA, Uchida T, Mahachai V, Vilaichone RK, Graham DY and Yamaoka Y (2015). 'Toll-like Receptor 10 in *Helicobacter pylori* Infection', J Infect Dis, **212**:(10) 1666-1676.
- Nanjundan M, Sun J, Zhao J, Zhou Q, Sims PJ and Wiedmer T (2003). 'Plasma membrane phospholipid scramblase 1 promotes EGF-dependent activation of c-Src through the epidermal growth factor receptor', J Biol Chem, **278**:(39) 37413-37418.

- Necchi V, Manca R, Ricci V and Solcia E (2009). 'Evidence for transepithelial dendritic cells in human *H. pylori* active gastritis', Helicobacter, **14**:(3) 208-222.
- Neuper T, Frauenlob T, Sarajlic M, Posselt G, Wessler S and Horejs-Hoeck J (2020). 'TLR2, TLR4 and TLR10 Shape the Cytokine and Chemokine Release of *H. pylori*-Infected Human DCs', Int J Mol Sci, **21**:(11).
- Noto JM, Gaddy JA, Lee JY, Piazuolo MB, Friedman DB, Colvin DC, Romero-Gallo J, Suarez G, Loh J, Slaughter JC, Tan S, Morgan DR, Wilson KT, Bravo LE, Correa P, Cover TL, Amieva MR and Peek RM, Jr. (2013). 'Iron deficiency accelerates *Helicobacter pylori*-induced carcinogenesis in rodents and humans', J Clin Invest, **123**:(1) 479-492.
- Odenbreit S, Gebert B, Püls J, Fischer W and Haas R (2001). 'Interaction of *Helicobacter pylori* with professional phagocytes: role of the *cag* pathogenicity island and translocation, phosphorylation and processing of CagA', Cell Microbiol, **3**:(1) 21-31.
- Odenbreit S, Kavermann H, Püls J and Haas R (2002). 'CagA tyrosine phosphorylation and interleukin-8 induction by *Helicobacter pylori* are independent from AlpAB, HopZ and *bab* group outer membrane proteins', Int J Med Microbiol, **292**:(3-4) 257-266.
- Odenbreit S, Swoboda K, Barwig I, Ruhl S, Borén T, Koletzko S and Haas R (2009). 'Outer membrane protein expression profile in *Helicobacter pylori* clinical isolates', Infect Immun, **77**:(9) 3782-3790.
- Odenbreit S, Till M and Haas R (1996). 'Optimized BlaM-transposon shuttle mutagenesis of *Helicobacter pylori* allows the identification of novel genetic loci involved in bacterial virulence', Mol Microbiol, **20**:(2) 361-373.
- Odenbreit S, Till M, Hofreuter D, Faller G and Haas R (1999). 'Genetic and functional characterization of the *alpAB* gene locus essential for the adhesion of *Helicobacter pylori* to human gastric tissue', Mol Microbiol, **31**:(5) 1537-1548.
- Olbermann P, Josenhans C, Moodley Y, Uhr M, Stamer C, Vauterin M, Suerbaum S, Achtman M and Linz B (2010). 'A global overview of the genetic and functional diversity in the *Helicobacter pylori* *cag* pathogenicity island', PLoS Genet, **6**:(8) e1001069.
- Oleastro M and Ménard A (2013). 'The Role of *Helicobacter pylori* Outer Membrane Proteins in Adherence and Pathogenesis', Biology (Basel), **2**:(3) 1110-1134.
- Olivera-Severo D, Uberti AF, Marques MS, Pinto MT, Gomez-Lazaro M, Figueiredo C, Leite M and Carlini CR (2017). 'A New Role for *Helicobacter pylori* Urease: Contributions to Angiogenesis', Front Microbiol, **8** 1883.
- Pachathundikandi SK, Tegtmeyer N, Arnold IC, Lind J, Neddermann M, Falkeis-Veits C, Chattopadhyay S, Brönstrup M, Tegge W, Hong M, Sticht H, Vieth M, Müller A and Backert S (2019). 'T4SS-dependent TLR5 activation by *Helicobacter pylori* infection', Nat Commun, **10**:(1) 5717.
- Papini E, de Bernard M, Milia E, Bugnoli M, Zerial M, Rappuoli R and Montecucco C (1994). 'Cellular vacuoles induced by *Helicobacter pylori* originate from late endosomal compartments', Proc Natl Acad Sci U S A, **91**:(21) 9720-9724.
- Peck B, Ortkamp M, Diehl KD, Hundt E and Knapp B (1999). 'Conservation, localization and expression of HopZ, a protein involved in adhesion of *Helicobacter pylori*', Nucleic Acids Res, **27**:(16) 3325-3333.
- Peek RM, Jr. and Blaser MJ (2002). '*Helicobacter pylori* and gastrointestinal tract adenocarcinomas', Nat Rev Cancer, **2**:(1) 28-37.
- Perrais M, Rousseaux C, Ducourouble MP, Courcol R, Vincent P, Jonckheere N and Van Seuning I (2014). '*Helicobacter pylori* urease and flagellin alter mucin gene expression in human gastric cancer cells', Gastric Cancer, **17**:(2) 235-246.
- Petri K (2020). 'Analysis of the interaction between *Helicobacter pylori* and members of the Annexin family', Ludwig-Maximilians-University, Doctoral Thesis (M.D.), Munich.
- Pfannkuch L, Hurwitz R, Traulsen J, Sigulla J, Poeschke M, Matzner L, Kosma P, Schmid M and Meyer TF (2019). 'ADP heptose, a novel pathogen-associated molecular pattern identified in *Helicobacter pylori*', Faseb j, **33**:(8) 9087-9099.
- Popa SJ, Stewart SE and Moreau K (2018). 'Unconventional secretion of annexins and galectins', Semin Cell Dev Biol, **83** 42-50.
- Raetz CR and Whitfield C (2002). 'Lipopolysaccharide endotoxins', Annu Rev Biochem, **71** 635-700.
- Rand JH, Wu XX, Lin EY, Griffel A, Gialanella P and McKittrick JC (2012). 'Annexin A5 binds to lipopolysaccharide and reduces its endotoxin activity', mBio, **3**:(2).
- Ren S, Higashi H, Lu H, Azuma T and Hatakeyama M (2006). 'Structural basis and functional consequence of *Helicobacter pylori* CagA multimerization in cells', J Biol Chem, **281**:(43) 32344-32352.

- Rescher U and Gerke V (2004). 'Annexins--unique membrane binding proteins with diverse functions', J Cell Sci, **117**:(Pt 13) 2631-2639.
- Rhead JL, Letley DP, Mohammadi M, Hussein N, Mohagheghi MA, Eshagh Hosseini M and Atherton JC (2007). 'A new *Helicobacter pylori* vacuolating cytotoxin determinant, the intermediate region, is associated with gastric cancer', Gastroenterology, **133**:(3) 926-936.
- Rickes S (2011). '[Walter Krienitz and one of the first descriptions of gastric bacteria]', Z Gastroenterol, **49**:(11) 1491-1492.
- Rieder G, Merchant JL and Haas R (2005). '*Helicobacter pylori* cag-type IV secretion system facilitates corpus colonization to induce precancerous conditions in Mongolian gerbils', Gastroenterology, **128**:(5) 1229-1242.
- Rossez Y, Gosset P, Boneca IG, Magalhães A, Ecobichon C, Reis CA, Cieniewski-Bernard C, Joncquel Chevalier Curt M, Léonard R, Maes E, Sperandio B, Slomianny C, Sansonetti PJ, Michalski JC and Robbe-Masselot C (2014). 'The lacdiNAc-specific adhesin LabA mediates adhesion of *Helicobacter pylori* to human gastric mucosa', J Infect Dis, **210**:(8) 1286-1295.
- Ruiter GA, Zerp SF, Bartelink H, van Blitterswijk WJ and Verheij M (2003). 'Anti-cancer alkyllysophospholipids inhibit the phosphatidylinositol 3-kinase-Akt/PKB survival pathway', Anticancer Drugs, **14**:(2) 167-173.
- Sahu SK, Gummadi SN, Manoj N and Aradhyam GK (2007). 'Phospholipid scramblases: an overview', Arch Biochem Biophys, **462**:(1) 103-114.
- Saunders NJ, Peden JF, Hood DW and Moxon ER (1998). 'Simple sequence repeats in the *Helicobacter pylori* genome', Mol Microbiol, **27**:(6) 1091-1098.
- Sayi A, Kohler E, Hitzler I, Arnold I, Schwendener R, Rehrauer H and Müller A (2009). 'The CD4+ T cell-mediated IFN-gamma response to *Helicobacter* infection is essential for clearance and determines gastric cancer risk', J Immunol, **182**:(11) 7085-7101.
- Schindele F, Weiss E, Haas R and Fischer W (2016). 'Quantitative analysis of CagA type IV secretion by *Helicobacter pylori* reveals substrate recognition and translocation requirements', Molecular Microbiology, **100**:(1) 188-203.
- Schmitt W and Haas R (1994). 'Genetic analysis of the *Helicobacter pylori* vacuolating cytotoxin: structural similarities with the IgA protease type of exported protein', Mol Microbiol, **12**:(2) 307-319.
- Sebrell TA, Hashimi M, Sidar B, Wilkinson RA, Kirpotina L, Quinn MT, Malkoç Z, Taylor PJ, Wilking JN and Bimczok D (2019). 'A Novel Gastric Spheroid Co-culture Model Reveals Chemokine-Dependent Recruitment of Human Dendritic Cells to the Gastric Epithelium', Cell Mol Gastroenterol Hepatol, **8**:(1) 157-171.e153.
- Segal ED, Falkow S and Tompkins LS (1996). '*Helicobacter pylori* attachment to gastric cells induces cytoskeletal rearrangements and tyrosine phosphorylation of host cell proteins', Proc Natl Acad Sci U S A, **93**:(3) 1259-1264.
- Sekiguchi M, Sakakibara K and Fujii G (1978). 'Establishment of cultured cell lines derived from a human gastric carcinoma', Jpn J Exp Med, **48**:(1) 61-68.
- Senkovich OA, Yin J, Ekshyyan V, Conant C, Traylor J, Adegboyega P, McGee DJ, Rhoads RE, Slepnev S and Testerman TL (2011). '*Helicobacter pylori* AlpA and AlpB bind host laminin and influence gastric inflammation in gerbils', Infect Immun, **79**:(8) 3106-3116.
- Sewald X, Gebert-Vogl B, Prassl S, Barwig I, Weiss E, Fabbri M, Osicka R, Schiemann M, Busch DH, Semmrich M, Holzmann B, Sebo P and Haas R (2008). 'Integrin subunit CD18 Is the T-lymphocyte receptor for the *Helicobacter pylori* vacuolating cytotoxin', Cell Host Microbe, **3**:(1) 20-29.
- Skoog EC, Morikis VA, Martin ME, Foster GA, Cai LP, Hansen LM, Li B, Gaddy JA, Simon SI and Solnick JV (2018). 'CagY-Dependent Regulation of Type IV Secretion in *Helicobacter pylori* Is Associated with Alterations in Integrin Binding', mBio, **9**:(3).
- Smoot DT, Resau JH, Naab T, Desbordes BC, Gilliam T, Bull-Henry K, Curry SB, Nidiry J, Sewchand J, Mills-Robertson K and et al. (1993). 'Adherence of *Helicobacter pylori* to cultured human gastric epithelial cells', Infect Immun, **61**:(1) 350-355.
- Sokolova O, Vieth M, Gnad T, Bozko PM and Naumann M (2014). '*Helicobacter pylori* promotes eukaryotic protein translation by activating phosphatidylinositol 3 kinase/mTOR', Int J Biochem Cell Biol, **55** 157-163.
- Somarajan SR, Al-Asadi F, Ramasamy K, Pandranki L, Baseman JB and Kannan TR (2014). 'Annexin A2 mediates *Mycoplasma pneumoniae* community-acquired respiratory distress syndrome toxin binding to eukaryotic cells', mBio, **5**:(4).

- Stead CM, Zhao J, Raetz CR and Trent MS (2010). 'Removal of the outer Kdo from *Helicobacter pylori* lipopolysaccharide and its impact on the bacterial surface', Mol Microbiol, **78**:(4) 837-852.
- Stein SC, Faber E, Bats SH, Murillo T, Speidel Y, Coombs N and Josenhans C (2017). '*Helicobacter pylori* modulates host cell responses by CagT4SS-dependent translocation of an intermediate metabolite of LPS inner core heptose biosynthesis', PLoS Pathog, **13**:(7) e1006514.
- Stewart SE, Ashkenazi A, Williamson A, Rubinsztein DC and Moreau K (2018). 'Transbilayer phospholipid movement facilitates the translocation of annexin across membranes', J Cell Sci, **131**:(14).
- Stout JG, Bassé F, Luhm RA, Weiss HJ, Wiedmer T and Sims PJ (1997). 'Scott syndrome erythrocytes contain a membrane protein capable of mediating Ca²⁺-dependent transbilayer migration of membrane phospholipids', J Clin Invest, **99**:(9) 2232-2238.
- Suerbaum S and Michetti P (2002). '*Helicobacter pylori* infection', N Engl J Med, **347**:(15) 1175-1186.
- Sun J, Nanjundan M, Pike LJ, Wiedmer T and Sims PJ (2002). 'Plasma membrane phospholipid scramblase 1 is enriched in lipid rafts and interacts with the epidermal growth factor receptor', Biochemistry, **41**:(20) 6338-6345.
- Sun J, Zhao J, Schwartz MA, Wang JY, Wiedmer T and Sims PJ (2001). 'c-Abl tyrosine kinase binds and phosphorylates phospholipid scramblase 1', J Biol Chem, **276**:(31) 28984-28990.
- Suzuki J, Denning DP, Imanishi E, Horvitz HR and Nagata S (2013). 'Xk-related protein 8 and CED-8 promote phosphatidylserine exposure in apoptotic cells', Science, **341**:(6144) 403-406.
- Suzuki J, Umeda M, Sims PJ and Nagata S (2010). 'Calcium-dependent phospholipid scrambling by TMEM16F', Nature, **468**:(7325) 834-838.
- Szabó I, Brutsche S, Tombola F, Moschioni M, Satin B, Telford JL, Rappuoli R, Montecucco C, Papini E and Zoratti M (1999). 'Formation of anion-selective channels in the cell plasma membrane by the toxin VacA of *Helicobacter pylori* is required for its biological activity', Embo j, **18**:(20) 5517-5527.
- Tabassam FH, Graham DY and Yamaoka Y (2008). 'OipA plays a role in *Helicobacter pylori*-induced focal adhesion kinase activation and cytoskeletal re-organization', Cell Microbiol, **10**:(4) 1008-1020.
- Takahashi-Kanemitsu A, Knight CT and Hatakeyama M (2020). 'Molecular anatomy and pathogenic actions of *Helicobacter pylori* CagA that underpin gastric carcinogenesis', Cell Mol Immunol, **17**:(1) 50-63.
- Tchoupa AK, Schuhmacher T and Hauck CR (2014). 'Signaling by epithelial members of the CEACAM family - mucosal docking sites for pathogenic bacteria', Cell Commun Signal, **12** 27.
- Tegtmeyer N, Hartig R, Delahay RM, Rohde M, Brandt S, Conradi J, Takahashi S, Smolka AJ, Sewald N and Backert S (2010). 'A small fibronectin-mimicking protein from bacteria induces cell spreading and focal adhesion formation', J Biol Chem, **285**:(30) 23515-23526.
- Tomb JF, White O, Kerlavage AR, Clayton RA, Sutton GG, Fleischmann RD, Ketchum KA, Klenk HP, Gill S, Dougherty BA, Nelson K, Quackenbush J, Zhou L, Kirkness EF, Peterson S, Loftus B, Richardson D, Dodson R, Khalak HG, Glodek A, McKenney K, Fitzegerald LM, Lee N, Adams MD, Hickey EK, Berg DE, Gocayne JD, Utterback TR, Peterson JD, Kelley JM, Cotton MD, Weidman JM, Fujii C, Bowman C, Watthey L, Wallin E, Hayes WS, Borodovsky M, Karp PD, Smith HO, Fraser CM and Venter JC (1997). 'The complete genome sequence of the gastric pathogen *Helicobacter pylori*', Nature, **388**:(6642) 539-547.
- Tran AX, Stead CM and Trent MS (2005). 'Remodeling of *Helicobacter pylori* lipopolysaccharide', J Endotoxin Res, **11**:(3) 161-166.
- Tran AX, Whittimore JD, Wyrick PB, McGrath SC, Cotter RJ and Trent MS (2006). 'The lipid A 1-phosphatase of *Helicobacter pylori* is required for resistance to the antimicrobial peptide polymyxin', J Bacteriol, **188**:(12) 4531-4541.
- Tsutsumi R, Higashi H, Higuchi M, Okada M and Hatakeyama M (2003). 'Attenuation of *Helicobacter pylori* CagA x SHP-2 signaling by interaction between CagA and C-terminal Src kinase', J Biol Chem, **278**:(6) 3664-3670.
- Tsutsumi R, Takahashi A, Azuma T, Higashi H and Hatakeyama M (2006). 'Focal adhesion kinase is a substrate and downstream effector of SHP-2 complexed with *Helicobacter pylori* CagA', Mol Cell Biol, **26**:(1) 261-276.
- van Genderen HO, Kenis H, Hofstra L, Narula J and Reutelingsperger CP (2008). 'Extracellular annexin A5: functions of phosphatidylserine-binding and two-dimensional crystallization', Biochim Biophys Acta, **1783**:(6) 953-963.
- Varga MG, Shaffer CL, Sierra JC, Suarez G, Piazuolo MB, Whitaker ME, Romero-Gallo J, Krishna US, Delgado A, Gomez MA, Good JA, Almqvist F, Skaar EP, Correa P, Wilson KT, Hadjifrangiskou M

- and Peek RM (2016). 'Pathogenic *Helicobacter pylori* strains translocate DNA and activate TLR9 via the cancer-associated *cag* type IV secretion system', *Oncogene*, **35**:(48) 6262-6269.
- Vermes I, Haanen C, Steffens-Nakken H and Reutelingsperger C (1995). 'A novel assay for apoptosis. Flow cytometric detection of phosphatidylserine expression on early apoptotic cells using fluorescein labelled Annexin V', *J Immunol Methods*, **184**:(1) 39-51.
- Viala J, Chaput C, Boneca IG, Cardona A, Girardin SE, Moran AP, Athman R, M emet S, Huerre MR, Coyle AJ, DiStefano PS, Sansonetti PJ, Labigne A, Bertin J, Philpott DJ and Ferrero RL (2004). 'Nod1 responds to peptidoglycan delivered by the *Helicobacter pylori* *cag* pathogenicity island', *Nat Immunol*, **5**:(11) 1166-1174.
- Voges M, Bachmann V, Kammerer R, Gophna U and Hauck CR (2010). 'CEACAM1 recognition by bacterial pathogens is species-specific', *BMC Microbiol*, **10** 117.
- Walz A, Odenbreit S, Mahdavi J, Bor en T and Ruhl S (2005). 'Identification and characterization of binding properties of *Helicobacter pylori* by glycoconjugate arrays', *Glycobiology*, **15**:(7) 700-708.
- Wang X, Dai Y, Zhao Y, Li M, Zhang J, Ci Y, Wang H and Li X (2021). 'AnnexinA5 Might Suppress the Phenotype of Human Gastric Cancer Cells via ERK Pathway', *Front Oncol*, **11** 665105.
- Watanabe T, Asano N, Fichtner-Feigl S, Gorelick PL, Tsuji Y, Matsumoto Y, Chiba T, Fuss IJ, Kitani A and Strober W (2010). 'NOD1 contributes to mouse host defense against *Helicobacter pylori* via induction of type I IFN and activation of the ISGF3 signaling pathway', *J Clin Invest*, **120**:(5) 1645-1662.
- Watanabe T, Tada M, Nagai H, Sasaki S and Nakao M (1998). '*Helicobacter pylori* infection induces gastric cancer in mongolian gerbils', *Gastroenterology*, **115**:(3) 642-648.
- Wesseling MC, Wagner-Britz L, Nguyen DB, Asanidze S, Mutua J, Mohamed N, Hanf B, Ghashghaieina M, Kaestner L and Bernhardt I (2016). 'Novel Insights in the Regulation of Phosphatidylserine Exposure in Human Red Blood Cells', *Cell Physiol Biochem*, **39**:(5) 1941-1954.
- Wiedemann T, Hofbauer S, Tegtmeyer N, Huber S, Sewald N, Wessler S, Backert S and Rieder G (2012). '*Helicobacter pylori* CagL dependent induction of gastrin expression via a novel $\alpha\beta 5$ -integrin-integrin linked kinase signalling complex', *Gut*, **61**:(7) 986-996.
- Wroblewski LE, Shen L, Ogden S, Romero-Gallo J, Lapiere LA, Israel DA, Turner JR and Peek RM, Jr. (2009). '*Helicobacter pylori* dysregulation of gastric epithelial tight junctions by urease-mediated myosin II activation', *Gastroenterology*, **136**:(1) 236-246.
- Yahiro K, Niidome T, Kimura M, Hatakeyama T, Aoyagi H, Kurazono H, Imagawa K, Wada A, Moss J and Hirayama T (1999). 'Activation of *Helicobacter pylori* VacA toxin by alkaline or acid conditions increases its binding to a 250-kDa receptor protein-tyrosine phosphatase beta', *J Biol Chem*, **274**:(51) 36693-36699.
- Yahiro K, Satoh M, Nakano M, Hisatsune J, Isomoto H, Sap J, Suzuki H, Nomura F, Noda M, Moss J and Hirayama T (2012). 'Low-density lipoprotein receptor-related protein-1 (LRP1) mediates autophagy and apoptosis caused by *Helicobacter pylori* VacA', *J Biol Chem*, **287**:(37) 31104-31115.
- Yahiro K, Wada A, Nakayama M, Kimura T, Ogushi K, Niidome T, Aoyagi H, Yoshino K, Yonezawa K, Moss J and Hirayama T (2003). 'Protein-tyrosine phosphatase alpha, RPTP alpha, is a *Helicobacter pylori* VacA receptor', *J Biol Chem*, **278**:(21) 19183-19189.
- Yakoob J, Abbas Z, Khan R, Salim SA, Awan S, Abrar A and Jafri W (2016). '*Helicobacter pylori* outer membrane protein Q allele distribution is associated with distinct pathologies in Pakistan', *Infect Genet Evol*, **37** 57-62.
- Yamaoka Y, Kwon DH and Graham DY (2000). 'A M(r) 34,000 proinflammatory outer membrane protein (*oipA*) of *Helicobacter pylori*', *Proc Natl Acad Sci U S A*, **97**:(13) 7533-7538.
- Yan F, Cao H, Chaturvedi R, Krishna U, Hobbs SS, Dempsey PJ, Peek RM, Jr., Cover TL, Washington MK, Wilson KT and Polk DB (2009). 'Epidermal growth factor receptor activation protects gastric epithelial cells from *Helicobacter pylori*-induced apoptosis', *Gastroenterology*, **136**:(4) 1297-1307, e1291-1293.
- Younan P, Iampietro M, Santos RI, Ramanathan P, Popov VL and Bukreyev A (2018). 'Role of Transmembrane Protein 16F in the Incorporation of Phosphatidylserine Into Budding Ebola Virus Virions', *J Infect Dis*, **218**:(suppl_5) S335-s345.
- Yuan S, Qu L and Shou C (2016). 'N-Terminal Polypeptide of Annexin A2 Decreases Infection of *Mycoplasma hyorhinis* to Gastric Cancer Cells', *PLoS One*, **11**:(1) e0147776.
- Zhao J, Zhou Q, Wiedmer T and Sims PJ (1998). 'Level of expression of phospholipid scramblase regulates induced movement of phosphatidylserine to the cell surface', *J Biol Chem*, **273**:(12) 6603-6606.

-
- Zhao Q, Busch B, Jiménez-Soto LF, Ishikawa-Ankerhold H, Massberg S, Terradot L, Fischer W and Haas R (2018). 'Integrin but not CEACAM receptors are dispensable for *Helicobacter pylori* CagA translocation', PLOS Pathogens, **14**:(10) e1007359.
- Zhou Q, Zhao J, Wiedmer T and Sims PJ (2002). 'Normal hemostasis but defective hematopoietic response to growth factors in mice deficient in phospholipid scramblase 1', Blood, **99**:(11) 4030-4038.
- Zobiack N, Rescher U, Laarmann S, Michgehl S, Schmidt MA and Gerke V (2002). 'Cell-surface attachment of pedestal-forming enteropathogenic *E. coli* induces a clustering of raft components and a recruitment of annexin 2', J Cell Sci, **115**:(Pt 1) 91-98.
- Zorio DAR, Monsma S, Sanes DH, Golding NL, Rubel EW and Wang Y (2019). 'De novo sequencing and initial annotation of the Mongolian gerbil (*Meriones unguiculatus*) genome', Genomics, **111**:(3) 441-449.

Danksagung

An dieser Stelle möchte ich all jenen Menschen meinen großen Dank aussprechen, die mir während dieser Zeit mit Rat und Tat zur Seite gestanden sind.

Zuerst möchte ich mich besonders bei Prof. Dr. Rainer Haas für die Chance bedanken, in diesem Forschungsbereich meine Dissertation zu absolvieren. Seine Betreuung und enorme Unterstützung, sowie die stete Diskussionsbereitschaft hat maßgeblich zum Gelingen der Arbeit beigetragen.

Mein Dank gilt außerdem der AG Haas, sowohl den derzeitigen als auch vergangenen Mitgliedern. Besonderes möchte ich Dr. Wolfgang Fischer danken, da er sich immer Zeit für produktive Gespräche genommen hat. Außerdem möchte ich mich bei Evelyn Weiß für ihre Hilfsbereitschaft in allen Lebenslagen bedanken, vor allem in labortechnischen Fragen. Ganz besonderer Dank gilt auch Clara Lettl, die mir immer mit Rat und Tat zur Seite gestanden ist und für viele lustige Stunden im Labor gesorgt hat. Außerdem möchte ich Ben, Pia, Ina und noch vielen anderen ehemaligen Mitgliedern der AG Haas meinen Dank aussprechen.

Bei unseren Kooperationspartnern möchte ich mich an dieser Stelle auch bedanken. Hellen Ishikawa-Ankerhold und Dominic van den Heuvel danke ich für ihre Unterstützung in der Konfokalmikroskopie. Für die Bereitstellung des *H. pylori* LPS bedanke ich mich bei Hong Li. Prof. Dr. Hauck danke ich für die Verfügungstellung der CEACAM Plasmide und Überstände und Prof. Dr. Zimmermann für die Erläuterung der CEACAM Sequenzen der mongolischen Wüstenrennmäuse.

Ganz besonderer Dank gilt meiner Familie, meinen Eltern, Johann und Elisabeth, und meiner Schwester Astrid für ihre Unterstützung und Zusprüche während der Arbeit an meiner Dissertation. Außerdem möchte ich mich von ganzem Herzen bei Tom bedanken, dessen Unterstützung ich keinesfalls missen wollte.

Zu guter Letzt möchte ich mich bei meinen Freunden Ingrid, Karin, Becky und Emilie für die Ermutigung auf meinem Weg zur Doktorarbeit bedanken.